

University of Ontario Institute of Technology
Faculty of Engineering and Applied Science

Development of Polymer Based Nanocomposite using Electrospinning for Sound Absorption and Isolation

Submitted By:
Mohamed Ali Elkasaby

Supervisors:
Associate Prof Dr. Atef Mohany
Associate Prof Dr. Ghaus M. Rizvi

January 2017

Abstract

Excessive noise has adverse effects on human health. Therefore, it is necessary to find innovative methods for decreasing the exposure to noise in the environment. Various materials are used for dampening noise. In order to obtain promising results for sound absorption, these materials should have a large volume. Nanofibers, derived from polymeric materials, offer enormous benefits, and therefore, there is an intense focus on how this technology can be implemented to improve the performance of different applications. Nanofibers have a high surface area to volume ratio as well as a high porosity. In addition, fillers like carbon nanotubes (CNTs), wollastonite (WS), graphene (GN) and fiberglass (FG) show significant results for improving the mechanical and other properties. Therefore, in this work, polymeric nanofibers with and without fillers, have been investigated as sound absorbing materials. The polymers used in this study were polyvinyl alcohol (PVA), polyvinyl chloride (PVC), and polystyrene (PS), which were processed using electrospinning to produce nanofiber mats and tested for the sound absorption properties. To optimize fiber diameters, the process parameters were studied including the solution concentration, the solution flow rate, the high voltage used for generating an electric field, the distance over which the fibers were collected, and the speed of the rotating drum on which the fibers were collected. Statistical analysis and multiple regression techniques were applied to investigate the effects of the process parameter on the fiber diameters. Solution concentration and flow rate were determined to have the most significant effects on the fiber diameters. The study resulted in the development of a predictive model, which can be used to determine the parameter values required to produce nanofibers with a specified average diameter in the range of interest.

Various fillers were added to the polymer matrix in order to enhance its mechanical and sound absorption properties. The fillers used were CNTs, WS, GN, and FG. Single and multi-layered mats, with different fiber diameters, were produced to investigate the sound absorbing properties. Also, a mixture solution of two different polymers was electrospun to obtain a mat that consists of two polymers.

The results show that the nanofiber mats exhibit good sound absorption in the mid and low frequency ranges. As the fiber diameter decreases, the sound absorption increases. The addition of fillers to the nanofibers increases the sound absorption and improves the mechanical properties. Multi-layer mats produced from different types of polymer show a good sound absorption. The sound absorption improved using mats with graded fiber diameters structure. Increasing the mats thickness enhances the sound absorption as well. Finally adding nanofibers mats to conventional sound absorbing materials improve the sound absorption in the low frequency range by 32%. This study presents a promising road map for using electrospun polymer materials, with and without different types of fillers, for sound absorption in the mid and low frequency ranges. These materials will be particularly cost-effective in applications where saving space or volume is a major consideration, such as in the aerospace industry or in electronic devices.

Acknowledgements

First, all thanks are to be for Merciful God who helps us to finish this work.

I would like to express my deepest sense of gratitude to supervisors, Dr. Atef Mohany and Dr. Ghaus M. Rizvi for their great support and encouragement to conduct this research. Their wide knowledge and great experience helped me a lot to overcome any obstacles during my research.

I express my deepest appreciation to my Ph.D. Committee members for their valuable suggestions and constructive comments.

I extend my thanks to all of my colleagues in aeroacoustics and noise control laboratory, and my colleagues in material lab as well.

I wish to record my gratefulness to all who have faithfully helped me through consultation, provision with material and performing the experiments reported in this study.

At last, I wish to express my great thanks to my parents, my wife and my kids for their continuous encouragement, support, and haleness during writing and doing this work.

Dedication

To soul of my father Mr. Ali Elkasaby

Contents

Abstract.....	ii
Acknowledgements	iv
Contents.....	vi
Tables.....	xii
Figures.....	xiii
Lists of abbreviations and symbols	xxii
Chapter 1: Introduction.....	1
1.1 Introduction.....	1
1.2 Motivation.....	2
1.3 Objective.....	3
1.4 Methodology.....	3
1.5 Main thesis contributions.....	3
1.6 Thesis outline.....	4
Chapter 2 : Background and literature review	6
2.1 Introduction.....	6
2.2 Nanofiber production methods	6
2.2.1 Drawing	6
2.2.2 Template synthesis.....	7
2.2.3 Phase separation.....	8
2.2.4 Self-assembly.....	8
2.2.5 Electrospinning	8
2.3 Electrospinning	8
2.4 Factors affecting electrospinning process.....	13
2.4.1 Solution parameters	13
2.4.1.1 Concentration.....	13

2.4.1.2 Molecular weight	13
2.4.1.3 Viscosity	16
2.4.1.4 Surface tension.....	17
2.4.1.5 Conductivity.....	18
2.4.1.6 Effect of solvent.....	19
2.4.2 Processing parameters.....	19
2.4.2.1 High Voltage.....	19
2.4.2.2 Flow rate	20
2.4.2.3 Distance	21
2.4.2.4 Collector.....	22
2.4.2.5 Spinneret	23
2.4.3 Ambient parameters.....	23
2.4.3.1 Humidity	23
2.4.3.2 Temperature	23
2.4.3.3 Pressure	24
2.4.3.4 Type of atmosphere	24
2.5 Techniques and apparatus used in electrospinning nanofiber	25
2.5.1 Magnetic electrospinning.....	26
2.5.2 External electric field.....	26
2.5.3 Needleless fiber production:	27
2.5.3.1 Rotating drum	27
2.5.3.2 Bubble electrospinning	28
2.5.3.3 Disc, ball and spiral coil	29
2.6 Sound and noise	30
2.6.1 Sound absorption coefficient	33
2.6.2 Sound reflection coefficient.....	34

2.6.3 Acoustic impedance	34
2.6.4 Factors affect the performance of sound absorbing materials	36
2.6.5 Low frequency:	38
2.6.6 Reducing the effect of low-frequency noise	39
2.7 Nanofiber as sound absorption material	41
2.7.1 Silica nanofiber sheet	41
2.7.2 Polyvinyl-chloride (PVC) and polyvinyl-pyrrolidone (PVP)	42
2.7.3 Polyamide (PA6)	43
2.7.4 Polyacrylonitrile (PAN)	44
2.7.5 Nylon (NY6)	46
2.7.6 Polyvinyl alcohol (PVA)	47
2.8 Nanofiber as thermally conductive material	50
2.9 Discussion	52
Chapter 3: Experimental setup and samples preparation.....	54
3.1 Introduction.....	54
3.2 Chemicals and solvents.....	54
3.3 Mechanical and physical characterization equipment	55
3.3.1 Thermogravimetric analyzer (TGA).....	55
3.3.2 Differential scanning calorimeters (DSC)	55
3.3.3 Dynamic mechanical analysis (DMA).....	55
3.3.4 Scanning electron microscopy (SEM) and digital optical microscope (DOM)..	55
3.4 The Electrospinning setup	56
3.5 Material formulations used	57
3.5.1 Solution preparation.....	57
3.5.2 Composite matrix.....	57
3.5.3 Electrospinning process	58
3.6 Acoustic characterization measurements.....	58

3.6.1 Impedance tube	58
3.6.1.1 Validation of impedance tube	61
3.6.2 Microphone	62
3.6.3 Data acquisition	62
3.6.4 Measurement of samples sounds absorption coefficient	63
Chapter 4 : Modeling and optimization of electrospinning of polyvinyl alcohol (PVA)	64
4.1 Introduction.....	64
4.2 Experimental setup, materials, procedure, and theory of experimental design	66
4.3 Results and analysis	67
4.3.1 Evaluating effects of control parameters using ANOVA:	68
4.3.2 Fiber morphologies:	69
4.3.3 Effects of control factors:	70
4.4 Verification of ANOVA:	71
4.5 Factorial ANOVA to study interactions:	72
4.6 Signal to noise ratio (S/N):	72
4.7 Electrospinning production model using RSM.....	73
4.8 Summary	77
Chapter 5: Mechanical and thermal properties	78
5.1 Introduction.....	78
5.2 Experimental work.....	78
5.2.1 Materials	78
5.2.2 Mats fabrication and sample preparation.....	78
5.2.3 Characterization	79
5.2.3.1 Dynamic mechanical analysis (DMA).....	79
5.2.3.2 Thermogravimetric analyzer (TGA).....	79
5.2.3.3 Differential scanning calorimeters (DSC)	79

5.3 Results and discussion	79
5.3.1 PVA nanocomposite	79
5.3.1.1 Tensile test	79
5.3.1.2 Thermal properties	82
5.3.2 PVC nanocomposite	84
5.3.2.1 Tensile tests.....	84
5.3.2.2 Thermal properties.....	87
Chapter 6 : Morphology	90
6.1 Introduction.....	90
6.2 PVA nanofibers and its blends.....	90
6.2.1 PVA nanofibers.....	90
6.2.2 PVA with fillers	91
6.2.2.1 PVA with CNTs.....	91
6.2.2.2 PVA with Graphene (GN)	92
6.3 PVC based materials.....	93
6.3.1 PVC/CNTs	94
6.3.2 PVC with fiberglass (FG)	95
6.4 Multi-polymers mats.....	95
6.4.1 Multi-layers of PVA and PS	95
6.4.2 Blends mats of PVC and PS	96
6.5 PVC and PS mat produced by coaxial needle.....	98
Chapter 7 : Characteristics of Sound absorption Nanofibers.....	99
7.1 Introduction.....	99
7.2 Sound absorption of PVC mat	99
7.2.1 Sound absorption of mats from mixture solutions of PVC and PS	100
7.2.2 Sound absorption of multi-layer mats of PVC-PS-PVC.....	102
7.2.3 Sound absorption of composites PVC	105

7.2.3.1 Carbon nanotubes and PVC.....	105
7.2.3.2 Fiberglass and PVC	106
7.2.4 Double layers of composite PVC mats	109
7.3 Sound absorption of PVA mats	111
7.3.1 Sound absorption of composite PVA mats	112
7.3.1.1 PVA and Carbon nanotubes (CNTs)	112
7.3.1.2 PVA and Graphene (GN).....	114
7.3.1.3 PVA and Wollastonite (WS).....	116
7.3.2 Sound absorption of several mats combination	118
7.3.3 Sound absorption of multi-layer mats PVA-PS-PVA.....	125
7.3.4 Sound absorption of PVA mats with graded structure	131
7.3.5 Sound absorption of PVA mats with different thickness.....	132
7.4 Nanofiber membrane with conventional sound absorbing material	133
7.5 Summary	136
Chapter 8 : Conclusions, contributions and future work.....	138
8.1 Conclusions.....	138
8.2 Contributions	139
8.3 Recommendation and future work.....	140

Tables

Table 2.1: Effect of changing electrospinning process parameters on the resultant fiber morphology[67]	25
Table 2.2: Effect of noise levels between 85-106 [db] on traffic wardens in Pakistan	31
Table 2.3: frequency and wavelength of low frequency sound [80]	39
Table 2.4: Average diameter (μm) of silica fiber laminates (SF1-4) and GW [95].....	42
Table 2.5: Outlet velocities of drum carry PVA solution [49]	48
Table 2.6: Distance of electrodes during electrostatic spinning that determines the average diameter of nanofiber [98]	48
Table 3.1: polymers concentrations range	57
Table 3.2 : Filler percent in polymer solution	57
Table 3.3: Measurement range according to distance between two microphones.....	59
Table 4.1: Assignment of levels to control factors	67
Table 4.2. Experimental results of fiber diameter using L27OA to plan experimentation..	68
Table 4.3: ANOVA results	69
Table 4.4: Results of the confirmation experiment for optimal fiber diameter values.....	71
Table 4.5: ANOVA results for interactions effect.....	72
Table 4.6: ANOVA results based on S/N ratio values	73
Table 5.1: Tensile properties of PVA mats and its composites	81
Table 5.2: TGA measurements of PVA and its composites nanofibers	83
Table 5.3: DSC measurements of PVA/PVA composites.	84
Table 5.4: Tensile properties of PVC and PVC composites mats	85
Table 5.5: TGA measurements of PVC and its composites nanofiber	88
Table 5.6: DSC measurements of PVC and PVC composites nanofibers.	89
Table 6.1: Fiber diameters of PVA/CNTs (nm)	92
Table 6.2: Fiber diameters of PVA/GN (nm)	92
Table 7.1: Percent of sound absorption improved with increasing the mats' thickness....	132
Table 7.2: Percent of sound absorption improving of DD2 using PVA mats	133

Figures

Figure 2.1: Drawing a molten of poly(trimethylene terephthalate) (PTT) [15].....	7
Figure 2.2: Templates of nanofiber [17].....	7
Figure 2.3: electrospinning setup[24]	9
Figure 2.4: Taylor cone [23].....	9
Figure 2.5: Morphology of PVA fiber with different concentration (wt%) at $M_{wt} = 18,000$ g/mol [42]	14
Figure 2.6: relation between the average fiber diameter and Berry number, for different molecular weight A: $M_{wt} = 9500$ g/mol, B: $M_{wt} = 18,000$ g/mol, C: $M_{wt} = 40,500$ g/mol, D: $M_{wt} = 67,500$ g/mol, E: $M_{wt} = 93,500$ g/mol and F: $M_{wt} = 155,000$ g/mol [42].....	15
Figure 2.7: various morphologies noticed in the electrospun polymer solution for different M_{wt} . I: Beads, II: beaded fibers, III: complete fibers and IV: flat fibers [42].....	16
Figure 2.8: PVP nanofibers electrospun dissolved in different solutions (a) ethanol, (b) MC, and (c) DMF [51].....	17
Figure 2.9: Effect of changing mass ratio of ethanol/DMF on surface tension and viscosity [51].....	18
Figure 2.10: Effect of different values of voltage on morphology and fiber diameter distribution of PVA solution with concentration 7.4wt% ,collecting distance = 15cm, flow rate = 0.2 ml/h and Voltages values a=5; b=8; c=10; and d=13 kV [56]	20
Figure 2.11: Effect of changing flow rate on the morphologies of 20% PSF polymer dissolved in DMAC (N,N-dimethyl acetamide) at 10 kV. Flow rate values a = 0.40 and b=0.66 ml/h, respectively [60]	21
Figure 2.12: Effect of changing collecting distance on the morphologies of 20% PSF polymer dissolved in DMAC at 10 kV. At collecting distance= 10cm fiber diameter was 438 ± 72 nm and at 15cm fiber diameter was 368 ± 59 nm, respectively [60]	22
Figure 2.13: Different types of collector disc, drum, mandrel and plate collector respectively [66].....	22
Figure 2.14: Effect of changing humidity on surface morphology of PS : a) 25%, b) 31–38%, c) 40–45%, d) 50–59% [63].....	24

Figure 2.15: a) Generating aligned fibers by using magnetic field b) direction of magnetic field generated between two parallel permanent magnets [70]	26
Figure 2.16: External electric field [26].....	27
Figure 2.17: (a) Electrospinning from the free liquid surface using the rotating drum. (b) Different rotating electrodes design [73]	28
Figure 2.18: Bubble electrospinning [2].....	29
Figure 2.19: Different types of electrospinning needleless disc, ball, and spiral coil [61]..	29
Figure 2.20: Chain of sound response [80].....	30
Figure 2.21: The path of the power of a sound wave impinging upon an absorptive obstacle [88].....	33
Figure 2.22: Incident and reflected wave at the surface of testing material	35
Figure 2.23: Relation between Matching ratio (ϵ) and (σ) for different thickness [88]	37
Figure 2.24: Design characteristics of sound absorbers with a matching ratio $\epsilon = 2$ (dashed line) and $\epsilon = 6$ (dotted line) [88].....	38
Figure 2.25: Annoyance rating, showing rapid growth at low frequencies [79]	39
Figure 2.26: Experimental and prediction values of sound absorption coefficient for combining three porous laminated composite materials [93].....	40
Figure 2.27: a) Sketch of micro-perforated panel absorber (MPA) from with diameter d of the orifice, spacing b between orifice, thickness t of the panel and air cavity depth D between the panel and backing wall b) Sketch of set-up and corresponding result for absorption coefficient [94].....	41
Figure 2.28: Three types of Helmholtz.....	41
Figure 2.29: Sound absorption coefficient of silica fiber laminates (SF1-4) and GW [95]	42
Figure 2.30: Absorption coefficient of PVC nanofiber mat samples compared with two thickness of melamine foam 1, 2 inches [13]	43
Figure 2.31: Absorption coefficient of PVP nanofiber mat samples compared with two thickness of melamine foam 1, 2 inches [13]	43
Figure 2.32: measured sound absorption coefficient of the nanofiber membrane as a function of sound frequency [96].....	44
Figure 2.33: PAN nanofibers with different thickness for different electrospinning time 10, 30, 60 min respectively [8]	45

Figure 2.34: sound absorption coefficient for PAN membrane with various back cavities at a) 0mm b) 10mm c) 20mm [8].....	45
Figure 2.35: a) Drawing of sample form; b, c) sound absorption coefficient of the perforated panel with PAN nanofiber membrane [8].....	46
Figure 2.36: a) Drawing of sample form; b) sound absorption coefficient of BASF with nanofiber membrane c) sound absorption coefficient of fiberglass with nanofiber membrane [8].....	46
Figure 2.37: Absorption coefficient of NY6 nanofiber layer over a) foam b) kenaf c) flet d) with back cavity [97]	47
Figure 2.38: Sound absorption coefficient for collecting nanofibers at a distance a) 50mm b) 90mm [49]	48
Figure 2.39: PVA nanofiber structures after exposing to water vapor for different duration a) 0 sec b) 60 sec c) 120 sec d) immersed in water for 60 sec [59]	49
Figure 2.40: sound absorption coefficient of PVA membrane exposes to water vapor for different time.....	50
Figure 2.41: Relation between the conductivity of the single composite fibers and a different mass fraction of MWCNT [10].....	50
Figure 2.42 : the relation between electrical conductance and concentration of MWNT dissolved in PEO by wt% and upper scale measure the volume fraction of MWNTs [107]	51
Figure 2.43: Effect of adding the different percent of MWCNTs (0wt%, 1wt% , and 4wt%) to nanocomposite fibers on heat flow and heat derivative of nanofibers [103].....	52
Figure 2.44: Relation between thermal conductivity and temperature for epoxy before and after add 1wt% SWCNT[109]	52
Figure 3.1: a) Electrospinning lab setup b) Schematic lab setup.....	56
Figure 3.2: Schematic of Impedance tube	59
Figure 3.3:a) Impedance tube setup b) schematic of measuring Impedance and Absorption of Acoustical Materials [125]	59
Figure 3.4: Theoretical and measured reflection coefficient of unflanged open-end tube .	62
Figure 3.5: Lab view interface for acoustic measurement.....	63

Figure 4.1: Different samples of fibers morphology produced from electro-spinning at various levels of concentration (wt%), high voltage (KV), and flow rate (ml/h). *(rpm& collecting distance)	70
Figure 4.2: Plot of control effect for all process designs variables.....	71
Figure 4.3: Experimental vs. model results based on the first model.....	75
Figure 4.4: Effect of concentration (wt%) and flow rate on fiber diameter for the 1st mathematical model.....	75
Figure 4.5: Experimental vs. model results based on the second model	76
Figure 4.6: Effect of concentration (wt%) and flow rate on fiber diameter for the second mathematical model.....	77
Figure 5.1: Tensile stress- strain curve for PVA 9wt% with CNTs 5wt%	80
Figure 5.2: Tensile Strength of PVA Composites	81
Figure 5.3: Young's modulus of PVA Composites	82
Figure 5.4: Elongation break of PVA Composites	82
Figure 5.5: TGA profile of PVA (sold line), DTGA of PVA (dash line).....	84
Figure 5.6: DMA curves for two samples of PVC 12wt% FG 10wt%	85
Figure 5.7: Tensile Strength of PVC Composites.....	86
Figure 5.8: Young's modulus of PVC Composites	86
Figure 5.9: Elongation break of PVC Composites	87
Figure 5.10: TGA profile (green line) and DTGA (blue line) of PVC 12wt% CNTs 10wt%	88
Figure 5.11: DSC curve of PVC12wt% PS10wt% (1:3)	89
Figure 6.1: SEM of a)PVA 12wt% b) PVA 9wt%	90
Figure 6.2: SEM of PVA 10wt% with a)1.5 wt% b) 2.5 wt% C) 3.5 wt% d)5wt% of CNTs	91
Figure 6.3: SEM of a) PVA 9wt% CNTs 5wt% b) PVA 9wt% CNTs 10wt% c) PVA 12wt% CNTs 5wt% d) PVA 12wt% CNTs 10wt%	92
Figure 6.4: SEM of a) PVA 9wt% GN 5wt% b) PVA 9wt% GN 10wt% c) PVA 12wt% GN 5wt% d) PVA 12wt% GN 10wt%	93
Figure 6.5: SEM of PVC 12wt%	94
Figure 6.6: SEM of composite PVC/CNTs nanofiber a) 5wt% b) 10wt%	94

Figure 6.7: SEM of PVC/FG nanofibers	95
Figure 6.8: SEM of PS nanofiber left) 20wt% right) 10wt%	96
Figure 6.9: SEM of multi-layer of PVC12PS20PVC12 (side view)	96
Figure 6.10: SEM of fibers of a mixture solution of PVC 12wt% and PS 10wt% with different volume% A) 3:1 B) 1:1 C)1:3 of PVC and PS respectively.	97
Figure 6.11: SEM of fibers of a mixture solution of PVC 12wt% and PS 20wt% with volume% (3:1)	97
Figure 6.12: SEM of PVC/PS mat produced by coaxial needle	98
Figure 7.1: Sound absorption coefficient of PVC at 3cm back cavity (FFT and 1/3 octave plot).....	100
Figure 7.2: Sound absorption coefficient of a mixture solution of PVC& PS A (3:1) at 3cm back cavity	101
Figure 7.3: Sound absorption coefficient of a mixture solution of PVC& PS with different ratios A(3:1), B(1:1) C (1:3) at 3cm back cavity (1/3 octave plot)	102
Figure 7.4: Sound absorption coefficient of multilayer mat PVC12 - PS10 - PVC12 at 3cm back cavity	103
Figure 7.5: Sound absorption coefficient of multilayer mat PVC12-PS10-PVC12 at 5cm back cavity.....	103
Figure 7.6: Sound absorption coefficient of multilayer mats PVC12-PS10-PVC12 at 3 and 5cm back cavity (1/3 octave plot).....	104
Figure 7.7: Sound absorption coefficient of multilayer mat PVC12-PS20-PVC12 at 3cm back cavity (FFT and 1/3 octave plot).....	104
Figure 7.8: Sound absorption coefficient of PVC12wt% CNTs 5wt% at 3cm back cavity	105
Figure 7.9: Sound absorption coefficient of PVC12 wt% CNTs 10 wt% at 3cm back cavity	105
Figure 7.10: Sound absorption coefficient of PVC12 CNTs5 and PVC12 wt% CNTs 10 wt% at 3cm back cavity (1/3 octave plot).....	106
Figure 7.11: Sound absorption coefficient of PVC 12wt% and FG 5wt% at 3cm back cavity	107

Figure 7.12: Sound absorption coefficient of PVC 12wt% and FG 10wt% at 3cm back cavity	107
Figure 7.13: Sound absorption coefficient of PVC 12wt% and FG 20wt% at 3cm back cavity	107
Figure 7.14: Sound absorption coefficient of PVC 12wt% and FG 30wt% at 3cm back cavity	108
Figure 7.15: Sound absorption coefficient of PVC 12wt% with (5, 10, 20, 30wt%) FG at 3cm back cavity (1/3 octave plot).....	108
Figure 7.16: Sound absorption coefficient of four composite samples of PVC 12% and FG with 2cm cavity and 2mm separation distance between each sample (FFT and 1/3 octave plot).....	109
Figure 7.17: Sound absorption coefficient of two composite attached PVC with CNTS mats at 3cm back cavity (FFT and 1/3 octave plot)	110
Figure 7.18: Sound absorption coefficient of two composite mats PVC/CNTs with 6mm gap and 3cm back cavity (1/3 octave plot).....	111
Figure 7.19: Sound absorption coefficient of PVA 9% at 3cm back cavity	111
Figure 7.20: Sound absorption coefficient of PVA 12% at 3cm back cavity	112
Figure 7.21: Sound absorption coefficient of PVA 9wt% and PVA 12wt% at 3cm back cavity (1/3 octave plot).....	112
Figure 7.22: Sound absorption coefficient of PVA 12wt% CNTs 5wt% at 3cm back cavity	113
Figure 7.23: Sound absorption coefficient of PVA 12wt% CNTs 10wt% at 3cm back cavity	113
Figure 7.24: Sound absorption coefficient of PVA 9wt% CNTs 5wt% at 3cm back cavity	113
Figure 7.25: Sound absorption coefficient of PVA 9wt% CNTs 10wt% at 3cm back cavity	114
Figure 7.26: Sound absorption coefficient of PVA 12wt%CNTs 5wt%, PVA 12wt%CNTs 10wt%, PVA 9wt% CNTs 5wt%, PVA 9wt%CNTs 10wt% at 3cm back cavity (1/3 octave plot).....	114

Figure 7.27: Sound absorption coefficient of composite mat PVA12wt% and GN 5wt% at 3cm back cavity	115
Figure 7.28: Sound absorption coefficient of composite mat PVA12wt% and GN 10wt% at 3cm back cavity	115
Figure 7.29: Sound absorption coefficient of composite mat PVA9wt% and GN 5wt% at 3cm back cavity	115
Figure 7.30: Sound absorption coefficient of composite mat PVA9wt% and GN 10wt% at 3cm back cavity	116
Figure 7.31: Sound absorption coefficient of PVA 12wt% GN 5wt%, PVA 12wt% GN 10wt%, PVA 9wt% GN 5wt%, PVA 9wt% GN 10wt% at 3cm back cavity (1/3 octave plot)	116
Figure 7.32: Sound absorption coefficient of composite mat PVA 9wt% WS 5wt% at 3cm back cavity	117
Figure 7.33: Sound absorption coefficient of composite mat PVA 9wt% WS 10wt% at 3cm back cavity	117
Figure 7.34: Sound absorption coefficient of composite mat PVA9wt% WS 20% with 3cm back cavity	117
Figure 7.35: Sound absorption coefficient of composite mat PVA 9wt% with (5, 10, 20wt %) WS at 3cm back cavity.....	118
Figure 7.36: Sound absorption coefficient of two samples of PVA 9wt% CNTs 5wt% no air gap and 3cm cavity (FFT and 1/3 octave plot)	119
Figure 7.37: Sound absorption coefficient of two composite mats of PVA/CNTs with 2mm air gap and 3cm back cavity	120
Figure 7.38: Sound absorption coefficient of two composite mats of PVA/CNTs with 5mm air gap and 3cm back cavity	121
Figure 7.39: Sound absorption coefficient of two composite mats of PVA/ CNTs with 2mm and 5mm air gap and 3cm back cavity (1/3 octave plot).....	121
Figure 7.40: Sound absorption coefficient of two composite mats PVA/ GN with 2mm air gap and 3cm back cavity.....	122
Figure 7.41: Sound absorption coefficient of two composite mats PVA/GN with 7mm air gap and 3cm back cavity.....	122

Figure 7.42: Sound absorption coefficient of two composite mats of PVA/GN with 2mm and 7mm air gap and 3cm back cavity (1/3 octave plot).....	123
Figure 7.43: Sound absorption coefficient of four composite mats and air gaps (PVA9GN5-2mm PVA9 GN10- 1mm- PVA12GN5-2mm- PVA12GN10) at 3cm back cavity (FFT and 1/3 octave plot)	124
Figure 7.44: Sound absorption coefficient of 4 composite mats and air gaps (PVA12GN5-2mm- PVA12GN10 -1mm- PVA9GN5-2mm- PVA9GN10) and 3cm back cavity (FFT and 1/3 octave plot)	125
Figure 7.45: Sound absorption coefficient of a multi-layer PVA12 PS10PVA12 without back cavity.....	126
Figure 7.46: Sound absorption coefficient of one mat consists layers of PVA 12wt% PS10wt% PVA12wt% respectively at 3cm back cavity	126
Figure 7.47: Sound absorption coefficient of one mat consists layers of PVA 12wt% PS10wt% PVA12wt% respectively at 0cm and 3cm back cavity (1/3 octave plot).....	126
Figure 7.48: Sound absorption coefficient of one mat consists layers of PVA 9wt% PS 10wt% PVA 9wt% respectively at 3cm back cavity	127
Figure 7.49: Sound absorption coefficient of one mat consists layers of PVA 9wt% PS20wt%PVA9wt% respectively at 3cm back cavity	127
Figure 7.50: Sound absorption coefficient of mats PVA9PS10PVA9 and PVA9PS20PVA9 respectively at 3cm back cavity (1/3 octave plot).....	128
Figure 7.51: Sound absorption coefficient of two multilayer PVA9PS20PVA9 with 3mm gap PVA12PS20PVA12 at 5mm back cavity.....	128
Figure 7.52: Sound absorption coefficient of two multi-layers PVA9PS20PVA9 with 3mm gap PVA12PS20PVA12 at 3cm back cavity	129
Figure 7.53: Sound absorption coefficient of two multilayer PVA9PS20PVA9 with 3mm gap PVA12PS20PVA12 at 5mm and 3cm back cavity(1/3 octave plot)	129
Figure 7.54: Sound absorption coefficient of PVA9PS20PVA9- 3mm- PVA12PS10PVA12- 5mm- PVC12PS20PVC12- 2mm- PVC12PS10PVC12 with 2mm cavity.....	130
Figure 7.55: Sound absorption coefficient multi-layer mats of PVA9PS20PVA9- 3mm- PVA12 PS10pvA12- 5mm- PVC12PS20PVC12- 2mm- PVC12PS10PVC12 with 1cm back cavity.....	130

Figure 7.56: Sound absorption coefficient multi-layer mats of PVA9PS20PVA9- 3mm- PVA12 PS10PVA12- 5mm- PVC12PS20PVC12- 2mm- PVC12PS10PVC12 with 2cm back cavity.....	130
Figure 7.57: Sound absorption coefficient of PVA9PS20PVA9- 3mm- PVA12PS10PVA12- 5mm PVC12PS20PVC12- 2mm- PVC12PS10PVC12 with 2.5cm cavity.....	131
Figure 7.58: Sound absorption coefficient of PVA9PS20PVA9- 3mm- PVA12PS10PVA12- 5mm-PVC12PS20PVC12- 2mm- PVC12PS10PVC12 at 2mm, 1cm, 2cm, 2.5cm cavity (1/3 octave plot)	131
Figure 7.59: Sound absorption coefficient of PVA mats with graded structure a) PVA9% with different flow rates b) mat from PVA 7, 9, 12wt% with fixed flow rate.....	132
Figure 7.60: Sound absorption coefficient of PVA mats electrospun for different time 10.5h, 7h, and 3.5h.....	133
Figure 7.61: Sound absorption coefficient of DD2.....	134
Figure 7.62: Sound absorption coefficient of DD2 with PVA nanofiber membrane at front	134
Figure 7.63: Sound absorption coefficient of DD2 with two PVA nanofiber membranes at both sides	134
Figure 7.64: Sound absorption coefficient of (DD2), (PVA-DD2), and (PVA-DD2- PVA)	135
Figure 7.65: Sound absorption coefficient of DD2 with PVA12-PS20-PVA12 nanofiber membrane at front (FFT and 1/3 octave plot).....	136

Lists of abbreviations and symbols

Abbreviations

ANOVA	Analysis of variance
CNTs	Carbone nanotube
DMA	Dynamic mechanical analysis
DSC	Differential scanning calorimeters
DOF	Degree of freedom
DW	Distilled water
DMF	N,N-dimethyl formalidede
DMAC	N,N- dimethylacetamide
GF	Fiberglass
GW	Fiberglass wool
GN	Graphene
h	Hour
KH ₂ PO ₄	Monopotassium phosphate
MWCNTs	Multiwall carbon nanotubes
MES	Magnetic electrospinning
MC	Methylene chloride
NaH ₂ PO ₄	Monosodium phosphate
MPA	Micro-perforated panel absorber
NaCl	Sodium chloride
NSF	National science foundation
NY6	Nylon
PVA	Polyvinyl alcohol
PS	Polystyrene
PVC	Polyvinylchloride
PTT	Poly(trimethylene terephthalate)
PVP	Polyvinyl-pyrrolidone
PSF	Polysulfone fibers
PA6	Polyamide
PAN	Polyacrylonitrile
PEO	Polyethylene oxide
rpm	Revolution per minute
RSM	Response surface methodology
SWCNT	Single wall carbon nanotube
SEM	Scanning electron microscopy
SWCNTs	Single wall carbon nanotube
S/N	Signal to noise ratio
SS	Statistical sum

SDS	Sodium dodecyl sulfate
SF	Silica fiber
TGA	Thermogravimetric analyzer
TEM	Transmission electron microscopy
WS	Wollastonite
WAXD	Wide-angle x-ray diffraction

Symbols

η	Intrinsic viscosity
E	Young's modulus
C	Solution concentration
C_i	Initial concentration
C_f	Final concentration
c	Speed of sound (m/s)
D	Diameter of fiber
d	Average diameter
F_c	Cut off frequency
f	Sound frequency
H_{12}	Transfer function between two microphone positions
H_I	transfer function of the incident wave
H_R	Ttransfer function of the reflected wave
H	Distance between needle tip and collector
I_r	Intensity of reflected sound
I_i	Intensity of incident sound
k_o	Wavenumber
L	Length of the capillary tube
p	Acoustic pressure
p_i	Pressure of the incident sound wave
p_r	Pressure of the reflected sound wave
P_i	Pressure amplitude of the incident sound wave
R	Sound reflection coefficient
ε	The matching ratio
S_{12}	Cross spectrum between the two microphones
S	Area of a neck
t	Time
v	Medium particle velocity
V	Volume

x	Distance from the material surface
Z	Acoustic impedance
Z_c	Characteristic impedance
Z'	Real part of acoustic impedance
Z''	Imaginary part of acoustic impedance
ρ_0	Air density (kg/m ³)
σ	Air flow resistivity (rayl/m)
σ_i	Standard deviation
ω	Angular frequency
α_t	Tortuosity
α	Sound absorption coefficient
γ	Surface tension of the fluid
μ	Viscosity
μ_i	Replications average
ε	Matching ratio
ε_b	Elongation at break
λ	Wavelength
ϕ	Porosity
σ_t	Tensile strength

Chapter 1: Introduction

1.1 Introduction

Nanotechnology is a promising research area due to its potential applications in many fields. The term nanotechnology was used as early as 1974 [1] to define the machining of tiny things and small-scale engineering. This term covers the activities related to manufacturing and engineering of nanoscale objects. Nanotechnology can be defined as a planned usage of methods of nano-measurement and nano-manipulation to make nanoscale objects with unique properties. There has been an exponential growth of publications on nanotechnology in the last two decades. More than 200 research centers worldwide have been established and are currently involved in research of nanotechnology and molecular manufacturing. The societal impact of the developments in nanotechnology in the 21st century is expected to surpass the effects of the industrial and information technology revolutions. A USA Presidential initiative in January 2000 named nanotechnology one of the U.S. national research priorities [2].

Nanofibers have the high specific surface area, high aspect ratio, and other useful properties [3]. The unique properties of nanofibers make them attractive for use in many applications such as medical products, personal care, drug industry, fuel cells, battery separators, energy storage, capacitors, transistors, filtration, and sound absorbing materials. From the literature, nanofibers are fibers that have diameters of one micron or less, but according to the National Science Foundation (NSF), nanofibers have diameters from 1 to 100 nanometers (nm) [2–5].

Electrospinning has proven to be an efficient and direct method for fabrication of nanofibers from many materials including polymers, ceramics, and composites [6, 7]. The fibers produced using electrospinning have diameters in the range of micro to nanometer. Electrospinning offers other unique possibilities such as adjustable porosity in electrospun fibers, hollow interiors, addition of fillers to nanofibers, the combination of several types of polymers in one nonwoven mat, and the flexibility to spin into a variety of shapes and sizes.

Some researchers have used the electrospinning process for producing sound absorbing materials [8]. They used the electrospun mats to improve the conventional sound

absorbing materials and obtained good results for absorption of sound at mid and high frequency ranges. However, they did not obtain a good sound absorption at low frequency, and they did not study the effect of fibers' morphology on the sound absorption. The mechanical and thermal properties of the electrospun fibers are improved by adding fillers such as carbon nanotubes (CNTs), graphene (GN), and wollastonite (WS) [9–11].

1.2 Motivation

Noise reduction is considered an important criterion when designing devices or equipment. It is important to design quiet spaces for work, leisure, and even for entertainment. Prevention of low-frequency noise is a challenge in industrial commercial, and residential buildings, and automotive and transportation industries. Although the traditional sound absorbing materials show good performance in absorbing high-frequency noise, they are not able to efficiently absorb lower frequencies. For instance, a foam sheet 8.5cm thick is able to dampen 1000Hz noise, while a thickness of 85cm is required to dampen 100Hz noise by the same factor. This shows that the materials needed for dampening low-frequency noise occupy large volumes, which may not be available in some applications, or may be very costly and hence become an obstacle for the application. Therefore, it is important to investigate and innovate solutions to noise problems that can be implemented in smaller volumes. The use of the electrospun nanofibers promises to yield workable and innovative solutions for noise reduction and mitigation in several applications.

Nanofibers present a large surface area to volume ratio, therefore, in a given volume, a large surface area is available for interaction between the sound waves and the fibrous sound absorbing material. This implies that the thickness of absorbing materials can be decreased to save space. Nanofiber membranes used in sound absorption are very thin and subsequently very fragile. Thus, the addition of fillers is preferred to improve the mechanical properties.

Few studies have investigated the types of fibrous polymers that can be effective in sound absorption [12, 13]. Such studies for electrospun fibers are rare, and the materials studied have mostly demonstrated acoustic dampening in mid and high-frequency range. A large

number of studies have to be undertaken before the advantages offered by electrospun nanofibers can be fully utilized in the fields of noise reduction, which constituted the motivation for performing this work.

1.3 Objective

The objective of this work was to develop innovative sound absorbing nanofiber materials that have a low thickness and are able to absorb sound using the electrospinning process. The sound absorbing nanofibers were also modified by the addition of fillers such as CNTs, GN, WS, and fiberglass (FG) to enhance both acoustic and mechanical properties. The focus was to find materials that can be electrospun and exhibit good acoustic absorption properties, especially in the low and mid frequency ranges (i.e. less than 2000Hz).

1.4 Methodology

A number of polymeric materials are selected for evaluation, which include two materials that are conventionally used for sound absorption and one biodegradable material in order to improve sustainable solutions. A number of reinforcements were also used. The polymers were dissolved in appropriate solvent at slightly elevated temperatures using a magnetic stirrer. When reinforcing materials were used, sonication was carried out to help in the dispersion. These solutions were processed using electrospinning, and the fibers were collected on a rotating drum in the form of mats. Parametric studies were carried out to find optimum conditions for fiber fabrication, and the interactions between different parameters were evaluated. For acoustic testing, a specimen with a diameter of 10cm was used, and other parts were used for characterization and testing using Scanning Electron Microscopy (SEM), Dynamic Mechanical Analyzer (DMA), Differential Scanning Calorimetry (DSC), and Thermogravimetric Analyzer (TGA).

1.5 Main thesis contributions

- The effects of five processing parameters on the PVA nanofibers production was estimated using a developed statistical model in the field of interest. In addition, the signal to noise ratio (S/N) was implemented to predict the effects of the noise variables.

- Adding different types of fillers such as CNTs, GN, and WS improved the dampening of sound waves.
- The multi-layered nanofiber mats consist of two different polymers with different fiber diameters, enhance the dampening efficiency by causing the sound waves travel in different medium.
- The existence of air gaps between the several mats combination increases the sound absorption in the low frequency, and increasing the air gaps shifted the sound absorption to the lower frequency.

1.6 Thesis outline

This thesis contains eight chapters. Chapter 1 introduces nanotechnology in general, the electrospinning process, and some of their applications. Also, it demonstrates the noise problem especially in the low frequency and the solutions for these problem using nanofibers. The motivation, main contribution, and thesis outline are found in this chapter.

Chapter 2 describes the different methods for producing nanofibers then discusses the fundamental basics and various approaches of the electrospinning process. In addition, the chapter discusses the noise problems and the important issues related to the measuring of sound reflection and absorption coefficient, then it reviews previous studies, which used nanofiber membranes as a sound absorption material using fillers to improve the membrane properties.

Chapter 3 provides the details of the experimental setup and explanation for apparatus used in this work. In addition, it includes a list of all materials used in sample production and the methods of sample preparation.

Chapter 4 presents a developed mathematical model for producing PVA nanofibers with a specific diameter by controlling the process parameters. This model contains the five main parameters that affect the production process (i.e. concentration, flow rate, high voltage, collecting distance, and rotating speed).

Chapter 5 reports the mechanical and thermal properties of all the samples used in this work and discusses the effect of adding fillers to the polymer matrices.

Chapter 6 shows the morphological properties of the samples and explains the effect of concentrations and addition of fillers on fibers' diameter.

Chapter 7 investigates the sound properties of the entire samples used in this work and discusses the effect of the back cavity and air gaps between these samples in improving the sound absorption. In addition, it provides many trials of combinations between several samples and their effects in the increase of sound absorption.

Chapter 8 summarizes the major contribution of this work and recommendations for future work.

Chapter 2: Background and literature review

2.1 Introduction

Polymeric nanofibers have gained much attention in the recent era for their promising application in the field of clinical products, drug development products, fuel cells, capacitors, transistors, filtration, battery separators, energy storage and sound absorbing materials. According to their potential application in various fields many of the researchers focus on the development and improvement of many fabrication methods for these fibers during the last two decades.

2.2 Nanofiber production methods

There are several methods that can be used for the fabrication of nanofibers such as drawing, phase separation, template synthesis, self-assembly and electrospinning [14]. Most of these methods have some drawbacks like long fabrication time, low yield production, and it is hard to obtain fibers with continuance. The most commonly used methods are described below.

2.2.1 Drawing

By using drawing technique, long single nanofibers can be fabricated and this can be used only for viscoelastic materials [15]. The drawing process mainly depends on the viscosity of the droplet, which changes over time due to the evaporation of the solvent. This affects the fiber diameter and prevents the continuous drawing of fibers. Ondarcuhu et al.[4] described the method for getting fibers from sodium citrate solution in chloric acid by using a micropipette. In their study, they dipped a sharp tip of an iron-silica rod into the polymer solution several times in order to get a consistency in the droplet as shown in Figure 2.1. Finally, a fiber appears between the tip and the polymer; then the fiber is pulled from its tip end into another liquid solution. So, it is possible to produce a micro and nanofiber using this direct drawing method.

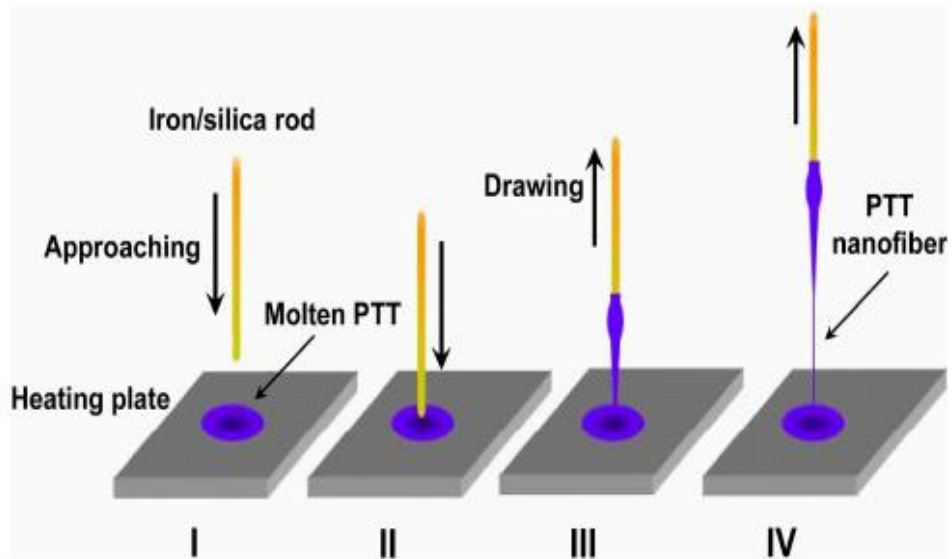


Figure 2.1: Drawing a molten of poly(trimethylene terephthalate) (PTT) [15]

2.2.2 Template synthesis

Template synthesis is a method of the production of micro- and nanostructures by using nano-scaled diameter membranes. Nanomaterials of the desired size can be fabricated using appropriate pore diameter of the template. Membranes have cylindrical pores or channels and each of them has a uniform diameter throughout the membrane [17, 18]. The polymer is forced to come out through the porous membrane with the desired diameter by using water pressure from one side. The extruded fibers exit from the other side, which contains a solidifying solution as shown in Figure 2.2.

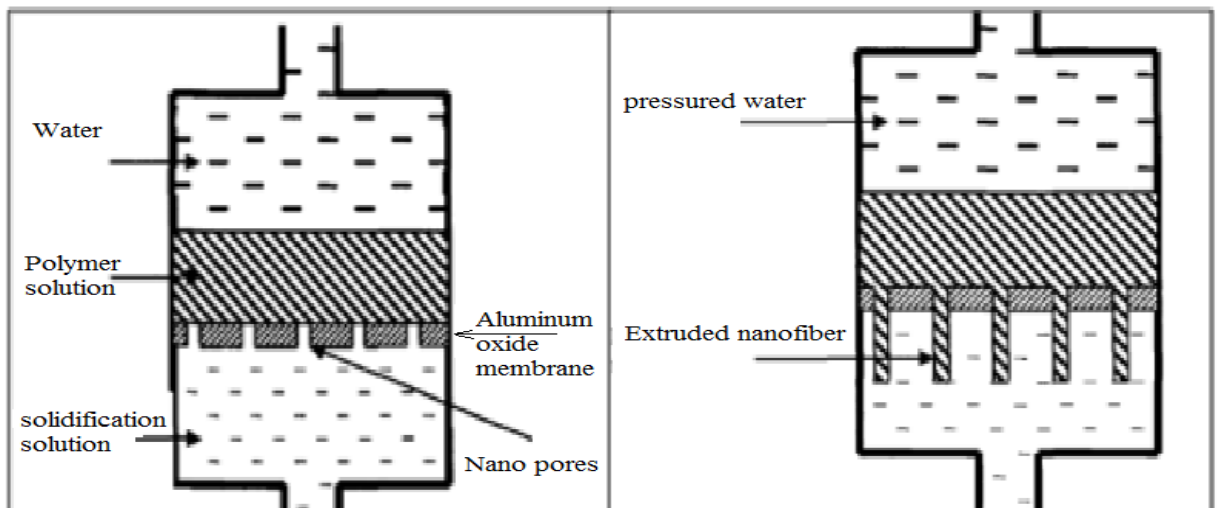


Figure 2.2: Templates of nanofiber [17]

2.2.3 Phase separation

Nanofibers, nanofiber matrices, porous 3-D scaffolds, and highly porous foams can be fabricated by phase separation technique. Generally, after dissolving the polymer in a solvent, the mixture is made to form a gel state. This procedure involves five steps; dissolution of the polymer, gelation, extraction of solvent, freezing and freeze-drying under vacuum [18,19].

2.2.4 Self-assembly

In the self-assembly technique, nanofibers can be derived from already existing single smaller molecules. These individual molecules organize themselves into desired nano-scale structures. It means that they act as basic building blocks. The idea behind the self-assembly method is that intermolecular forces between those tiny molecules give the overall shape of the resulting nanofibers [18, 20].

2.2.5 Electrospinning

Nano or microfibers can be produced by using ‘Electrospinning’ technique. This technique, for fiber production, electrostatic forces accelerate and stretch a polymeric solution towards an electrode on which nano or microfibers are deposited. This process is discussed in detail in the next section.

2.3 Electrospinning

Electrospinning is a novel approach for fiber production, which has attracted enormous attention in the last two decades. The fibers produced using electrospinning have diameters in the range of micro to nanometer. Electrospinning offers other unique possibilities such as adjustable porosity in electrospun fibers, hollow interiors, addition of fillers to nanofibers, combining different types of polymers in one nonwoven mat, and the flexibility to spin into a variety of shapes and sizes. Another major advantage of this method is the vast variety of materials that can be used to produce the nanofibers.

In addition, electrospinning is one of the fastest, least expensive, and most direct ways to obtain nanomaterials [18, 21]. Compared to the fibers created from conventional melt spinning, dry spinning, or wet spinning, they possess several unique properties as described earlier, and therefore, they can be used in numerous applications of diverse fields.

In this method, an electrical charge is applied to a jet of the polymer solution, which accelerates in a high potential electrical field to produce fibers from micro-scale to nano-scale. Figure 2.3 shows an electrospinning setup, comprising of the three basic components: a source of high voltage, a needle or pipette with a small diameter, and a collection screen. The polymer solution or polymer melt extrudes from the syringe with a controlled constant flow rate using a precision pump [22, 23]. The high voltage source is connected to the syringe needle and applies an electrical charge on the jet of material flowing through it. When the electrical field intensity increases, the surface of fluid at the needle tip elongates and takes a conical shape known as the Taylor cone, which shown in Figure 2.4 [18, 24].

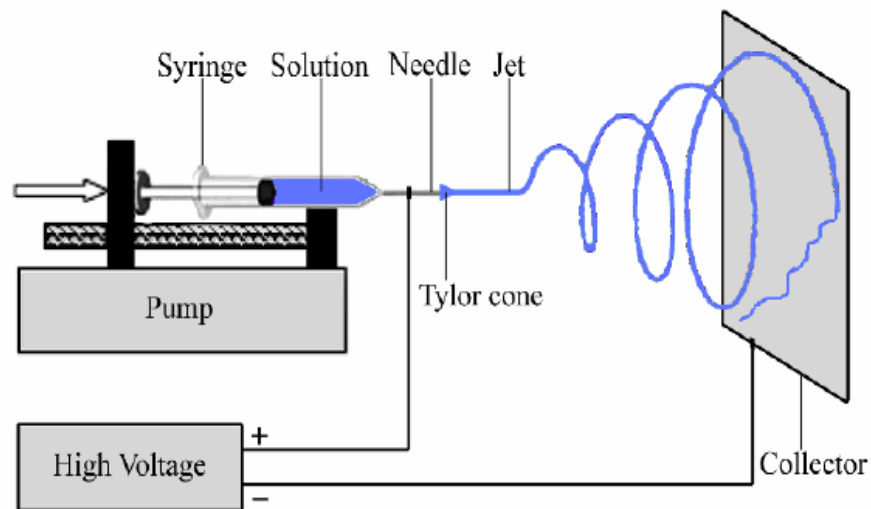


Figure 2.3: electrospinning setup[24]

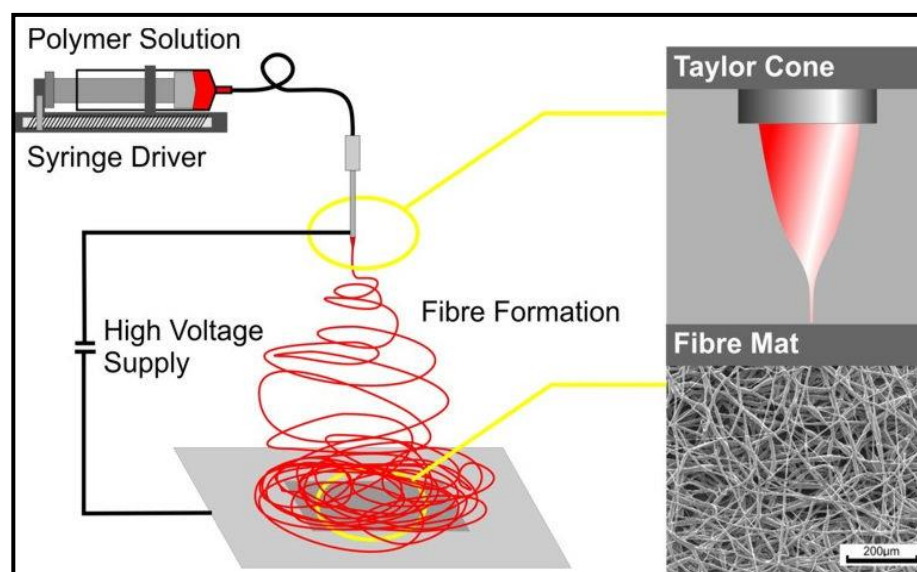


Figure 2.4: Taylor cone [23]

By increasing the electrical field, the repulsive electrostatic force overcomes the surface tension and the charged jet comes out from the vertex of the Taylor cone. The charged solution jet stretches as it accelerates towards the opposite electrode, and in addition, the similar charges on it repel each other causing further stretch. The flow instabilities induce a whipping motion and elongation process, which create longer and thinner fibers [25]. Meanwhile, the solvent in the jet evaporates, the polymer solidify into fibers before reaching the collector [26]. Frequently the positive electrode is connected to the polymer solution while the negative one is connected to the collector, as indicated in Figure 2.3.

The fiber morphology is affected by several factors, such as aerodynamic, gravitational, inertial, and rheological [6]. In addition, the charges tensile force exists in the axial direction of the polymer flow and is caused by induced charges that are attracted towards the electrode and the repulsion between the similar charges, which are responsible for the fiber spinning [28 –30].

After the discovery of electricity, there were several attempts to produce artificial thread by using an electric field, but they were not successful until Formhals [31,32] invented his first apparatus in 1934. The major problem faced by early researchers was collecting and drying the fibers produced as they would not properly dry and stick together due to incomplete solvent evaporation. Formhals improved his device to overcome this problem by increasing the distance between the nozzle tip and the collector to increase the time for solvent evaporation. In 1940, Formhals developed another device to produce the fibers from many polymers by using a moving base substrate [28].

In 1952, Vonnegut et al. [32] developed electrical atomization device, which used the flow of highly electrified uniform droplets with a diameter of 0.1mm using a capillary tube has a diameter of a few tenths of a millimeter. They filled the tube with a solution and then inserted an electric wire connected to a variable high voltage source 5-10KV. In 1955, Drozin [32] studied the dispersion of some liquids into aerosol under specific conditions by using Vonnegut's setup. He obtained photographs for different stages of dispersion.

Taylor [34, 35] in 1960 investigated the fundamental process of jet formation. Later in 1969, Taylor studied the shape of polymer droplets at the needle tip, which appeared after

applying the electric field. His studies showed that the droplets take a conical shape and that the jet starts to eject from the tip of the cone. After that, other researchers referred to this conical shape as the 'Taylor cone'. Taylor electrospun different viscous fluids and he claimed that the angle of 49.3° achieved the balance of the surface tension of polymer solution with electrostatic forces. Now, it is accepted generally, this cone is the place where the jet starts to form and fibers begin to get their extensional velocity gradients in the fiber forming process.

Some recent researches have indicated that Taylor cone angle is valid for only a specific solution. Cone angles of 33.5° have been reached both experimentally and theoretically with the initiation of a critical electric field. The electrospinning process is initiated when mutual repulsive electrostatic forces overcome surface tension and a charged jet of polymer solution or melt is ejected from the Taylor cone at the needle tip. Polymer jet travels through a short stable region then suddenly gain a chaotic motion as it enters an unstable region. The solution jet evaporates or solidifies before fibers reach the collector. Frequently the positive electrode is connected to the polymer solution and the negative connected to the collector, as indicated in Figure 2.3 [35].

As mentioned above, a straight jet is formed at the vertex of the Taylor cone after overcoming the surface tension. The straight jet keeps its stability up to few centimeters and then followed by an unstable region, which can be described by three models. The first is the Rayleigh instability that occurs at low charge density, and it yields axisymmetric instability. The second is axisymmetric instability and occurs at high electric field. The third causes whipping instability, which is nonaxisymmetric and occurs due to the alterations in the bipolar component of the charge's distributions. These bending instabilities are responsible for elongation of the polymer jet and allow it to bend and stretch. Sometimes a high repulsive force carried by the electrical charges is responsible for the formation of multi-jet from a single polymer fluid [39]. This is because radical forces from electrically charged polymer jets overcome coherent forces of the jet. Each polymer jet then separates into multiple smaller jets before reaching the collector. The jets formed have equal fiber diameter and in each splayed jet, the electrical charge is distributed uniformly. This process causes the formed fibers to be very thin. Fibers are generally collected as non-woven filaments.

Simons [36] invented his electrospinning apparatus in 1966. He immersed a positive electrode into a polymer solution and connected a negative one to a belt, where the fibers were collected. He claimed that as the viscosity of solution decreased the fibers became thinner and shorter. In 1971, Baumgarten electrospun acrylic fibers using an infusion pump instead of a capillary tube to get a constant flow rate. He obtained fibers with diameters in the range of 0.05–1.1 microns [28].

Hayati et al. [29] investigated the parameters that affect the fiber stability and atomization, such as electric fields and experimental conditions. They concluded that liquid conductivity has a high influence on the electrostatic disturbance of the liquid surface. They also observed that for fluids with high conductivity values, when the applied voltage was increased, the instability increased and larger whipping action appeared in different directions. On the other hand, they found that stable jets were produced from semiconducting solutions.

Wannatong et al. [37] claimed that there are six forces affecting fiber formation. They concluded that these forces as follow: (1) gravitational or body force, (2) electrostatic force, acting during electrospinning from the needle tip to collector, (3) Coulombic force is responsible for the charged polymer jet stretching, (4) viscoelastic force responsible for prohibiting a polymer jet stretching, (5) surface tension has the same effect as the viscoelastic force and (6) drag force due to friction between the polymer jet and the air in jet pass.

Many researchers determine the relationship between fibers structures and process parameters. They have studied the morphology of nanofibers produced using electrospinning. The most common equipment for morphology examination are Wide-angle X-ray diffraction (WAXD), Scanning Electron Microscopy (SEM), Transmission Electron Microscopy (TEM), and Differential Scanning Calorimetry (DSC).

2.4 Factors affecting electrospinning process

The parameters that affect electrospinning process can be grouped into three categories as follows: solution parameters, process parameters, and ambient parameters. Each set of parameters has effects on the fibers morphology. By controlling, these parameters, the morphology and the diameter of electrospun fibers can be regulated.

2.4.1 Solution parameters

These parameters have dominant role on the morphology of the fibers produced. The studies on them are described below:

2.4.1.1 Concentration

Concentration has a vital effect on the formation morphology of the fiber. As concentration decreases, the micro or nanoparticles turn into an electrospray, rather than fiber, as a result of the low viscosity of the solution. As concentration increases, the formation of beads decreases, and fibers begin to appear until a suitable concentration for uniform fibers production is obtained [40, 41]. At higher concentrations, ribbon fibers start to appear. Figure 2.5 [40] shows the effects of changing concentration of PVA solution from low value of 7wt% which results in a disjointed spray, fibers and beads at 16wt%, and uniform fibers at a concentration of 22wt%. Further increase in the wt% of PVA leads to the formation of ribbon-like morphology.

At any molecular weight, there are two critical concentrations at which electrospun fibers can be formed: the initial concentration (C_i) and the final concentration (C_f). These two concentrations are known as the structural transition points, at which the beads-only to beads free fibers transition takes place. At lower initial concentrations, only beads can be noticed, due to the scanty chain entanglement in solution. Above C_i , the mixture of beads and fibers appears. As concentration comes to C_f the full fibers are noticed. Koski et al. [41] claim that with further high concentration levels, the fiber diameter and interfiber spacing increase. After this point, the fiber profile slowly converts from circular to flat.

2.4.1.2 Molecular weight

Electrospun fibers morphology is also affected by the molecular weight of the polymer used. Molecular weight demonstrates the entanglement of the polymer chains in the solution. For different molecular weights of the same polymer and concentration, the

beads appear in low concentration while circle smooth fibers appear as the molecular weight increases. Then flat ribbon fibers form with further raise of the molecular weight [41].

Berry number $[\eta]C$ which is the product of intrinsic viscosity $[\eta]$ and concentration C plays a major role in electrospinning of fibers. When $[\eta]C < 4$, the fibrous structure could not be stabilized and when $[\eta]C > 9$ flat fiber begin to form as shown in Figure 2.6. Mark-Houwink [42] obtained the relationship that connects the molecular weight with intrinsic viscosity shown below.

$$[\eta] = K (M_{wt})^a \quad (2.1)$$

Where 'K' and 'a' depend on the particular polymer-solvent system

The diameter of fiber formed could be obtained from the relation below [42].

$$D \text{ (nm)} = 18.6 ([\eta] C)^{1.11} \quad (2.2)$$

Demir et al. [43] claimed that there is a relation between fiber diameter and concentration where $D \propto C^3$.

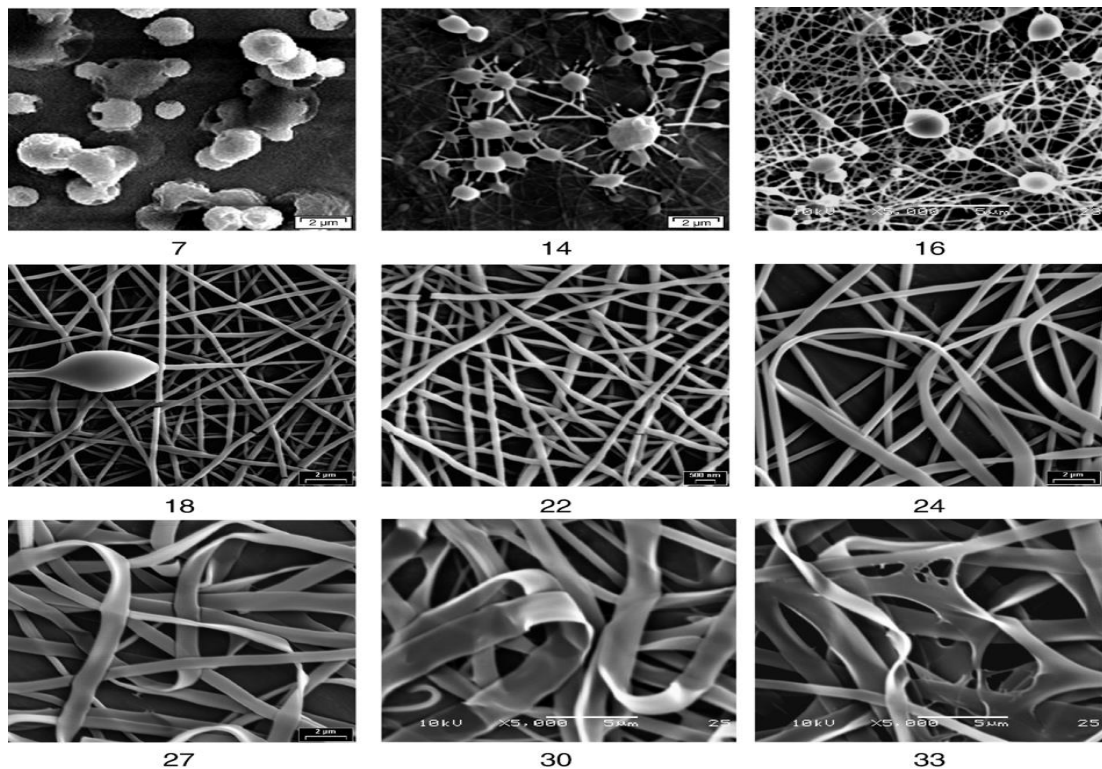


Figure 2.5: Morphology of PVA fiber with different concentration (wt%) at $M_{wt} = 18,000$ g/mol [42]

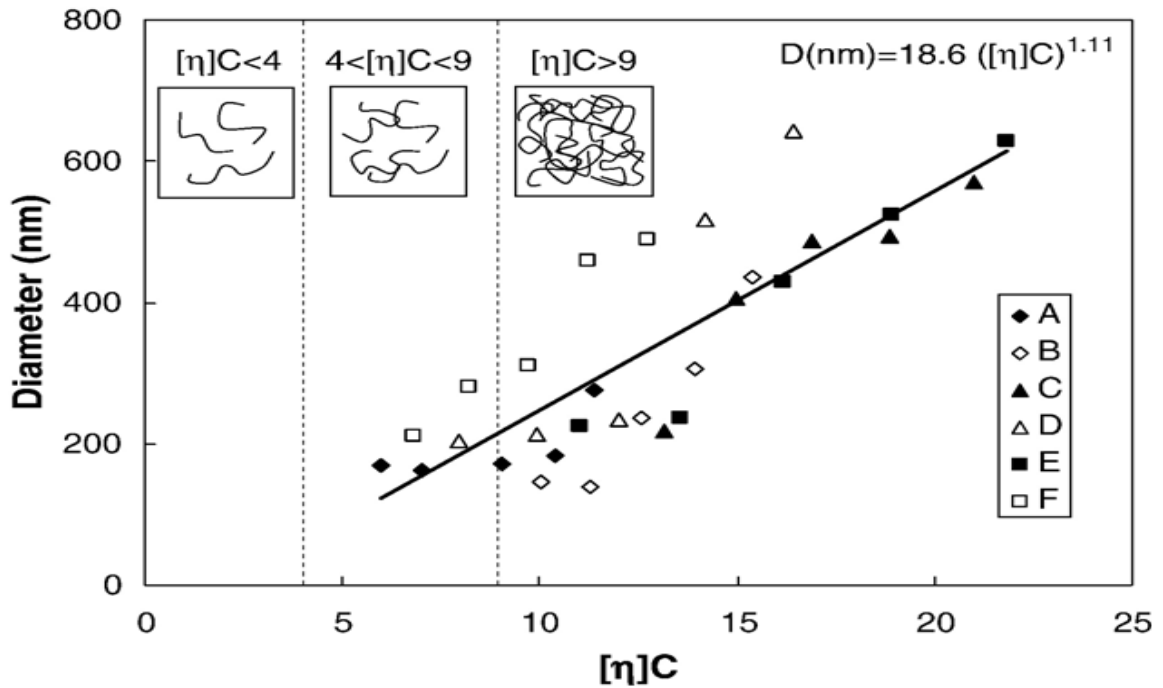


Figure 2.6: relation between the average fiber diameter and Berry number, for different molecular weight A: $M_{wt} = 9500$ g/mol, B: $M_{wt} = 18,000$ g/mol, C: $M_{wt} = 40,500$ g/mol, D: $M_{wt} = 67,500$ g/mol, E: $M_{wt} = 93,500$ g/mol and F: $M_{wt} = 155,000$ g/mol [42]

It is noticed that at very high molecular weight, the polymers tend to form ribbon even at low concentration [44]. However, McKee et al. [45] postulated that electrospinning process does not necessarily depend on the molecular weight when there is sufficient intermolecular interaction similar to the case of oligomers. They obtained oligomer sized of phospholipids fibers from lecithin solutions at a concentration over than 35%. Jing et al. [42] declared that there are limiting values of concentrations and molecular weights for obtaining electrospun fibers; and at lower than these values, only beads are obtained and at higher values ribbons are produced instead of fibers. They obtained a relation between molecular weight and concentration for PVA shown in Figure 2.7.

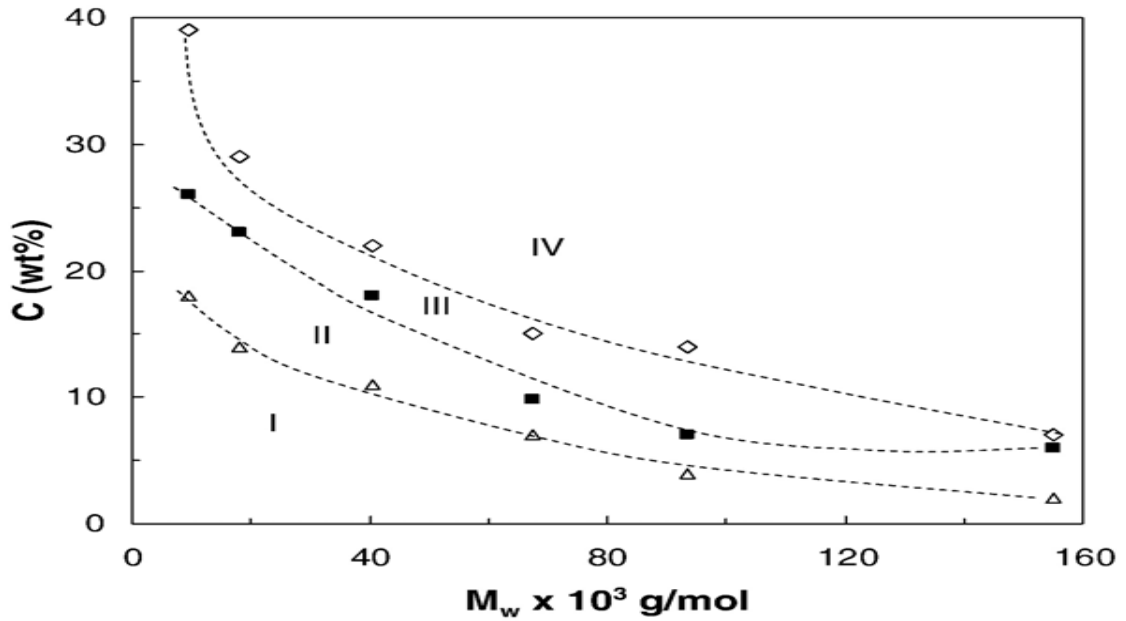


Figure 2.7: various morphologies noticed in the electrospun polymer solution for different M_{wt}. I: Beads, II: beaded fibers, III: complete fibers and IV: flat fibers [42].

2.4.1.3 Viscosity

The morphology of fiber depends on its viscosity. The average diameter of the fibers has an exponential relation with solution viscosity [48, 49].

$$D \text{ (nm)} = 88.7 + 0.804 e^{(0.00137\mu)} \quad (2.3)$$

Where D is the average diameter in nm and μ is the viscosity in cp.

The viscosity of a material is the measure of the resistance to flow. There are several parameters affecting solution viscosity like molecular weight, concentration, polymer chain entanglement and temperature. The viscosity of the solution will be greater when a polymer with a higher molecular weight is dissolved in its solvent [35]. It has been shown that very low viscosity solutions are not able to produce continuous and smooth fibers and it is hard to get fibers from very high viscosity solution due to the difficulty in the formation of the jet from the solution [46], [48]. Therefore, the suitable viscosity is required to get electrospun fibers. In general, the viscosity is adjusted by changing the polymer concentration. It is also important to recognize the relation between viscosity, concentration, and molecular weight of the polymer [49]. The temperature of the spinning solution can have an effect on the solution viscosity so that for high viscosity solutions, the heating spinneret can be used.

2.4.1.4 Surface tension

Surface tension is the force that is applied to the plane surface per unit length. The water drop falling in the air takes a spherical shape due to surface tension. Polymer drop at the tip of the needle takes the shape of a cone, called “Taylor cone”, in the presence of the applied electric field. When the value of electric field reaches a critical value, it overcomes the surface tension of the solution and a jet comes from the tip of Taylor cone [27]. High surface tension solutions produce beads during the electrospinning process. Yang et al. [50] investigated the effect of surface tension on the morphology of (polyvinyl-pyrrolidone) PVP fibers with many solvents such as ethanol, *N,N*-Dimethylformamide (DMF), and methylene chloride (MC). The effect of using different solvents on morphology is shown in Figure 2.8. The surface tensions changes if the solvent is changed for the same concentration of polymer [51]. They found that by reducing surface tension for fixed concentration, smooth fibers could be formed instead of beads. They also claimed that the surface tension of solution can be controlled by varying the mass ratio of a blend of solvents, like ethanol with DMF, as depicted in Figure 2.9. Zeng et al. [35] explained that, the surface tension of solution decreases by adding surfactant and less beads and smoother fibers are obtained. The surface tension has a great influence on determining the higher and lower values of the high voltage required for the electrospinning process [40], [52].

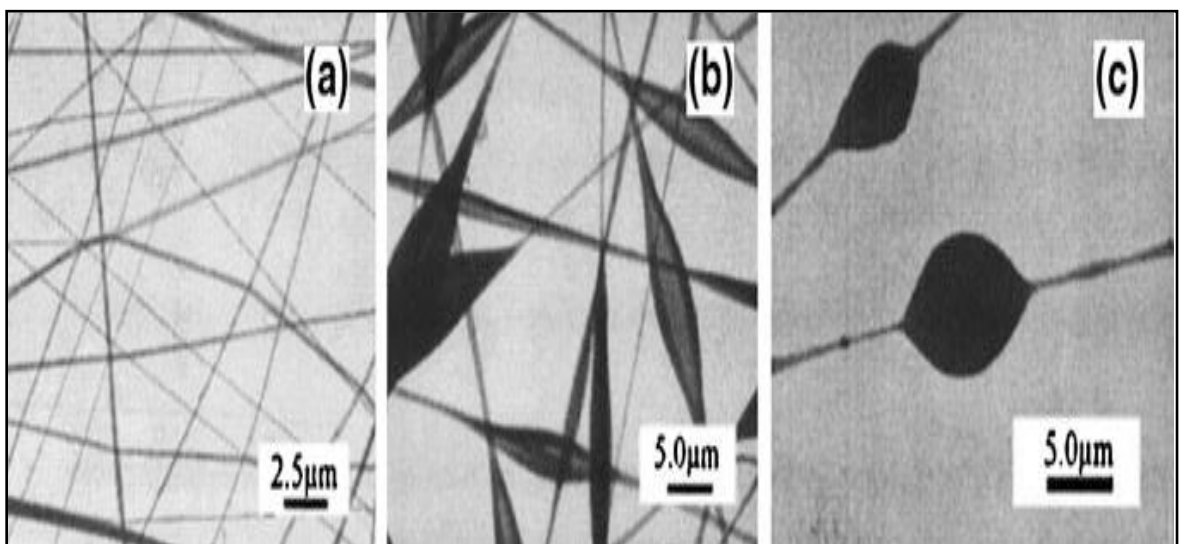


Figure 2.8: PVP nanofibers electrospun dissolved in different solutions (a) ethanol, (b) MC, and (c) DMF [51]

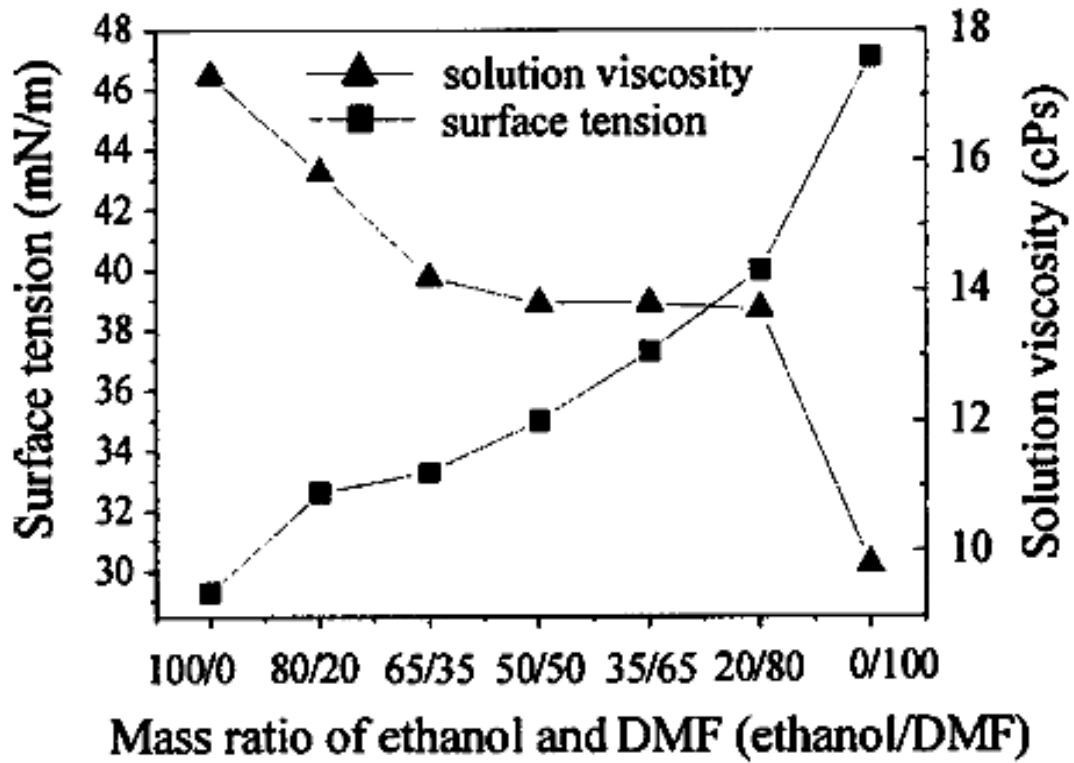


Figure 2.9: Effect of changing mass ratio of ethanol/DMF on surface tension and viscosity [51]

2.4.1.5 Conductivity

To start the electrospinning process, a sufficiently high number of charges are needed to enable the jet to be attracted towards the oppositely charged electrode and overcome the surface tension of the polymer solution. Mutual repulsive forces cause the jet to be stretched and this repulsion is proportional to the charge density on the jet's surface.

Solution conductivity is influenced by several factors such as polymer type, solvent, and salt. For instance, using ionic salts like monopotassium phosphate (KH_2PO_4) or sodium chloride (NaCl), increases the electrical conductivity of the polymer solution and produces small diameter fibers [38]. Also, using organic acid as a solvent increases the solution conductivity [40]. Zong et al. [53] found that when they add 1wt% of the salt to the polymer solution, the produced fibers were bead-free and thinner. They attributed this as the charge density over the jet surface increases by adding salt, the stretching forces increase.

2.4.1.6 Effect of solvent

Selection of the solvent depends on its solubility and its volatility. A volatile solvent with high evaporation rate is required for efficient electrospinning process [35]. Ideally, it should evaporate during the time needed for the polymer fiber's passage from the needle to the opposite electrode so that dry polymeric fibers are collected on it.

2.4.2 Processing parameters

Processing parameters also affect the electrospinning process, although this effect is generally less significant than the solution parameters.

2.4.2.1 High Voltage

A high voltage difference is applied between the spinneret electrode and the collector. This high voltage is responsible for the formation of the Taylor cone and overcoming the surface tension of the solution and causing the fibers to be ejected and travel towards the other electrode. There are two types of polarity for high voltage; first is the positive polarity and it is most commonly used while the second is the negative polarity [54]. At low applied voltage, the polymer droplet at the needle tip tries to reduce its size due to the interaction between the electric field and the surface tension.

As the applied voltage comes to critical value (V_c), the shape of droplet changes from hemisphere to a Taylor cone and fiber emits from the tip of the cone. The critical voltage can be modeled as:

$$V_c = 4 \frac{H^2}{L^2} \left[\ln \frac{2L}{r} - 1.5 \right] (0.117\pi r \gamma) \quad (2.4)$$

Where H is the distance between needle tip and collector, L is the length of the capillary tube, r is the radius of the tube, and γ is the surface tension of the fluid (units: H, L, and r in cm, γ in dyne/cm) [55].

Demir et al. [43] found that as the high voltage increases, the fibers diameter increase. They explained that as more fluid ejected by increasing the applied voltage, resulting in increasing the fiber diameter as shown in Figure 2.10. Zhang et al. [56] reported the same results. Nevertheless, Deitzel et al [57] reported that rough fibers and more beads appear with increasing the voltage and this is due to less stability in the initiating jet. Several

research groups have reported that higher applied voltages can raise the electrostatic repulsive force on the charged jet which reduces the fiber diameter [58]. Thus, different tendencies have been reported for voltage effects on electrospun fiber's diameter, the level of significance varies with the polymer solution concentration, the mass of polymer fed out from the needle tip, and elongation level of a jet by the electrical forces [59].

In general, the increasing of high voltage is proportional to the surface tension of solution; because as the surface tension of solution increases, a higher voltage is needed to start the jet of fiber.

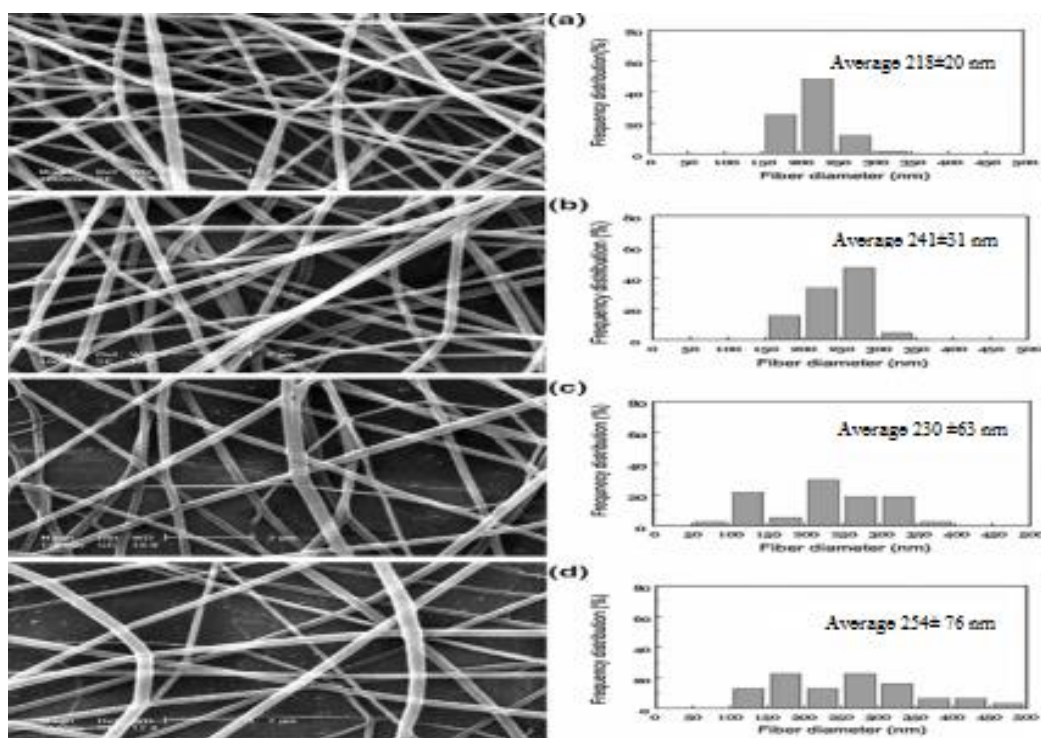


Figure 2.10: Effect of different values of voltage on morphology and fiber diameter distribution of PVA solution with concentration 7.4wt% ,collecting distance = 15cm, flow rate = 0.2 ml/h and Voltages values a=5; b=8; c=10; and d=13 kV [56]

2.4.2.2 Flow rate

The solution flow rate during the electrospinning process effects both the jet velocity and the diameter of the fibers produced. Megelski et al. [18] noticed that in the case of polysulfone fibers (PSF); pore and fiber diameter increase as the flow rate increases. Also, the rate of beads formation increases due to the limited evaporation rate compared to the increased amount of solvent which requires a longer time to evaporate. Therefore, when the fibers dry while on the collector, the uneven evaporation results in bead formation. Thus, the low flow rate is preferred for obtaining bead free fibers. Yean et al.

[60] studied the influence of changing the flow rate of PSF on fiber morphology. In addition, they found beads formation with thicker fiber diameters as the feeding rate increases as shown in Figure 2.11.

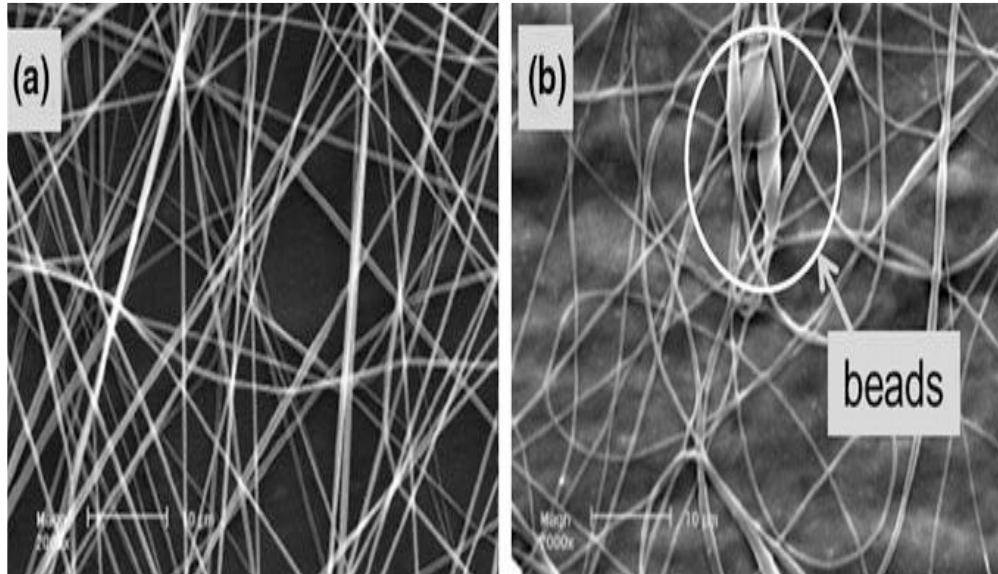


Figure 2.11: Effect of changing flow rate on the morphologies of 20%PSF polymer dissolved in DMAC (N,N-dimethyl acetamide) at 10 kV. Flow rate values a = 0.40 and b=0.66 ml/h, respectively [60]

Pump extrudes has been used to have a constant flow rate from the spinneret in horizontal or vertical position. As mentioned before the flow rate has a substantial effect on fiber diameter, thus the control of flow rate by using the pump is very important [35]. The pump can be single or multi syringes to increase the production rate, or to use different solutions from different materials to have a mixture of nonwoven mat.

2.4.2.3 Distance

It is the spacing between the grounded collector and the needle connected to the high voltage source. It controls the intensity of the electric field, which maintain the time required for the fiber jet to reach the opposite electrode. The distance should be adjusted to obtain a good fiber morphology [60]. The minimal collecting distance depends on the geometry of fibers and solution characteristics; also the distance should not be too large, as higher applied voltage will be required to initiate the process [61]. If the distance is short, the solvent may not have enough time to evaporate in which case the fiber may stick together and merge into thick fibers. Moreover, the velocity of fibers increases due to increased strength of electric field over a short distance, which leads to less time to evaporate the solvent and more beads will be formed. For larger distances, the solvent

has enough time to evaporate and the fibers are stretched more and become thinner. Yuan et al. [60] demonstrated this as shown in Figure 2.12.

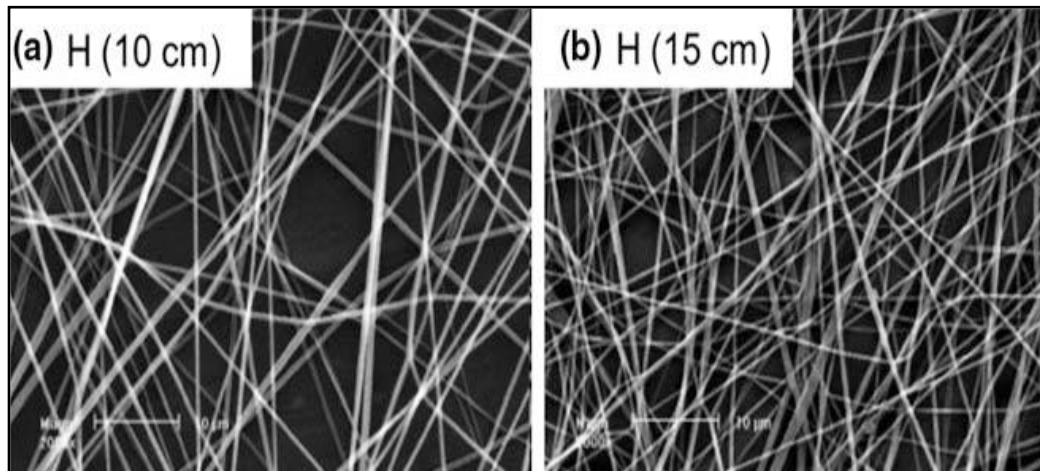


Figure 2.12: Effect of changing collecting distance on the morphologies of 20% PSF polymer dissolved in DMAC at 10 kV. At collecting distance= 10cm fiber diameter was $438 \pm 72\text{nm}$ and at 15cm fiber diameter was $368 \pm 59\text{nm}$, respectively [60]

2.4.2.4 Collector

It is the electrode on which the fibers are collected and the shape of collected fiber depends on the type of electrode and how the fibers are collected on the surface of the collector, as shown in Figure 2.13 [63–66].

- a) Disc Collector: for aligned fibers.
- b) Drum Collector: for random mesh or sheet of aligned fibers, depending on the speed of rotation.
- c) Mandrel Collector: for tubular nanofibers with different inner diameter.
- d) Plate collector: for random mesh.

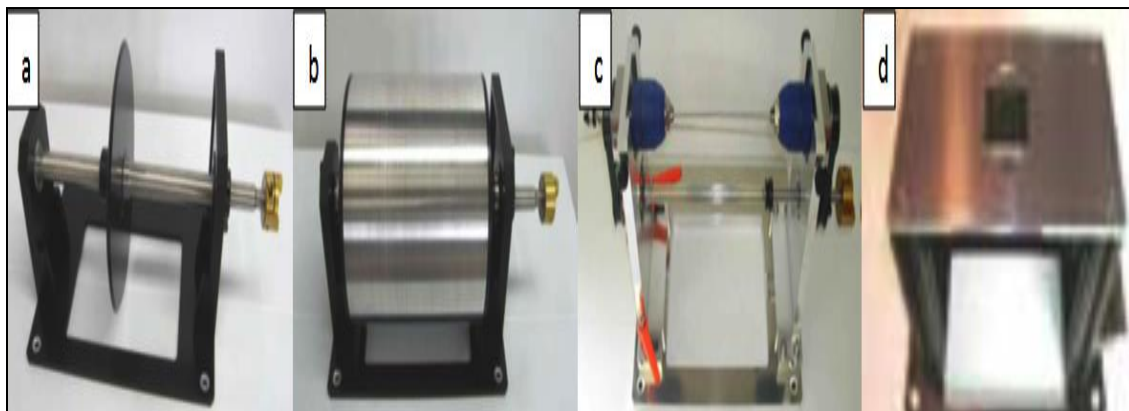


Figure 2.13: Different types of collector disc, drum, mandrel and plate collector respectively [66]

2.4.2.5 Spinneret

The spinneret is usually a syringe or a pipette with the end in micro scale. It is responsible for extruding the fibers from its end. There are many different types of spinnerets [66].

- a) Single Spinneret : produce one type of fiber
- b) Coaxial Spinneret: produce Core/Sheath and Hollow Fibers. It is also used for material, which shows low spin ability. The shell contains material with good electrospinning ability and the core contains the other.
- c) Heating Spinneret: for melting solid polymer up to 200 °C.

2.4.3 Ambient parameters

The final fiber morphology may be affected by the changing ambient parameters like air pressure, temperature, humidity, and electrical field from other devices near the electrospinning process. These are elaborately discussed in below:

2.4.3.1 Humidity

The humidity during the process has an influence on the electrospinning process. It affects directly the morphology of the electrospun fibers. Low humidity increases the rate of solvent evaporation. On the other hand, increased humidity leads to increase fiber diameter and pores which appear on the surface of fiber [9], [51]. Casper et al. [63] reported that such changes appear on the surface morphology of PS fiber with change of the humidity as shown in Figure 2.14

2.4.3.2 Temperature

Temperature has high influence on electrospinning process. In the warmer environment, the evaporation of solvent from the jet is easier. Increasing the temperature decreases the solution viscosity and increasing the polymer solubility. This improves the mobility of the polymer chain and more uniform fibers can be obtained [35]. The higher solution temperature produces thinner fiber due to the decrease in viscosity. However, some researchers' opinion that changes in temperature have two effects. It increases the evaporation rate which yields thicker fibers and decreases the viscosity resulting in thinner fibers [64].

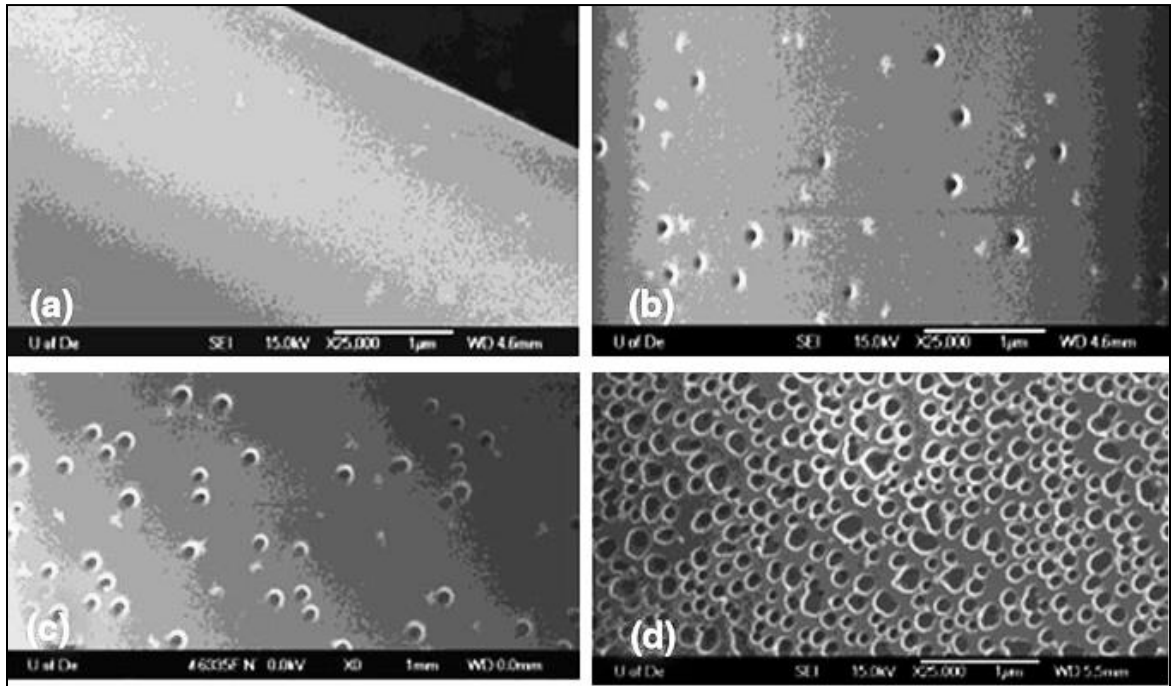


Figure 2.14: Effect of changing humidity on surface morphology of PS : a) 25%, b) 31–38%, c) 40–45%, d) 50–59% [63]

2.4.3.3 Pressure

Pressure has also some effect on the electrospinning process. If the pressure is lower than atmospheric pressure, the polymer solution inside the reservoir will have an affinity to come out and this results in the unstable jet initiation and wet fibers at the collector with less uniform diameters [35]

2.4.3.4 Type of atmosphere

Atmospheric gasses have notable effects on the electrospinning process. Like in helium environment, the electrospinning process is impossible due to the breakdown of the helium under high voltage. For feron-12, the fiber diameter will be double that of fibers produced under similar conditions in the atmospheric air [65].

Table 2.1 concise all the parameters affect the electrospinning and shows the effect of these parameters on the final shape of fibers' morphology

Table 2.1: Effect of changing electrospinning process parameters on the resultant fiber morphology[67]

	Process parameter	Effect on fiber morphology
1	Viscosity/concentration	<ul style="list-style-type: none"> • Low concentrations/viscosities yielded defects in the form of beads and junctions; increasing concentration/viscosity reduced the defects • Fiber diameters increased with increasing concentration/ viscosity
2	Conductivity/solution charge density	<ul style="list-style-type: none"> • Increasing the conductivity aided in the production of uniform bead-free fibers • Higher conductivities yielded smaller fibers in general (exceptions were PAA and polyamide-6)
3	Surface tension	<ul style="list-style-type: none"> • No conclusive link established between surface tension and fiber morphology
4	Polymer molecular weight	<ul style="list-style-type: none"> • Increasing molecular weight reduced the number of beads and droplets
5	Dipole moment and dielectric constant	<ul style="list-style-type: none"> • Successful spinning occurred in solvents with a high dielectric constant
6	Flow rate	<ul style="list-style-type: none"> • Lower flow rates yielded fibers with smaller diameters • High flow rates produced fibers that were not dry upon reaching the collector
7	Field strength/voltage	<ul style="list-style-type: none"> • At too high voltage, beading was observed • Correlation between voltage and fiber diameter was ambiguous
8	Distance between tip and collector	<ul style="list-style-type: none"> • A minimum distance was required to obtain dried fibers • At distances either too close or too far, beading was observed
9	Needle tip design	<ul style="list-style-type: none"> • Using a coaxial, 2-capillary spinneret, hollow fibers were produced • Multiple needle tips were employed to increase throughput
10	Collector composition and geometry	<ul style="list-style-type: none"> • Smoother fibers resulted from metal collectors; more porous fiber structure was obtained using porous collectors • Aligned fibers were obtained using a conductive frame, rotating drum, or a wheel-like bobbin collector • Yarns and braided fibers were also obtained
11	Ambient parameters	<ul style="list-style-type: none"> • Increased temperature caused a decrease in solution viscosity, resulting in smaller fibers • Increasing humidity resulted in the appearance of circular pores on the fibers

2.5 Techniques and apparatus used in electrospinning nanofiber

Electrospinning is not like other mechanical driven spinning method. In electrospinning, the force of extrusion comes from the interaction between the charged polymer fluid and an applied electric field [68]. After the connecting with the high voltage, the solution is charged and two forces, the surface tension and the electrostatic repulsion force affect the droplet at the needle tip. Under the influence of these forces the Taylor cone starts to appear [7], [69]. As mentioned earlier, electrospinning process should have a continuous flow rate of the polymer solution, and the voltage differential between the needle electrode through which it exits and the collector. There are several types of apparatus, which can use different techniques to produce the electrospun fiber.

2.5.1 Magnetic electrospinning

Dayong Yang et al. [70] employed the magnetic electrospinning (MES) technique to fabricate well-aligned nanofiber arrays and multilayer grids as shown in Figure 2.15. MES simply demands the addition of two magnets to the traditional setup as shown in Figure 2.1. In MES, the polymer solution is magnetized by adding few magnetic nanoparticles. The magnetic field stretches the fibers across the gap to form a parallel array as they land on the magnets. When the fibers fall down, the segments of the fibers close to the magnets are attracted to the surface of the magnets. Finally, the fibers land on the two magnets and stay over the gap [71].

MES has several advantages:

- a) The magnetic field can be manipulated accurately
- b) The resultant nanofibers can be transferred onto any substrate with full retention
- c) The area of the aligned fibers is large compared to other techniques

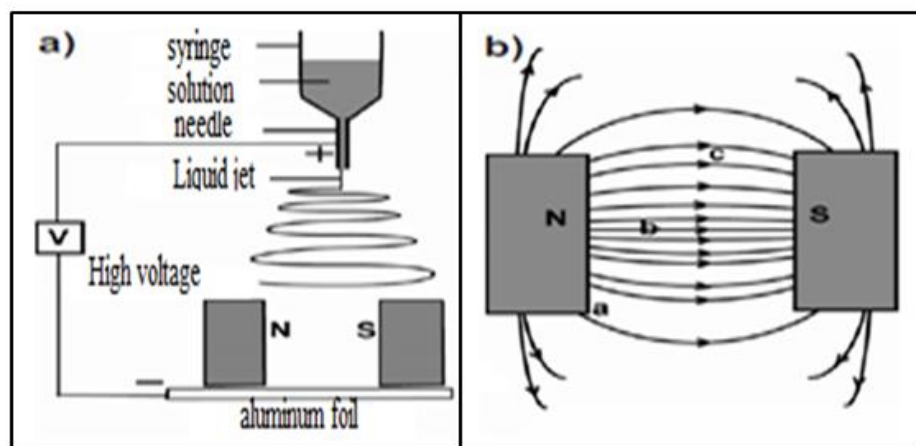


Figure 2.15: a) Generating aligned fibers by using magnetic field b) direction of magnetic field generated between two parallel permanent magnets [70]

2.5.2 External electric field

The external electric field can be used to control the electrospinning jet. A shape, a position and a polarity of the charges applied to the auxiliary electrode have to be considered. A single ring, or multiple rings, can be used as auxiliary electrodes to control the electrospinning jet. Deitzel et al. [26] used rings after the tip of the spinneret, as auxiliary electrodes and connected them with the same positive charge as the solution. The positively charged rings prevented the charged electrospinning jet from going outside the rings. A negative charge can also be applied to the collector screen to cause the jets stay inside the positive rings as shown in Figure 2.16. The lines of electric field meet at a centerline over collector screen. Stankus et al. [72] controlled the electrospinning jet

and reduced the deposition area from 7cm to 1cm with the charged rings. Although, the deposition area of 1cm in diameter is not good enough for precise patterning. This method still offers advantages such as controlled fiber deposition area and location. Otherwise, the chaotic flight of the electrospinning jet and the residual charge accumulation on the deposited fibers and the electrospun fibers may be deposited on outside areas rather than the designated collector. Buttafuoco et al.[25] used a single charged ring to designate and reduce the deposition area.

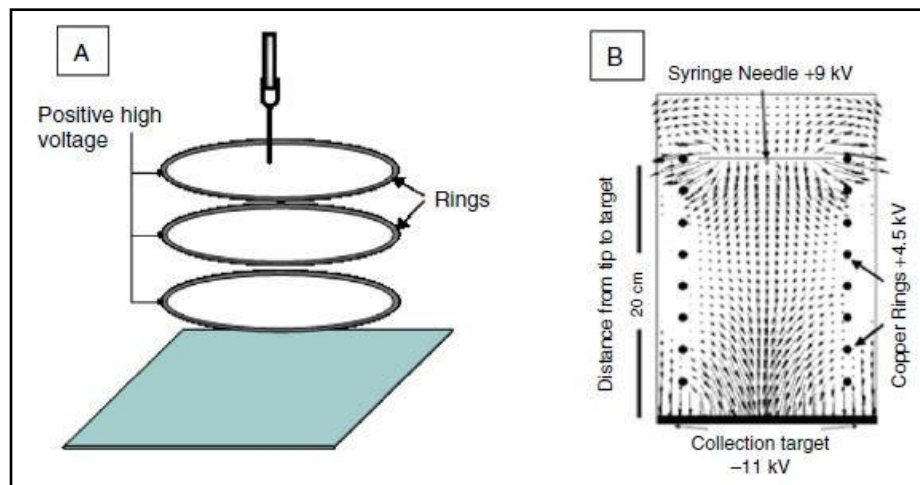


Figure 2.16: External electric field [26]

2.5.3 Needleless fiber production:

2.5.3.1 Rotating drum

Jirsak et al. [73] developed a needleless electrospinning setup by using a rotating roller to generate nanofibers as shown in Figure 2.17. Others have used a porous tubular surface [74]. The roller is partially submerged in the polymer solution and rotates with slow velocity.

A thin layer of polymer is carried onto the drum surface and exposed to a high voltage electric field. If the voltage exceeds the critical value, numerous numbers of electrospinning jets are generated. The jets are distributed over the electrode surface with periodicity and this is one of the main advantages of nozzle-less electrospinning. The number and location of the jets are set up naturally in their optimal positions. In the case of multi-needle spinning heads, the jet distribution is made artificially. The mismatch between “natural” jet distribution and the real mechanical structure leads to instabilities in the process [75]. There are several types of rotating electrodes for free liquid surface

electrospinning have been developed for industrial machines. However, the drum type is still one of the most productive.

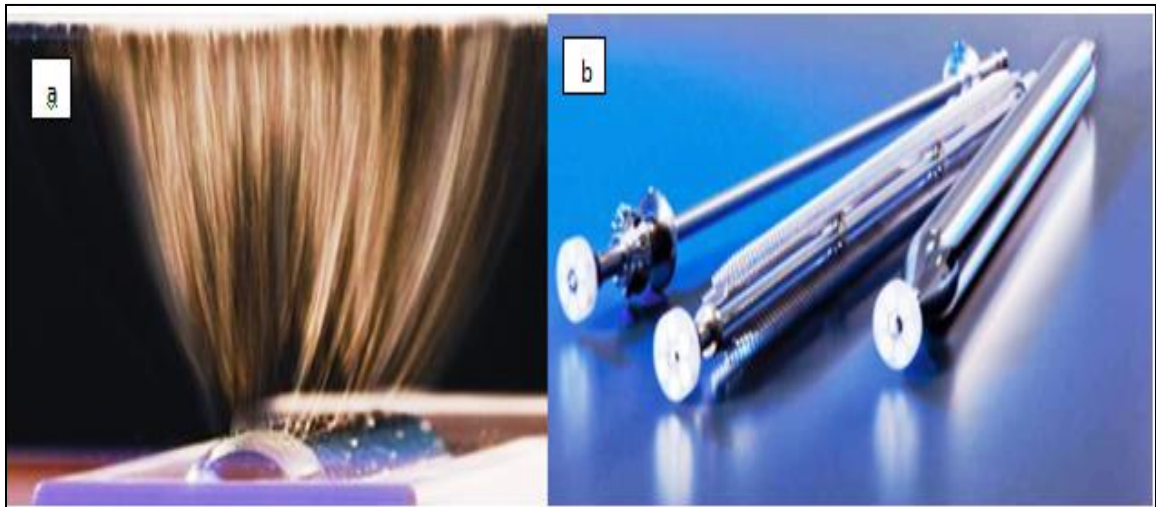


Figure 2.17: (a) Electrospinning from the free liquid surface using the rotating drum. (b) Different rotating electrodes design [73]

2.5.3.2 Bubble electrospinning

This design overcomes the bottleneck in present electrospinning technology and minimizes the surface tension of electrospun solutions. The system consists of vertical solution reservoir with a tube feeding gas from the bottom, with a metal electrode fixed along the centerline of the tube and ground collector over the reservoir as shown in Figure 2.18. Many small bubbles with different sizes were produced on the solution surface [17]. In the absence of an electric field, the aerated solution forms various bubbles on the surface. When an electric field is present, it induces charges into the bubble surface. When the electric field exceeds the critical value needed to overcome the surface tension a fluid jet ejects from the apex of the conical bubble as shown in Figure 2.18. However, there are large beads in the produced fibers [76].

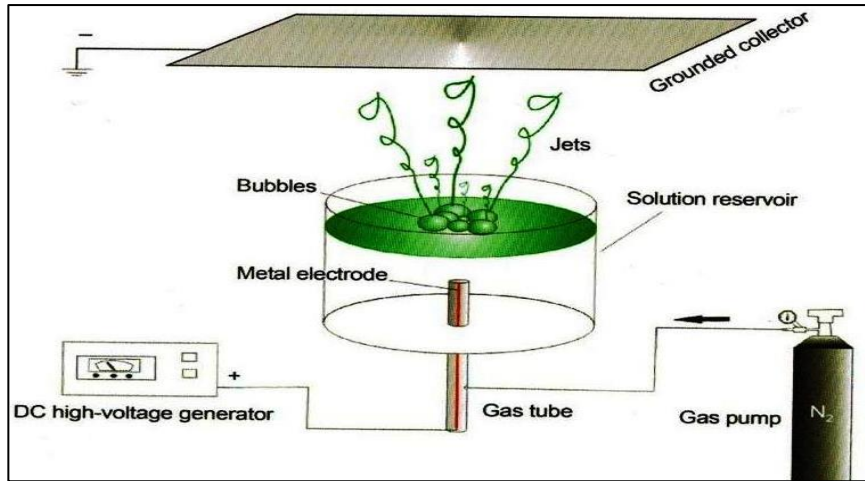


Figure 2.18: Bubble electrospinning [2]

2.5.3.3 Disc, ball and spiral coil

Niu et al. [61] compared the needleless electrospinning using different rotary fiber-generators (disc, ball, spiral coil) as shown in Figure 2.19 to electrospinning PVA solution. When PVA solution is charged with a high electric voltage via a copper wire inside the solution vessel, numerous jets/filaments were generated from the spinnerets, which deposited on the collector. With the rotation of the spinneret, PVA solution was loaded onto the spinneret surface constantly, leading to the continuous generation of polymer jets/filaments. They also used finite element method to analyze electric field and examine the influence of spinneret shape on the electric field profile. They found that the spinneret with a highly concentrated and evenly distributed electric field is the key to efficient needleless electrospinning of uniform nanofibers.

It was also found that the spiral coil had higher fiber production rate than cylinder spinneret of the same dimension, and the fiber diameter was fine with a narrower diameter distribution[77].



Figure 2.19: Different types of electrospinning needleless disc, ball, and spiral coil [61]

2.6 Sound and noise

The sound is the vibrations that transmitted through an elastic solid, a gas or liquid with frequencies in the range of 20- 20000Hz and can be detected by human ears.

The perception of sound needs three things: a sound source, a medium to transfer sound, and a receiver to sound. The observed incident sound at a point has two main distinguished attributes. First, is a timbre (frequency is the quantity of timbre) and second, is a loudness (represent by sound pressure).

Noise is the sound that is not desired by the receiver because it is unpleasant, loud, and interferes with hearing. In another word, it is the unpleasant sound, which is disruptive, dangerous and can cause harm to life, nature, and property. This results in the subjective discretion between sound and noise, where any sound may be considered as a noise depending on the receiver. Noise differs from other forms of pollution in that, once abated, noise leaves no residual accumulation in the environment or the human body not like air pollution [78]. However, these can change after continued exposure to harmful sounds. Therefore, it is not true, firmly speaking, that noise leaves no observable evidence. Ear detect the sound by mechanical process, where the sound waves mutate into vibrations inside the ear [79].

Figure 2.20 shows the response chain for detecting the sound by ear where the mechanical vibrations in eardrum convert to electrical signals, which are transmitted, to the brain and the perception occurs and the sensation of sound. The reaction response for the sound perception is varied between people according to their age and health state [80].

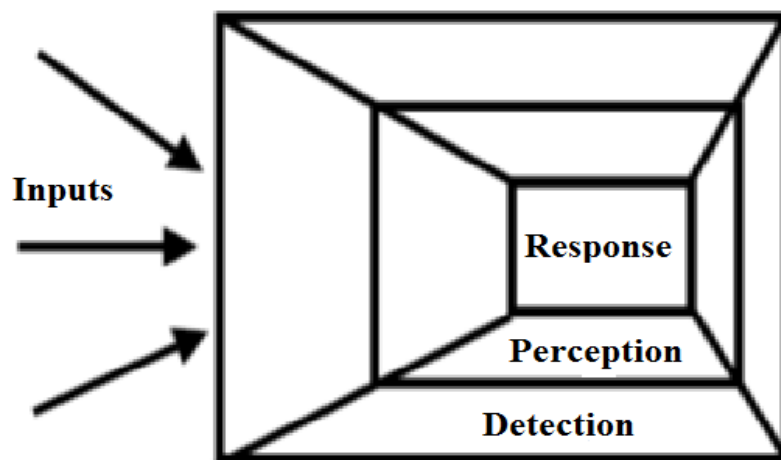


Figure 2.20: Chain of sound response [80]

Noise pollution may increase raising the risk of serious health conditions, such as heart disease, the risk of hearing loss, stress, sleep disturbances, and heart disease [81]. A new analysis conducted an environmental assessment of USA noise pollution as a cardiovascular health hazard and revealed small decreases in noise could add up to major economic savings. According to a research published in Environmental Health Perspectives, long-term exposure to traffic noise may account for approximately 3 percent of coronary heart disease deaths (or about 210,000 deaths) in Europe each year [82]. Also, Children in noisier neighborhoods were shown to suffer from increased stress and diminished motivation and a fetus exposed to noise may experience a change in heart rate, or it may suffer the impact of its mother’s noise related stress [83]. Research also suggests long-term exposure to noise pollution may have an effect on cognitive development in children and cognitive and psychological functions in adults; although more research is needed in this area [84]. One study of traffic wardens in Pakistan, who are exposed to noise levels between 85-106 decibels, found significant physio-psychological effects due to traffic noise pollution, as shown in Table 2.2 [85].

Table 2.2: Effect of noise levels between 85-106 [db] on traffic wardens in Pakistan

Aggravated depression: 58%	Stress: 65%	Public conflict: 71%
Irritation and annoyance: 54%	Behavioral effects: 59%	Speech interference: 56%.
Hypertension: 87%	Muscle tension: 64%	Exhaustion: 48%
Low performance levels: 55%	Concentration loss: 93%	Hearing impairment: 69%
Headache: 74%	Cardiovascular issue: 71%	

Noise pollution can be controlled through reduction at the source, interruption of transmission paths, or protection of the receiver. There are several methods of reduction at the source reengineering machines and simply turning down the volume when possible are methods of reduction at the source. Barriers, enclosures, and other forms of soundproofing can interrupt transmission paths. The use of hearing protection is the main form of receiver protection. Experts recommend a multifaceted approach, including appropriate training on the use of equipment and on why ear protection matters,

enforcement of hearing protection regulations, and the use of new technologies to reduce noise at the source [86]. Like many other environmental problems, issues of shared responsibility and jurisdiction, making some conventional economic approaches less effective and inviting new interdisciplinary solutions, complicate addressing noise pollution.

Acoustic treatments are very important for such cases not only to improve the quality of life, which is achieved by providing quiet and friendly acoustic surroundings but most importantly to protect health. To reduce or eliminate the bad effect of sound (noise), there are two grouped for that; active and passive methods. The active method differs from the passive method in that it is necessary to apply external energy for reducing the noise process [87].

In active noise control, it is necessary to have a noise or vibration meter based on various sensors in order to act on the system via adequate actuators to cancel the noise or vibrations. This is why it is also necessary to have a feedback control to close the sensor-control-actuator loop. Therefore, the various control algorithms will play a major role in active noise control.

The sound absorbing materials consider passive mediums that decrease the noise by disseminating energy and turning it into heat. Acoustic absorption depends on the frequency of the sound waves. In porous materials at high frequencies, an adiabatic process takes place that produces heat loss due to friction when the sound wave crosses the irregular pores. The absorption phenomenon differs from that of insulation or shock absorption. This process causes a vibrating movement to diminish in size with time. The origin can vary due to the friction between two surfaces, as a result of internal friction or hysteresis of the material itself.

Poroelastic materials are divided into two phases: a solid phase is known as the skeleton and a liquid phase that is normally air. There are different types of poroelastic materials: fibrous, such as cloth and rock wool, foam, granular and vegetable binders such as straw. At high frequencies, parameters of porosity, tortuosity, and characteristic lengths play a very important role, while at low frequencies, porosity, air flow resistivity, and thermal permeability [87].

2.6.1 Sound absorption coefficient

A sound wave which has a sound power P_i , a sound pressure p_i , a sound particle velocity v_i and a frequency f impinges on an obstacle, which is large compared to its wavelength (λ). It is partially reflected (P_r) (and may be also, possibly diffracted and scattered), allowed to pass through (P_t), transmitted as structure-borne sound (P_f), as well as absorbed (P_a) [88], see Figure 2.21.

$$P_i = P_r + P_t + P_f + P_a \quad (2.5)$$

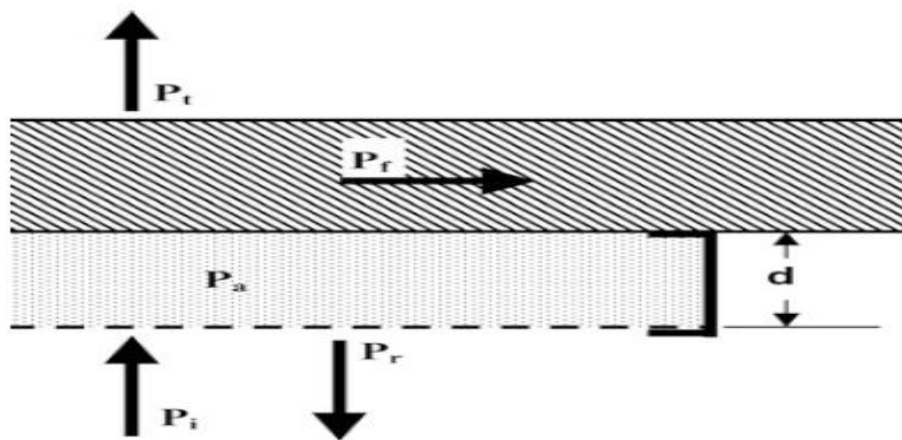


Figure 2.21: The path of the power of a sound wave impinging upon an absorptive obstacle [88]

Sound absorption coefficient (α) is used as a performance index to assess the efficiency of sound absorbing materials such as fibers, foams, mineral wool and glass fiber. It describes the sound energy fraction, which not reflected (R) back to the surrounding and is dampened inside the material, when sound waves impinge on the surface of the material. For the normal incidence of sound wave, it is expressed mathematically as:

$$\alpha = \frac{P_t + P_f + P_a}{P_i} = \frac{P_i - P_r}{P_i} = 1 - \frac{P_r}{P_i} = 1 - \frac{I_r}{I_i} \quad (2.6)$$

Sound absorption in fine-fiber or open-pore materials having prevailed in noise control and room acoustics since the 1950s [88].

2.6.2 Sound reflection coefficient

Another way to assess the efficiency of sound absorbing materials is the sound reflection coefficient (R). It is defined as the ratio of the reflected intensity over the incident intensity [89]:

$$|R|^2 = \frac{I_r}{I_i} \quad (2.7)$$

Where I_r the intensity of reflected sound and I_i is the intensity of incident sound.

The sound reflection coefficient is a complex quantity with a phase term expressing the phase lag between these two pressure waves. The sound pressure and sound intensity for a plane sound wave have a relation to each other as shown in the following equation [89]:

$$I_i = \frac{p_i^2}{\rho_0 c_0}, \quad I_r = \frac{p_r^2}{\rho_0 c_0} = \frac{|R|^2 p_i^2}{\rho_0 c_0} \quad (2.8)$$

Where ρ_0 is the air density, and c_0 is the sound speed in air. For the pervious equations, the relation between sound absorption and sound reflection can be concluded as the follow:

$$\alpha = 1 - \frac{\frac{|R|^2 p_i^2}{\rho_0 c_0}}{\frac{p_i^2}{\rho_0 c_0}} = 1 - |R|^2 \quad (2.9)$$

2.6.3 Acoustic impedance

The acoustic impedance between two media causes the sound reflection when it transfers between them. The impedance defined as the ratio of acoustic pressure to particle velocity in the medium.

$$Z(x, t) = \frac{p(x, t)}{v(x, t)} = Z' + j Z'' \quad (2.10)$$

Where Z is the acoustic impedance, p and v are the acoustic pressure and the medium particle velocity, respectively. Acoustic impedance is a complex number, which has a real part Z' that expresses the resistance magnitude of the sound wave through the medium and an imaginary part Z'' that shows the reactance or the lag phase between the

medium particle velocity and acoustic pressure. The acoustic impedance of air is shown in the following equation:

$$Z_c = c_0 \rho_0 \quad (2.11)$$

Where Z_c is the characteristic impedance and at normal condition for atmospheric temperature and pressure $Z_c = \rho_0 c_0 = 1.21 \times 344 = 416.24 \text{ Pa.s.m}^{-1} (\text{MKS rayl})$. The surface impedance is defined as the measuring impedance at the interface between two media. There are many factors affect the surface impedance. The first group related to the material properties such as flow resistivity, tortuosity, porosity, viscous characteristic length, and thermal characteristic length. The second group related to outer conditions such as mounting condition, incidence angle of sound waves, and material thickness.

There is a relation can be concluded between the surface impedance and the sound reflection by imagining the plane sound wave propagation in + x-direction facing the surface of the sound absorbing material as presented in Figure 2.22.

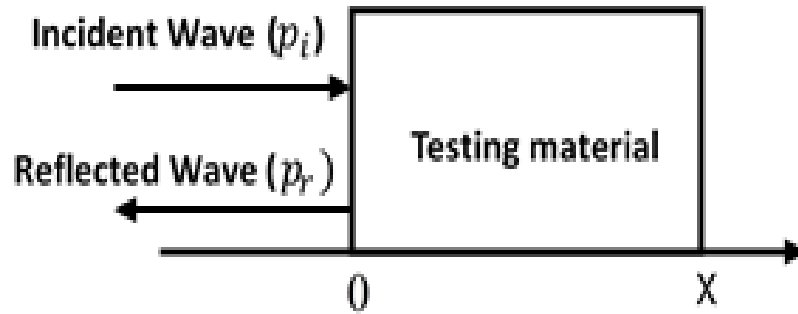


Figure 2.22: Incident and reflected wave at the surface of testing material

Due to the impingement of incident wave with the material surface, a part of the reflected wave in the reverse direction interferes with the incident wave and form a standing wave. The total pressure of this standing wave can be estimated from the superposition principle [89]:

$$P(x, t) = p_i - p_r = P_i e^{j(\omega t - \bar{k}x)} + R P_i e^{j(\omega t + \bar{k}x)} \quad (2.12)$$

Where p_i is the pressure of the incident sound wave, p_r is the pressure of the reflected sound wave, P_i is the pressure amplitude of the incident sound wave, t is the time, x is the distance from the material surface, ω is the angular frequency ($= 2\pi f$), \bar{k} is the

wavenumber ($= \omega/c_0 = 2\pi/\lambda$), c_0 is the speed of sound in air, f and λ are the sound frequency and wavelength, respectively. The particle velocity is given by the following equation [89]:

$$v(x) = \frac{p(x)}{Z_c} = \frac{P_i}{Z_c} e^{j(\omega t - \bar{k}x)} - \frac{RP_i}{Z_c} e^{j(\omega t + \bar{k}x)} \quad (2.13)$$

At the surface of the material, the value of P and v can calculate as follow:

$$P(0) = (1 + R)e^{j(\omega t)} \quad (2.14)$$

$$v(0) = (1 - R)\frac{P_i}{Z_c} e^{j(\omega t)} \quad (2.15)$$

The corresponding surface impedance in this case

$$Z_s = \frac{P(0)}{v(0)} = \frac{(1+R)e^{j(\omega t)}}{(1-R)\frac{P_i}{Z_c} e^{j(\omega t)}} = Z_c \frac{(1+R)}{(1-R)} \quad (2.16)$$

From this equation (R) can be obtained it terms of (Z)

$$R = \frac{Z_s - Z_c}{Z_s + Z_c} \quad (2.17)$$

In addition, (α) can be expressed in terms of (Z)

$$\alpha = 1 - |R|^2 = \frac{4Z_s'Z_c}{(Z_s' + Z_c)^2 + Z_s''^2} \quad (2.18)$$

The influence of the acoustic impedance at the surface of the material on the sound reflection is shown in equation 2.18 and it is called the matching law [79].

2.6.4 Factors affect the performance of sound absorbing materials

There are four parameters that characteristic the performance of the sound absorbing materials as follow: porosity (ϕ), tortuosity (α_∞), the characteristic impedance (Z_c), and static airflow resistivity (σ). The surface impedance (Z_s) can collect of these parameters in the following equation 2.19 [88]:

$$Z_s = Z_c \frac{\sqrt{\alpha_\infty}}{\phi} \sqrt{1 - j \frac{\sigma \phi}{2\pi f \alpha_\infty \rho_0}} \quad (2.19)$$

The material thickness (d) and the air flow resistivity (σ) are considering important factors in choosing sound absorbing materials. The increasing of one or both of them increases dissipate of sound energy by the viscous losses. However, their increase also,

increase the surface impedance of the material, which by sequence will lead to sound reflection at the surface of material. From this, it can be conclude that there are a limitation for choosing the values of (d) and (σ) to have the best performance. The following equation shows the limitation for choosing these values.

$$2 < \varepsilon = \frac{\sigma d \phi}{\rho_0 c_0 \sqrt{\alpha_\infty}} < 6 \quad (2.20)$$

Where ε is called the matching ratio.

By considering $\phi \approx \alpha_\infty \approx 1$, the equation 2.20 becomes

$$800 < \sigma d < 2400 \text{ (MKS rayl)} \quad (2.21)$$

The relation between the material flow resistivity and thicknesses of sound absorbing materials is shown in Figure 2.23. The vertical line at $\sigma > 7500 \text{ Pa.s.m}^{-2}$ (MKS rayl/m) represents the minimum flow resistivity value for most commercial sound absorbing materials. Figure 2.24 shows the design characteristic of the sound absorbing material and it is clear that the material thickness should not be too less than the wavelength to be able to absorb sound. For example to absorb 90%, sound the thickness of absorbing material should be equal a quarter of an incident wavelength.

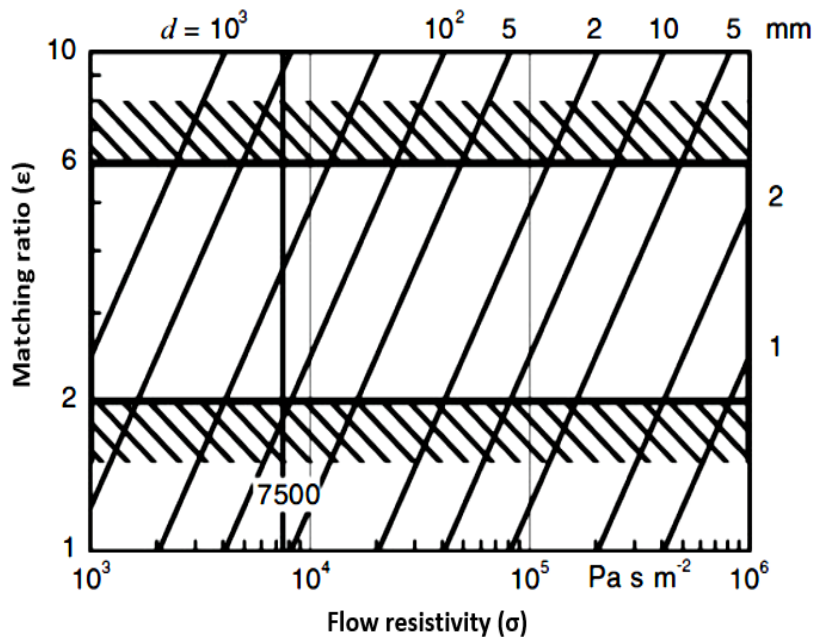


Figure 2.23: Relation between Matching ratio (ε) and (σ) for different thickness [88]

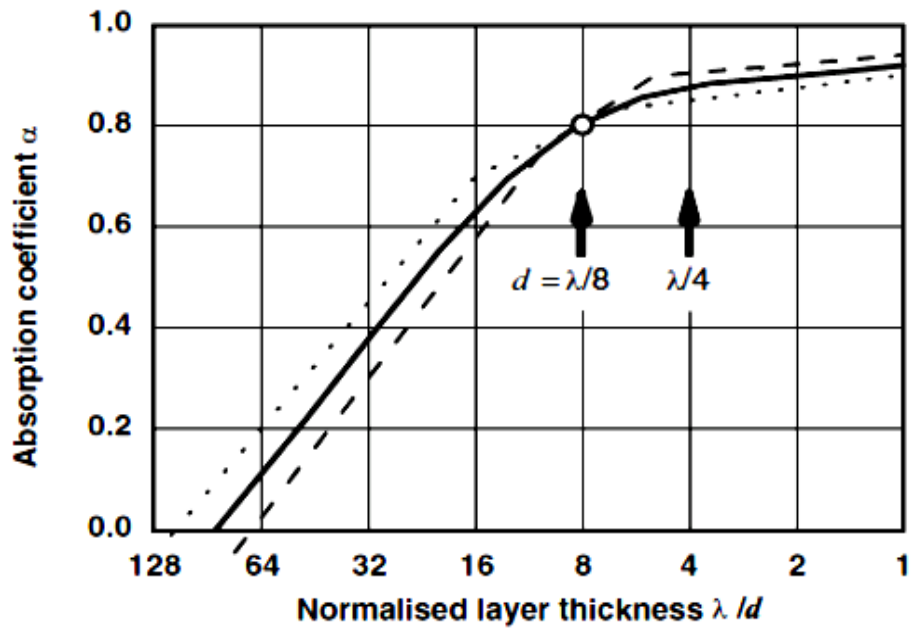


Figure 2.24: Design characteristics of sound absorbers with a matching ratio $\epsilon = 2$ (dashed line) and $\epsilon = 6$ (dotted line) [88]

2.6.5 Low frequency:

Low-frequency noise is produced by many sources in our life such as different means of transportation, (i.e. Lorries, diesel-driven buses and trains, airplanes and helicopters), heating- cooling or ventilation of buildings, wind turbines, gas transmission grid, industrial plants, sewerage, and so on. The low-frequency range is between (20 -200Hz). It may propagate for long distances and penetrate thick walls. It is reported that the low-frequency noise has energy responsible for sleep disturbance, concentration difficulties, irritability, anxiety, and tiredness. Also, people complain about the presence of hum, buzz, and rumble are often not recognized as a nuisance [93, 92].

The sound frequency is the number of oscillations/second and it measured by hertz (Hz). The sound travels through the air with velocity 340m/s but this velocity may little change with temperature.

$$\text{The sound velocity (c) = wavelength } (\lambda) \times \text{frequency (f)} \quad (2.22)$$

Table 2.3 shows the relation between the frequency and wavelength. It is noticed that the frequency region from 25Hz to 200Hz have wavelengths similar the room dimensions, which lead to resonances in the room. Therefore, it is difficult to stop or absorb unless there are thick heavy walls for preventing attenuation or a thickness of absorbing material

up to about a quarter wavelength thick, which could be several meters to absorb the noise [80].

Table 2.3: frequency and wavelength of low frequency sound [80]

Frequency (Hz)	1	10	25	50	100	150	200
Wavelength (m)	340	34	13.6	6.8	3.4	2.27	1.7

Moller (1987) studied contours of equal annoyance for pure tones in the frequency range 4Hz to 31.5Hz. He found that the annoyance contours are influenced by the narrowing of the range of equal loudness contours at low frequencies [79]. Figure 2.25 shows the annoyance rating vs the sound pressure level. It is shown that the lowest frequencies should be at a higher level than other frequencies to become audible. As lower frequencies become audible, their annoyance increases rapidly. For instance, the frequency at 4Hz is about 10dB between extremes of annoyance but for 8Hz and 16Hz have a 20dB range, whilst 31.5Hz has nearly 40dB range.

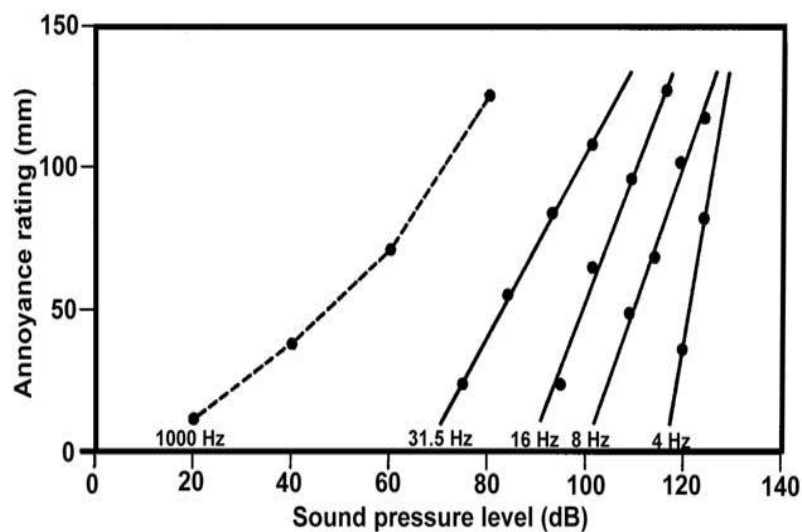


Figure 2.25: Annoyance rating, showing rapid growth at low frequencies [79]

2.6.6 Reducing the effect of low-frequency noise

To reduce the low-frequency noise, the process starts from choosing the material that will be able to absorb or dissipate the sound at low frequency. The ability of homogeneous sound absorbing materials can be improved by increasing their surface wrinkle [92]. Surface wrinkle enhances the impedance matching with air and allows the sound dissipate by viscous losses.

T Yang et al. [93] introduce a laminated structure as a sound absorbing material for low frequency by gradually increase the impedance using several layers of different thickness and different density which will lead to increase the sound dissipation across the sample as shown in Figure 2.26.

Micro-perforated panels (MMP) is one the effective methods to absorb sound in low and mid frequency range. Metal, polycarbonate, wood, plastics, and many others are used as planes and it perforated in a design pattern. The holes diameter should be close to the thickness of viscous boundary layer to create frictional losses. Besides, that the diameter of the holes should be near from the sheet thickness to enhance the sound dissipation [94].

Helmholtz resonator device consists of a rigid –walled cavity of volume V with a neck of area S and L length. For the frequency of interest assume that, $\lambda \gg V^{1/3}$, $\lambda \gg L$, $\lambda \gg S^{1/2}$. The open end of the neck radiates sound, providing radiation resistance and radiation mass. The fluid in the neck, moving as a unit, provides another mass element and thermoviscous losses at the neck walls provide additional resistance. The compression of the fluid in the cavity provides stiffness. This stiffness can adjust by changing the design of Helmholtz resonator like length and/or diameter of the neck, and the depth of the hole.

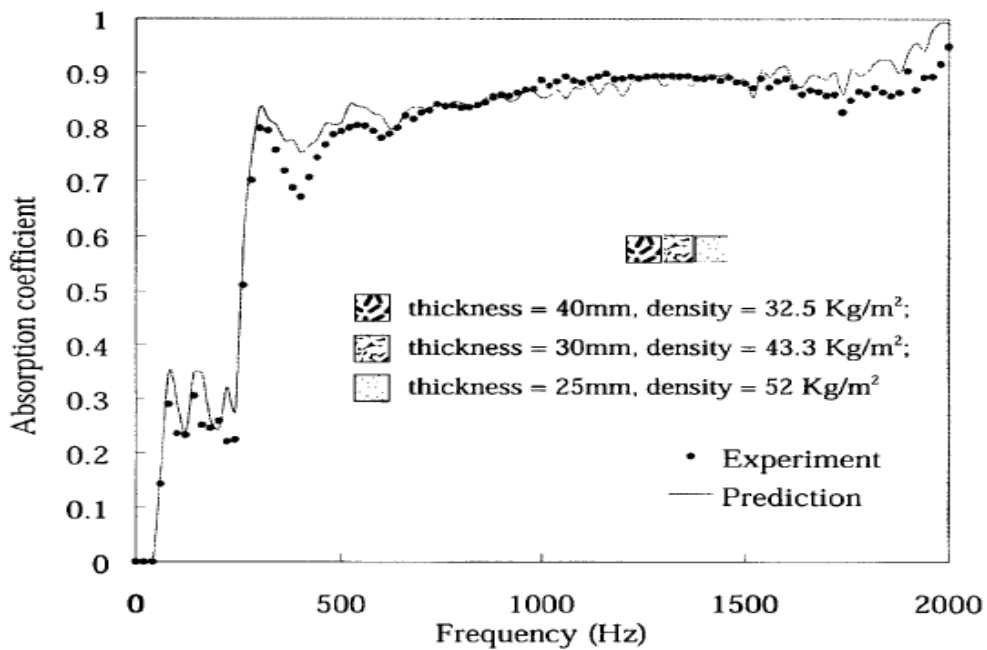


Figure 2.26: Experimental and prediction values of sound absorption coefficient for combining three porous laminated composite materials [93]

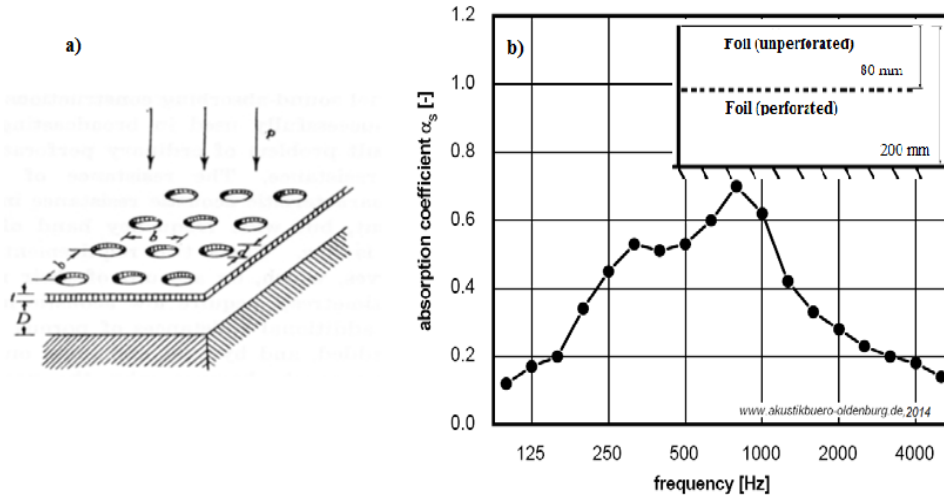


Figure 2.27: a) Sketch of micro-perforated panel absorber (MPA) from with diameter d of the orifice, spacing b between orifice, thickness t of the panel and air cavity depth D between the panel and backing wall b) Sketch of set-up and corresponding result for absorption coefficient [94]

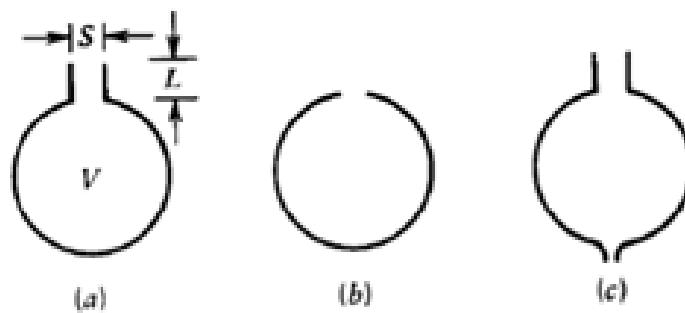


Figure 2.28: Three types of Helmholtz

2.7 Nanofiber as sound absorption material

Sound absorption for lower frequency generally requires thicker material, but increase in the thickness has the disadvantage of using up larger interior space architecture. Therefore, there are requirements of materials with lighter weight, which are thin and have high sound absorption performance.

Application of nanofibers in the acoustic field is relatively new. Therefore, a substantial amount of studies is required to better understanding and improvement of sound absorption using nanofibers.

2.7.1 Silica nanofiber sheet

Shuichi et al. [95] produced laminates of silica fibers (SF) with fiber diameters between (0.5-3.5 μ m) and the overall thickness of 3mm. They studied the influence of fibers diameter on the absorption of sound and they found that the flow resistivity increased with decreasing fiber diameters due to increasing in the surface area of the fiber. Table 2.4

shows the average diameters of silica fiber laminates and diameter of fiberglass wool (GW), they used to compare with silica. Figure 2.29 shows the sound absorption coefficient of measured samples and it is observed that as the fiber diameter decreases, the sound absorption increases and shifts to the lower frequencies.

Table 2.4: Average diameter (μm) of silica fiber laminates (SF1-4) and GW [95].

SF1	SF2	SF3	SF4	GW
0.52	0.67	2.01	3.48	8.24

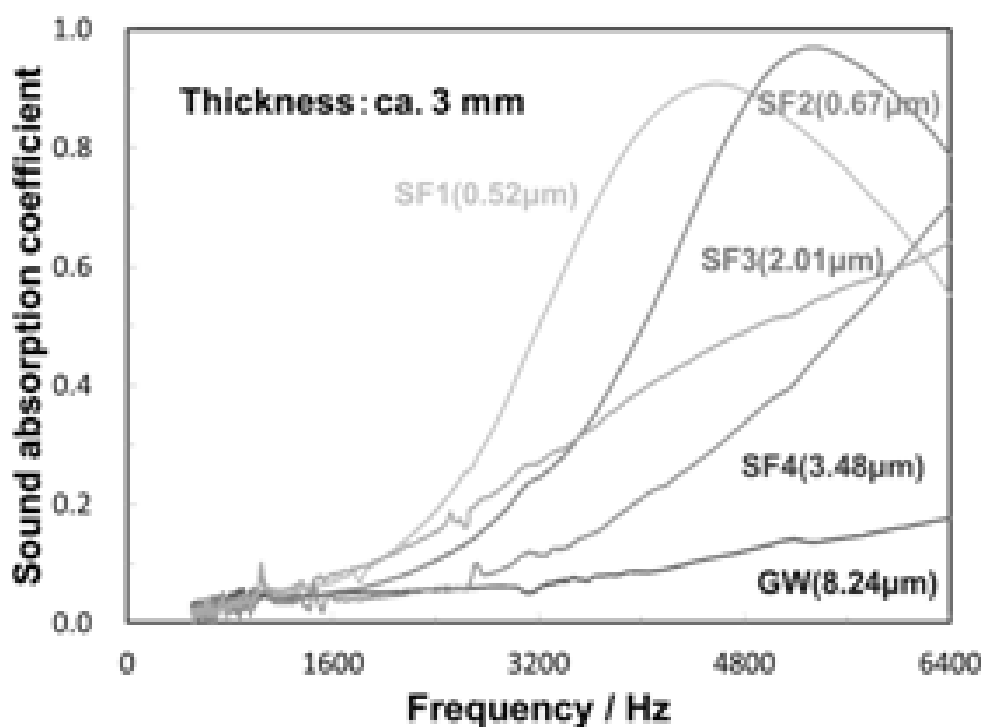


Figure 2.29: Sound absorption coefficient of silica fiber laminates (SF1-4) and GW [95]

2.7.2 Polyvinyl-chloride (PVC) and polyvinyl-pyrrolidone (PVP)

PVC and PVP were used by Asmatulu et al. [13] for reducing noise inside aircraft. They produced PVC nanofibers with a diameter of 150- 900nm by using N,N-dimethylformamide (DMF) as a solvent. Also, they produced PVP nanofiber with a diameter between 4- 5 μm by dissolving in ethanol. They compared the absorption coefficient of PVC and PVP with Melamine foam by preparing three samples with different weights and used two thickness of Melamine foam for comparison. They found that nanofibers have a good absorption coefficient and the absorption coefficient of PVC shifts to lower frequency by increasing the sample weight as shown in Figure 2.30, but for PVP, sound absorption increases with increasing the weight as shown in Figure 2.31.

However, Asmatulu et al. [13] did not investigate the morphology of the fibers and at which fibers diameter the sound absorption increases.

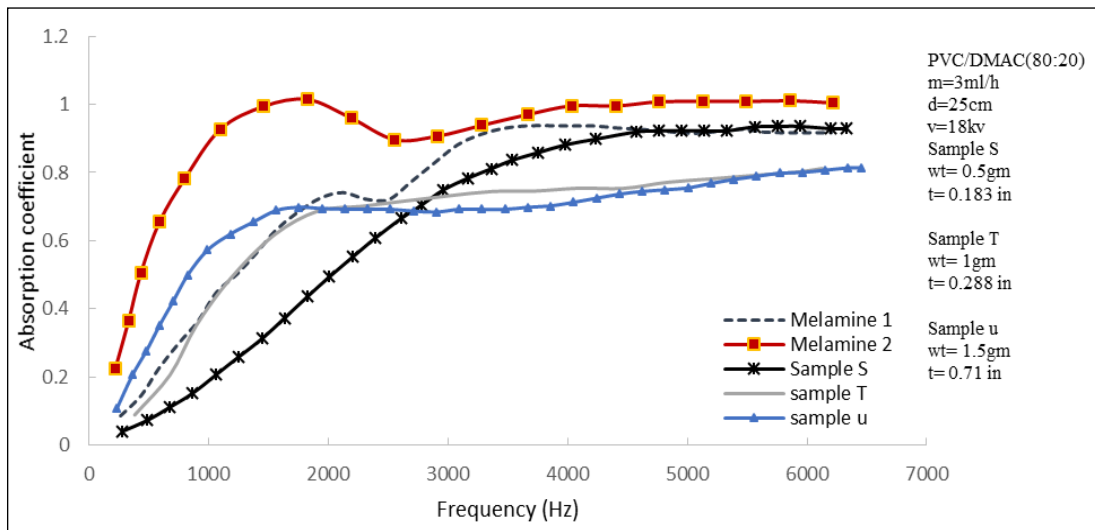


Figure 2.30: Absorption coefficient of PVC nanofiber mat samples compared with two thickness of melamine foam 1, 2 inches [13]

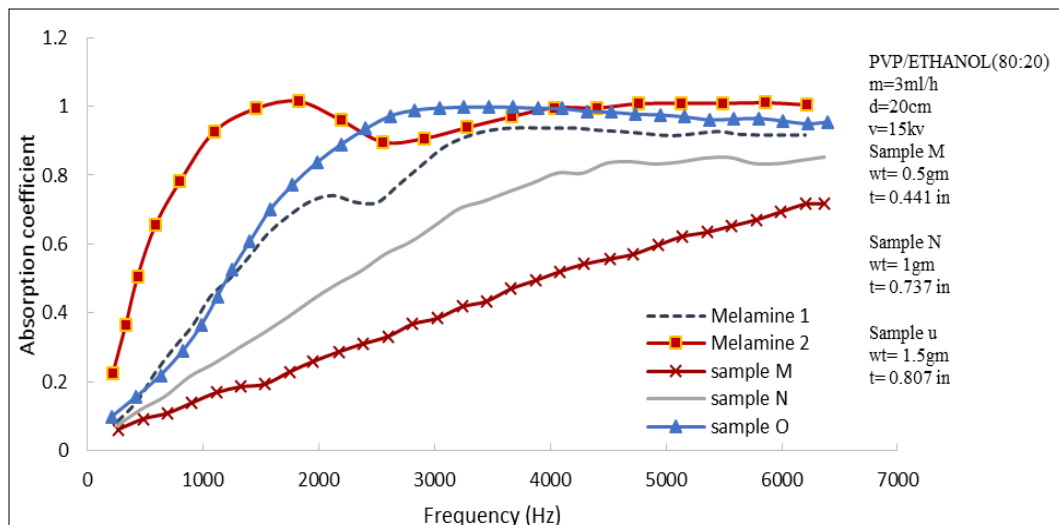


Figure 2.31: Absorption coefficient of PVP nanofiber mat samples compared with two thickness of melamine foam 1, 2 inches [13]

2.7.3 Polyamide (PA6)

Kucukali et al. [96] used PA6 to produce nanofibers. PA6 dissolved in acetic acid and formic acid followed by heating to 80 °C and stirred for 5 h. They used the mat of PA6 to produce nanofiber resonant membrane and measured its efficiency as a sound absorbing material and they studied the influence of several air gaps spaces between the sample and the back wall. They found that the existence of air gap between the rigid wall

and nanofiber membrane enhanced the sound absorption proprieties, and the absorption increased as the gap size increased as shown in Figure 2.32. However, they did not study the effect of fibers diameter or the sample thickness on the sound absorption of the fibers mat produced in their work.

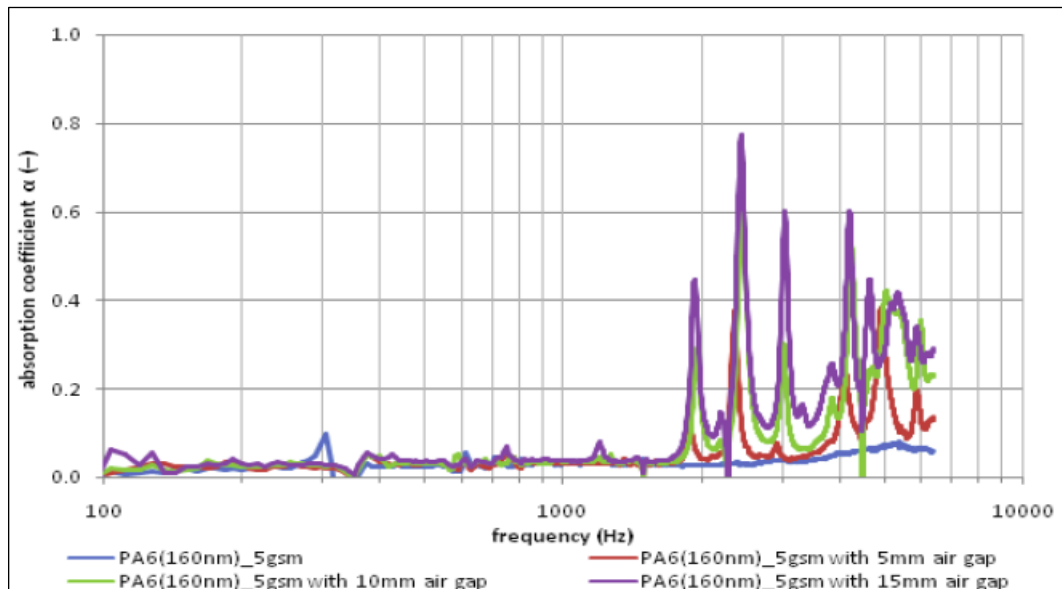


Figure 2.32: measured sound absorption coefficient of the nanofiber membrane as a function of sound frequency [96]

2.7.4 Polyacrylonitrile (PAN)

The acoustical proprieties of PAN was investigated by Xiang et al. [8]. They concluded that PAN has good sound absorption coefficient in low and mid frequencies, that hard to detect by the traditional material. They produced mats of PAN using the same concentration and different electrospinning time. The concentration was 8wt% of PAN dissolved in N,N-dimethylformamide (DMF) and the production times were 10, 30, 60min and the average thickness of these samples were (17 ± 3) , (38 ± 3) , $(205\pm4)\mu\text{m}$ respectively as shown in Figure 2.33.

In that work, they measured the acoustic absorption for PAN samples with three forms [8]:

- 1- PAN membrane with different back cavities
- 2- PAN membrane over perforated panel with different back cavities
- 3- PAN membrane as upper layers on conventional acoustic materials

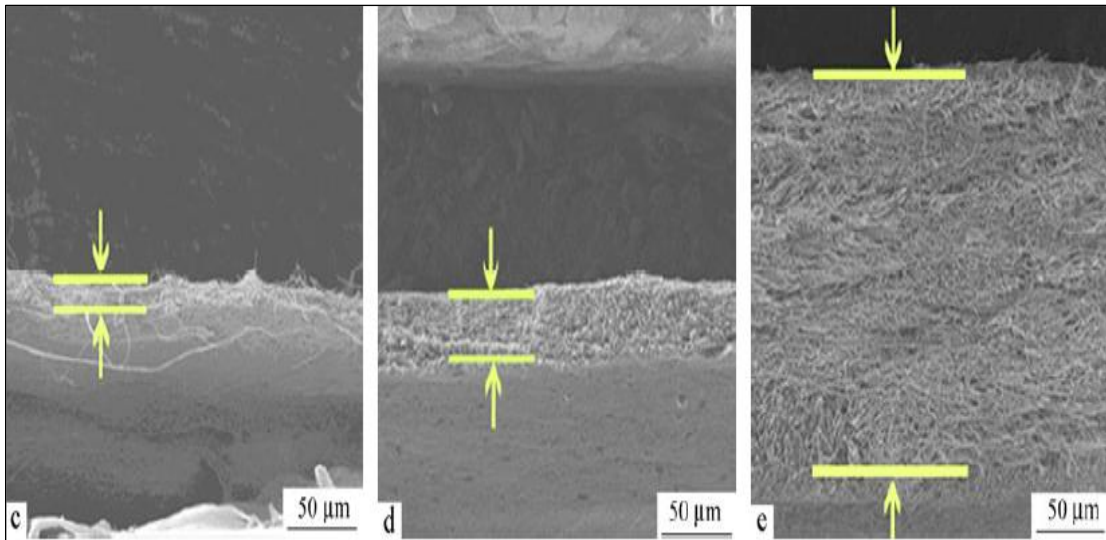


Figure 2.33: PAN nanofibers with different thickness for different electrospinning time 10, 30, 60 min respectively [8]

For the first case nanofiber, PAN membrane showed that its absorption coefficient for all sample was lower than 0.1 but as back cavity increased the absorption coefficient increased and it moved to the low frequency with increasing the cavity space as shown in Figure 2.34.

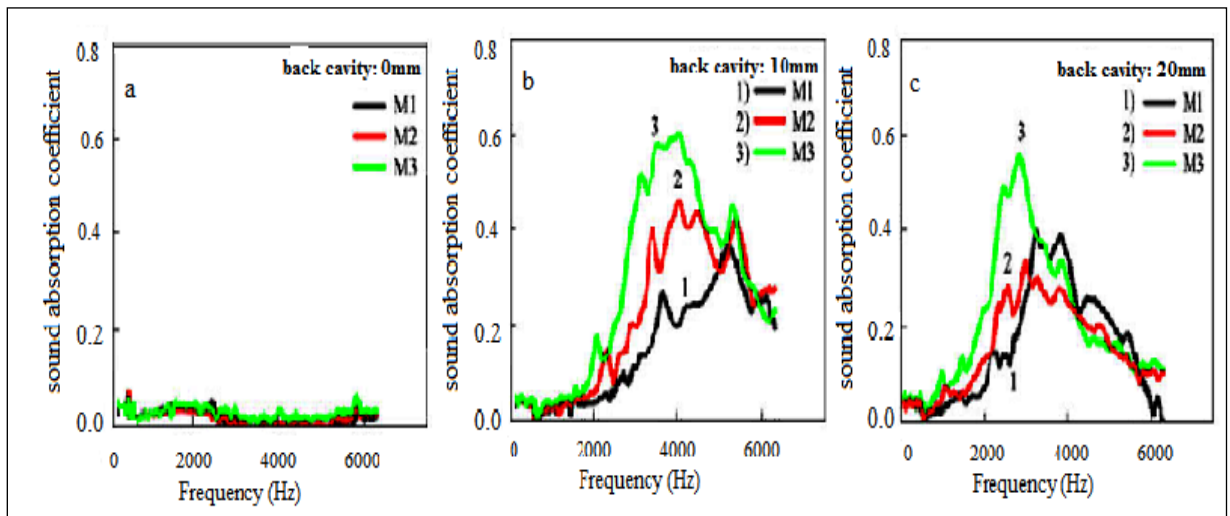


Figure 2.34: sound absorption coefficient for PAN membrane with various back cavities at a) 0mm b) 10mm c) 20mm [8]

In the second case nanofiber, PAN membrane is fixed on the top of the perforated panel with different back cavities. The absorption coefficient of the perforated panel with nanofiber membrane increased more than the perforated panel alone and it is increased with increasing the membrane thickness. The curve shifted to a lower frequency with increasing the back cavity as shown in Figure 2.35.

In the third case nanofiber, PAN membrane over the traditional acoustical material (BASF foam, fiberglass, polyester layers) with different back cavities. The absorption coefficient of traditional acoustical material with nanofiber membrane increased more than the traditional material alone as shown in Figure 2.36. Although, they did a lot of work, they did not use several layers from different types of polymer or produced mat that contain two different polymers.

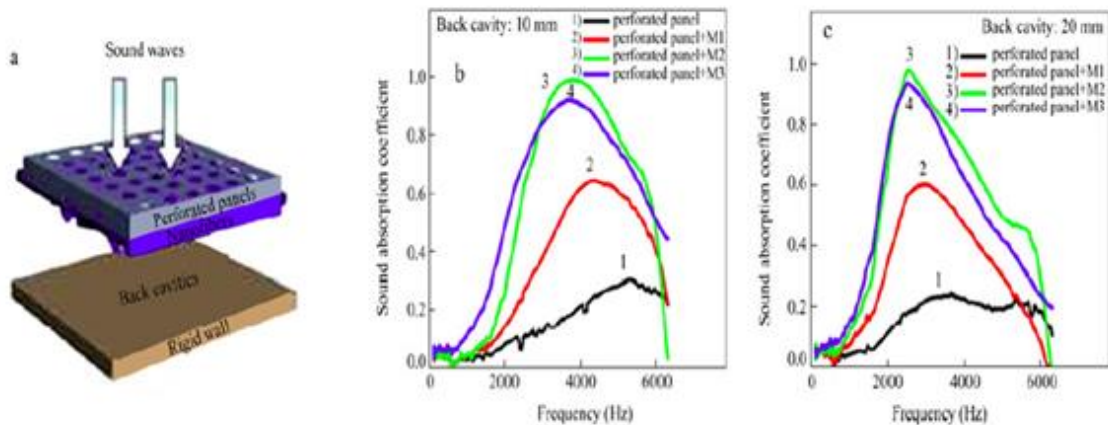


Figure 2.35: a) Drawing of sample form; b, c) sound absorption coefficient of the perforated panel with PAN nanofiber membrane [8].

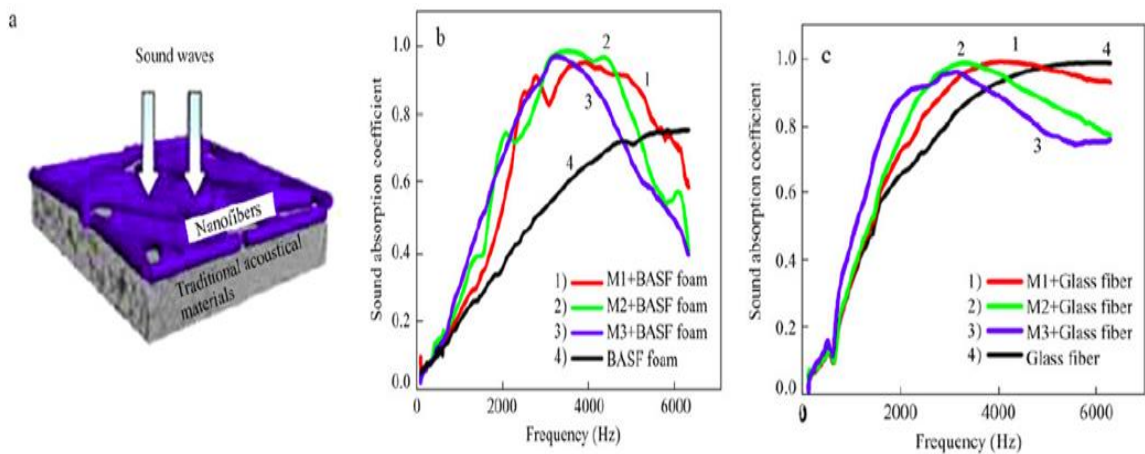


Figure 2.36: a) Drawing of sample form; b) sound absorption coefficient of BASF with nanofiber membrane c) sound absorption coefficient of fiberglass with nanofiber membrane [8]

2.7.5 Nylon (NY6)

Trematerra et al. [97] used NY6 as nanofibers membrane with fibers diameter 150 - 200nm and thickness of 10 μm to coat traditional acoustic material like foam, kenaf, felt and the result showed that nanofiber membrane improves the acoustic performance of traditional material as shown in Figure 2.37. Also, they measured the absorption

coefficient for NY6 membrane with 20mm and 30mm back cavity. However, they did not mention at which diameter the fiber mat will give better sound absorption.

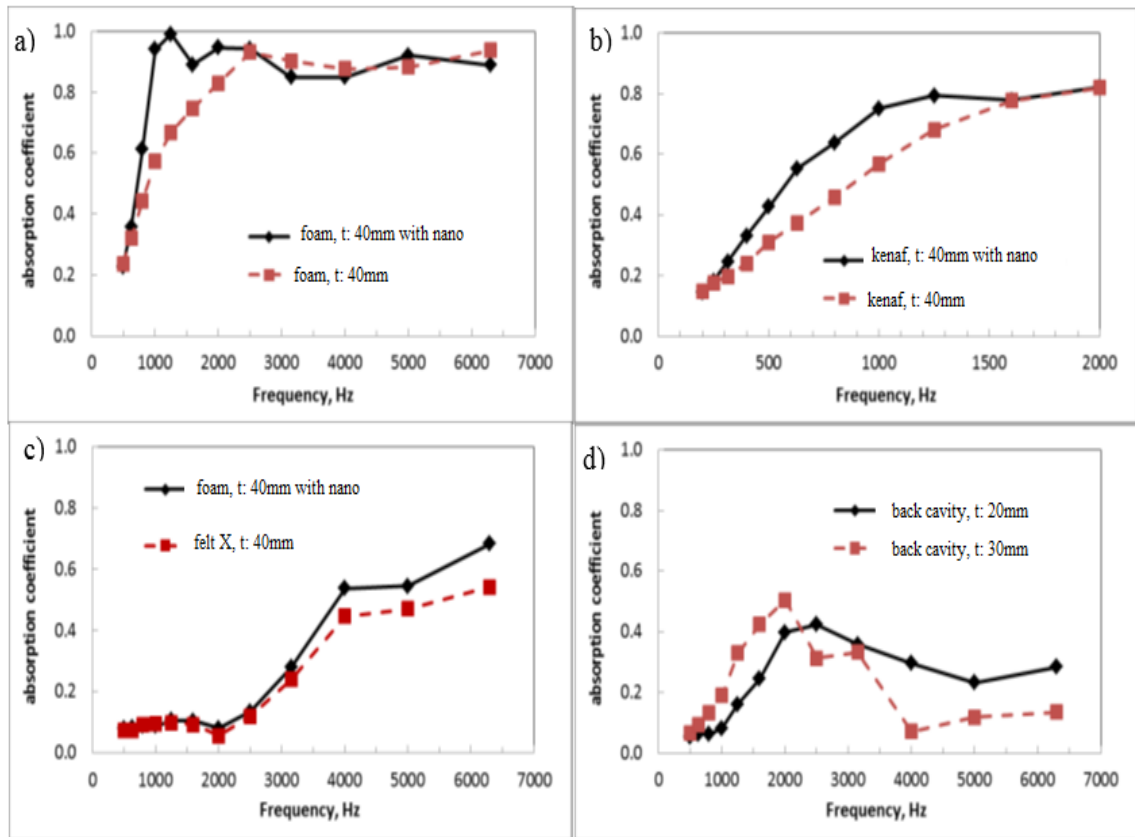


Figure 2.37: Absorption coefficient of NY6 nanofiber layer over a) foam b) kenaf c) felt d) with back cavity [97]

2.7.6 Polyvinyl alcohol (PVA)

Kalinová [98] produced PVA nanofiber membrane as acoustic absorbing material. A thin nanofiber membrane absorbed the sound wave at low frequency according to the principle of resonance membrane. She claimed that some materials have the ability to convert the acoustic energy to thermal energy. She changed two parameters in her experiments to produce PVA membrane. The first is the speed of the rotating drum, which produced fiber from its surface to obtain the different density of fiber membrane as shown in Table 2.5. The second is the distance between the collector and the drum as shown in Table 2.6. It is observed that the sound absorption coefficient increases with decreasing the fiber diameter as shown in Figure 2.38; this may be due to increasing in surface area which causes increasing in the flow resistivity and converts sound wave to vibration [99], [95].

Table 2.5: Outlet velocities of drum carry PVA solution [49]

Outlet velocity of nanofibrous material during electrostatic spinning ($\text{m} \cdot \text{min}^{-1}$)	Area density of the nanofibrous layer ($\text{g} \cdot \text{m}^{-2}$)
0.0171	28.8
0.0342	17.2
0.0855	6.3
0.1197	4.8
0.171	3.3

Table 2.6: Distance of electrodes during electrostatic spinning that determines the average diameter of nanofiber [98]

Distance of electrodes during electrostatic spinning (mm)	Average diameter of nanofibers (nm)
50	79.9
70	77.6
90	76.3
110	73.3
130	68.6

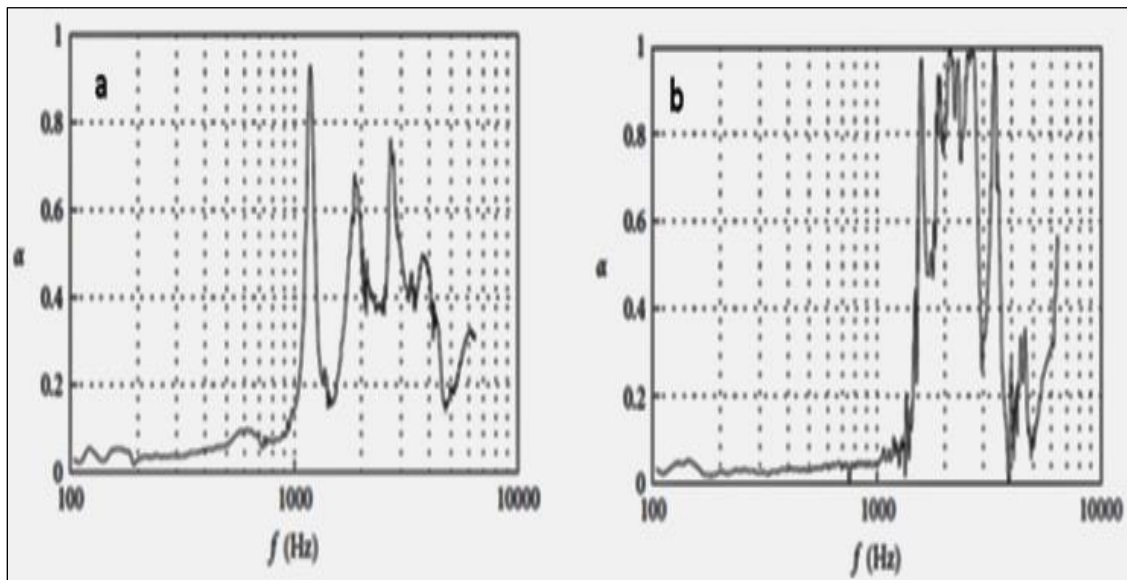


Figure 2.38: Sound absorption coefficient for collecting nanofibers at a distance a) 50mm b) 90mm [49]

The structure of nanofiber membrane can be varied by changing the conditions of the fibers production or by applying external conditions for the produced fibers. Jana

Mohrova et al. [100] exposed PVA membrane to water vapor for different duration (10 - 120 s). Also, they immersed the membrane in water for 60 s as shown in Figure 2.39.

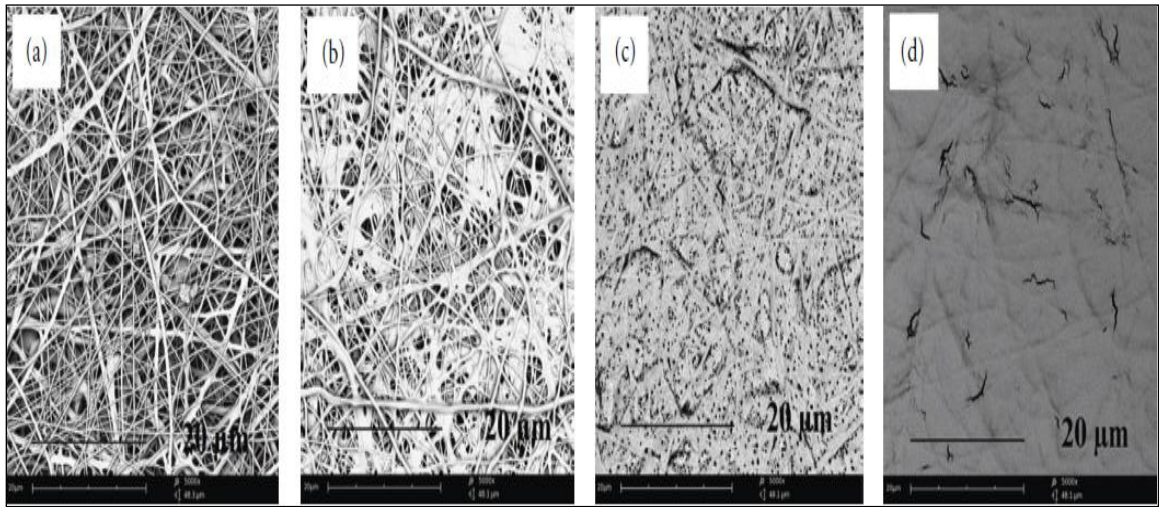


Figure 2.39: PVA nanofiber structures after exposing to water vapor for different duration a) 0 sec b) 60 sec c) 120 sec d) immersed in water for 60 sec [59]

It is obvious that there are changing in the structure shape of membrane depending on the duration of exposure to water vapor. The percentage of merged fibers increases proportional to the time of water vapor exposed. This led to changing the vibration of the resonant frequency of the thin membrane, due to weight area change. Jana et al. [100] concluded that the structure of PVA membrane has an effect on the amount of sound absorbed energy. The movement of fibers inside the structure and the inner friction between the fiber layers lead to sound absorption as shown in Figure 2.40. From that, the irregularity of a fiber's ability to absorb sound increases, but it has a limit and after that, the absorption will decrease again.

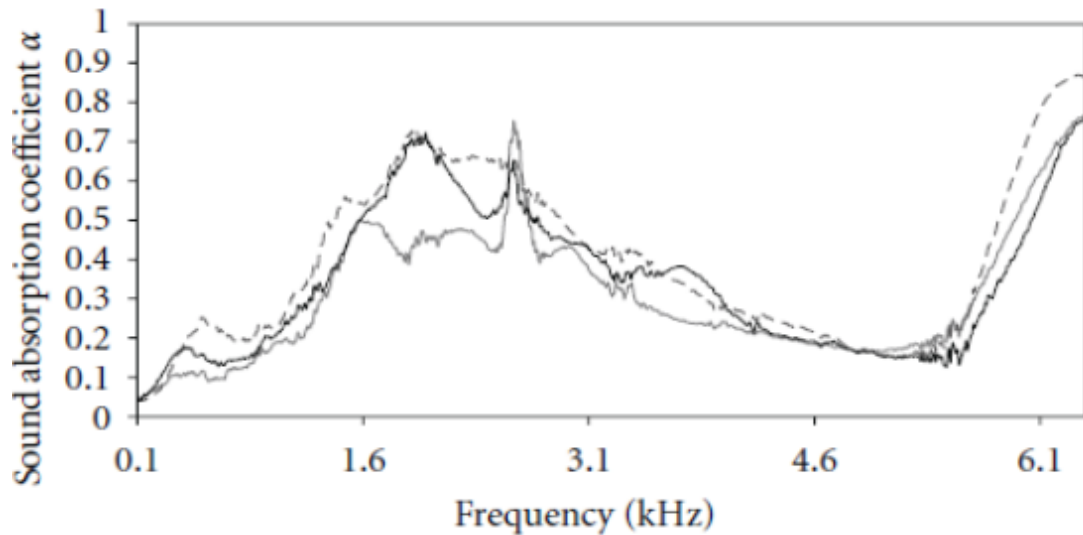


Figure 2.40: sound absorption coefficient of PVA membrane exposes to water vapor for different time —30 seconds (grey line), 90 seconds (dashed grey line) and 120 seconds (black line) [50]

2.8 Nanofiber as thermally conductive material

Carbon nanotubes (CNTs) improves the properties of nanofibers. It enhances the mechanical, electrical, and thermal properties of the material. Figure 2.41 shows the improving in electrical conductivity of polymer after the addition of CNTs. CNTs have two types, a single wall carbon nanotube (SWCNTs) and a multiwall carbon nanotube (MWCNTs). Electrospinning polymers, which contain CNTs show good properties in mechanical, electrical and thermal properties, which candidate it to work as a thermally conductive material in heat dissipation of the electrical device to have high performance for long time [10, 62, 63, 64].

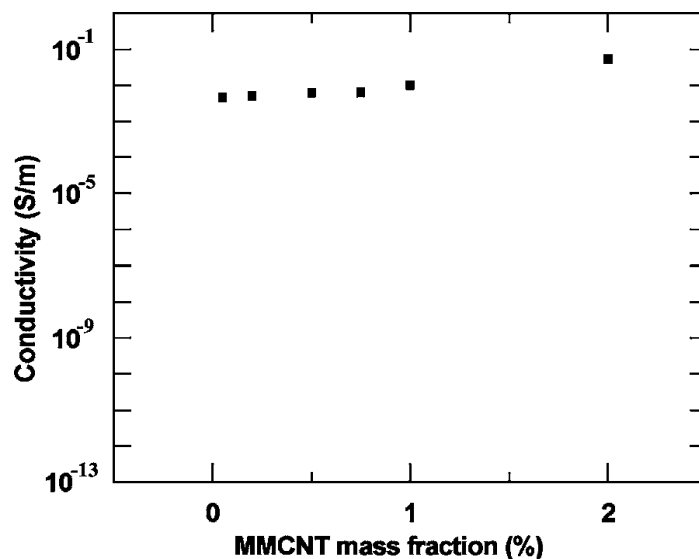


Figure 2.41: Relation between the conductivity of the single composite fibers and a different mass fraction of MWCNT [10]

The greatest challenge in doing composites with CNTs is getting the uniform dispersion in the polymer matrix. The agglomerations may be formed due to the van der Waals force between the individual CNT and decrease the anticipated properties of nanocomposites. For better dispersion low concentration of CNTs were added to a composite matrix. Some surfactants may be added to improve the dispersion of CNTs as sodium dodecyl sulfate (SDS), polyvinylpyrrolidone, natural polysaccharide (gum Arabic) and triton [12, 64, 66].

Mccullen et al. [107] added MWCNTs to polyethylene oxide (PEO) with different concentration (0.35 -1wt%) and they found that the electrical conductivity is improved by increasing the percent of MWCTs up to concentration of 1wt% and stay constant even for more concentration as shown in Figure 2.42 [107].

Yarns et al. [108] noticed that the straight alignment of CNTs in the electrospun fibers becomes better as the diameter of fiber become lower. Also, Khan et al. [103] found that the thermal conductivity of nanofiber polymer increases with increasing the percent of CNTs up to 4wt% in the solution and the conduction process become easier. This may be due to the increasing of polarizability value of composite fibers as shown in Figure 2.43. Biercuk et al. [109] added CNTs to epoxy by 1wt% and its thermal conductivity increased by 70%. However, there are no trials to investigate the effect of adding CNTs to improve the sound absorption of nanofiber.

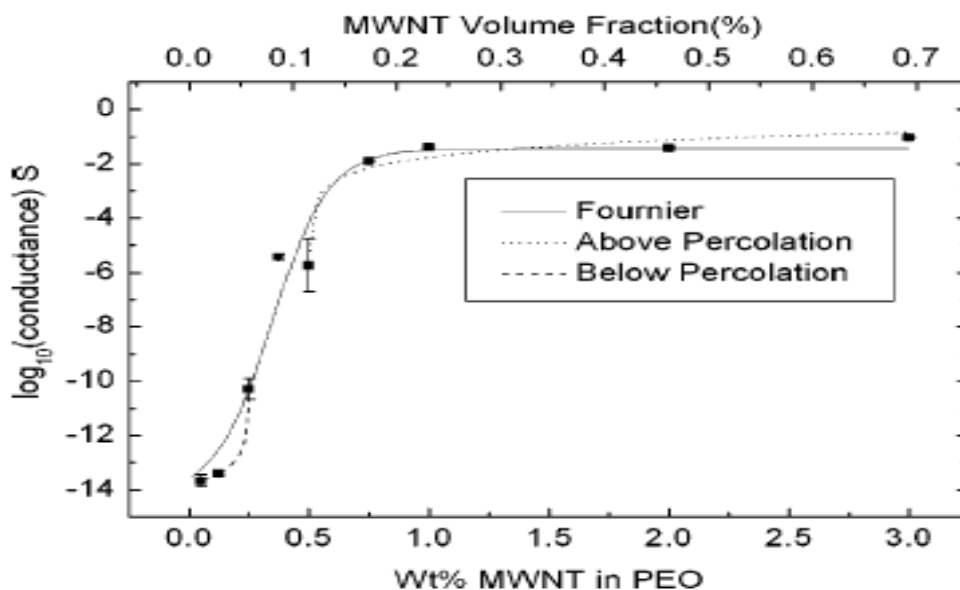


Figure 2.42 : the relation between electrical conductance and concentration of MWNT dissolved in PEO by wt% and upper scale measure the volume fraction of MWNTs [107]

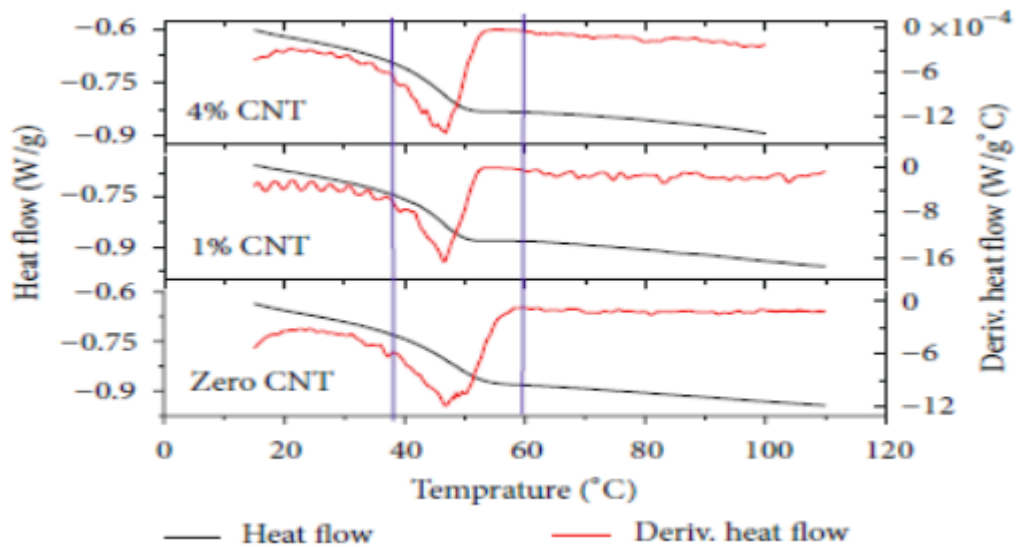


Figure 2.43: Effect of adding the different percent of MWCNTs (0wt%, 1wt% , and 4wt%) to nanocomposite fibers on heat flow and heat derivative of nanofibers [103]

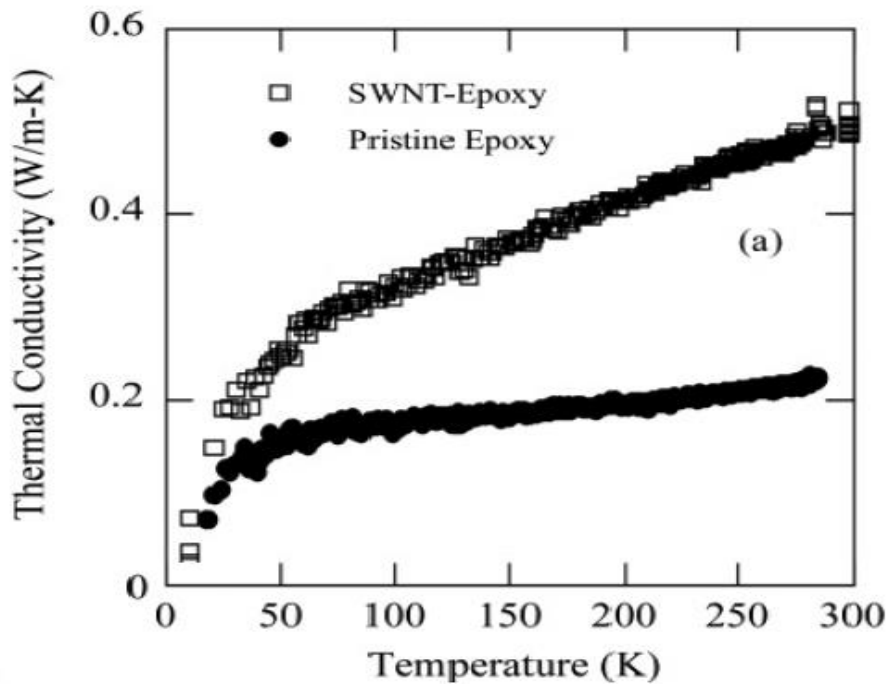


Figure 2.44: Relation between thermal conductivity and temperature for epoxy before and after add 1wt% SWCNT[109]

2.9 Discussion

A large number of studies show that nanofibers produced by electrospinning have good properties, which can be useful in many applications. The addition of fillers to electrospun fibers improves its mechanical and physical properties. This work aims to fabricate innovative materials that have good sound absorbing properties, particularly in low to mid frequency ranges. Very few studies could be found on the use of electrospun

fibers for mitigation of sound propagation using nanofibers. The effects of adding filler to nanofiber mats on the sound absorption properties have not addressed in the literature at all. Therefore, this work highlights the technique of improving the mechanical and physical properties of nanofibers by adding fillers like carbon nanotubes, graphene, wollastonite, and fiberglass in electrospinning process. The mechanical and the acoustic properties of these nanofibers were measured and characterized. In addition, mats containing two types of polymers and multiple layers of mats were studied. Therefore, the investigation of this work will cover as given below:

- 1- The interaction between the different parameters that affect the production of nanofibers
- 2- The effect of using two types of nanofibers polymers in one mat on the sound characteristics
- 3- Using several layers of nanofiber mats from the same or different types of polymers and investigate their effect on the sound and thermal characteristics.
- 4- Investigate the effect of using graded fiber mats on the sound characteristics
- 5- The effect of adding fillers in nanocomposite mat on the sound characteristics
- 6- Investigate the effect of adding fillers such as carbon nanotubes, graphene, fiberglass and wollastonite to nanofibers
- 7- Electrospinning polymer that has hydrophobic properties that will be good as a water repels beside sound insulation

Chapter 3: Experimental setup and samples preparation

3.1 Introduction

In this work, the nanofibers were produced using an electrospinning process, consisting of a high voltage source, a precision pump, and a collector to collect the fibers. Polymers were dissolved in a suitable solvent and were electrospun to produce the nanofibers. The mechanical and physical characteristics of the nanofibers were carried out using Dynamic Mechanical Analyzer (DMA, Q800), Differential Scanning Calorimetry (DSC, Q20) and Thermogravimetric Analyzer (TGA, Q50). Finally, the sound absorption coefficient of the fabricated mats was measured using a house-built impedance tube.

3.2 Chemicals and solvents

In this study, different types of chemicals and materials were used. The polymers of interest were polyvinyl alcohol (PVA) with a molecular weight of 130,000 g/mol, polyvinyl chloride (PVC) with a high molecular weight, and polystyrene (PS) with a molecular weight 190,000 g/mol, while sodium dodecyl sulfate (SDS) was used as a surfactant. All these chemicals were purchased from "Sigma-Aldrich". In these experiments different types of solvents were used; N, N-Dimethylformamide (DMF) purchased from "ACP" Montreal, Quebec; Chloroform purchased from Fisher scientific. 1-methyl-2pyrrolidinone (MP) with a grade of >99.7%, purchased from "Sigma-Aldrich", and distilled water. Wollastonite (CaSiO₃) type 520U was supplied by Fibertec, USA. Milled fiberglass of 2 μ m diameter was supplied from Owens corning company. Multi-wall carbon nanotubes (MWCNTs) of length (10-20 μ m) with outer diameter (30-50nm) as well, graphene nanoplatelets grade M with average particles diameter 5 μ m and surface area (120- 150 m²/g) from XGNP both were obtained in courtesy of Dr. Simon Park of University of Calgary.

PVA was selected for the study due to its good biodegradability, has several applications in many industrial fields, and shows a good indication as sound absorbing materials [98], [110], [111]. Polystyrene has a good thermal and acoustic insulation properties when it is used in a foam form [112],[113], [114]. In addition, it has good hydrophobic properties. This gives an additional privilege so it is worth the trial to be used as electrospun mat for absorbing sound. PVC is used as high-density foam for sound insulation [115],[116]. MWCNTs has unique and exceptional physical properties and is used as a filler in composites to improve the mechanical, thermal, and electrical properties [3], [106],

[101]. Adding graphene to the polymers matrix shows an improvement in the mechanical and thermal properties [117]. Fiberglass improves the thermal properties of nanofibers, it is also, used as a sound absorbing material [118], [119]. Wollastonite was used as a filler and it shows a promising reinforcement for the composite matrix [59],[11].

3.3 Mechanical and physical characterization equipment

3.3.1 Thermogravimetric analyzer (TGA)

Thermogravimetric analysis (TGA) was carried out using Q50 (TA Instruments, USA) to investigate the thermal stability of the fibers. During the TGA tests, nitrogen environment was introduced around the sample to avoid oxidative degradation. Also, during the experiments, the temperature range was from 0°C to 600°C at a heating rate of 10 °C/min under nitrogen atmosphere. Approximately 3.5 mg of sample was used for each test. T_{onset} is the degradation temperature, at which the temperature slope changes.

3.3.2 Differential scanning calorimeters (DSC)

The thermal transition properties of nanofiber mats were measured with differential scanning calorimeter using Q20 (TA instruments, USA). The samples were heated from room temperature to 350 °C with a heating rate 20 °C/min and held for 5 minutes to remove any previous thermal history. Then, the specimens were cooled at a rate 20 °C/min up to 40 °C. Finally, the thermal data was collected while reheating the sample from 40 °C to 350 °C at 20 °C/min.

3.3.3 Dynamic mechanical analysis (DMA)

Dynamic Mechanical Analysis Q800 (TA instruments, USA) was used to measure the tensile strength of nanofiber mats at 30 °C with ramp force 0.5 N/min. The sample was prepared in a rectangle shape with a width (5- 7mm) and length (15- 20mm). The sample thickness was measured using a digital optical microscope. For this analysis, some conditions like maximum force=18 N, an initial preload force= 0.05 N. The average values of four tested samples were calculated and reported for Young's modulus (E), tensile strength (σ_t), and elongation at break (ϵ_b).

3.3.4 Scanning electron microscopy (SEM) and digital optical microscope (DOM)

The morphological characteristics of electrospun fibers were investigated by using a Scanning Electron Microscopy (SEM) (JSM 6060) and digital optical microscope (DOM) (KEYENCE VHX-1000). The diameter of fibers was measured by analyzing the pictures of SEM using ImageJ software. ImageJ is a public domain Java based image processing

and analysis program that was used to estimate the diameter of fibers from the images obtained from the microscope. The program code is available free online from the link <http://imagej.nih.gov/ij/features.html> [120].

3.4 The Electrospinning setup

The main components for the electrospinning setup used in this work were high voltage source model ES100 purchased from Gamma High Voltage Research Inc (USA), precision pump model NE-1600 purchased from New Era Company (USA), and rotating collector with varying speed. The polymer solution was loaded into a syringe with a metallic needle, which was connected to the source of high voltage. As the solution started to extrude from the tip of the syringe needle with the adjusted flow rate, and the suitable high voltage, the fibers began to deposit over the surface of the rotating collector drum, which was connected to the ground. The electrospinning process was housed in a closed acrylic cabinet to avoid any injury from the high voltage or the inhalation of vapor coming from the solution. Figure 3.1 shows the electrospinning setup used in this work.

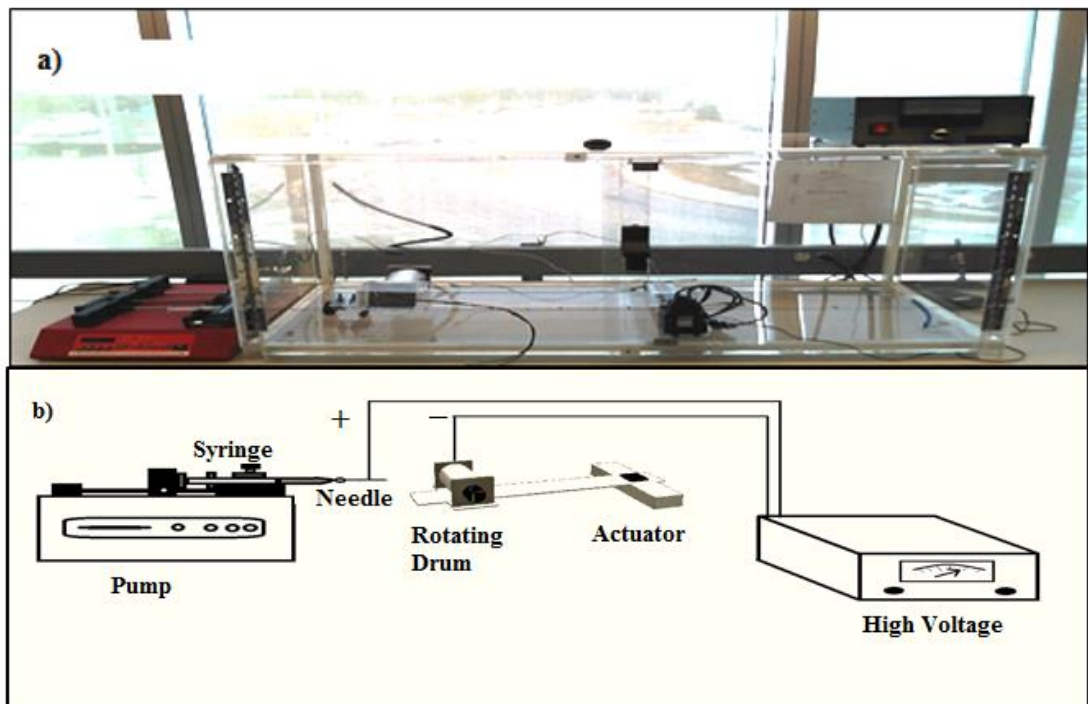


Figure 3.1: a) Electrospinning lab setup b) Schematic lab setup

3.5 Material formulations used

3.5.1 Solution preparation

Different types of polymers were used in this work. Each polymer had certain ranges of concentration at which it could produce nanofibers using electrospinning technique. Table 3.1 shows the concentration ranges for each polymer which were used in this work.

Table 3.1: polymers concentrations range

	Type of polymer	Concentration range wt%
1	PVA	7-15
2	PS	10-30
3	PVC	10-15

PVA was weighted and dissolved in distilled water and stirred at 70 °C for about 3h using magnetic stirrer hot plate. PS was weighted and dissolved in DMF and stirred for 4h using magnetic stirrer. PVC was weighted and added slowly to the solution of DMF at 60 °C for 4-5h and stirred using magnetic stirrer hot plate

3.5.2 Composite matrix

The filler materials were added to the solution with different concentrations according to the polymer weights. Table 3.2 shows the filler concentrations in the polymer solutions. The filler was added to the solvent and sonicated for 30 min followed by the addition of the polymer and then the solution was moved to the magnetic stirrer. For MWCNTs and graphene, the surfactant (SDS) was dissolved in the solvent first to improve the fillers dispersion and prevent the fillers agglomeration.

Table 3.2 : Filler percent in polymer solution

Polymer \ Filler	PVA	PVC
MWCNTs	(1.5 – 5- 10) wt/wt%	(5- 10) wt/wt%
Graphene	(5- 10) wt/wt%	(5- 10) wt/wt%
Fiberglass	----	(5- 10- 20- 30) wt/wt%
Wollastonite	(5- 10- 20) wt/wt%	----

3.5.3 Electrospinning process

After the solution preparation, the solution was loaded into a 5 ml syringe with 21 gauge needle and electrospun at the planned conditions. The produced nanofiber mats had the dimension of (12cm X 16cm). A circular part of this mat was assembled over a ring with 10cm diameter to measure the sound absorption characteristics. The remaining mat material had been used in the mechanical and physical properties characterization tests.

3.6 Acoustic characterization measurements

According to the acoustic measurement, the absorption coefficient is the most significant property of any sound absorbing material. It can be a judgment whether the material can be used as a sound absorber or not. There are three main standardized methods to measure the sound absorption coefficient: transfer function method (ISO 10534-2) [121], standing wave ratio (ISO 10534-1) [122] and reverberation chamber (ISO 354) [123]. The first two methods measure the absorption coefficient at a normal incident angle but reverberation chamber measures at a random incident angle and requires a large sample to be tested in a space of which volume may be more than 150 m³ [124].

3.6.1 Impedance tube

Impedance tube was developed in the lab according to ASTM1050 and ISO10534-2 [125], [126] to measure acoustic properties of nanofiber membranes as shown in Figure 3.2. The diameter of the impedance tube is 10cm and the cut off frequency is 2000Hz according to the equation (3.1). The length of the tube is 117cm which is greater than three times its diameter to avoid any non-plane sound wave. The sound source (speaker) is enclosed in a wooden box and isolated with a sound absorbing material to prevent any flanking transmission to the microphones. The speaker is connected to a signal generator, which produces a white noise at all frequency ranges using a sine wave. Three 1/4" microphones holes are drilled through the wall of the tube to position the microphones. The first hole from the speaker side is at a distance larger than three times tube's diameter to dissipate the cross modes come from the speaker. The distance between each two hole covers a certain range of frequency as shown in Table 3.3. A stainless steel sample holder with a movable piston allows the adjustment of the back cavity depth. It is attached at the other end of the impedance tube and sealed with clay to prevent any acoustic leakage. The piston is made from aluminum with 5cm thickness and it resembles a closed acoustic termination.

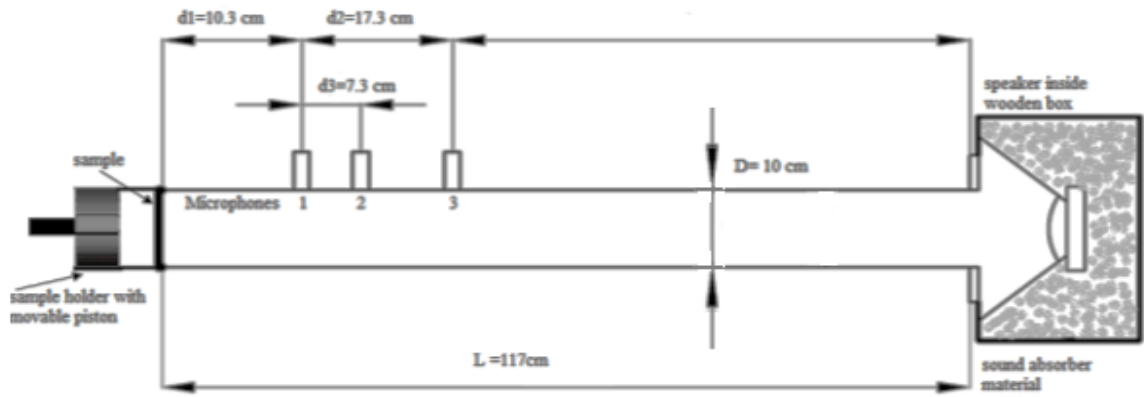


Figure 3.2: Schematic of Impedance tube

Table 3.3: Measurement range according to distance between two microphones

Distance between two microphones (m)	The corresponding frequency measurement range	
	low range (Hz)	high range (Hz)
0.073	234	2000
0.173	99	892
0.100	171	1543

The transfer function method is implemented for the measurement of the acoustic absorption coefficient because it is the most suitable method for impedance tube and small samples. The transfer function method is less time consuming than standing wave method. Two microphones are connected with data acquisition system that conveys the signals recorded to the PC. Lab View software is used to analyze the signals and calculates sound absorption coefficient of the membrane.

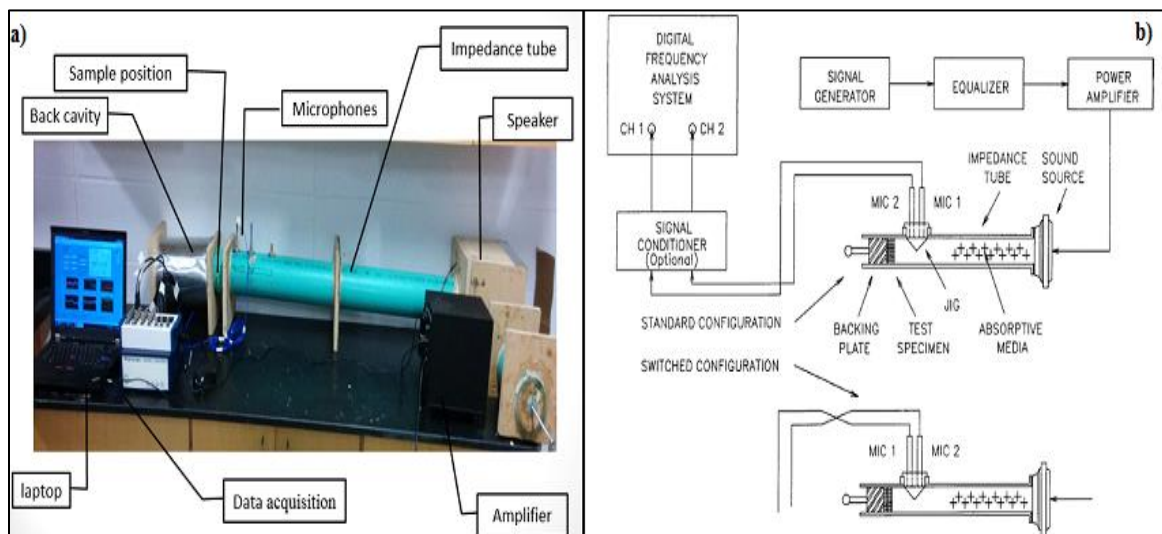


Figure 3.3: a) Impedance tube setup b) schematic of measuring Impedance and Absorption of Acoustical Materials [125]

The sound source was placed at the end of the tube and the tested specimen was placed on the other side as shown in Figure 3.3 (b). The decay of sound pressure wave was measured at two different positions on the wall of the tube. The normal incidence absorption coefficient for the acoustical material was calculated by processing an array of complex data from the measured transfer function. Frequency ranges depend on the tube diameter and the separating distance between the two microphones [125]. The following equations show the calculation method for sound absorption, reflection coefficient and cut off frequency. The latter is the maximum frequency that could be measured corresponding to the tube's diameter, and it is given by the equation.

$$F_c = 1.84C/\pi d \quad (3.1)$$

Where C is the speed of the sound [m/s], and d is the tube diameter [m].

The sound reflection factor (r) is measured at normal incidence, and the transfer function (H_{12}) between the two microphone positions in front of the tested specimen is obtained using the relation:

$$H_{12} = S_{12}/S_{11} \quad (3.2)$$

Where

$$S_{12} = p_2 \cdot p_1 \quad (3.3)$$

$S_{12} \dots$ is the cross spectrum between the two microphones; $S_{11} = p_1 \cdot p_1$ is the auto-spectrum of the Microphone 1.

$$r = \frac{H_{12} - H_I}{H_R - H_{12}} e^{2jk_o x_1} \quad (3.4)$$

Where H_I is the transfer function of the incident wave, H_R is the transfer function of the reflected wave. These two transfer functions are calculated as shown in equations (3.6) and (3.7). x_1 is the distance between the tested specimen and the first microphone, and k_o is the wave number defined as

$$k_o = \frac{2\pi f}{c} \quad (3.5)$$

Where f is the frequency in hertz

$$H_I = e^{-jk_o(x_1-x_2)} = e^{-jk_o s} \quad (3.6)$$

$$H_R = e^{jk_o(x_1-x_2)} = e^{jk_o s} \quad (3.7)$$

Where the separation between the two microphones is $s = x_1 - x_2$.

The normal incidence sound absorption coefficient is:

$$\alpha = 1 - |r|^2 \quad (3.8)$$

The specific acoustical impedance ratio is

$$\frac{z}{\rho c} = \frac{R}{\rho c} + \frac{jX}{\rho c} = \frac{1+r}{1-r} \quad (3.9)$$

Where R is the real component of the impedance, X is the imaginary component of the impedance and ρc is the characteristic impedance.

$$s = c/2f \quad (3.10)$$

$$f_{\text{lower}} = 0.1c/2s \quad (3.11)$$

$$f_{\text{upper}} = 0.8c/2s \quad (3.12)$$

$$f_{\text{ideal}} = c/4s \quad (3.13)$$

3.6.1.1 Validation of impedance tube

The impedance tube has been validated by measuring the reflection coefficient of unflanged open end tube. The measured data was compared with the theoretical reflection coefficient of unflanged open end tube given by the equation:

$$R = 1 + 0.01336(ka) - 0.59079(ka)^2 + 0.33576(ka)^3 - 0.06432(ka)^4 \quad (3.14)$$

Where R is the magnitude of the reflection coefficient, a is the radius of the tube, and k is the wave number ($=2\pi f/c$). Figure 3.4 shows that the measurements and the theoretical values for the reflection coefficient of the unflanged open-end tube are in a good agreement over the measuring frequency range.

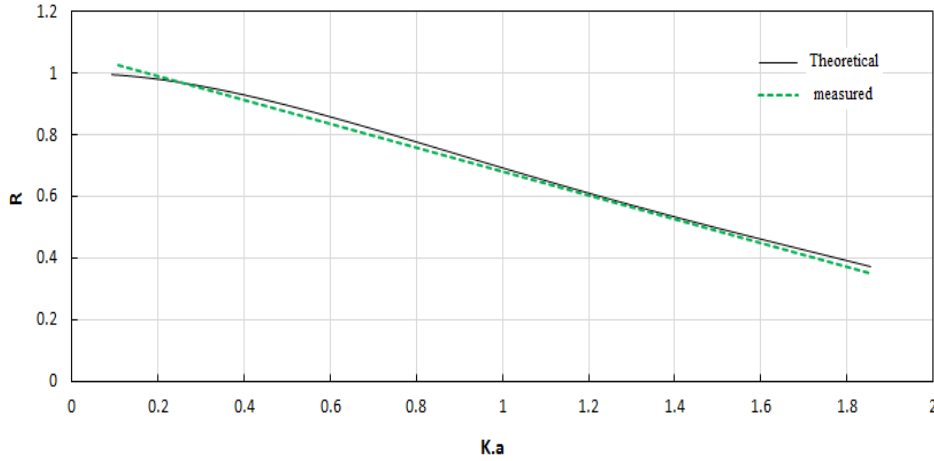


Figure 3.4: Theoretical and measured reflection coefficient of unflanged open-end tube

3.6.2 Microphone

Microphones are used to measure the acoustic pressure. The microphones have 1/4 inch diameter and are manufactured by PCB Pizotronics (model number: 377A12). The microphone is amplified by a PCB Pizotronics preamplifier (model number: 426B03). This microphone-preamplifier arrangement is powered by a PCB Pizotronics Signal conditioner (model number: 482C15). The whole arrangement is calibrated by a G.R.A.S pistonphone (model number: 42AB) and it gives a sensitivity of 0.2545 mV/Pa. The microphones are fixed on the top side of the impedance tube.

3.6.3 Data acquisition

The acoustic pressure signal is obtained from a National Instruments data acquisition card (model number: BNC-2110) connected to the desktop computer. The signal is recorded and analyzed by using the National Instruments LabVIEW software (version: 8.6). A code for measuring the sound absorption coefficient, sound reflection coefficient, and normalized surface impedance were developed using lab view software and the interface of the program shown in Figure 3.5 . A code for measuring the signal and performing FFT analysis was designed and calibrated with known signals and pistonphone measurements.

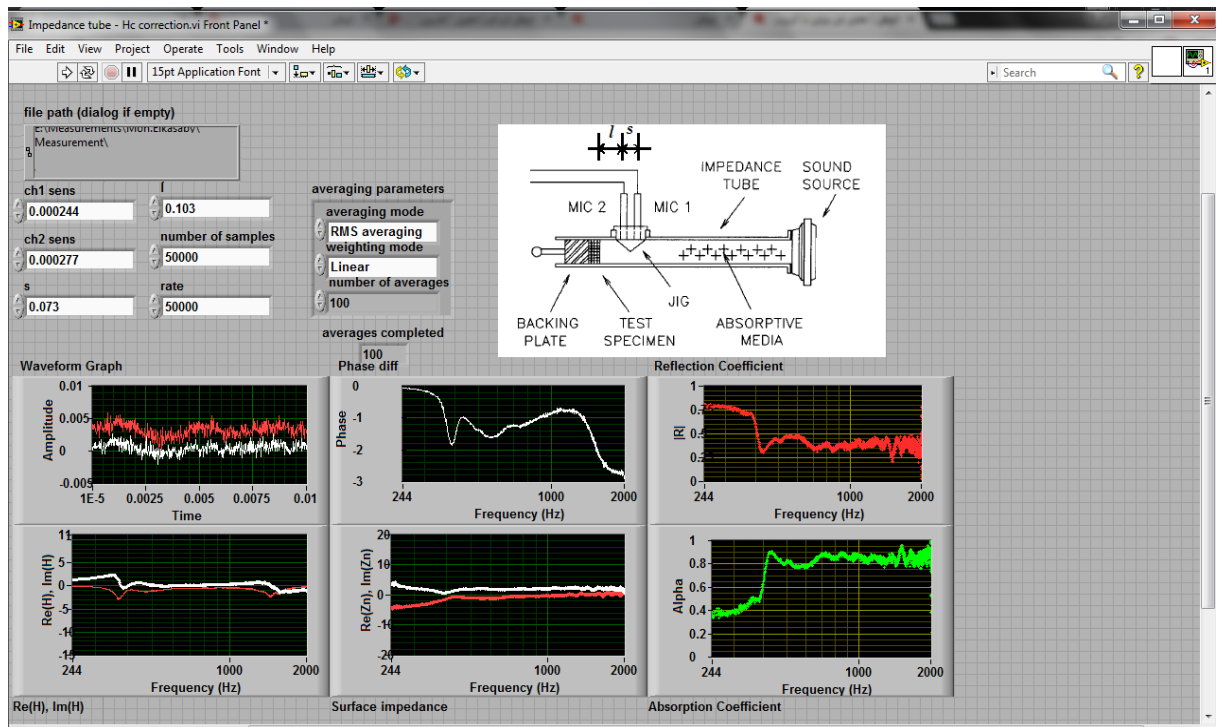


Figure 3.5: Lab view interface for acoustic measurement

3.6.4 Measurement of samples sounds absorption coefficient

After collecting the nanofiber mat from the collector drum. It is loaded to the sample holder ring using glue. The impedance tube is connected to the microphone, signal generator and data acquisition as shown in Figure 3.3. The speaker is turned on for 10 min before running the experiment to adjust the temperature inside the tube. The microphone is calibrated and the mismatch correction is calculated before the sample test. The sample is mounted to the sample holder at the end of impedance tube. All the measurements have been taken as output file from LabView software and the absorption and reflection curve are drawn, using MS excel.

Chapter 4: Modeling and optimization of electrospinning of polyvinyl alcohol (PVA)

4.1 Introduction

The electrospinning process is an economical and simple process for nanomaterial fabrication. [127]. The three main components of the electrospinning process in this work are a high voltage source, a syringe pump with a needle of small diameter and a rotating collecting drum as shown in Figure 3.1. These parameters that effect electrospinning can be optimized to produce electrospun fibers with desired morphologies and diameters[57], [129–131]. Many researchers have extensively studied the effects of these parameters. Deitzel et al. [57] used Polyethylene oxide (PEO) at a concentration range from 4 to 10wt% and reported that the fiber diameter increased with increase in the polymer concentration. Boland et al. [131] used poly (glycolic acid) and came to the same conclusion. Demir et al.[43] and Reneker et al. [6] also found the significant dependence of fiber diameter on concentration but showed that the fiber diameter did not change significantly with changes in the applied voltage. However, other researchers claimed that the diameter of Poly (l- lactide- co-e-caprolactone) fiber decreased with the increase in the applied voltage [133, 134] but the effect of the high voltage is not significant compared to the polymer concentration. Sukigara et al. [49], [134] discussed the effect of the electrospinning parameters (e.g. electric field, tip-to-collector distance and concentration) for Bombyx mori silk on the morphology and the fiber diameter. They found that the solution concentration is the most important parameter in producing uniform fibers having diameters less than 100nm.

The theory and the dynamics of the electrospinning process are complex, and several parameters affect fiber production. Many researchers have tried to model the electrospinning process. However, the fluid jet motion is chaotic in nature and is not readily subjected to the development of accurate models. Karatay & Dogan [135] used an external electric field to focus the deposition in a small area of interest and developed a model for it. Hohman et al. [136] and Reneker et al. [137] demonstrated that repulsive forces on the charged fiber are responsible for the chaotic random motion and developed a model for the onset of instability.

Some models describe the shape of the jet and model the jet tracks due to the change in physical parameters [138]. However, this is limited to the initial stable region. Moreover, some models show the effect of adding salts (e.g. NaCl, LiCl, and NH₄Cl) to increase the conductivity and study its effect on the final fibers' shape [139].

None of these studies attempt to model the effects of more than two or three parameters due to the complexity of the electrospinning phenomenon. In such cases, statistical models can be developed and effectively used to optimize the process. A literature search yielded only few studies in which statistical models were used to optimize the electrospinning process. Yordem et al. [140] modeled concentration, high voltage and collector distance for PAN nanofibers using RSM and found that the concentration played a significant role compared to the other two parameters. Sukigara et al. [134] studied regeneration of Bombyx mori silk by electrospinning. In addition, they applied RSM methodology and found an optimum processing window for specified values of concentrations and voltages. Dong et al. [141] used the Taguchi design to model electrospinning of PLA/HNT composite and found the HNT concentration and applied voltage to be effective. They have studied effects of voltage, feed rate, collector distance, and HNT concentration. Gu et al. [142] modeled the effect of two parameters, concentration, and high voltage, on the fibers' diameter and found that the concentration has a main significant effect on the diameter. Considerable opportunities exist for the development of such models for prediction and/or optimization of various electrospinning production systems.

RSM has been applied successfully for several materials and process optimization studies such as including thermoplastic elastomers, diamond-like carbon films, and polyvinyl alcohol hydrogels [143],[144],[145]. This approach has the advantage of taking into account the combined effects of several parameters. It uses statistical techniques to establish an empirical model from the experimental data [146]. RSM provides an overview of the impact of processing parameters on the average fiber diameter. This Chapter investigates the parameters that affect the production of PVA microfiber and optimizing the fiber diameter in order for it to work as a sound absorption membrane. Some studies related the fiber's diameter to the sound absorption coefficient. They claimed that the relation is inversely proportional [98, 99]. Modeling and optimization of the electrospinning process parameters will be discussed by applying the principles of

design of experiments, analysis of variance and response surface methodology (RSM) to produce PVA fibers with the optimal diameter. Five parameters (i.e. concentration, flow rate, high voltage, the speed of rotating collector, and the distance between needle tip and collector) are investigated in this Chapter in order to control and predict the average fiber diameter of PVA.

4.2 Experimental setup, materials, procedure, and theory of experimental design

The experimental setup is shown in Figure 3.1. It consists of a precision syringe pump filled with a polymer solution, which flows out from a needle connected to a high voltage source. The charged solution accelerates towards a grounded electrode causing the polymer to stretch and the solvent to evaporate. The grounded electrode is a rotating drum on which the polymer fibers are collected. The solution of PVA, with three different concentrations, is prepared by dissolving the PVA in distilled water and stirring for 3h at 70°C. The morphology of electrospun fibers is investigated by using a digital optical microscope (KEYENCE VHX-1000). The diameter of fibers is measured by the analysis of optical microscope micrographs using image J software. About one hundred measurements were recorded randomly for each sample to calculate the average diameter. The design of experiments technique is applied to optimize the electrospinning process. Analysis of variance (ANOVA), and orthogonal array (L27OA) are employed to analyze the influence of the process parameters. Another objective is to build a mathematical model of the polymer fiber diameter as a function of significant process parameters using response surface methodology (RSM)

Taguchi's robust design is used to provide a simple and systematic approach in order to optimize the fiber diameter. Orthogonal arrays (OA) are the main tools used in the robust design. Taguchi's robust design evaluates the mean performance and its variation by applying two arrays. Inner array consists of control variables and an outer array consist the noise variables. Taguchi uses the quality loss to combine the effects of mean performance and performance variation [148, 149]. An L27 orthogonal array based on the Taguchi robust is employed for experiments. L27 has 27 rows corresponding to the number of tests (26 degrees of freedom) with maximum 13 columns at three levels [148].

The design consists of 27 tests in which the first column is assigned to high voltage (KV), the second column to concentration weight percentage (wt%), the third column to rotational speed (RPM), the fourth column to collecting distance (cm), and the fifth column to flow rate (ml/h) as shown in Table 4.1. Tests are replicated, and the average values of the diameter of the fiber are obtained. The five factors are applied at three levels. The full factorial array is L243. However, fractional factorial array L27OA is used in this study. The experimentally observed fiber diameter value is “the lower the better” (LB) as smaller fiber diameter of the proposed material can improve some specific properties (e.g. the sound absorption coefficient).

Table 4.1: Assignment of levels to control factors

		Symbol	Level 1	Level 2	Level 3
Control Factors	High voltage (KV)	A	15	20	25
	Concentration (wt%)	B	7	12	15
	Rotational speed (RPM)	C	500	1500	2500
	Collecting distance (cm)	D	5	10	15
	Flow rate (ml/h)	E	0.1	0.2	0.3

4.3 Results and analysis

The five parameters are evaluated using ANOVA. Data from the Taguchi design is used for this purpose. Table 4.2 shows the 27 runs according to the Taguchi design, which incorporates five parameters each varied at three levels and the resulting fiber diameters. It demonstrates the influence of control variables on the measured responses. It is observed that the smaller diameters are obtained in runs 19, 3, and 1. It is noticed that all these occur at the lowest concentration used. Minimum diameters at these runs varied in the range of 0.51 to 0.59 micrometer. The higher values ranged up to 1.87 micrometers.

Table 4.2. Experimental results of fiber diameter using L27OA to plan experimentation.

Run no.	[A]	[B]	[C]	[D]	[E]	Fiber Diameter(μm) (Average Value)
1	15	7	500	5	0.1	0.59 ± 0.07
2	15	7	1500	10	0.2	0.64 ± 0.08
3	15	7	2500	15	0.3	0.57 ± 0.06
4	15	12	500	10	0.3	0.79 ± 0.09
5	15	12	1500	15	0.1	1.53 ± 0.13
6	15	12	2500	5	0.2	1.27 ± 0.11
7	15	15	500	15	0.2	1.87 ± 0.19
8	15	15	1500	5	0.3	1.45 ± 0.12
9	15	15	2500	10	0.1	0.67 ± 0.07
10	20	7	500	5	0.1	0.93 ± 0.08
11	20	7	1500	10	0.2	0.86 ± 0.06
12	20	7	2500	15	0.3	0.88 ± 0.05
13	20	12	500	10	0.3	1.22 ± 0.12
14	20	12	1500	15	0.1	1.30 ± 0.11
15	20	12	2500	5	0.2	1.42 ± 0.16
16	20	15	500	15	0.2	1.59 ± 0.12
17	20	15	1500	5	0.3	1.73 ± 0.15
18	20	15	2500	10	0.1	1.40 ± 0.13
19	25	7	500	5	0.1	0.51 ± 0.03
20	25	7	1500	10	0.2	1.23 ± 0.11
21	25	7	2500	15	0.3	1.55 ± 0.15
22	25	12	500	10	0.3	1.03 ± 0.1
23	25	12	1500	15	0.1	1.05 ± 0.12
24	25	12	2500	5	0.2	1.42 ± 0.13
25	25	15	500	15	0.2	1.47 ± 0.11
26	25	15	1500	5	0.3	1.35 ± 0.11
27	25	15	2500	10	0.1	1.36 ± 0.12

4.3.1 Evaluating effects of control parameters using ANOVA:

The results shown in the previous table were investigated using analysis of variance (ANOVA) based on the mean response values for each run and the statistics of the analysis are shown in Table 4.3. The results show that the concentration percentage has a major effect on the diameter size and is significant at 99% confidence level, while the flow rate has a slightly lower effect and is significant at 90% confidence level. The high voltage and collecting distance are not significant with 90% confidence level. The

rotational speed (RPM) is considered an insignificant control variable as it has the least statistical sum contribution of only 0.103.

Table 4.3: ANOVA results

	*SS	**DOF	Variance	F_o	Results
A	0.24	2	0.120	1.580	Non-Significant
B	1.483	2	0.741	9.743	Significant @ 99% confidence level
C	0.103	2	0.051	0.682	Non-Significant
D	0.261	2	0.130	1.715	Non-Significant
E	0.373	2	0.186	2.454	Significant @ 90% confidence level
Error	1.307	16	0.081		*Statistical Sum
Total	3.770	26			**Degree of freedom

4.3.2 Fiber morphologies:

The fiber morphologies of nine different samples are shown in Figure 4.1. In order to demonstrate the effects of high voltage, polymer concentration, and flow rate on the fibers' diameter. These pictures of the fibers diameter and their measured values show that the concentration and flow rate have high effects on the fiber's diameters. The lowest diameter is exhibited by run 19 when the concentration was 7wt%, the flow rate was 0.1 ml/hr and the voltage was 25 kV. It is also shown that as the concentration and flow rate increase the fibers diameter increases. Increasing the high voltage does not necessarily increase the fiber's diameter.

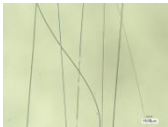








Concentration (wt%)	High voltage (KV)			Flow rate (ml/h)
	15	20	25	
7	(500&5)  590nm	(500&5)  937nm	(500&10)  510nm	0.1
12	(2500&5)  1270nm	(2500&5)  1428nm	(2500&5)  1420nm	0.2
15	(1500&5)  1457nm	(1500&5)  1730nm	(1500&5)  1350nm	0.3

Figure 4.1: Different samples of fibers morphology produced from electro-spinning at various levels of concentration (wt%), high voltage (KV), and flow rate (ml/h). *(rpm& collecting distance)

4.3.3 Effects of control factors:

The control factors (parameters) effect in terms of a summation of fiber diameters are displayed graphically in Figure 4.2. Each summation point represents the summation of all the fiber diameters at this level of the parameter being considered. A larger variation between the high and low values represents a greater influence of the control factor. The figure shows that A1, B1, C1, D1, and E1 are the optimal level of the control parameters, which means that in general the lower levels of all parameters usually lead to smaller fiber diameters. In addition, it is observed that the difference between the highest and lowest summation of fiber diameters for the concentration (B) and flow rate (E) are 5.10 and 2.60 respectively, so these two parameters have the most significant effect on fibers diameter. On the other hand, the corresponding value for the high voltage, collecting distance and rotating speed are 1.97, 1.93 and 1.32 respectively, which mean that these factors have lower effects in determining the output diameter of the fibers being produced.

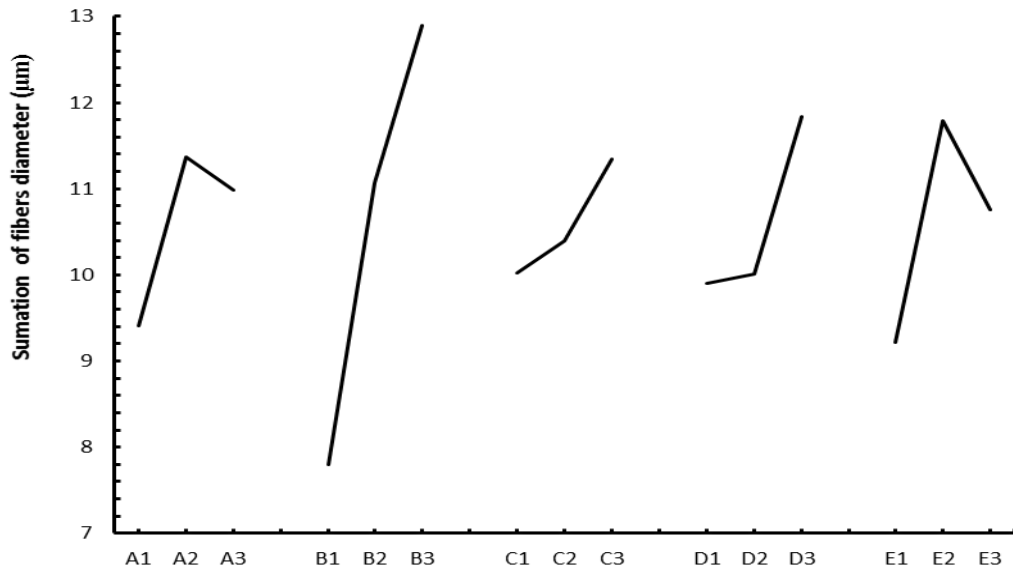


Figure 4.2: Plot of control effect for all process designs variables

4.4 Verification of ANOVA:

Once the optimal level of design parameters is selected, the final step is to verify the improvement of quality characteristics using the optimal level of design parameters. The estimated optimal level of parameters is calculated as [149]:

$$Y_{\text{Predicted}} = Y_{\text{Mean}} + \sum_{i=1}^n (Y_i - Y_{\text{Mean}}) \quad (4.1)$$

Where Y_i is the mean response at an optimal level for the main design parameters that affect the quality characteristics, and Y_{Mean} is the total mean response.

Table 4.4 shows the comparison of the predicted and actual values of fiber diameter. Good agreement between the predicted and the actual response is observed and verification accuracy of 93% is calculated as well.

Table 4.4: Results of the confirmation experiment for optimal fiber diameter values

Verification of Experimental Results		
Optimal levels: B1, E1		
Experimental	Theoretical	Accuracy
0.513	0.549	93%

4.5 Factorial ANOVA to study interactions:

In order to investigate the effects of the interaction variables on the measured response, the factorial ANOVA test was used and the results are shown in Table 4.5. It uses different trials which have been selected to include all interaction effects. The results show that the concentration percentage (B) and the interaction (BE) between flow rate (E) and concentration percentage (B) are the two significant factors at 99% confidence levels. The pooling technique has been used in order to modify all of the possible interactions using L27OA. The variables with lowest statistical summation values have been pooled (e.g. E, AD), during this test, in order to avoid the ANOVA limitation and to determine the most significant design parameters.

Table 4.5: ANOVA results for interactions effect

	*SS	**DOF	Variance	Fo	Results
B	1.483	2	0.741	78.15	Significant @ 99% confidence level
E	0.373	2	0.186	Pooled	---
AE	1.137	4	0.284	Pooled	---
BE	2.097	4	0.524	55.30	Significant @ 99% confidence level
DE	1.504	4	0.376	Pooled	---
Error	0.189	20	0.009		*Statistical Sum
Total	3.771	26			**Degree of freedom

4.6 Signal to noise ratio (S/N):

Gu et al [143] have shown that the diameter of Polyacrylonitrile (PAN) electrospun nanofibers are significantly affected by variation in solution concentration. They also found that voltage variations have no significant effect on fiber diameters. Reneker et al [6] have also, confirmed that the high-voltage does not have a significant effect on the diameters of polyethylene oxide nanofiber. However, other researchers such as Fennessey et al [150] and Ding et al [151] have observed significant effects of the high voltage on nanofibers diameter of PAN and PVA respectively. Thus, it can be concluded that some parameters like high voltage may be affected by the noise variables.

The effect of noise variables on the control factors was studied by subjecting them to S/N test in the domain of interest. The high voltage exhibits the highest influence by the noise variables as shown in The S/N analysis demonstrates that the applied voltage is a

confounding parameter, and this is supported in the literature. Therefore, further quantifications are recommended to determine its clear effect on the proposed fiber diameter.

Table 4.6, where it is significant at 95% confidence level. The S/N results are based on "the nominal- the better criteria" and is applied to equation (4.2), where μ is the replications average and σ is the standard deviation.

$$\text{The nominal-the better criteria} = \sum_{i=1}^n -\log\left(\frac{\mu_i^2}{\sigma_i^2}\right) \quad (4.2)$$

The S/N analysis demonstrates that the applied voltage is a confounding parameter, and this is supported in the literature. Therefore, further quantifications are recommended to determine its clear effect on the proposed fiber diameter.

Table 4.6: ANOVA results based on S/N ratio values

	*SS	**DOF	Variance	F _o	Results
A	1.138193328	2	0.5691	5.38041	Significant @ 95% confidence level
B	0.08259	2	0.0413	0.3904	Non-Significant
C	0.085877122	2	0.04294	0.40595	Non-Significant
D	0.15369	2	0.07685	0.72653	Non-Significant
E	0.452410326	2	0.22621	2.13861	Non-Significant
Error	1.6923	16	0.1057		
Total	3.6501	26			

*Statistical Sum **Degree of freedom

4.7 Electrospinning production model using RSM

Multiple regression techniques are used to analyze the influence of the independent variables on a specific response. Response surface methodology is used to develop a predictive electrospinning model. The purpose of mathematical models is to relate the process responses and facilitate the optimization of the process. The mathematical model commonly used for the process responses is represented as:

$$Y=F(X_1, X_2, X_3\dots) + \varepsilon \quad (4.3)$$

Where $X_1, X_2\dots X_n$ process parameters and ε are the error which is normally distributed about the observed response Y .

Two mathematical models have been developed to demonstrate the effects of process parameters. The first model relates to first ANOVA test as shown in equation (4.4), and the second model is developed in terms of the interaction effects as shown in equation (4.5).

$$\begin{aligned} Y_1 = & (- 5.861 * 10^{-4} * A^2)+ (7.745 * 10^{-3} * B^2)+ (3.957 * 10^{-3} * D^2) - (18.267 * E^2)- \\ & (3.111 * 10^{-3} * A*B) - (2.061*10^{-3} * A * D) + (4.793*10^{-1} * A * E) - (8.049*10^{-4} * B \\ & *D) - (1.64 \cdot 10^{-1} *B*E) - (7.075*10^{-2} *D*E) + (5.389 * 10^{-1}) \end{aligned} \quad (4.4)$$

$$Y_2 = (0.1501 * B) + (11.607 * E) - (5.975 * 10^{-4}*B^2) - (20.108 * E^2) - (0.331*B*E) - (1.075) \quad (4.5)$$

To validate the 1st mathematical model, the average residual error (RE) and the average model accuracy are calculated as shown in equations (4.6) and (4.7) [149] and the results are shown in Figure 4.3. This model shows 84.34% average model accuracy, which is considered as an acceptable percentage.

$$RE = \text{Absolute (Experimental value - Predicted)} \quad (4.6)$$

$$\text{Average model accuracy} = 1 - \frac{RE}{\text{Experimental value}} \quad (4.7)$$

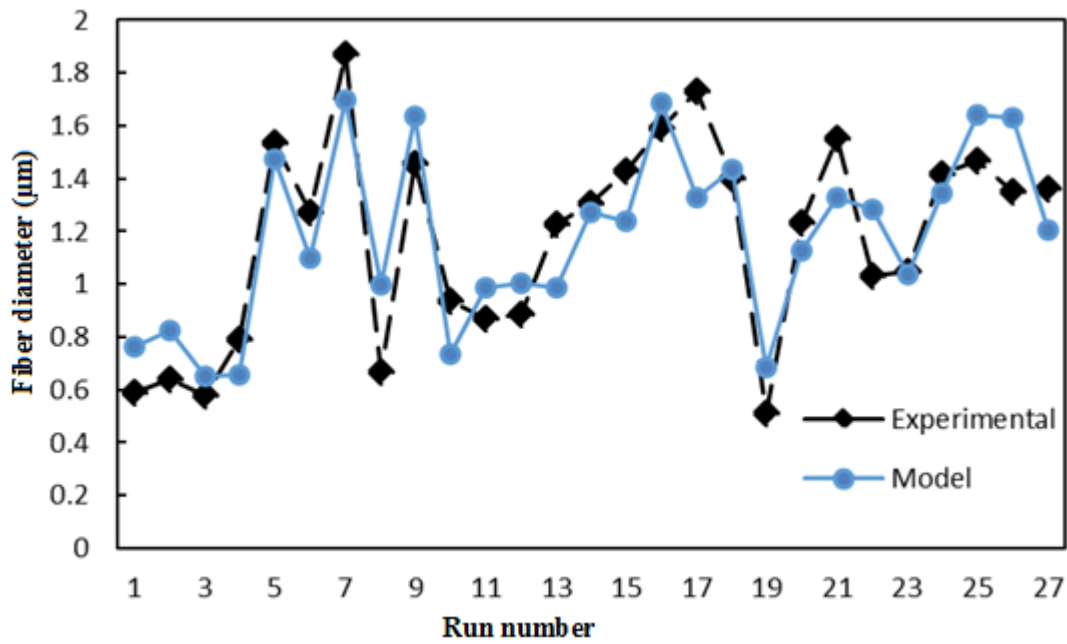


Figure 4.3: Experimental vs. model results based on the first model

Figure 4.4 indicates the estimated three-dimensional surface and contour plot for the first developed the model as a function of all design parameters where the other three variables are held constant at center points. It is obvious that decreasing the flow rate and concentration values result in lower fiber diameter values as it has been mentioned earlier through the first ANOVA test.

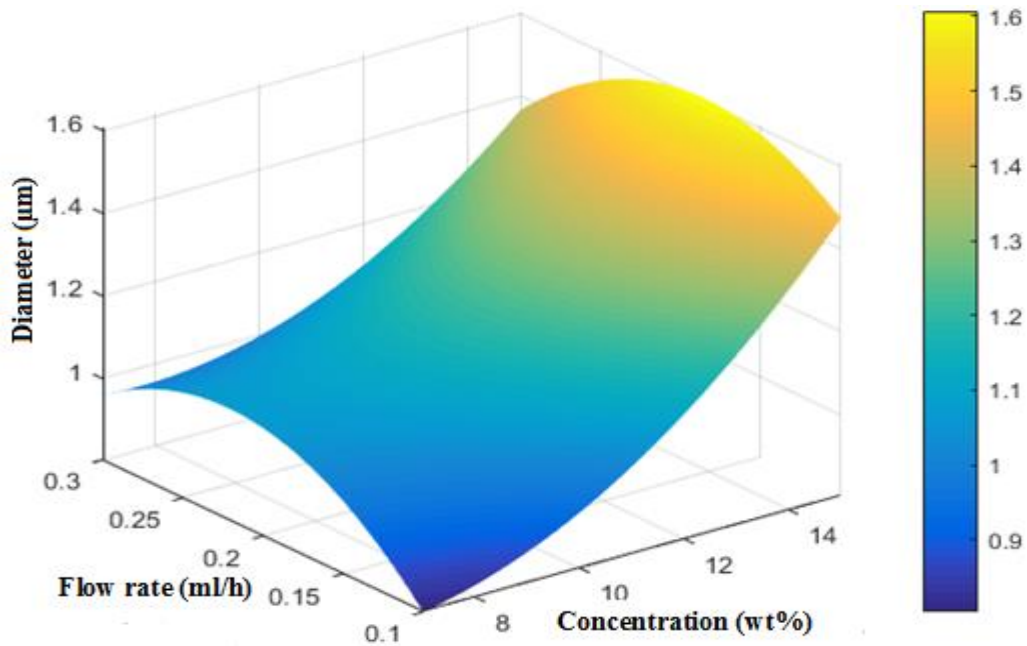


Figure 4.4: Effect of concentration (wt%) and flow rate on fiber diameter for the 1st mathematical model

Similarly, the average residual error and average model accuracy are calculated for the second model where it shows about 80% average model accuracy. In addition, Figure 4.5 graphically shows a comparison between the predicted and experimental results for the second model, while Figure 4.6 shows the estimated three-dimensional surface for the second developed the model. The interaction effect between the polymer concentration and flow rate can be clearly noticed through the non-linearity effect of the second 3-D surface model and lower levels for both variables are still the optimal levels to produce lower fiber diameters. Model accuracies for both of the two estimated models can be improved using a higher orthogonal array as this study deals only with 27 trials out of 243 actual trials through principles of design of experiment and Taguchi's method.

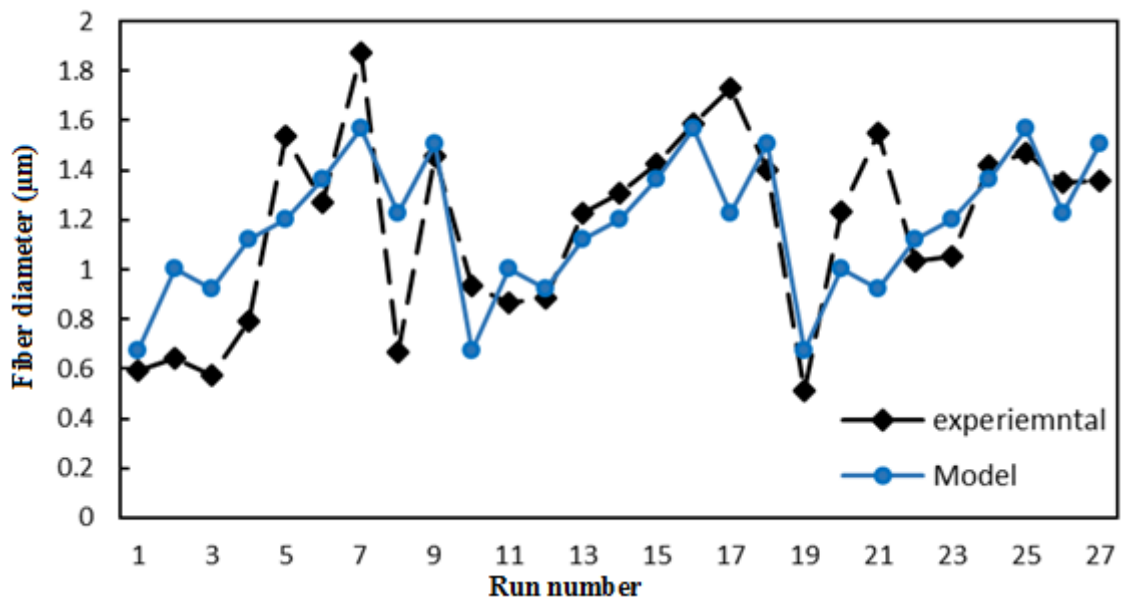


Figure 4.5: Experimental vs. model results based on the second model

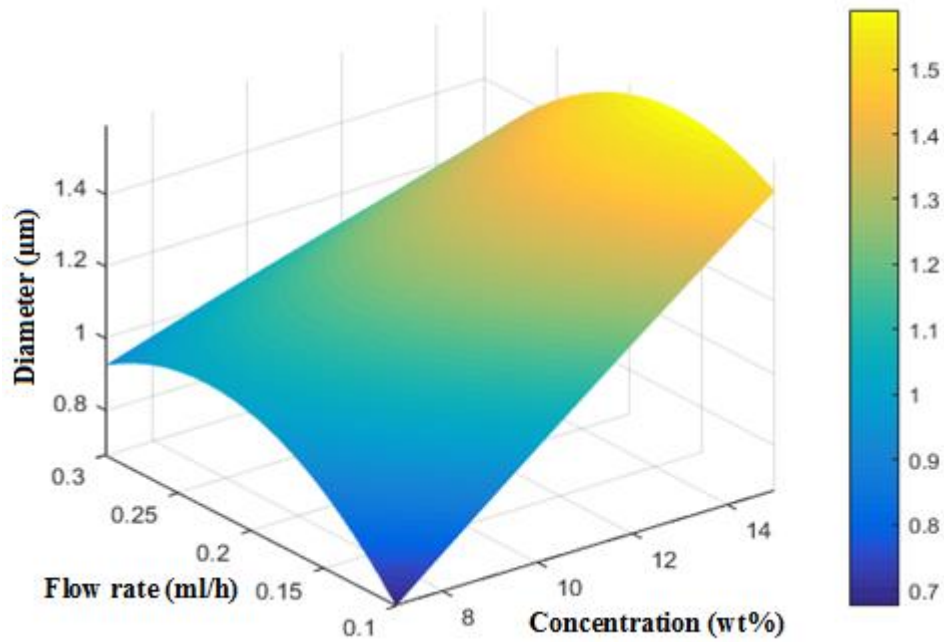


Figure 4.6: Effect of concentration (wt%) and flow rate on fiber diameter for the second mathematical model

4.8 Summary

Electrospinning of PVA micro/nanofibers is studied using the design of the experiment. The influence of five parameters is investigated using Taguchi's L27 Orthogonal Arrays (3-levels, 5-variables). PVA micro/nanofibers with diameters ranging from 0.51 μm to 1.87 μm have been obtained. The concentration and the flow rate are the main parameters that have a significant effect on the diameter of the fibers whereas; the high voltage and rotating speed have nonsignificant effects on the fibers' diameter. The concentration of 7wt% and flow rate of 0.1 ml/h yield minimal fiber diameter. ANOVA tests have revealed that interaction between flow rate and concentration also has a significant effect at 99% confidence level. RSM has been used to develop predictive models for fibers diameter for the chosen material and range of the control variables. The accuracy of these models can be enhanced by increasing the number of trials over wider domains of process variables. In addition, more interactions can be included in model development.

Chapter 5: Mechanical and thermal properties

5.1 Introduction

Nanofibers structures have a promising potential due to its unique properties such as the high surface area to the volume ratio, controllable porosity and desired functional properties [153, 154]. The addition of fillers improves the functional properties of the nanofiber and enhances the thermal and mechanical properties such as the high strength to weight ratio [155–158]. Different types of fillers can be used according to the field of interest, such as Carbon nanotubes (CNTs), nano-clays, graphene (GN), fiberglass (FG), wollastonite (WS), and titanium dioxide etc. The problem faced in the addition of fillers is the agglomerations, which prevent the fillers from being properly dispersed in the solution [2], [155], [158]. The dispersion of nanoscale fillers into the polymers can be facilitated in the liquid solution state by using surfactants and/or by mechanical means such as stirring or sonication. During the electrospinning process, the solution converts into nanofibers, and the particles dispersed in it are solidifies and remain in a dispersed state. This Chapter discusses the results of the tests carried out by using Dynamic Mechanical Analysis (DMA), Differential Scanning Calorimeters (DSC) and Thermogravimetric Analyzer (TGA).

5.2 Experimental work

5.2.1 Materials

Three types of polymers used are Polyvinyl chloride (PVC), polyvinyl alcohol (PVA), and polystyrene (PS). CNTs, GN, FG, and WS are used as fillers. The methods of samples preparation, characterization, and properties of all involved materials are mentioned in Chapter 3.

5.2.2 Mats fabrication and sample preparation.

The pure polymer and polymers with fillers were electrospun and the fibers were collected on the rotating drum electrode collector. The deposited materials were collected as rectangular mats of nanofibers of polymers and polymers containing the fillers. These mats were used to prepare the specimen for testing the mechanical, thermal, and acoustic properties. Samples prepared for the DMA test had the following dimensions: length between 5 - 30mm, width less than 6.5mm and thickness of around 100 μ m. For TGA and DSC, the weight of samples used was between 2.5- 5mg.

5.2.3 Characterization

5.2.3.1 Dynamic mechanical analysis (DMA)

Dynamic Mechanical Analysis Q800 (TA instruments, USA) is used to measure the tensile strength of nanofiber mats at 30 °C with ramp force 0.5 N/min. The sample is prepared in a rectangle shape with a width 5- 7mm and length 15- 20mm. The sample thickness is measured using a digital optical microscope. The test conditions are set as follows: maximum force equals to 18N and an initial preload force equals to 0.05N. The average results of four samples are calculated and data are reported (i.e. Young's modulus (E), tensile strength (σ_t), and elongation at break (ϵ_b)).

5.2.3.2 Thermogravimetric analyzer (TGA)

Thermogravimetric test (TGA) is applied to the samples using Q50 (TA Instruments, USA) to investigate the thermal stability of the fibers. The TGA uses a nitrogen environment during analyses in order to avoid the oxidative degradation. The chosen working temperatures range is from 0°C to 600°C at heating rate of 10 °C/min under nitrogen atmosphere. Approximately 3.5mg of sample is used for each test. T_{onset} is the degradation temperature, at which the slope of temperature changes.

5.2.3.3 Differential scanning calorimeters (DSC)

The thermal properties of nanofiber mats are conducted with differential scanning calorimeters Q20 (TA instruments, USA). The samples are initially heated from room temperature to 350 °C with a heating rate of 20 °C/min and held for 5 minutes to remove any previous thermal history. Then, the specimens were cooled at a rate of 20 °C/min up to 40 °C. Finally, the thermal results are collected by reheating the sample from 40 °C to 350 °C at 20 °C/min.

5.3 Results and discussion

5.3.1 PVA nanocomposite

5.3.1.1 Tensile test

The tensile strength for the nanocomposite mats increased significantly after adding fillers. For PVA 9wt%, it was noticed that adding CNTs by 5 and 10wt% improved the tensile strength by 23% and 61% respectively. Figure 5.1 shows the stress-strain curve for three samples of PVA 9wt% with CNTs 5wt%. The average value of the three measurements is calculated to measure the percentage of improvement. In addition,

adding WS with 5, 10, and 20wt% improved the tensile strength by 30, 73 and 121%, respectively. GN was also used, with 5 and 10wt% and it improved the tensile strength by 31 and 53.6%. Another concentration of PVA 12wt% solution is used to produce nanofiber mats. The used fillers CNTs and GN are loaded into the solution. The improvement in tensile strength for CNT and GN with 5 and 10wt% are 26.3, 83, 15, and 63% respectively. The explanation for this improvement is that the fillers are properly dispersed in the matrix so the superior load is easily transferred from the matrix to reinforcement. Table 5.1 shows the measurement values of the tensile strength (Mpa), elongation at break (%) and Young's modulus (Mpa) for PVA and their matrix which include the fillers. The figures 5.2, 5.3, and 5.4 represent the values of Table 5.1. The fillers' addition improves the tensile strength and Young's modulus, which indicates that a sufficient dispersion of the fillers inside the polymer matrix occurs. In addition, as the fillers' concentration increases, the samples' deformation decreases.

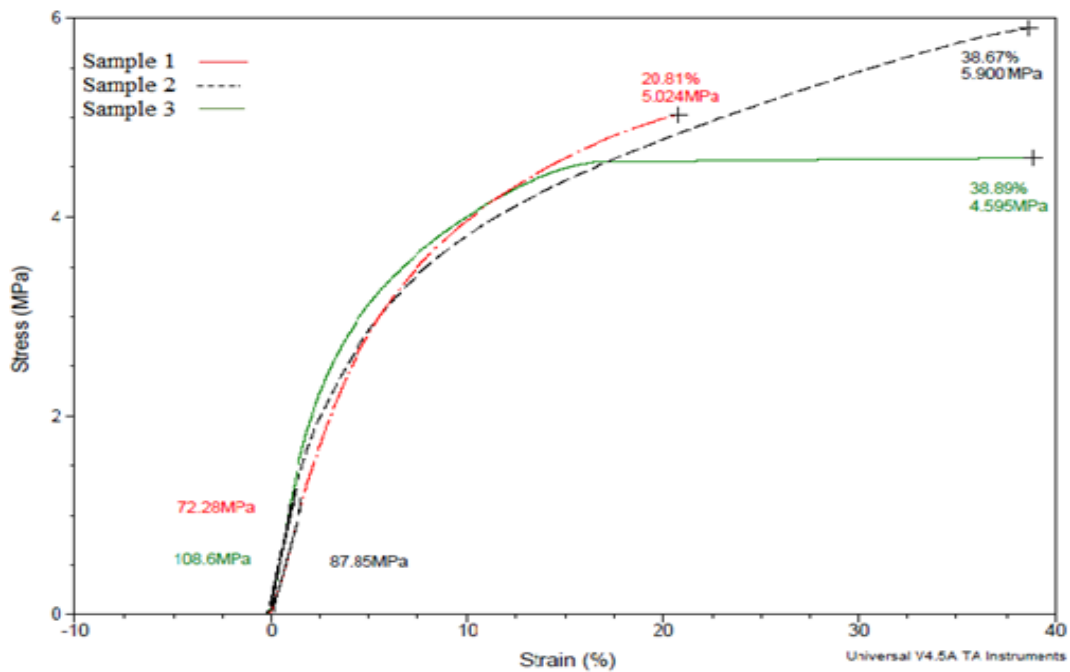


Figure 5.1: Tensile stress- strain curve for PVA 9wt% with CNTs 5wt%

Table 5.1: Tensile properties of PVA mats and its composites

	Material	Tensile Strength (Mpa)	Elongation at break (%)	Young's modulus (Mpa)
1	PVA9wt%	3.9 ±0.23	53.9 ±3.50	85.2 ±5.96
2	PVA9wt% + CNT 5wt%	4.9 ±0.34	22.9 ±2.06	127.3 ±8.14
3	PVA9wt% + CNT 10wt%	6.4 ±0.32	18.4 ±1.28	138.8 ±6.94
4	PVA9wt% + WS 5wt%	4.1 ±0.30	40.5 ±3.44	92.4 ±7.39
5	PVA9wt% + WS 10wt%	6.9 ±0.65	41.5 ±3.32	139.1 ±10.29
6	PVA9wt% + WS 20wt%	8.8 ±0.70	30.1 ±1.65	152 ±9.12
7	PVA9wt% + GN 5wt%	5.2 ±0.34	38.7 ±2.70	98.2 ±4.91
8	PVA9wt% + GN 10wt%	6.1 ±0.45	34.0 ±2.04	120 ±7.80
9	PVA 12wt%	3.5 ±0.19	35.8 ±3.04	90.1 ±8.10
10	PVA12wt% + CNT 5wt%	4.4 ±0.40	38.9 ±2.72	130.3 ±10.42
11	PVA12wt% + CNT 10wt%	6.4 ±0.42	18.0 ±1.44	147.5 ±8.85
12	PVA12wt% + GN 5wt%	4.1 ±0.28	19.1 ±1.14	97.4 ±5.30
13	PVA12wt% + GN 10wt%	5.8 ±0.49	21.1 ±1.37	112.7 ±9.12

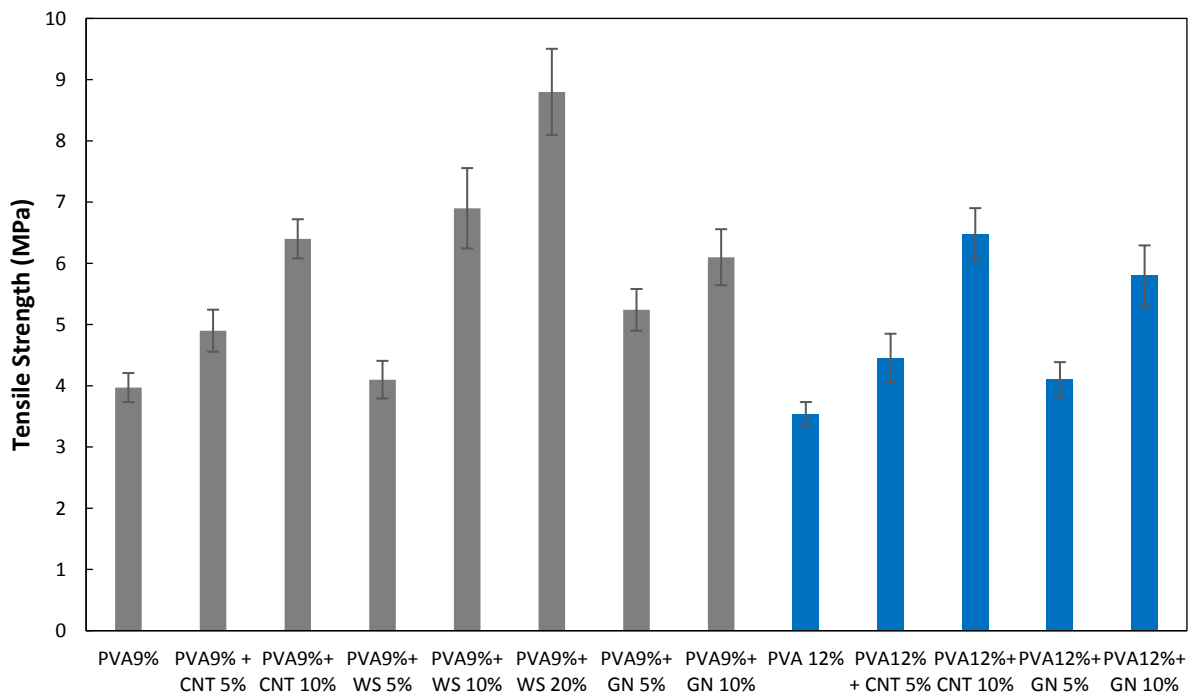


Figure 5.2: Tensile Strength of PVA Composites

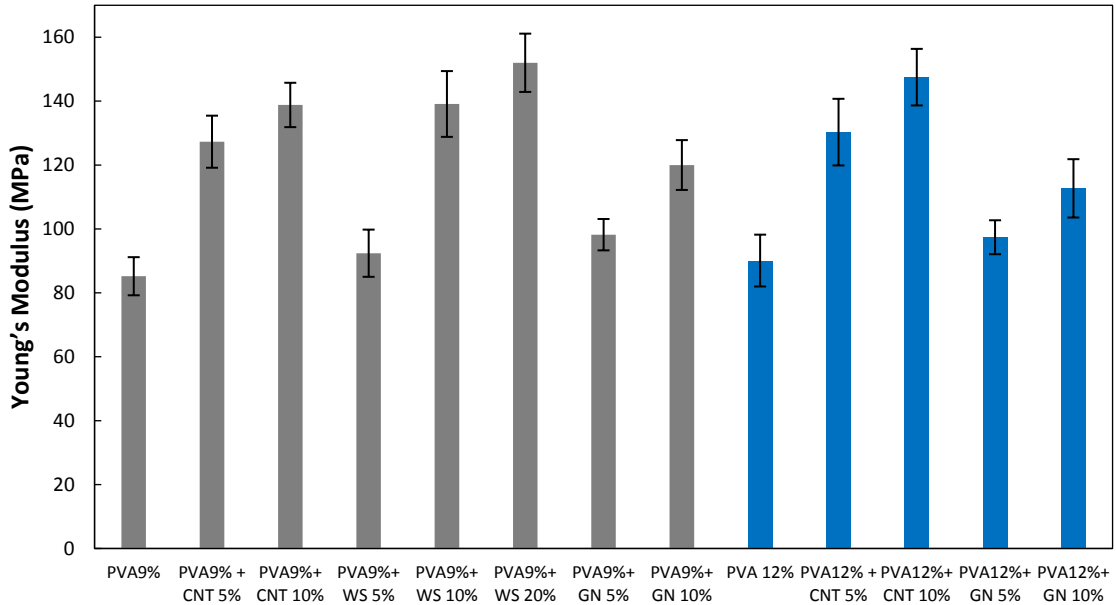


Figure 5.3: Young's modulus of PVA Composites

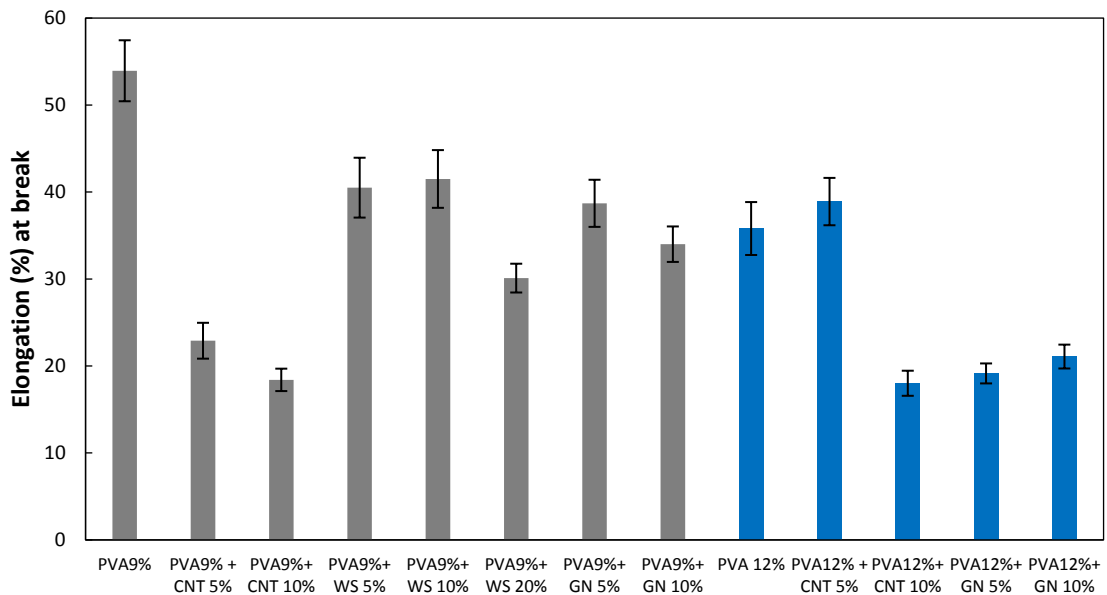


Figure 5.4: Elongation break of PVA Composites

5.3.1.2 Thermal properties

TGA measurements show that the onset temperature of electrospun PVA is less than PVA pellets. Also, the addition of CNTs and GN decrease the onset temperature of the PVA mats. The WS wt% did not shown any significant effects in terms of onset temperature. However, a slight decrease is observed with increasing the WS wt%. It is observed that the residue percentage increases as the percent of fillers increase, while the degradation rate decreases as the fillers' percent increases. Table 5.2 shows the summary result of TGA measurements and Figure 5.5 shows an example for TGA and DTGA data of PVA 9wt%.

The data analysis of DCS measurements shows that there is no significant difference in glass transition temperature (T_g) between the PVA pellets and PVA nanofibers with or without fillers. The differences range is between 1- 4°C. The melting temperature (T_m) of the electrospun nanofibers of PVA and PVA composite is lower than PVA pellets. Table 5.3 shows the data for DSC measurements.

Table 5.2: TGA measurements of PVA and its composites nanofibers

	Materials	Onset temperature (°C)	Maximum decomposition temperature (°C)	Residue (%)
1	PVA pellets	309.0	349.7	4.5
2	PVA 9wt%	269.8	307.3	3.4
3	PVA 12wt%	280.5	315.5	6.2
4	PVA 9wt% + CNTs 5wt%	234.6	239.1	7.4
5	PVA 9wt% + CNTs 10wt%	226.2	231.1	12.8
6	PVA 9wt% + GN 5wt%	223.4	213.1	19.5
7	PVA 9wt% + GN 10wt%	216.4	222.4	16.5
8	PVA 9wt% + WS 5wt%	272.8	313.6	6.5
9	PVA 9wt% + WS 10wt%	261.7	295.9	3.2
10	PVA 9wt% + WS 20wt%	251.8	246.1	3.6
11	PVA 12wt% + CNTs 5wt%	246.0	250.1	10.1
12	PVA 12wt% + CNTs 10wt%	230.0	233.0	9.6
13	PVA 12wt% + GN 5wt%	240.1	245.1	10.1
14	PVA 12wt% + GN 10wt%	217.0	221.3	12.6

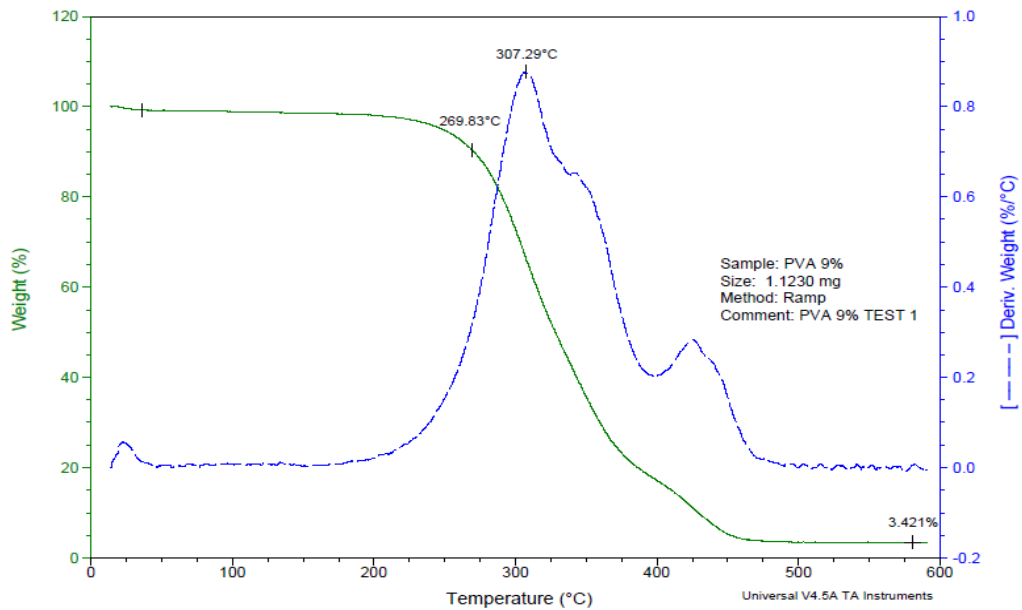


Figure 5.5: TGA profile of PVA (solid line), DTGA of PVA (dash line)

Table 5.3: DSC measurements of PVA/PVA composites.

	Material	T_g	T_m
1	PVA pellets	68.1	185.2
2	PVA9wt%	72.6	174.8
3	PVA12wt%	71.2	176.4
4	PVA 9wt% + CNTs 5wt%	64.9	178.3
5	PVA 9wt% + CNTs 10wt%	65.7	174.9
6	PVA 12wt% + CNTs 5wt%	67.6	175.9
7	PVA 12wt% + CNTs 10wt%	64.5	174.0
8	PVA 9wt% + WS 5wt%	69.7	163.9
9	PVA 9wt% + WS10wt%	70.4	168.7
10	PVA 9wt% + WS20wt%	67.6	162.0

5.3.2 PVC nanocomposite

5.3.2.1 Tensile tests

The tensile tests are implemented for the PVC nanofibers mat and its composite mats. CNTs and fiberglass are used as fillers to prepare the composite mats of PVC. PS solution of 10wt% concentration is prepared and mixed with PVC 12wt% solution with different ratio and the mixture solution is used to produce composite PVC/PS mats. The addition of CNTs with 5 and 10wt% improve the tensile strength by 41% and 63% respectively. However, adding fiberglass does not improve the tensile strength of the composite mats. Furthermore, the addition of PS to PVC does not improve the tensile strength as well. The Young's modulus is improved by adding fillers to PVC matrix by 89% for CNTs

10wt% and 140% for FG 30wt%. However, Young's modulus for PVC/PS composite mats does not show any improvements. Fillers addition decreases the elongation of the composite mats, which indicates that a sufficient dispersion of the fillers inside the polymer matrix occurs. As the fillers concentrations increase, the samples get more resisting to deformation. Figure 5.6 depicts the DMA curves of two samples of PVC 12wt% FG 10wt%. The summary of DMA results for PVC and PVC composites mats is shown in Table 5.4 and the figures 5.7, 5.8, and 5.9 represent the values of Table 5.4.

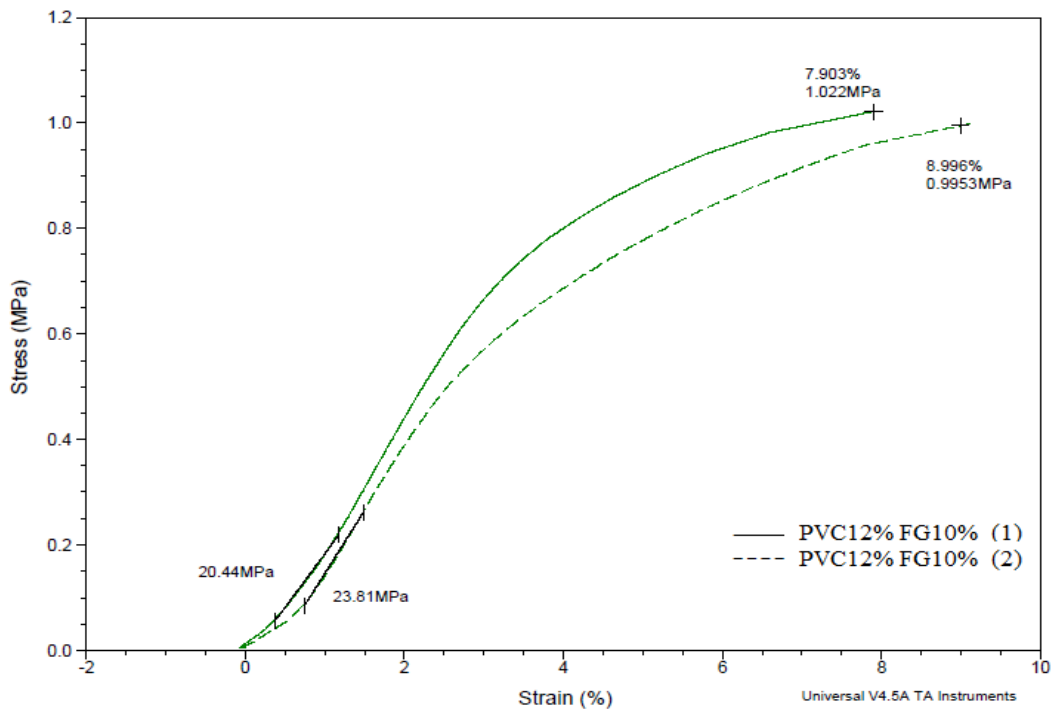


Figure 5.6: DMA curves for two samples of PVC 12wt% FG 10wt%

Table 5.4: Tensile properties of PVC and PVC composites mats

	Material	Tensile Strength (Mpa)	Elongation at break (%)	Young's modulus (Mpa)
1	PVC 12wt%	2.2 ±0.14	31.4 ±1.88	12.3 ±0.86
2	PVC 12wt% + CNT5wt%	3.1 ±0.28	25.02 ±1.75	19.4 ±1.24
3	PVC 12wt% + CNT10wt%	3.6 ±0.25	11.66 ±0.58	23.3 ±1.16
4	PVC 12wt% + FG 5wt%	1.35 ±0.11	9.80 ±0.73	20.0 ±1.61
5	PVC 12wt% + FG 10wt%	1.00 ±0.08	8.40 ±0.79	22.1 ±1.63
6	PVC 12wt% + FG 20wt%	2.70 ±0.14	6.48 ±0.51	23.5 ±1.41
7	PVC 12wt% + FG 30wt%	2.60 ±0.18	4.04 ±0.26	29.6 ±1.48
8	PVC 12wt% + PS10wt% (3:1)	2.17 ±0.13	24.1 ±1.81	10.9 ±0.71
9	PVC 12wt% + PS10wt% (1:1)	1.84 ±0.15	21.3 ±1.17	9.40 ±0.85
10	PVC 12wt% + PS10wt% (1:3)	1.50 ±0.11	17.42 ±1.56	7.41 ±0.62

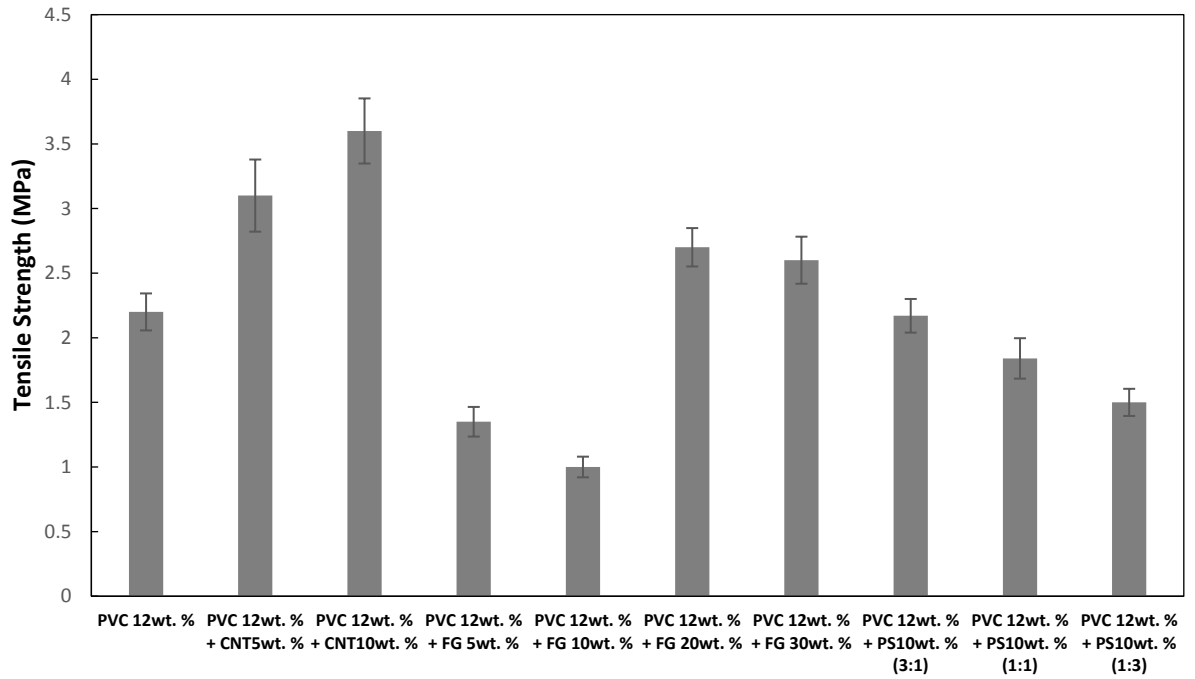


Figure 5.7: Tensile Strength of PVC Composites

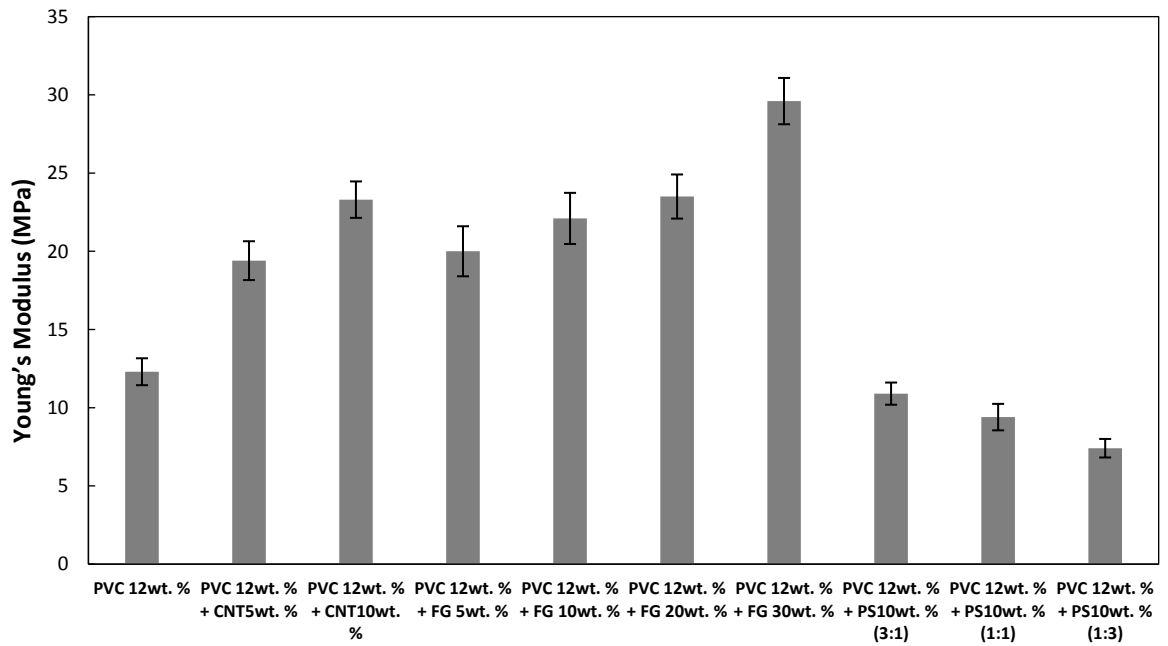


Figure 5.8: Young's modulus of PVC Composites

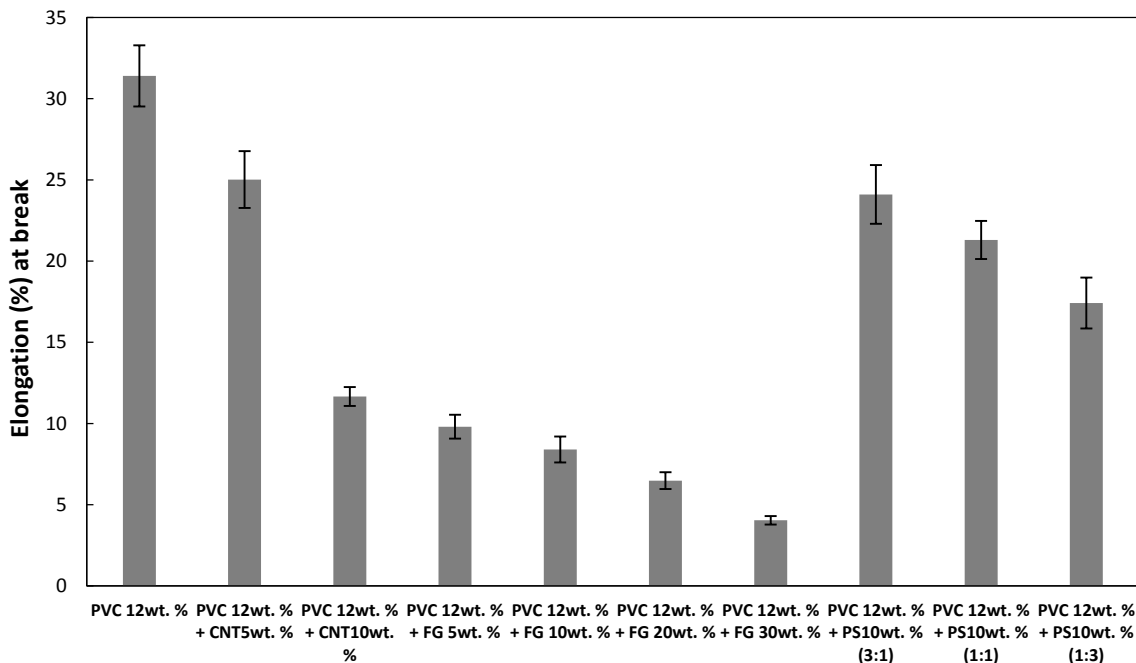


Figure 5.9: Elongation break of PVC Composites

5.3.2.2 Thermal properties

The onset temperature of the PVC pellets is approximately the same onset temperature for the electrospinning PVC nanofibers. The addition of CNTs as filler for PVC matrix does not change the onset temperature. However, the addition of FG increases the onset temperature for PVC composites about 23 °C for FG 10wt%. For mixture mats of PVC/PS, the onset temperature for both materials PVC and PS is approximately the same. The degradation rates for PVC nanofibers and PVC nanofibers composites are higher than degradation rate for the PVC pellets. The difference in degradation rate between the PVC nanofibers and the composites of PVC nanofibers is only about 3°C, so the fillers have no observed effect on the degradation rate. The residues % increase as the fillers % increases. Table 5.5 shows the TGA analysis results for PVC/PVC composites, while Figure 5.10 shows the samples of TGA and DTGA of PVC 12wt% CNTs 10wt%.

Table 5.5: TGA measurements of PVC and its composites nanofiber

	Materials	On- set temperature (°C)	Maximum decomposition temperature (oC)	Residue (%)
1	PS pellets	390.2	419.5	0.57
2	PS 10wt%	258.7	415.0	0.33
3	PVC pellets	251.0	267.0	7.16
4	PVC 12wt%	253.0	285.9	5.65
5	PVC 12wt% + CNTs 5wt%	250.0	289.0	10.90
6	PVC 12wt% + CNTs 10wt%	251.8	309.0	14.10
7	PVC 12wt% + FG 5wt%	266.2	290.0	11.50
8	PVC 12wt% + FG 10wt%	275.5	307.0	9.10
9	PVC 12wt% + FG 20wt%	276.0	304.6	10.20
10	PVC 12wt% + FG 30wt%	265.0	298.0	13.00
11	PVC12PS10(1:3)	250 (PVC), 390 (PS)	281(PVC), 413(PS)	6.22
12	PVC12PS10(1:1)	249 (PVC), 395(PS)	290(PVC), 423(PS)	4.61
13	PVC12PS10(3:1)	253 (PVC), 397(PS)	287(PVC), 422(PS)	11.20

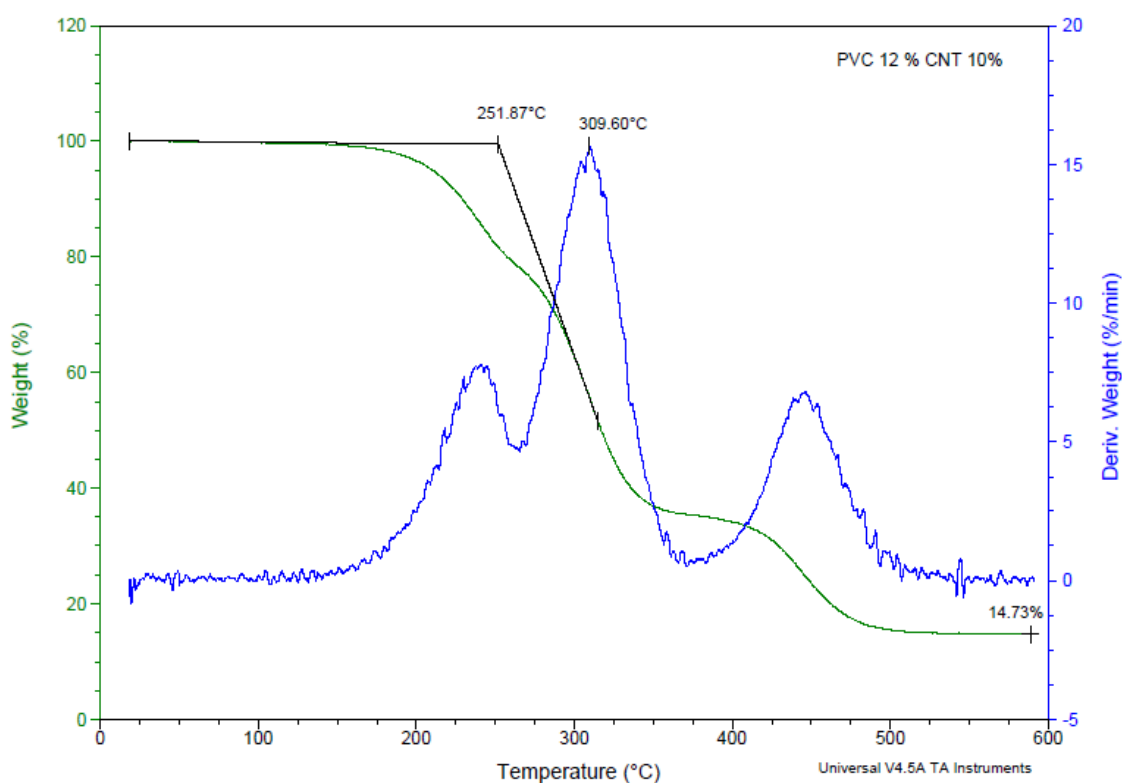


Figure 5.10: TGA profile (green line) and DTGA (blue line) of PVC 12wt% CNTs 10wt%

The data analysis of DCS measurements shows that there are no significant difference in glass transition temperature (T_g) between the PVC pellets and PVC nanofibers. The addition of fillers decreases the glass transition temperature about 15 °C. In addition, the

mixing PVC/PS solutions have no effect on the changing of the glass transition temperature. The melting point of PVC nanofibers is less than the PVC pellets, but it is approximately the same for the PVC composites nanofibers. Table 5.6 shows the data analysis of DSC for PVC/ PVC composites nanofibers and Figure 5.11 depicts the third cycle of DSC curve for analysis of sample PVC 12wt% PS 10wt% (1:3).

Table 5.6: DSC measurements of PVC and PVC composites nanofibers.

	Material	T_g	T_m
1	PVC pellets	90.00	174
2	PVC12wt%	89.00	168
3	PVC12wt% + FG 5wt%	84.10	165
4	PVC12wt% + FG 10wt%	85.14	163
5	PVC12wt% + FG 20wt%	83.54	158
6	PVC12wt% + FG 30wt%	84.90	161
7	PVC 12wt% + CNTs 5wt%	85.00	169
8	PVC 12wt% + PS 10wt% (1:3)	90.00	161(PVC), 243 (PS)
9	PVC 12wt% + PS 10wt% (1:1)	92.00	156(PVC), 240(PS)
10	PVC 12wt% + PS 10wt% (3:1)	92.50	150(PVC), 244(PS)

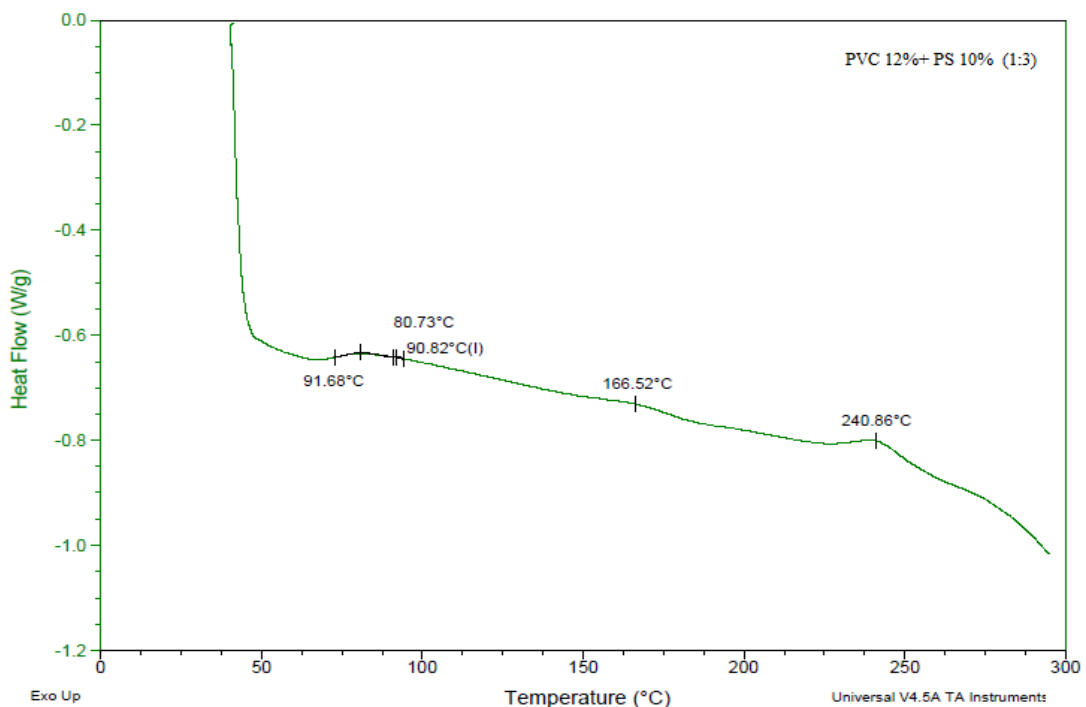


Figure 5.11: DSC curve of PVC12wt% PS10wt% (1:3)

Chapter 6: Morphology

6.1 Introduction

Several mats were produced from different polymers, with and without fillers, using electrospinning process. The detailed description of this method has been discussed in Chapter 3. In this Chapter, the morphology of electrospun mats produced during the experimental frame work is discussed elaborately. The effects of solution concentrations, fillers addition, and mixing the solutions of two polymers on fibers' morphology are investigated and characterized in this chapter.

6.2 PVA nanofibers and its blends

6.2.1 PVA nanofibers

PVA solutions were prepared using three different concentrations 7, 9 and 12wt% by dissolving in distilled water with stirring over a hot plate for 3-4h at temperature range from 60 -70 °C. The final solution was loaded into the syringe and electrospun to produce the mats. During the electrospinning process, the flow rate of the solution was maintained at 0.3ml/h. The applied high voltage was 15KV, the speed of the collecting drum was 1000rpm, and the collecting distance was 10cm. The mats were characterized by using SEM images and ImageJ software to measure the fiber diameters. The fiber diameters were calculated by taking the average of around 50 measurements and the results found that average fiber diameters for 7wt%, 9wt% and 12wt% of PVA are 109nm, 158nm and 267nm, respectively. It is observed that as the solution concentration increases the fibers diameter increases as discussed in Chapter 4. Concentration is a significant factor in controlling the fiber diameter thus, the fibers at these concentrations have smooth circular shapes without any beads. Figure 6.1 shows that internal space between the fibers decreases with increase the solution concentration.

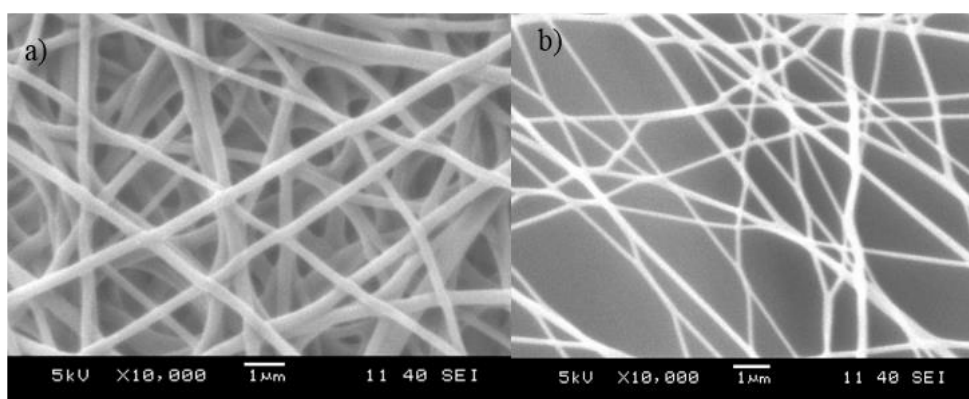


Figure 6.1: SEM of a)PVA 12wt% b) PVA 9wt%

6.2.2 PVA with fillers

PVA composite solutions are prepared using two types of fillers such as carbon nanotube (CNTs), and graphene (GN). Sodium dodecyl sulfate (SDS) was used as a surfactant to facilitate the dispersion of the fillers in the solution by adding 1wt%. After dissolving the surfactant, the fillers were added to the solution according to the desired concentration. Then the solution was sonicated for 30 min, followed by adding PVA pellets. The mixture is stirred over a hot plate for 3h at 70 °C.

6.2.2.1 PVA with CNTs

Electrospun fibers of PVA/CNTs prepared by using different concentrations of CNTs such as 1.5, 2.5, 3.5, 5, and 10wt% according to PVA weight. It was noticed that the fibers' diameter decreased with increase the CNTs concentration up to 5wt% and after that it increased. The fiber's diameters of the above-mentioned concentrations are 281.9, 265.9, 213.0 and 284.7nm, respectively.

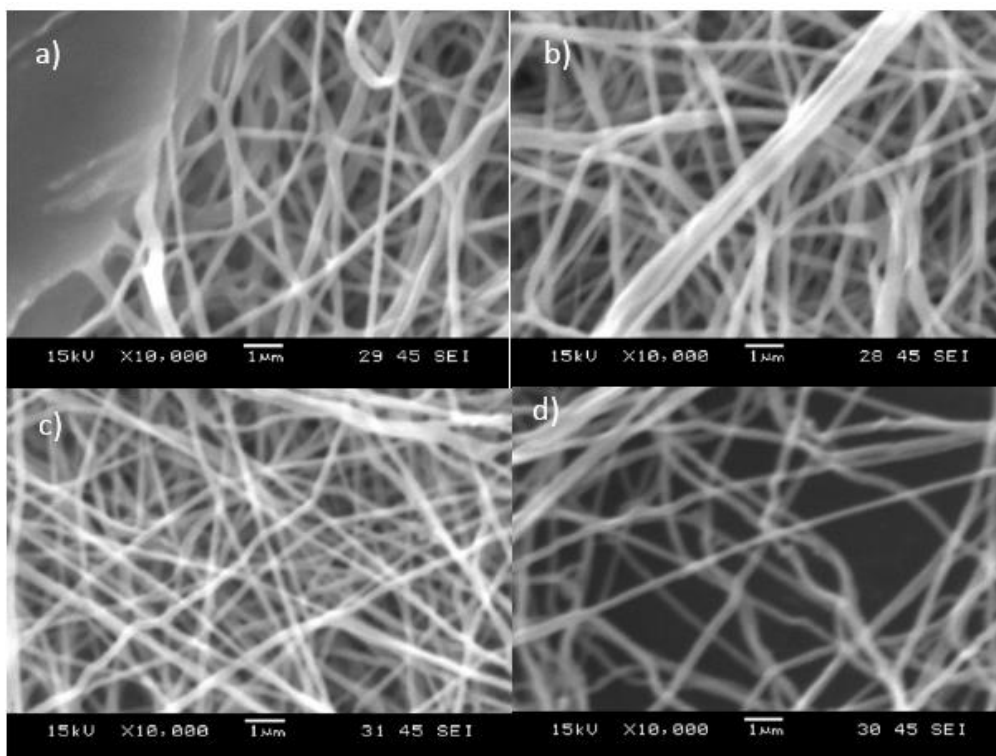


Figure 6.2: SEM of PVA 10wt% with a)1.5 wt% b) 2.5 wt% C) 3.5 wt% d)5wt% of CNTs

Solutions PVA of 9 and 12wt % concentrations were prepared. CNTs of 5 and 10wt% concentrations were added to the previous solutions of PVA. Table 6.1 shows the values

of fiber diameters at different concentrations. Figure 6.3 shows the smooth and circular shape fibers without any beads.

Table 6.1: Fiber diameters of PVA/CNTs (nm)

Polymer \ Fillers	CNTs 5wt%	CNTs 10wt%
PVA 9wt%	169.0	198.8
PVA 12wt%	298.9	309.3

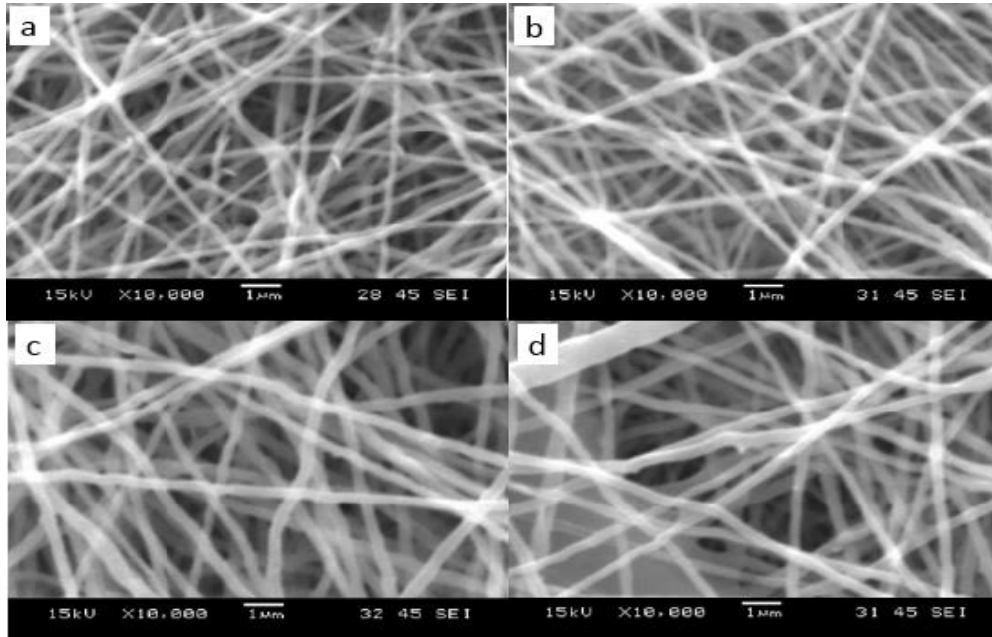


Figure 6.3: SEM of a) PVA 9wt% CNTs 5wt% b) PVA 9wt% CNTs 10wt% c) PVA 12wt% CNTs 5wt% d) PVA 12wt% CNTs 10wt%

6.2.2.2 PVA with Graphene (GN)

GN was also used as filler for preparation of PVA/GN electrospun fibers by loading 5 and 10wt% of GN to 9 and 12wt% of PVA. The measured fiber diameters shown that as the percent of graphene increased, the fibers diameters decreased. Table 6.2 shows the values of fiber diameters at different concentrations.

Table 6.2: Fiber diameters of PVA/GN (nm)

Polymer \ Fillers	GN 5wt%	GN 10wt%
PVA 9wt%	302	186
PVA 12wt%	425	404

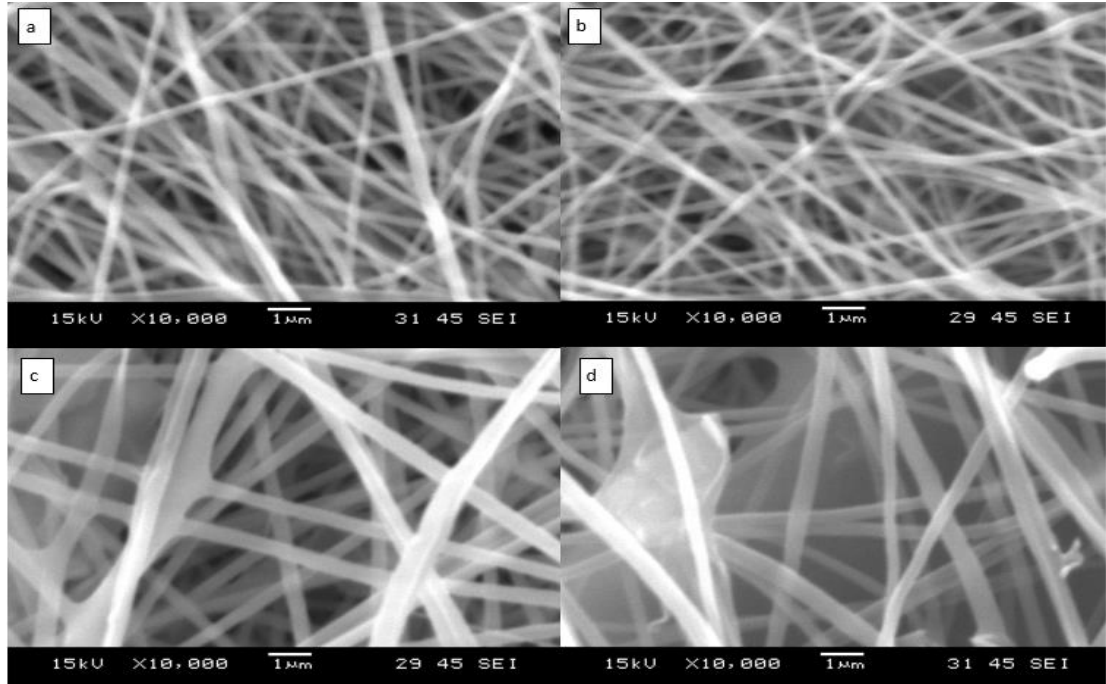


Figure 6.4: SEM of a) PVA 9wt% GN 5wt% b) PVA 9wt% GN 10wt% c) PVA 12wt% GN 5wt% d) PVA 12wt% GN 10wt%

6.3 PVC based materials

The solution of PVC was prepared by dissolving in DMF and stirring over a hot plate for 4-5h at 70 °C. The solution was loaded into the syringe for running the experiments. During the electrospinning process, the flow rate was adjusted at 1ml/h, the applied voltage was fixed at 15Kv, the collecting speed at 1000rpm and the collecting distance maintained at 10cm. From the series of experiments, it was found that the most convenient concentration to use was 12wt% with compared to other concentrations. At concentration lower than 12wt%, beads started to appear, and higher than 12wt% concentration the solution became more viscous and hard to electrospun. Moreover, the fibers fabricated were thicker and not preferable to acoustic applications. The average diameter of the produced fibers was 137nm.

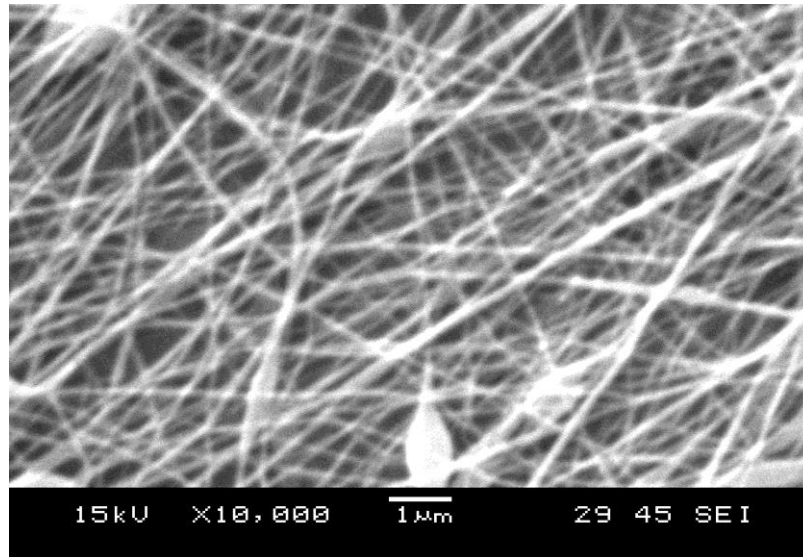


Figure 6.5: SEM of PVC 12wt%

The fillers such as CNTs, and Fiberglass (FG) were added to the solution of PVC 12wt%. The fillers were dispersed in the solvent using ultrasound probe for 30min, then PVC was added, followed by stirring for about 4-5h. For the electrospinning process, the composite solutions were loaded into the syringe with a needle gauge 21 to be electrospun using high voltage at 15KV, drum speed at 1000 rpm and drum to needle distance was 10cm.

6.3.1 PVC/CNTs

CNTs were added to the PVC using two concentrations of 5 and 10wt%. It was found that the addition of CNTs increased the diameters of the PVC fibers produced. The fiber diameters were 144nm and 270nm for concentrations of 5 and 10wt% of CNTs, respectively.

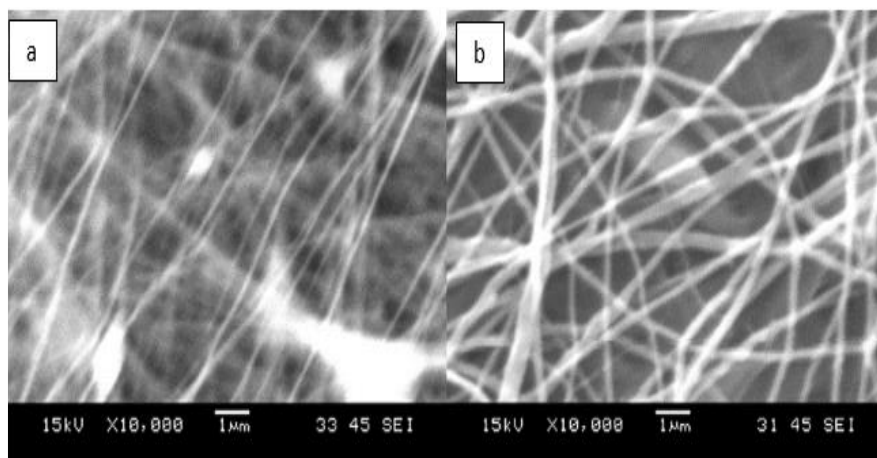


Figure 6.6: SEM of composite PVC/CNTs nanofiber a) 5wt% b) 10wt%

6.3.2 PVC with fiberglass (FG)

For preparation of PVC/FG fibers, a solution of PVC 12wt% was using with different weight percentage concentrations of FG such as 5, 10, 20, and 30wt% according to PVC weight. It was noticed that the fiber diameters decreased, as the percentage of FG increased as follows: 448, 409, 267, and 252nm for the FG concentrations of 5, 10, 20, and 30wt%, respectively.

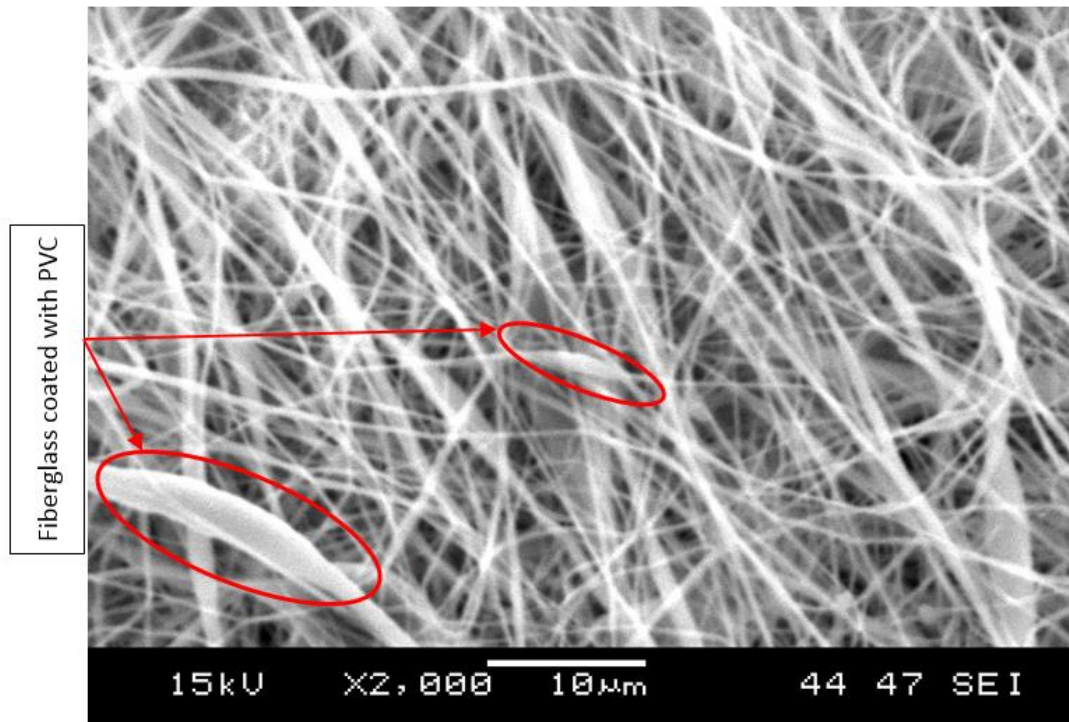


Figure 6.7: SEM of PVC/FG nanofibers

6.4 Multi-polymers mats

Multi-polymers mats were produced and its sound absorption properties were investigated.

6.4.1 Multi-layers of PVA and PS

The multi-layer mats of PVA and PS were prepared using two concentrations of both polymers. These mats consisted of three layers; the lower and upper layers were PVA and the middle layer was PS. The first layer of PVA was electrospun for 90 min with flow rate 0.3 ml/h and the second layer of PS was electrospun for 180 min with flow rate 0.8ml/h, finally, the last layer was the same as the first. PS mat was brittle and could not remove from the drum as one piece, so it was essential to have non-brittle lower and

upper mats to sandwich the PS layer. The solution of PS 10wt% produced beads, however the solution of PS 20wt% produced smooth fibers without beads and had average diameter 2584nm as shown in Figure 6.8.

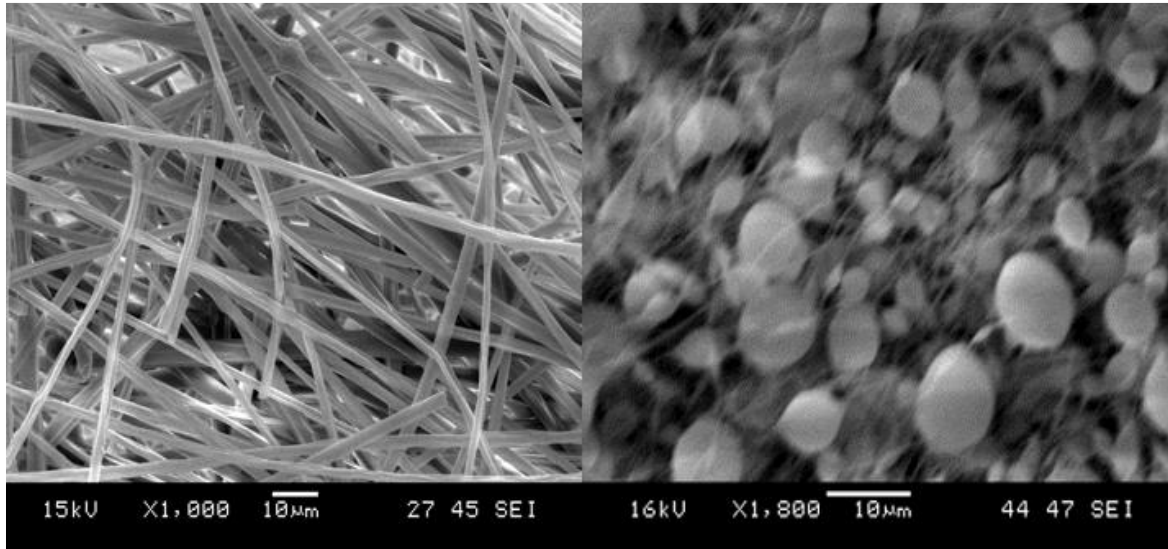


Figure 6.8: SEM of PS nanofiber (left) 20wt% (right) 10wt%

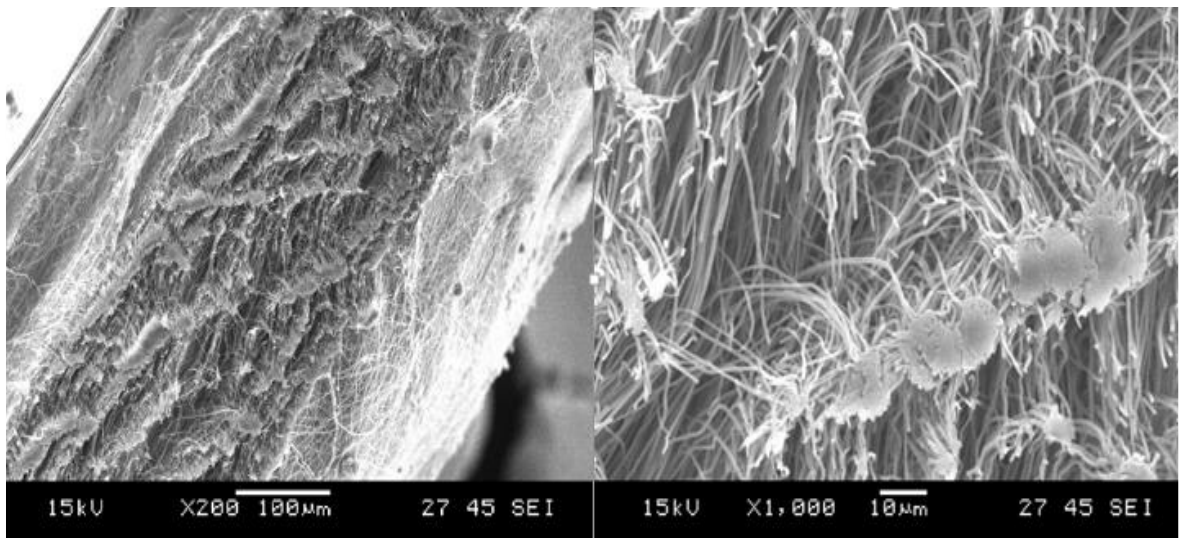


Figure 6.9: SEM of multi-layer of PVC12PS20PVC12 (side)

6.4.2 Blends mats of PVC and PS

Solutions of PVC 12wt% and PS 10wt% were prepared separately then mixed together using a magnetic stirring for 1h with the volume ratios A(3:1), B(1:1), and C(1:3) of PVC and PS, respectively. The obtained fiber diameters were 145nm, 456nm, and 690nm, for A, B and C, respectively. The fiber diameters increased, and the gap spaces between

fibers decreased, as the ratio of PS increased in the solution. The beads started to form as amount of PS as seen in Figure 6.10.

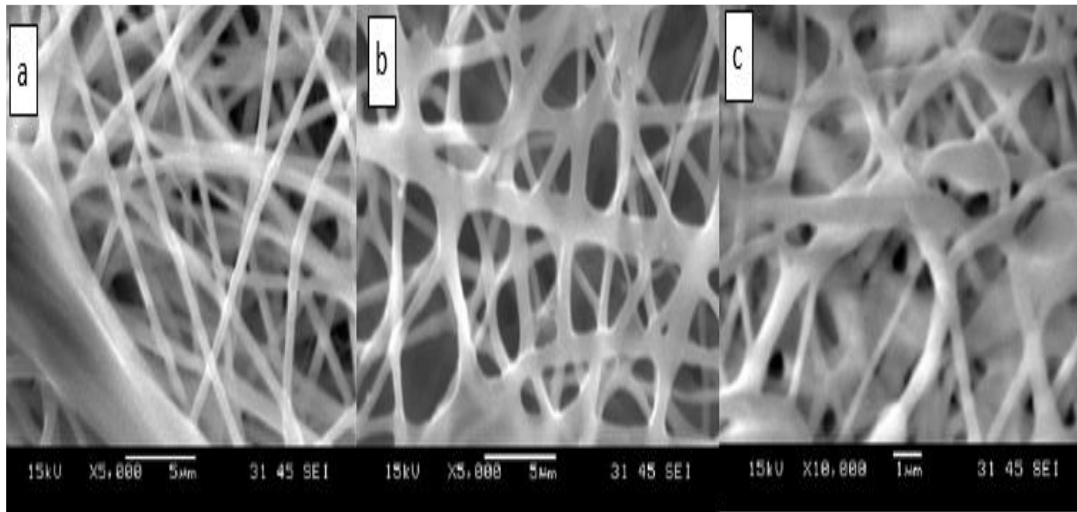


Figure 6.10: SEM of fibers of a mixture solution of PVC 12wt% and PS 10wt% with different volume% A) 3:1 B) 1:1 C)1:3 of PVC and PS respectively.

Solutions of PVC 12wt%, and PS 20wt% were prepared separately, then mixed together with a volume percentage 3:1 of PVC and PS, respectively. The fibers were beads free and thicker due to increase PS concentration and the average fibers diameter was 722nm as shown in Figure 6.11.

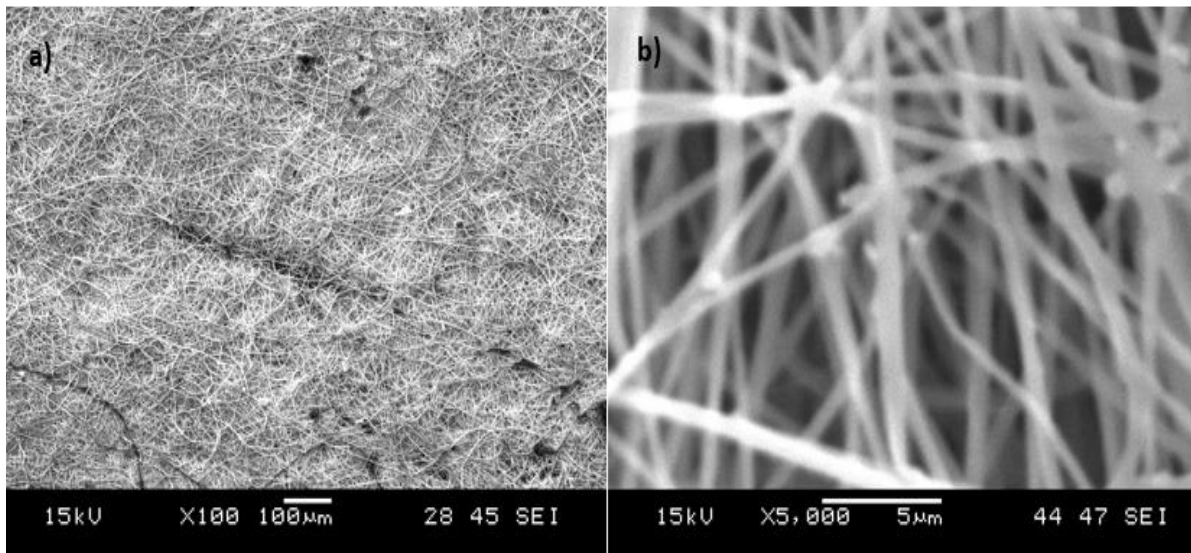


Figure 6.11: SEM of fibers of a mixture solution of PVC 12wt% and PS 20wt% with volume% (3:1)

6.5 PVC and PS mat produced by coaxial needle

The coaxial needle was used to produce a nanofiber mat of PVC 12wt% and PS 10wt% dissolved in 1-methyl-2-pyrrolidinone. PVC solution was used in the shell and PS solution in the core and the flow rates of PVC and PS were 0.8ml/h and 0.4ml/h, respectively. It was observed that the fibers not showing the expected result, i.e. not coming in one thread as core and shell, but a bubble started to form at the tip of the coaxial needle and grew, then it blew up and fibers moved towards the collector. It is clear from the Figure 6.12 that there are two major fibers diameters. The thin fibers have average diameter 437nm and the thick fibers have average diameter 1267nm.

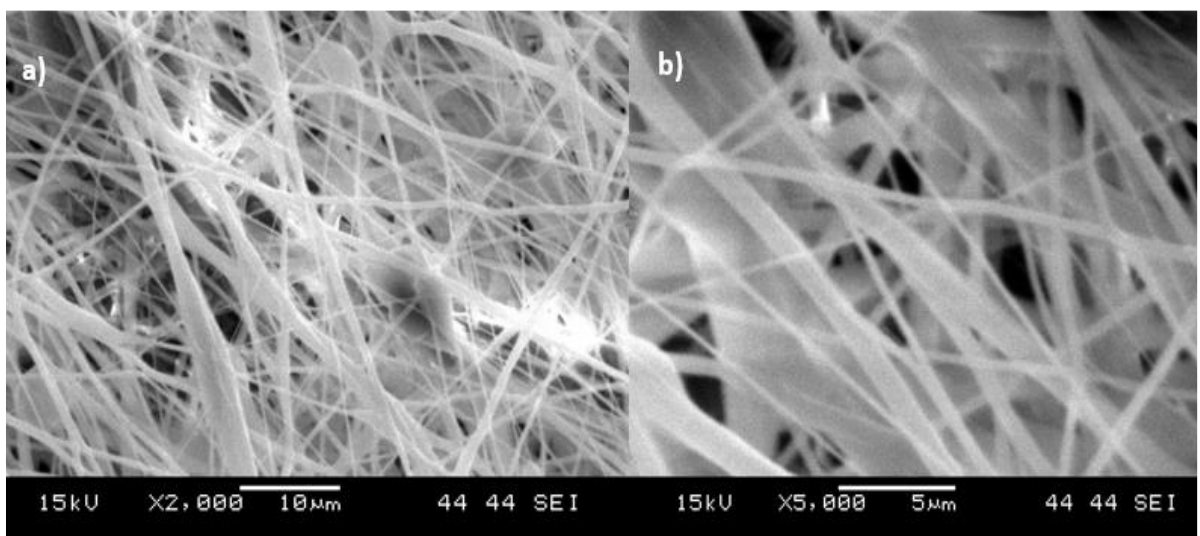


Figure 6.12: SEM of PVC/PS mat produced by coaxial needle

Chapter 7: Characteristics of Sound absorption Nanofibers

7.1 Introduction

The sound absorption coefficient expresses the amount of sound absorption inside the material. Sound absorbing materials convert sound energy to another type of energy (i.e. heat energy) due to the friction between the sound waves and the walls of the material or kinetic energy in the case of membrane. The samples' sound absorption coefficient has been measured using the developed impedance tube. The detail procedure of the measurement has been mentioned in Chapter 3, and it follows ASTM1050 and ISO 10534-2 standards. In this work, different nanofiber mats are produced and evaluated the sound absorption coefficient of each of the products. For evaluate the sound absorption coefficient, samples are prepared and mounted inside the impedance tube and recorded the data. The mats used in this work are PVC mats, composites of (PVC/CNTS), composites of (PVC/FG), PVA mats, composites of (PVA/CNTS), composites of (PVA/GN), composites of (PVA/WS), multilayers of PVC-PS-PVC and multilayers of PVA-PS-PVA. A 3cm cavity is used behind all the samples for the measurement and the fiber diameters are measured using ImageJ software as mentioned in Chapter 6.

7.2 Sound absorption of PVC mat

PVC has many applications as electrical insulation, waterproofing, and soundproofing. PVC is a cheap material, which is easy to prepare and electrospun. PVC solution of 12wt% concentration is prepared to be electrospun. A nanofiber mat of PVC with average diameter 137nm and thickness 52.6 μ m shows an acceptable sound absorption behavior between 700-900Hz and 1100-1300Hz and the sound absorption coefficient reaches (0.3-0.5) and (0.2- 0.9) at these frequency ranges, respectively as shown in Figure 7.1.

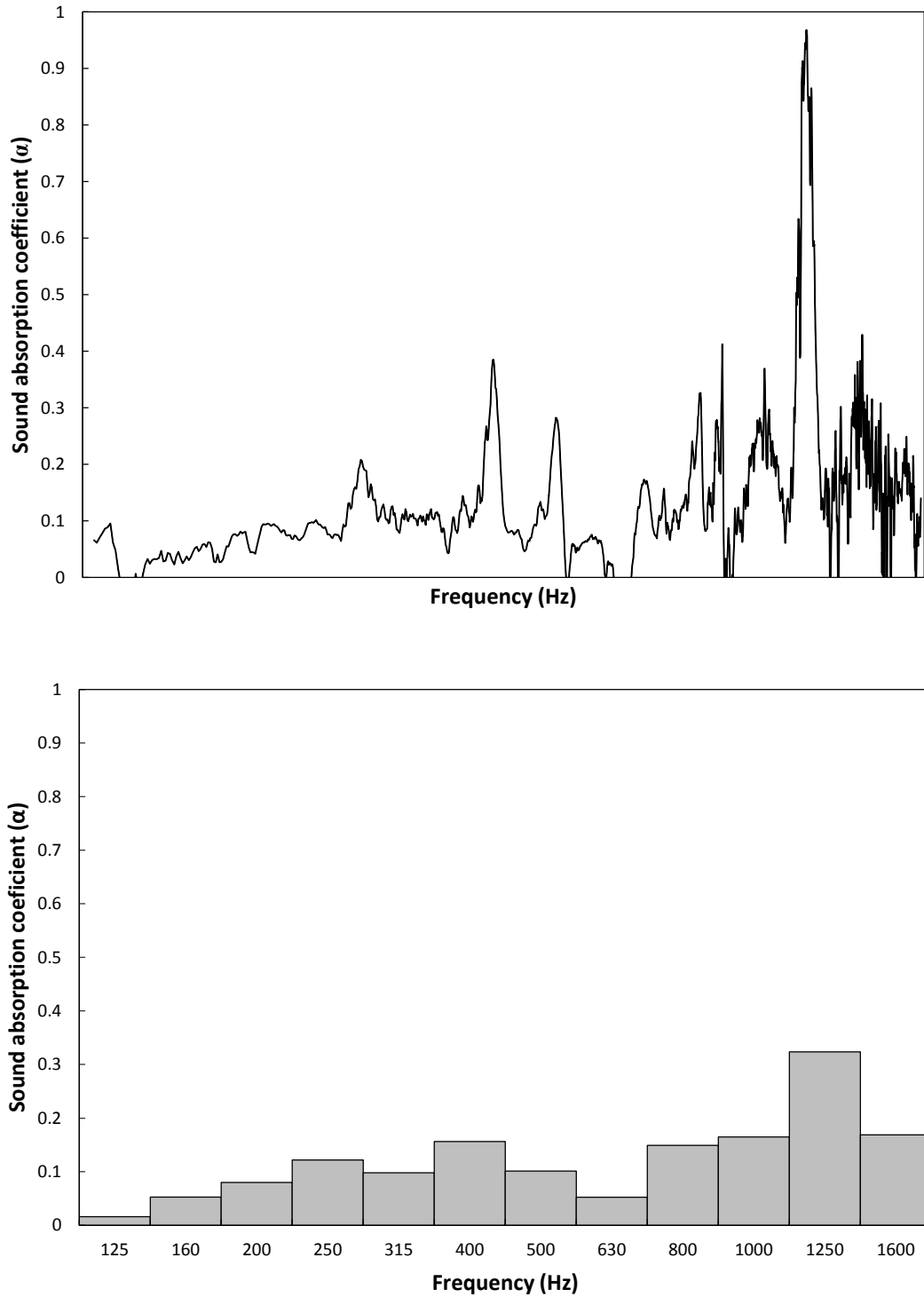


Figure 7.1: Sound absorption coefficient of PVC at 3cm back cavity (FFT and 1/3 octave plot).

7.2.1 Sound absorption of mats from mixture solutions of PVC and PS

The mixture solutions of PVC 12wt% and PS 10wt% with different volume ratios are prepared. First, each solution (i.e. PVC 12wt% and PS 10wt%) is prepared separately. Then, three mixture solutions of PVC and PS are prepared by mixing different volume ratios as follows; A (3:1), B (1:1) and C (1:3), respectively. The mixture solutions are

stirred vigorously for 1 hour. Finally, the sound absorption coefficient is measured for the nanofibers mat produced from each solution. The first mat, A (3:1), shows an absorption coefficient of 0.1- 0.35 at 580-900Hz and reaches 0.9 at 1200Hz as shown in Figure 7.2. It was observed that the sound absorption is adversely affected by the increase of the volume ratio of PS in the mixture solution, and this is clearly shown in Figure 7.3. This can be attributed to the reduction in the specific surface areas of the nanofiber. This happens due to the enlargement of the nanofibers cross-section with the increase of PS ratio in the solution. This was justified by the nanofiber diameter measurements for the different volume ratios. The fiber diameters was 144nm for the first sample, 456nm for the second sample, and 690nm for the third sample as mentioned in Chapter 6. Therefore, the electrospun fibers from the mixture of PS and PVC did not show any significant improvements in terms of the sound absorption results as the fiber diameters increased with the increase of the PS ratio in the mats.

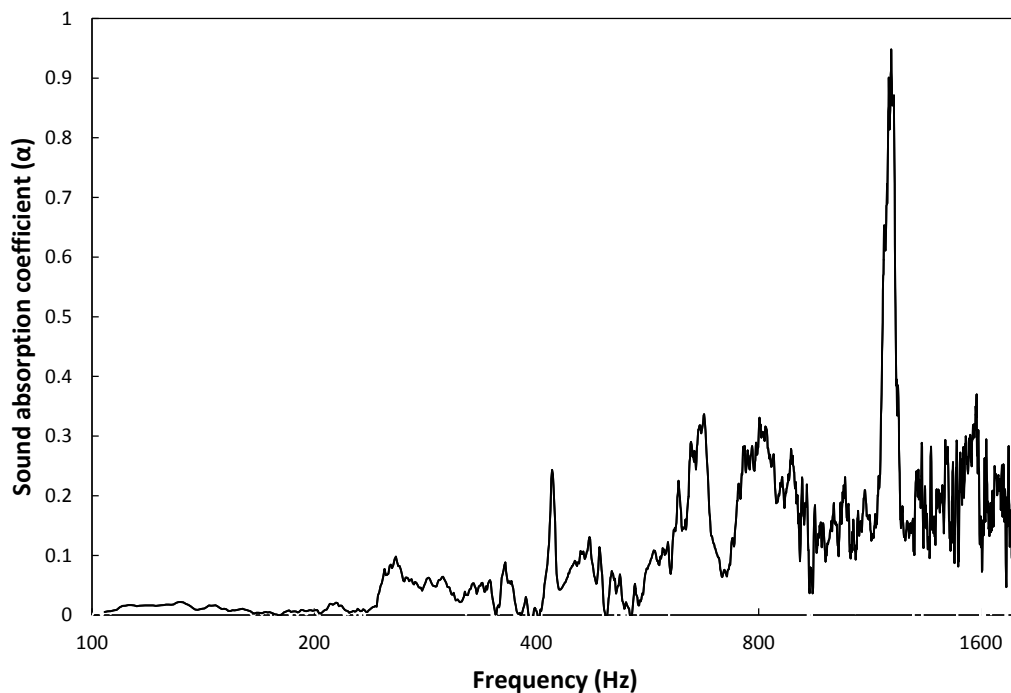


Figure 7.2: Sound absorption coefficient of a mixture solution of PVC& PS A (3:1) at 3cm back cavity

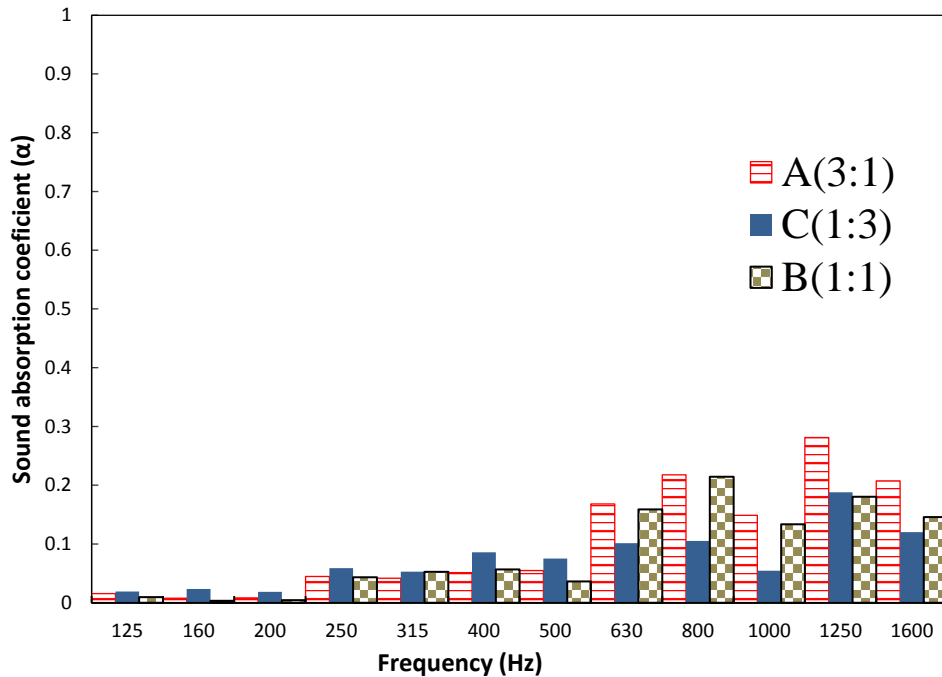


Figure 7.3: Sound absorption coefficient of a mixture solution of PVC& PS with different ratios A(3:1), B(1:1) C (1:3) at 3cm back cavity (1/3 octave plot)

7.2.2 Sound absorption of multi-layer mats of PVC-PS-PVC

Mats of three layers consists of two different polymers were produced. The lower and upper layers were produced from PVC, and the middle was produced from PS. The idea behind the use of PS in the middle layer was that PS foam had been widely used as a sound absorbing material, and its mat is brittle and fragile, thus it could be easily shredded as it was taken out from the surface of the drum. Therefore, the lower and the upper layers of PVC were produced to keep the PS as one layer without shredding.

In this experiment, the concentration of PVC was 12wt% (PVC12), and the concentrations of PS were 10wt% (PS10) and 20wt% (PS20). Two mats were produced using these concentrations. The first mat (PVC12-PS10-PVC12) had a thickness of 219 μ m, and the second mat had (PVC12-PS20-PVC12) a thickness of 501 μ m, respectively. The absorption coefficient for the first mat was measured at two different back cavities 3 and 5cm. It was noticed that the absorption coefficient increased at certain frequencies of (f_c) 397, 500 and 794Hz as the back cavity increased, while it was unaffected at others frequencies as shown in Figure 7.4, Figure 7.5, and Figure 7.6. For the second mat (PVC12-PS20-PVC12), the absorption coefficient was measured at 3cm back cavity. It was shown that the second mat enhanced the sound absorption coefficient due to its thickness, and the gradient fiber' diameters difference between the PVC and PS as shown

in Figure 7.7. In addition, it was shown PS10wt% mat had beads, however, the PS 20wt% mat was free of beads, as the beads existence decreased the sound absorption efficiency.

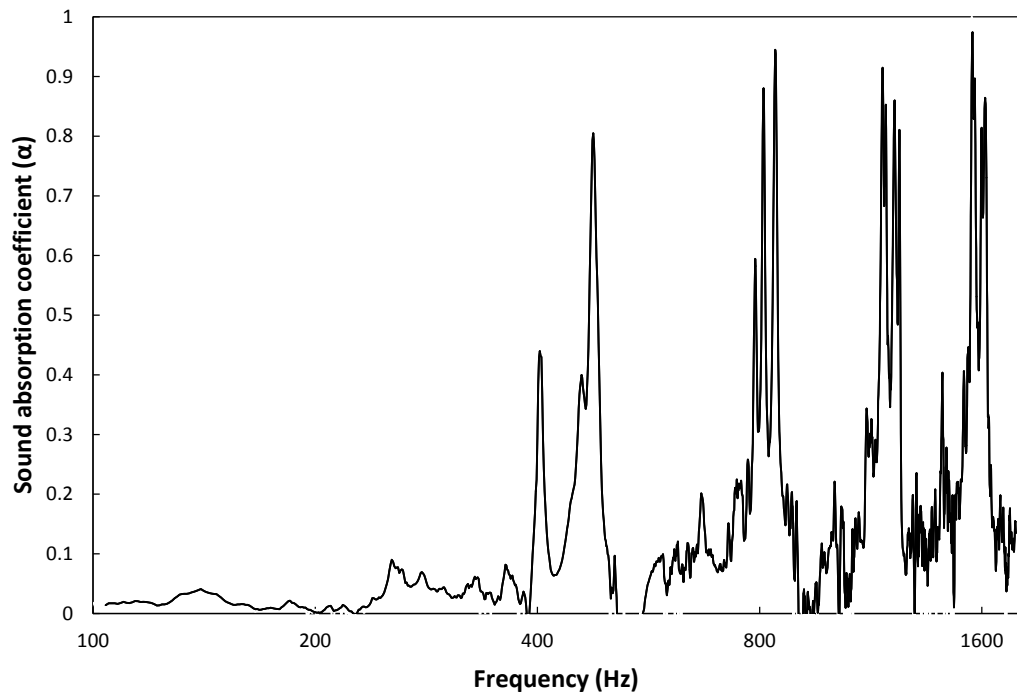


Figure 7.4: Sound absorption coefficient of multilayer mat PVC12 - PS10 - PVC12 at 3cm back cavity

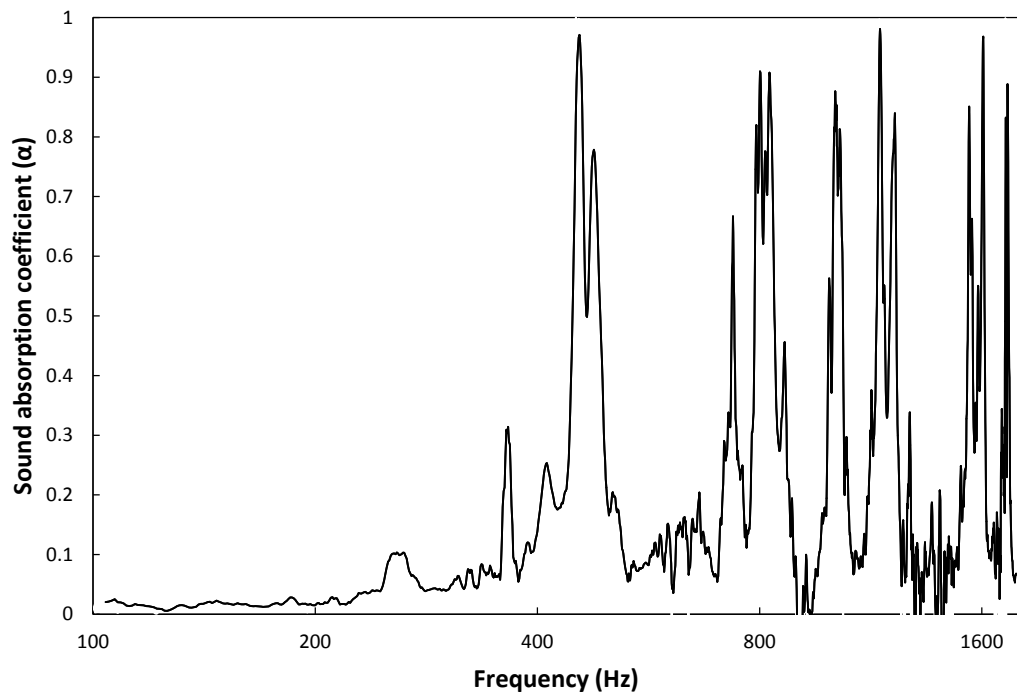


Figure 7.5: Sound absorption coefficient of multilayer mat PVC12-PS10-PVC12 at 5cm back cavity

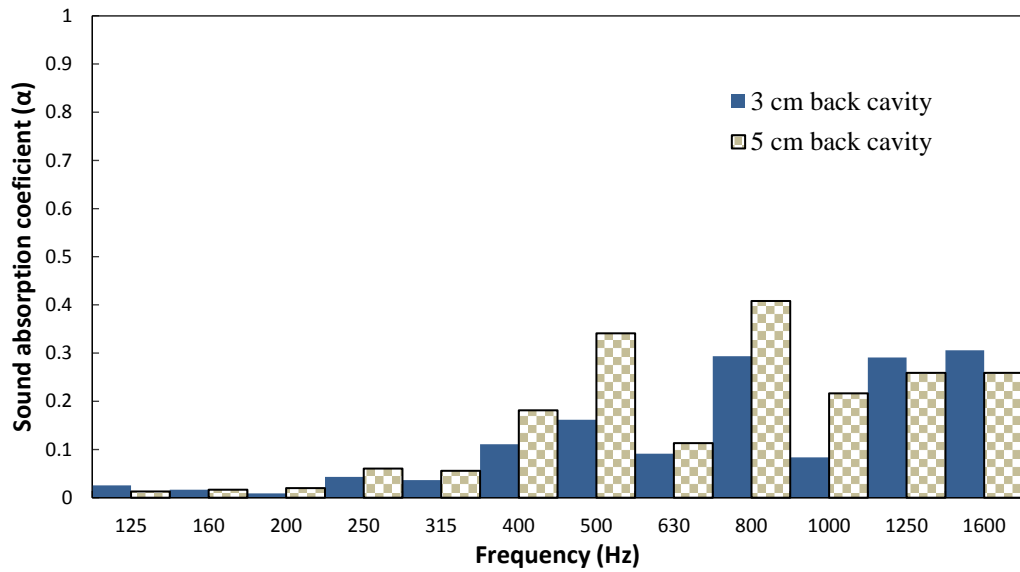


Figure 7.6: Sound absorption coefficient of multilayer mats PVC12-PS10-PVC12 at 3 and 5cm back cavity (1/3 octave plot)

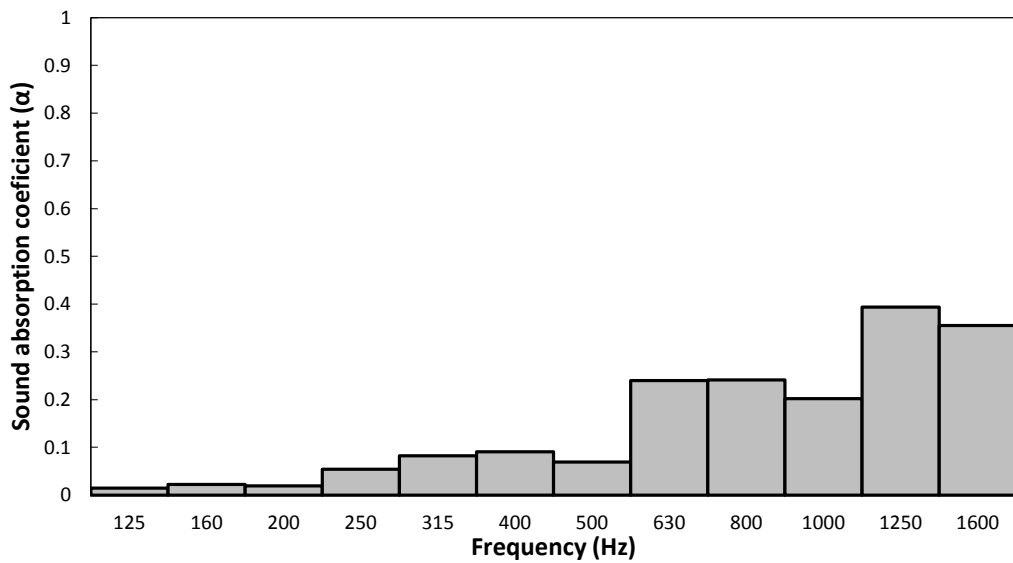
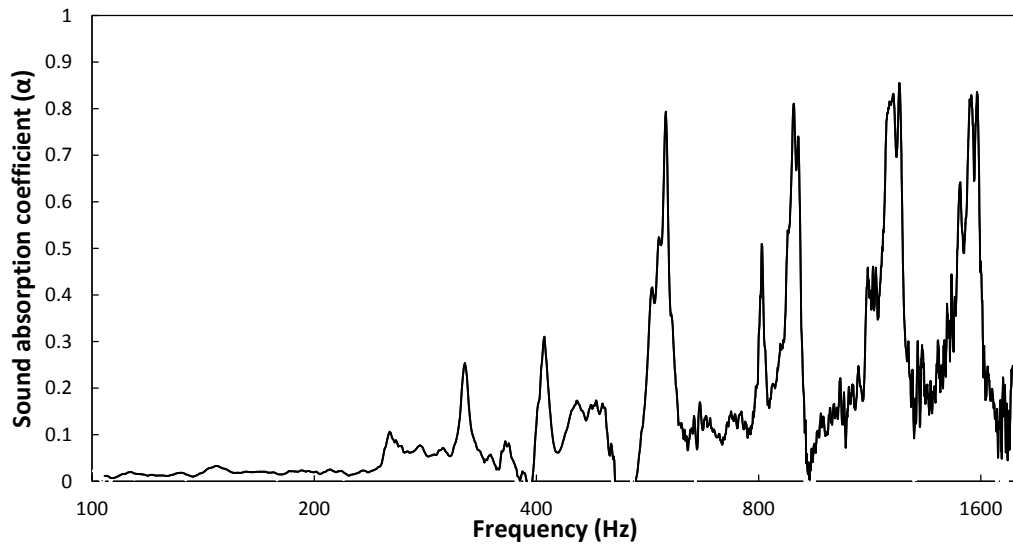


Figure 7.7: Sound absorption coefficient of multilayer mat PVC12-PS20-PVC12 at 3cm back cavity (FFT and 1/3 octave plot)

7.2.3 Sound absorption of composites PVC

7.2.3.1 Carbon nanotubes and PVC

Carbon nanotubes were sonicated in N,N-dimethyl formalidede (DMF) then PVC is added to the solution, and stirred vigorously for 3h at 60 °C. CNTs of 5 and 10wt% were added to PVC solution. The addition of 5wt% CNTs to PVC solution improved the sound absorption of PVC nanofiber mats, and the sound absorption increased twice at 397Hz, four times at 500Hz, and 1.5 times at 1587Hz by comparing the measurements in Figure 7.1 and Figure 7.8. However, increased the CNTs to 10wt% decreased the sound absorption of PVC mats as shown in Figure 7.9 and Figure 7.10. The fibers diameter of the mat increased from 144nm to 270nm, as the percent of CNTs increased to 5wt% and 10wt%, respectively.

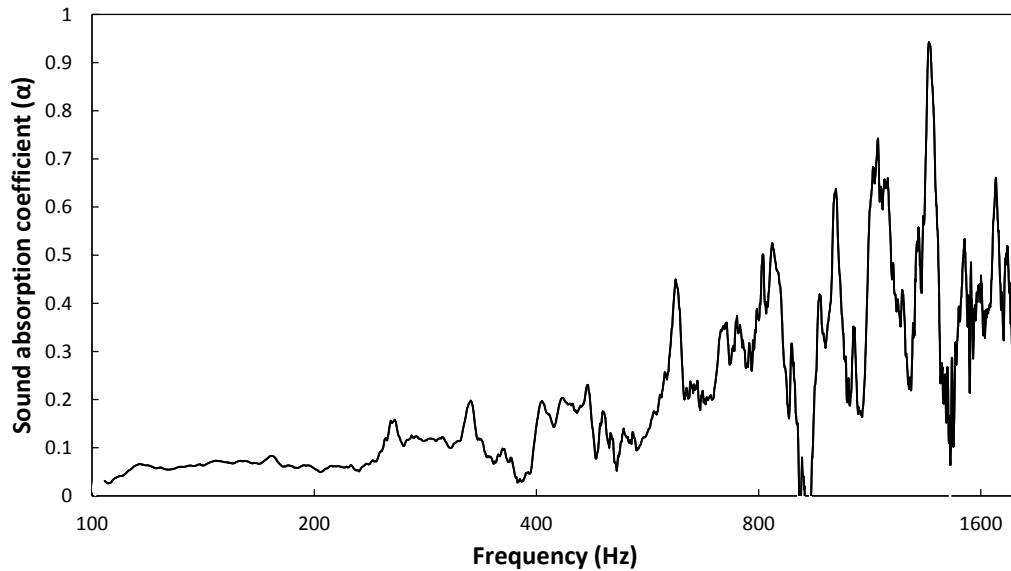


Figure 7.8: Sound absorption coefficient of PVC12wt% CNTs 5wt% at 3cm back cavity

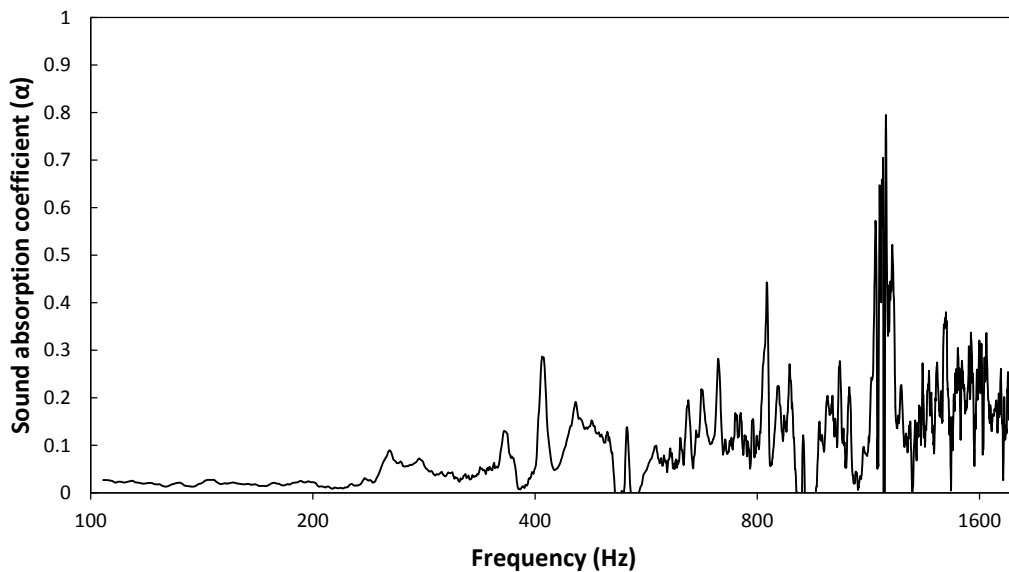


Figure 7.9: Sound absorption coefficient of PVC12 wt% CNTs 10 wt% at 3cm back cavity

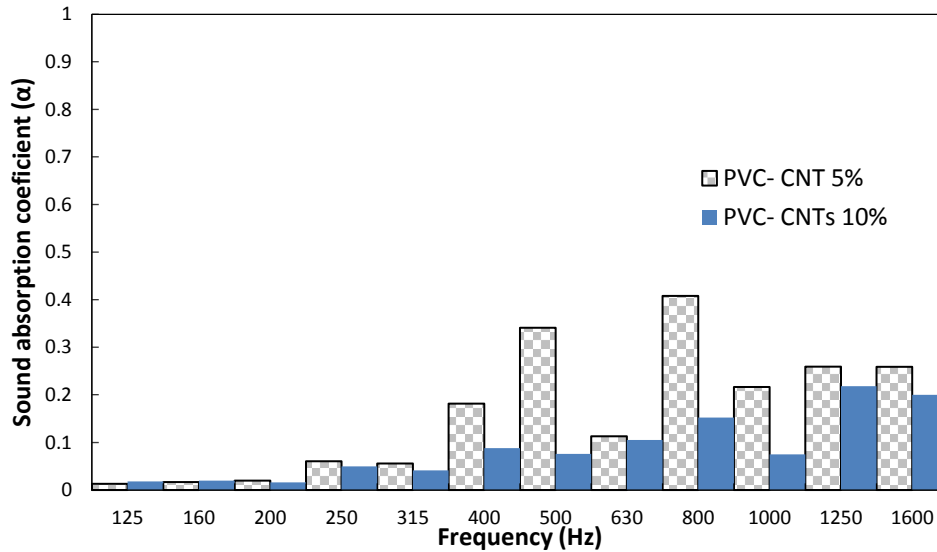


Figure 7.10: Sound absorption coefficient of PVC12 CNTs5 and PVC12 wt% CNTs 10 wt% at 3cm back cavity (1/3 octave plot)

7.2.3.2 Fiberglass and PVC

Fiberglass (FG) was added to the PVC 12wt% by different concentrations of 5, 10, 20 and 30wt% according to the weight of PVC. First, FG was sonicated in DMF for 30 min then PVC was added to the solution, and stirred vigorously for 3h at 60 °C. The addition of FG with different percentages to PVC did not show improvement in the sound absorption for PVC mats except at frequency 1260Hz, the sound absorption increased from 0.31 to 0.4 for 20wt%, and 30wt% as observed in Figure 7.15.

The previous four samples were mounted together with a separation distance 2mm between each mat, and using 2cm back cavity. The sound absorption had a noticeable improvement at frequency bands 1260 and 1587Hz as shown in Figure 7.16. The existence of air space between samples plays an effective role in increasing the ability to absorb the sound wave. The air gaps act as a gradient structure within the mats, where the sound waves moved between the mediums had different densities.

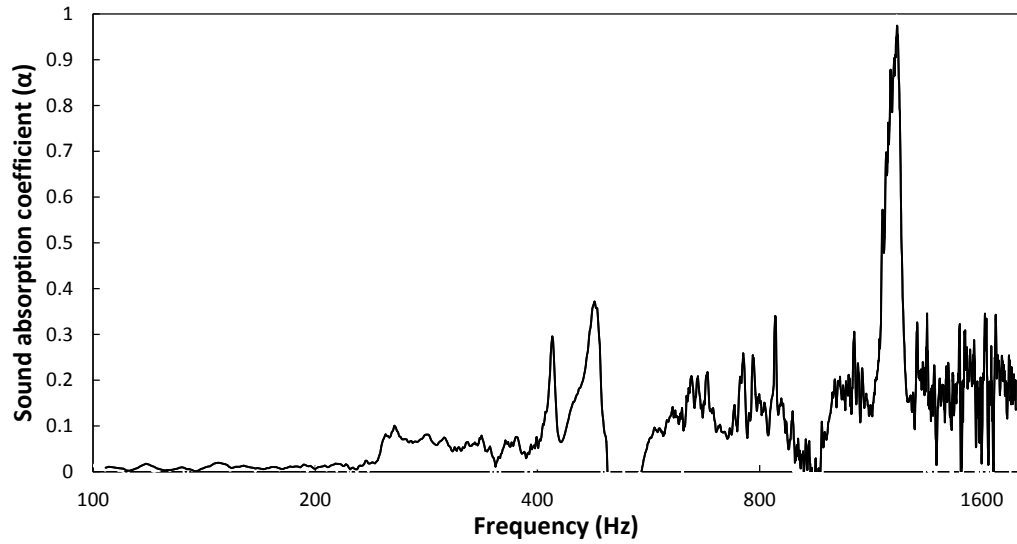


Figure 7.11: Sound absorption coefficient of PVC 12wt% and FG 5wt% at 3cm back cavity

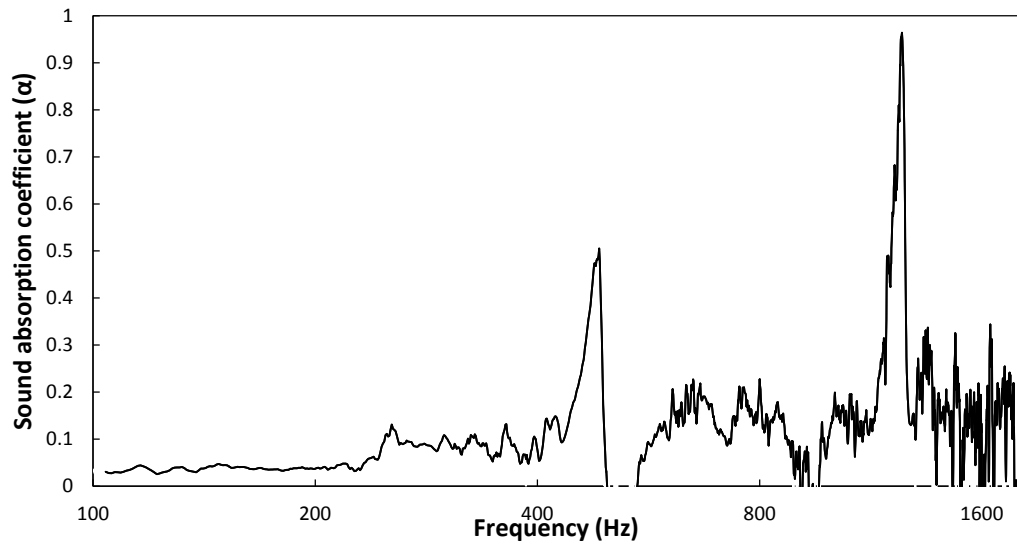


Figure 7.12: Sound absorption coefficient of PVC 12wt% and FG 10wt% at 3cm back cavity

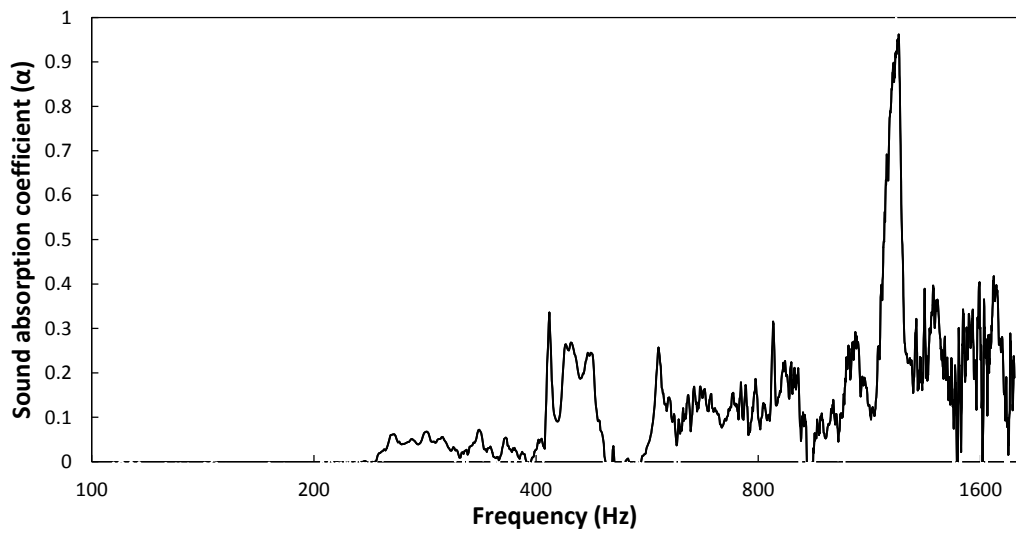


Figure 7.13: Sound absorption coefficient of PVC 12wt% and FG 20wt% at 3cm back cavity

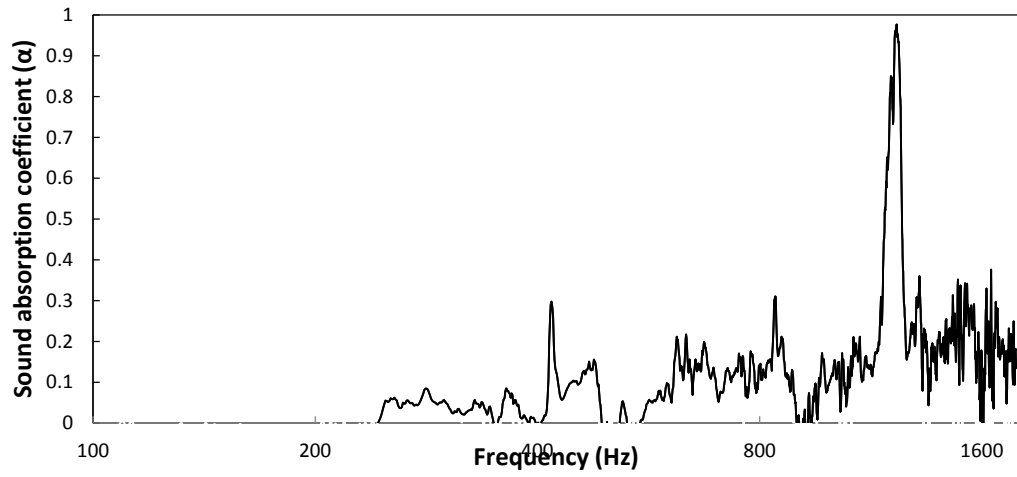


Figure 7.14: Sound absorption coefficient of PVC 12wt% and FG 30wt% at 3cm back cavity

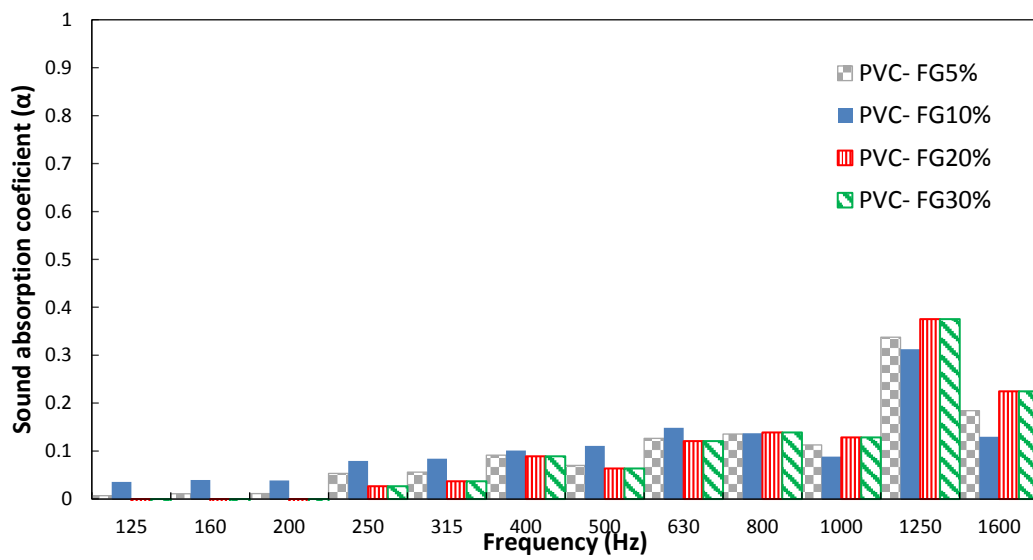


Figure 7.15: Sound absorption coefficient of PVC 12wt% with (5, 10, 20, 30wt%) FG at 3cm back cavity (1/3 octave plot)

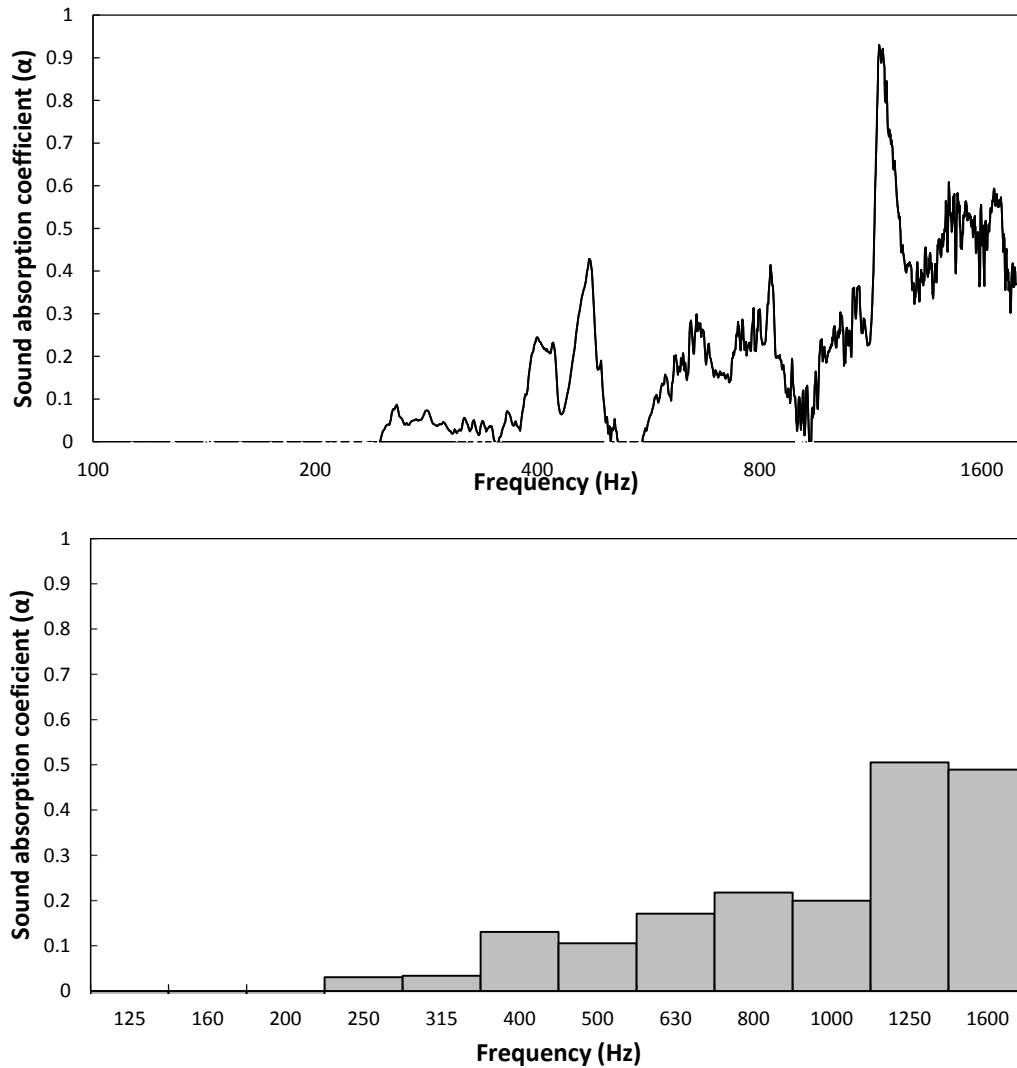


Figure 7.16: Sound absorption coefficient of four composite samples of PVC 12% and FG with 2cm cavity and 2mm separation distance between each sample (FFT and 1/3 octave plot)

7.2.4 Double layers of composite PVC mats

Two composite PVC mats were added over each other without any air gap to obtain a double layer of composite of PVC mat. The first mat was PVC with 10wt% CNTs and the second was PVC with 5wt% CNTs. The double layer mats showed an acceptable improving for sound absorption. The sound absorption increased from 0.2 to 0.6 at 500-1850Hz as seen in Figure 7.17. This enhancement was due to the grade arrangement of the diameter of the fiber of the two mats where the fiber's diameters were 270nm and 144nm, respectively as mentioned in Chapter 6.

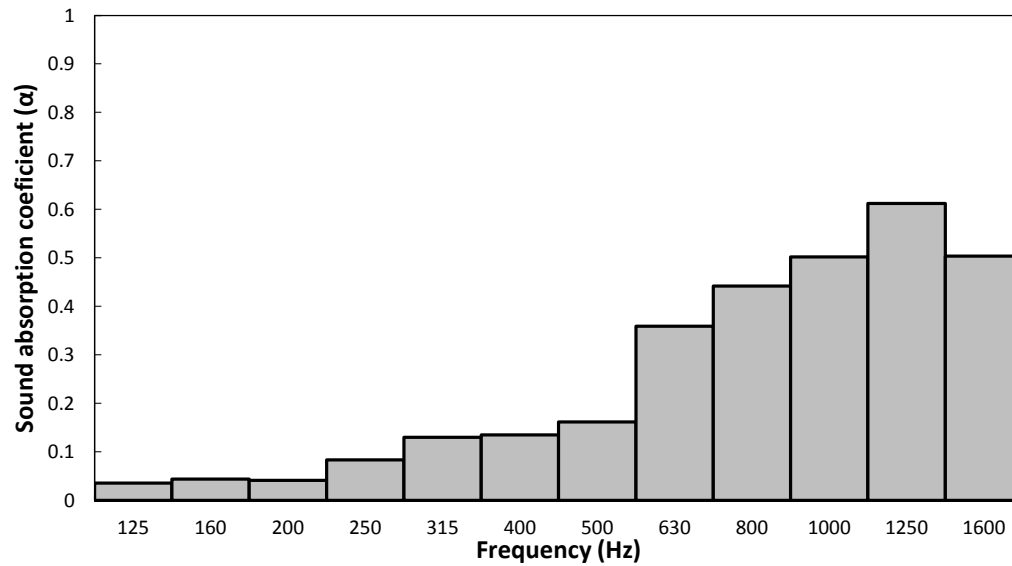
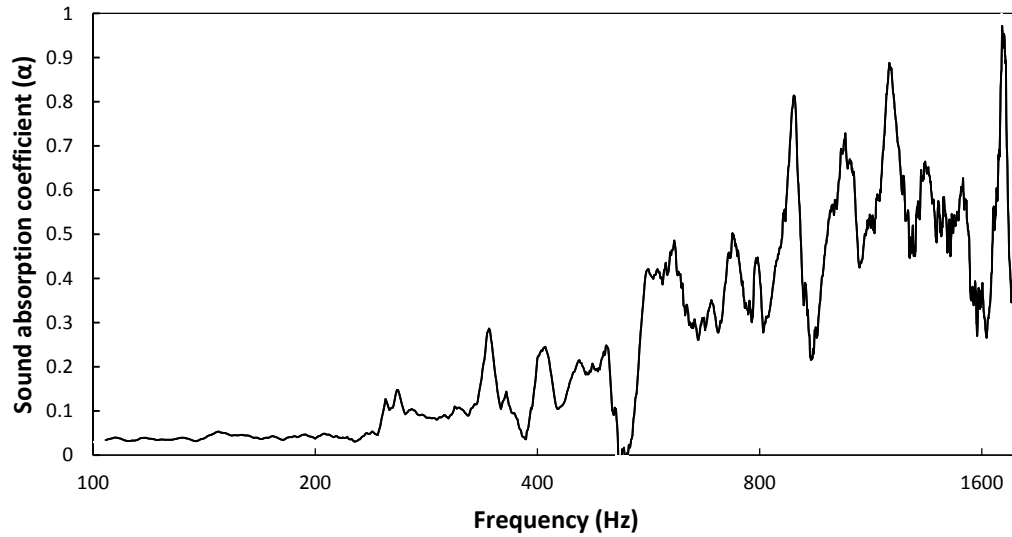


Figure 7.17: Sound absorption coefficient of two composite attached PVC with CNTS mats at 3cm back cavity (FFT and 1/3 octave plot)

The air gaps effect were studied using the previous two composite mats of PVC/CNTs. The existence of air gaps increased the sound absorption for the sample all over the frequency range as shown in Figure 7.18 compared to the measurements shown in Figure 7.17.

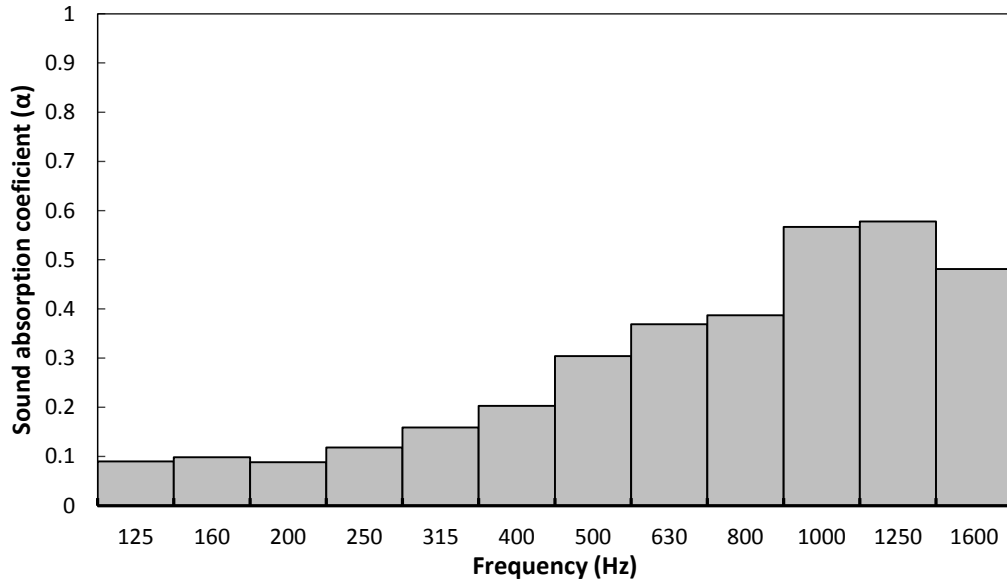


Figure 7.18: Sound absorption coefficient of two composite mats PVC/CNTs with 6mm gap and 3cm back cavity (1/3 octave plot)

7.3 Sound absorption of PVA mats

Polyvinyl alcohol (PVA) was a biodegradable material that had many applications in textile and food industry. Solutions of 9wt% and 12wt% PVA were prepared. Some research groups used PVA as a sound absorbing material. PVA was electrospun and its sound absorption coefficient was measured at 3cm back cavity. PVA mats had a good sound absorption coefficient up to 0.95 at a frequency range between 1150-1250Hz. Regarding the sound absorption measurements, it was observed that mat of PVA with low concentration had better sound absorption than the high concentration mat due to its low fibers diameter, which increased the surface areas as observed in Figure 7.19, Figure 7.20, and Figure 7.21.

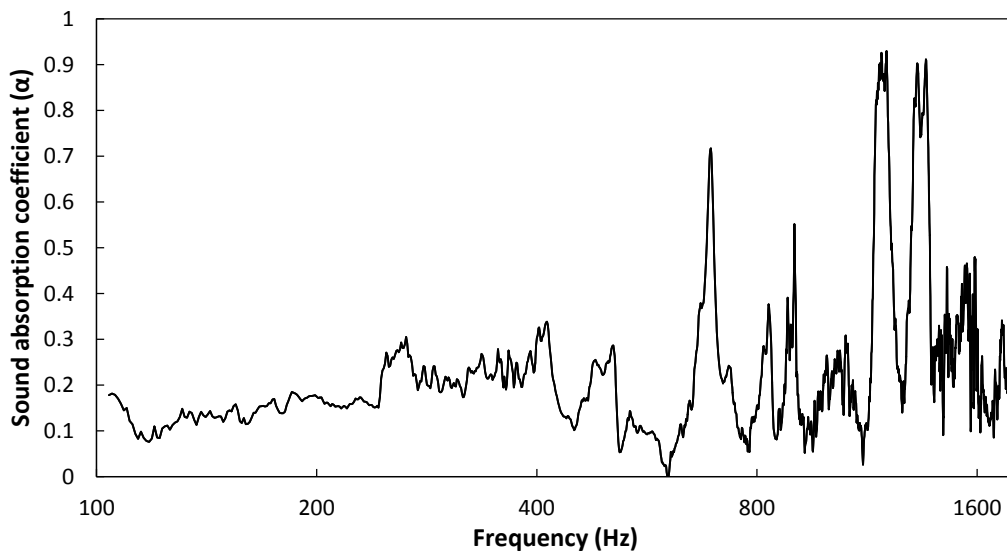


Figure 7.19: Sound absorption coefficient of PVA 9% at 3cm back cavity

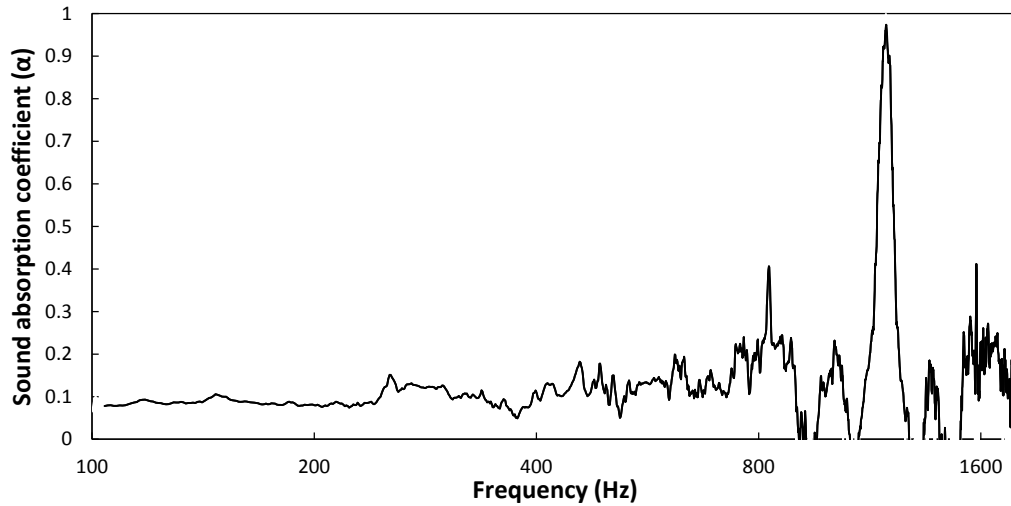


Figure 7.20: Sound absorption coefficient of PVA 12% at 3cm back cavity

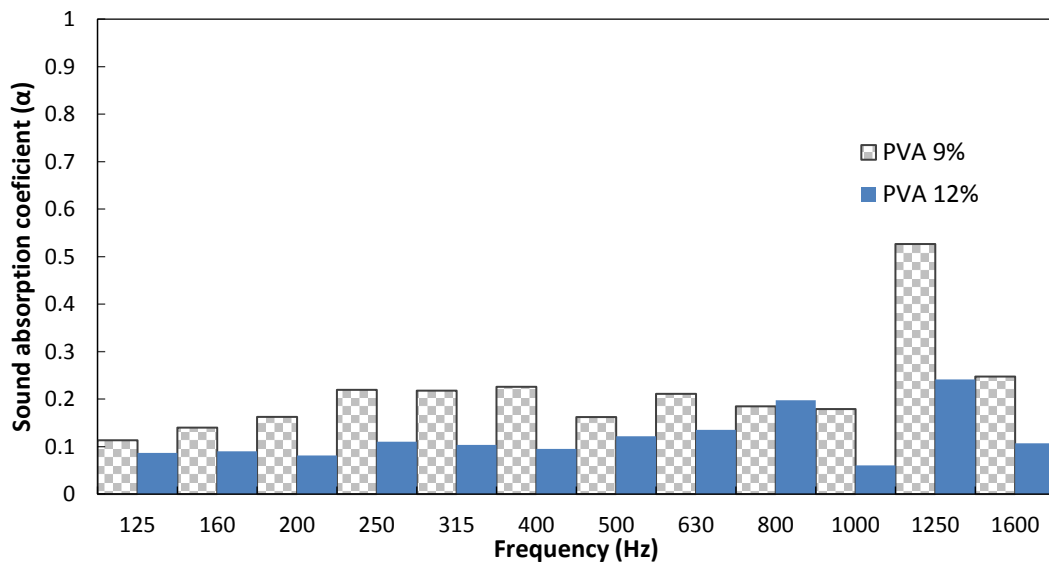


Figure 7.21: Sound absorption coefficient of PVA 9wt% and PVA 12wt% at 3cm back cavity (1/3 octave plot)

7.3.1 Sound absorption of composite PVA mats

7.3.1.1 PVA and Carbon nanotubes (CNTs)

The composite mats of PVA/CNTs were produced, where PVA used as a matrix and CNTs as a filler. Two concentrations of PVA 9 and 12wt% were used to prepare the polymer solutions. CNTs were added with two concentrations 5 and 10wt%. The sound absorption coefficients of the samples were investigated using 3cm back cavity. The results showed that addition of CNTs improved the sound absorption for PVA 9wt% membrane. In addition, a significant improvement was noticed for the mat of PVA 9wt% with CNTs 5wt. In addition, Figure 7.26 showed the mats with low concentration of 9wt% of PVA have better sound absorption, and it noticed that the low concentration of 5wt% of CNTs has higher sound absorption than 10wt% at 1000 and 1600Hz.

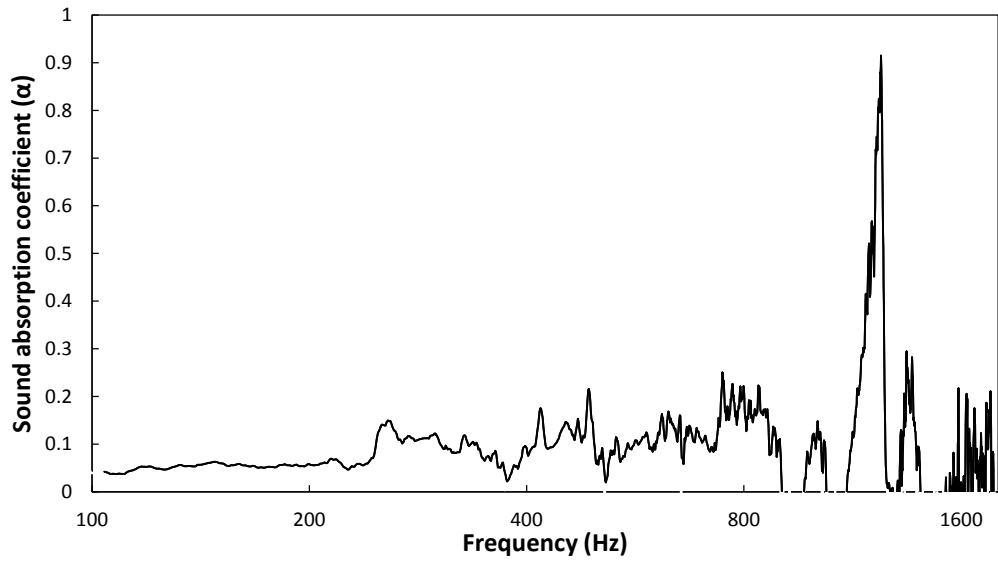


Figure 7.22: Sound absorption coefficient of PVA 12wt% CNTs 5wt% at 3cm back cavity

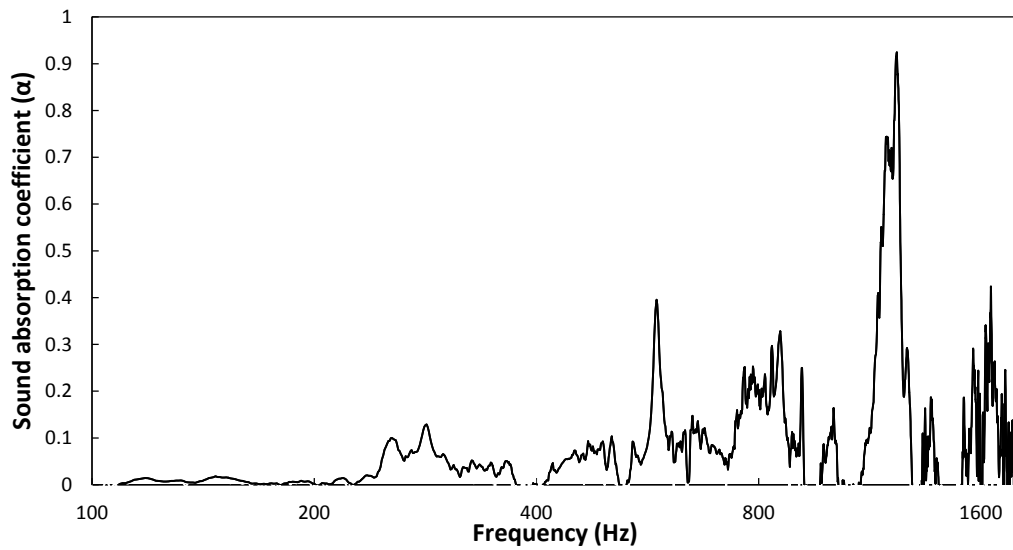


Figure 7.23: Sound absorption coefficient of PVA 12wt% CNTs 10wt% at 3cm back cavity

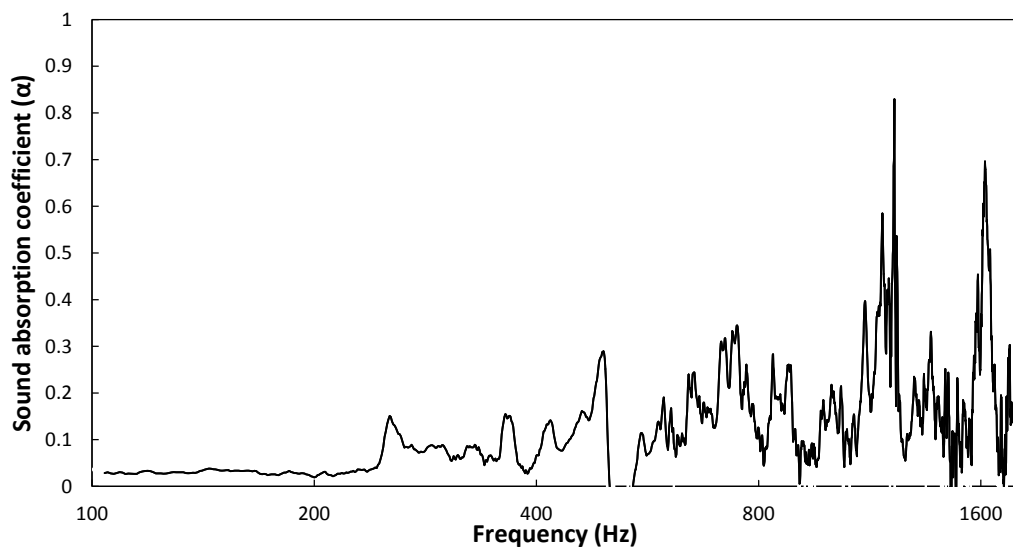


Figure 7.24: Sound absorption coefficient of PVA 9wt% CNTs 5wt% at 3cm back cavity

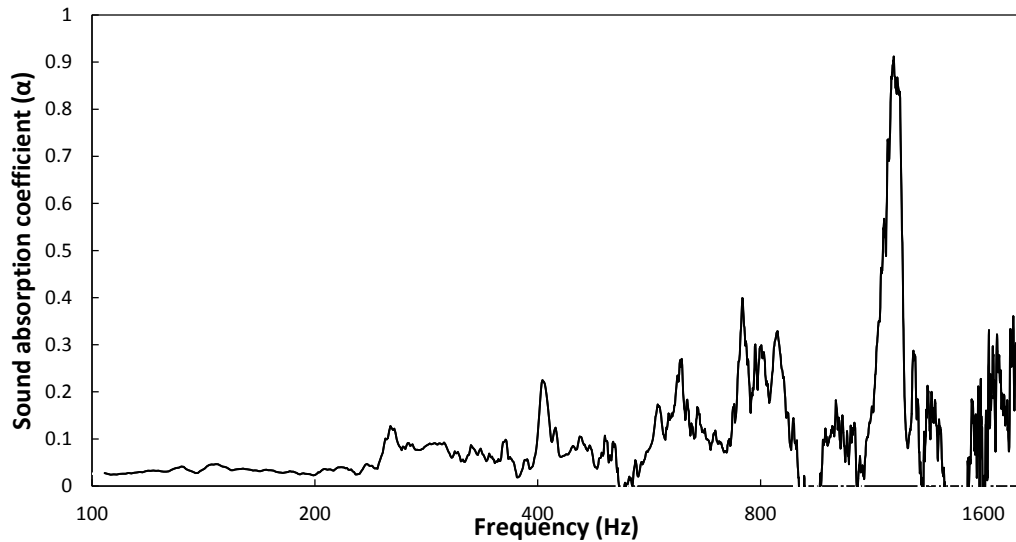


Figure 7.25: Sound absorption coefficient of PVA 9wt% CNTs 10wt% at 3cm back cavity

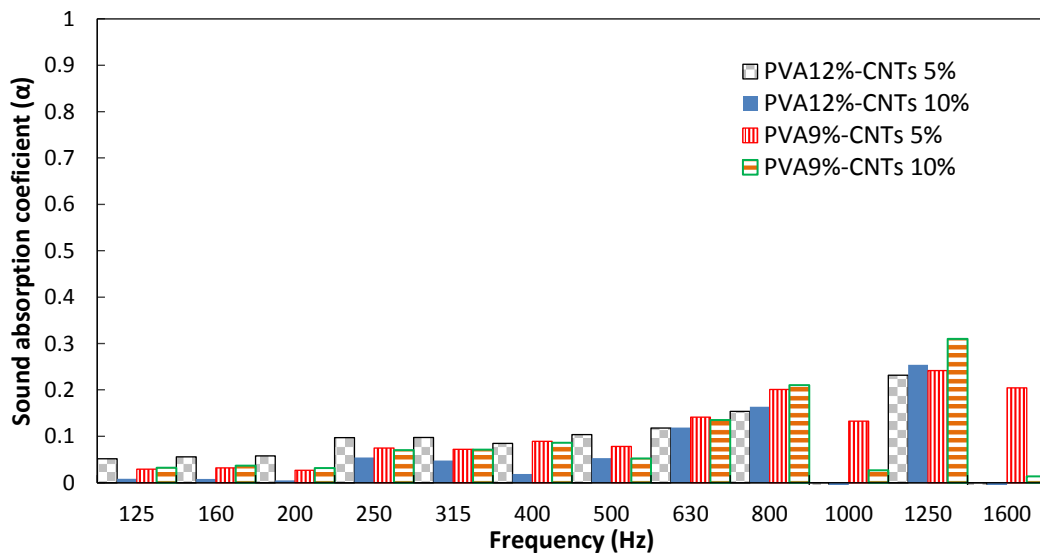


Figure 7.26: Sound absorption coefficient of PVA 12wt% CNTs 5wt%, PVA 12wt% CNTs 10wt%, PVA 9wt% CNTs 5wt%, PVA 9wt% CNTs 10wt% at 3cm back cavity (1/3 octave plot)

7.3.1.2 PVA and Graphene (GN)

GN was used as a filler with PVA mats and the sound absorption for the samples was investigated at 3cm back cavity. The fiber diameters decreased with the increase of GN concentration. Two concentrations of PVA solution were prepared 9 and 12wt%. GN were added to the PVA solutions with 5 and 10wt% according to the weight of PVA. AS the percentage of GN increased the sound absorption of mats increased due to the decrease in the fibers diameter as shown in Figure 7.31.

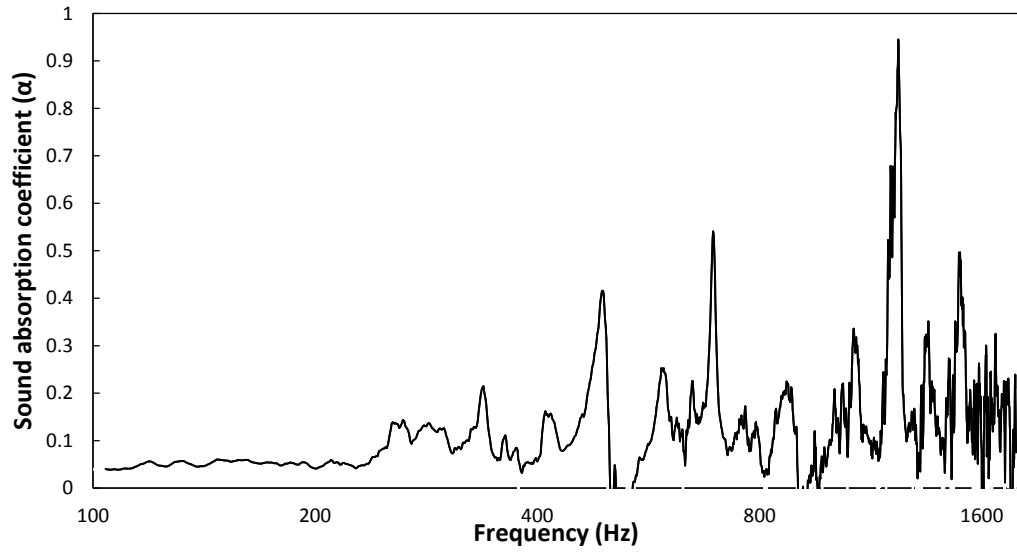


Figure 7.27: Sound absorption coefficient of composite mat PVA12wt% and GN 5wt% at 3cm back cavity

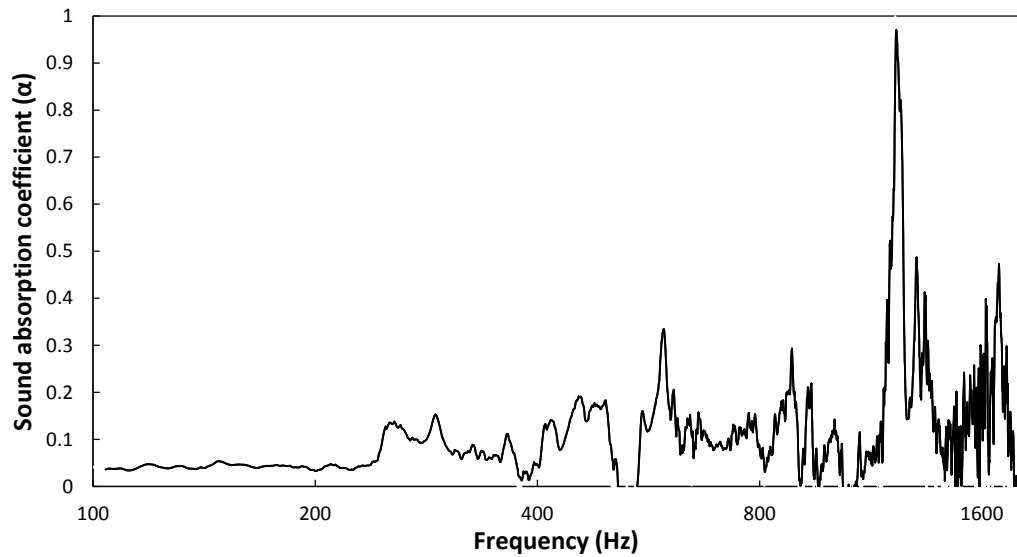


Figure 7.28: Sound absorption coefficient of composite mat PVA12wt% and GN 10wt% at 3cm back cavity

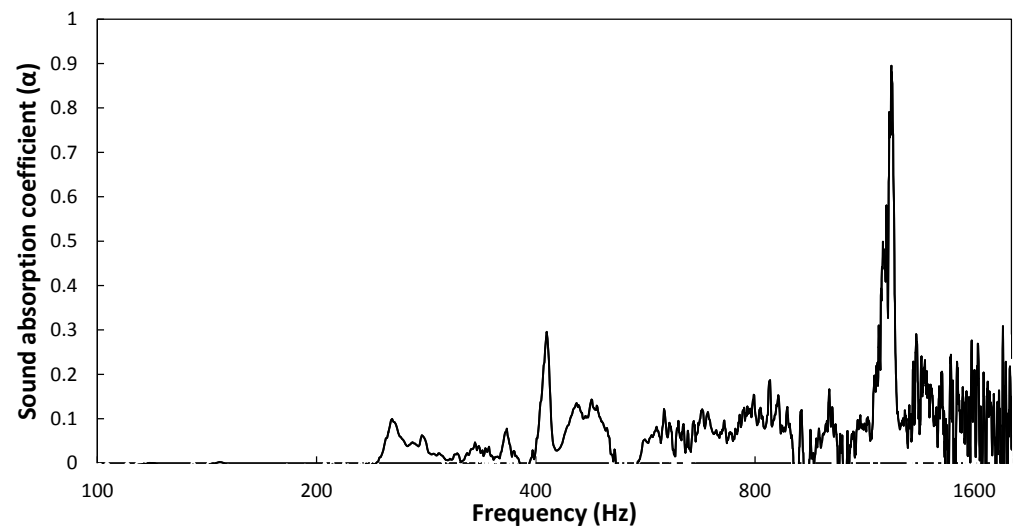


Figure 7.29: Sound absorption coefficient of composite mat PVA9wt% and GN 5wt% at 3cm back cavity

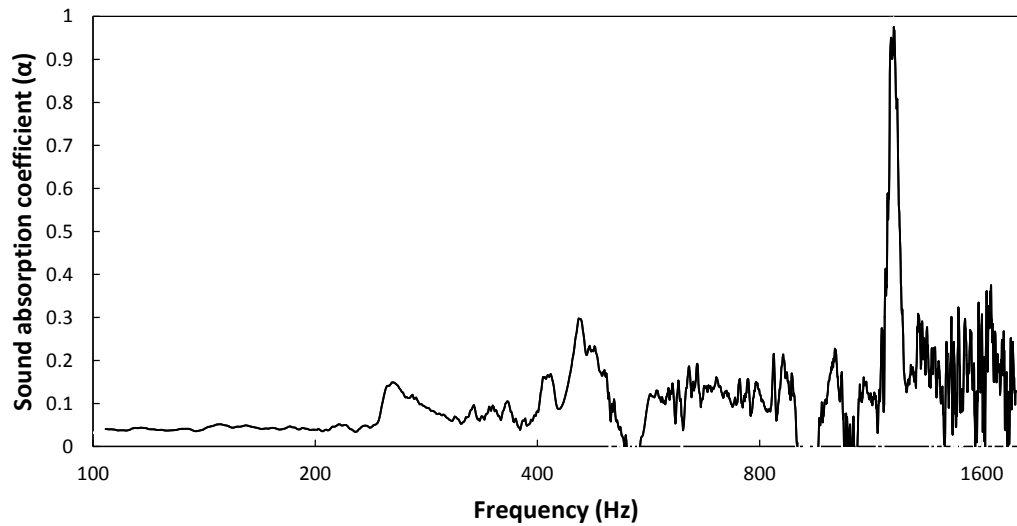


Figure 7.30: Sound absorption coefficient of composite mat PVA9wt% and GN 10wt% at 3cm back cavity

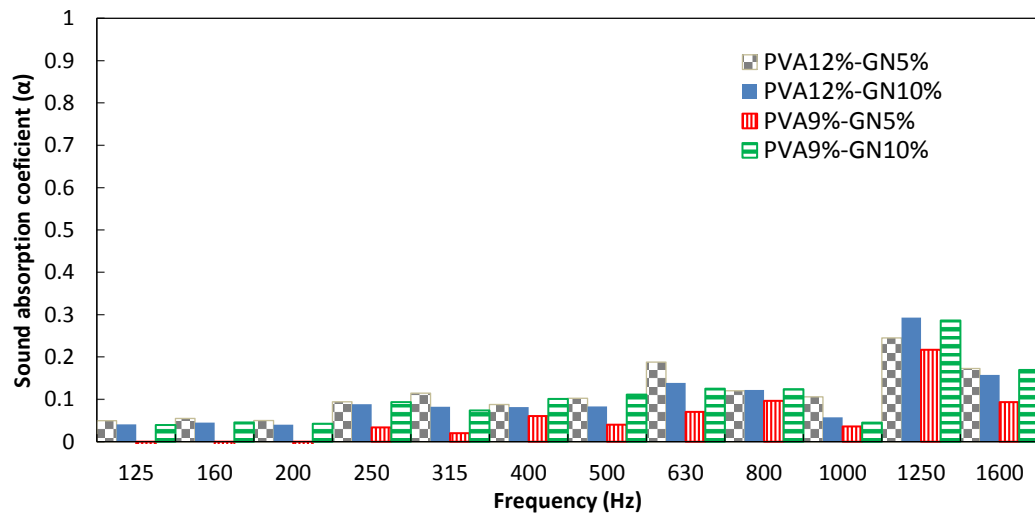


Figure 7.31: Sound absorption coefficient of PVA 12wt%GN 5wt%, PVA 12wt% GN 10wt%, PVA 9wt% GN 5wt%, PVA 9wt% GN 10wt% at 3cm back cavity (1/3 octave plot)

7.3.1.3 PVA and Wollastonite (WS)

WS was added to PVA 9wt% using three concentrations 5, 10, and 20wt% and it was noticed that WS improved the sound absorption of PVA after 630Hz. Although, the increase of WS weights percent had minor effects on the sound absorption as illustrated in Figure 7.35.

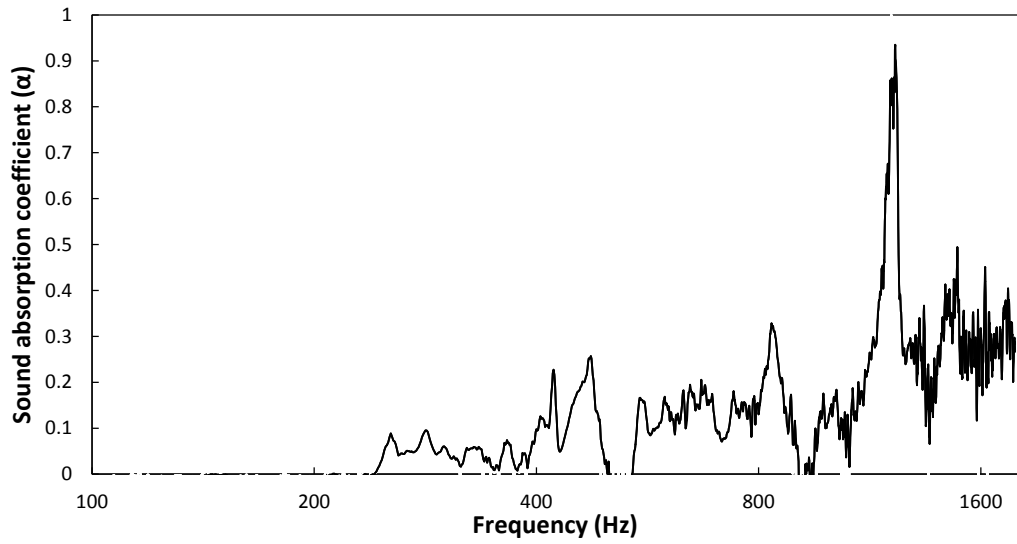


Figure 7.32: Sound absorption coefficient of composite mat PVA 9wt% WS 5wt% at 3cm back cavity

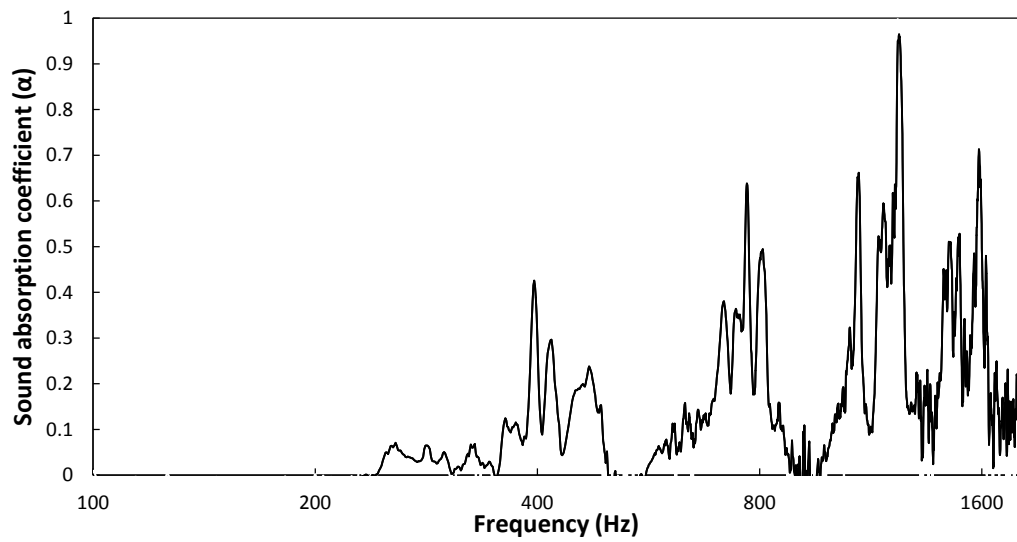


Figure 7.33: Sound absorption coefficient of composite mat PVA 9wt% WS 10wt% at 3cm back cavity

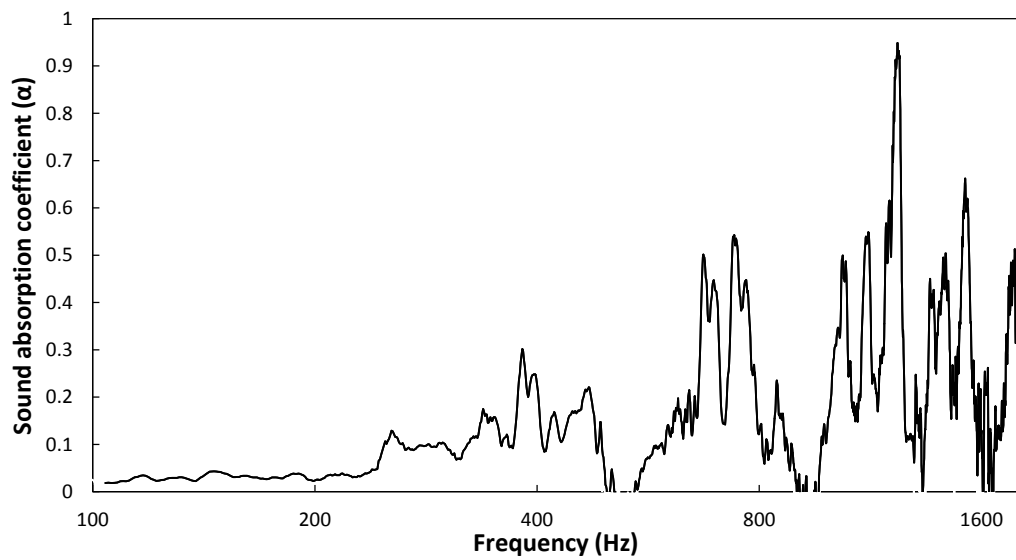


Figure 7.34: Sound absorption coefficient of composite mat PVA9wt% WS 20% with 3cm back cavity

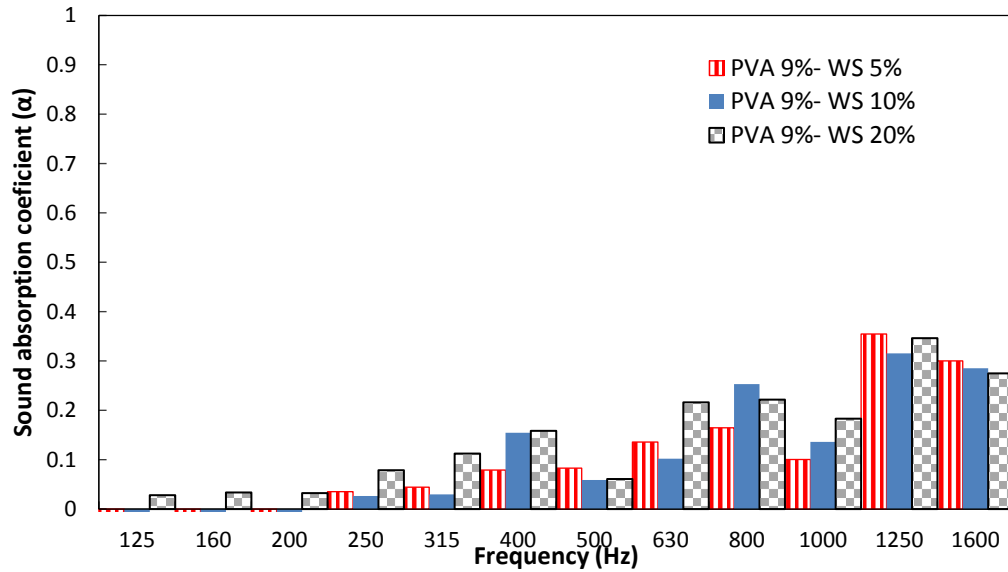


Figure 7.35: Sound absorption coefficient of composite mat PVA 9wt% with (5, 10, 20wt %) WS at 3cm back cavity

7.3.2 Sound absorption of several mats combination

The combination of several attached mats to each other and/or had a gap distances between each other enhanced the sound absorption. First, the sound absorption coefficient of two attached composite mats PVA/CNTs at 3cm back cavity was measured as shown in Figure 7.36, and it was observed that the sound absorption increased to the single mat shown in Figure 7.24 for PVA 9wt% CNTs 5wt% mat. The improvement percentages were as follows: 50% at 800Hz, 42% at 1250Hz and 66% at 1600Hz.

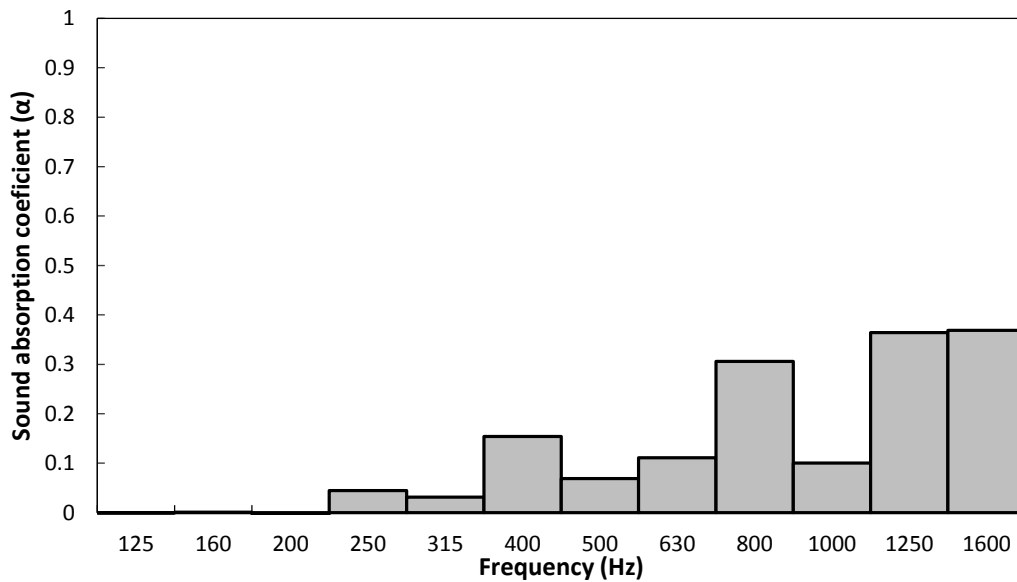
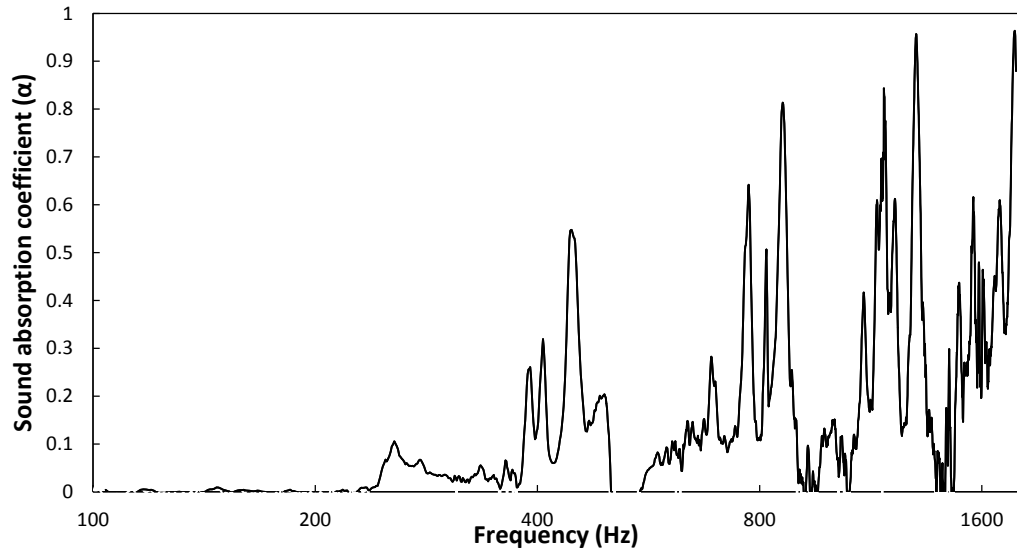


Figure 7.36: Sound absorption coefficient of two samples of PVA 9wt% CNTs 5wt% no air gap and 3cm cavity (FFT and 1/3 octave plot)

Second, the sound absorption coefficient of two composite mats PVA/CNTs with 2mm separation air gap and 3cm back cavity was measured. This sample showed a good sound absorption at different ranges of frequencies (i.e. 630, 800, 1000, 1250 and 1600Hz) as shown in Figure 7.37 and Figure 7.39.

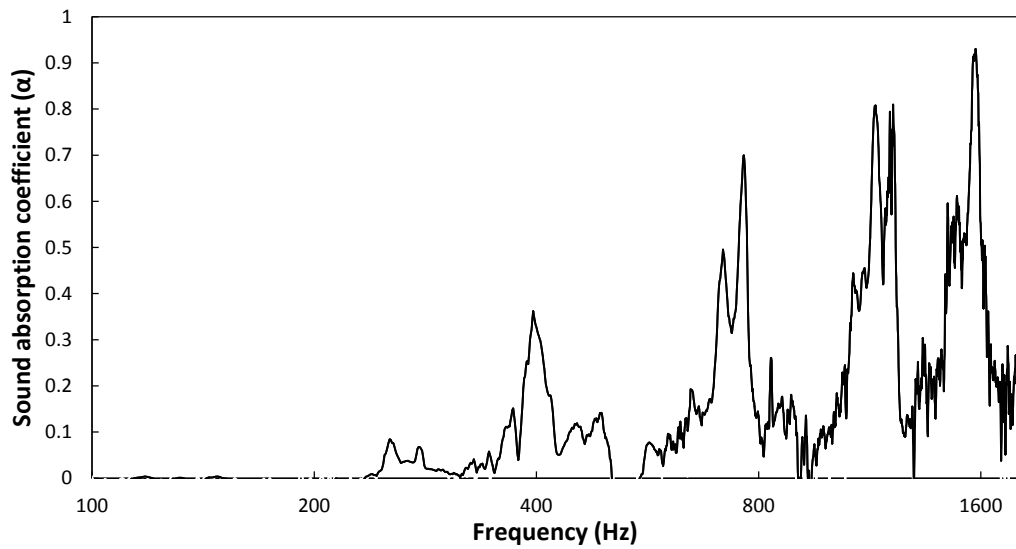
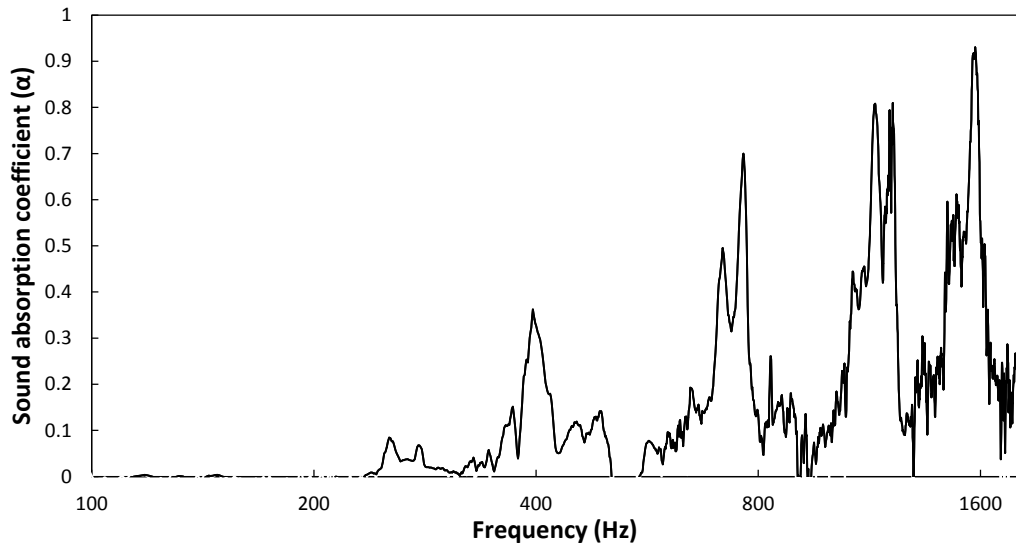


Figure 7.37: Sound absorption coefficient of two composite mats of PVA/CNTs with 2mm air gap and 3cm back cavity

The previous experiment was repeated by increasing the separation gap distance between the two samples to 5mm. It is observed that the increase in the gap distance had a favorable effect on the sound absorption increased at the low-frequency range from 125 to 630Hz as shown in Figure 7.38 and Figure 7.39. This was due to the sound wave had to travel more distance in the air medium which increase the time of sound wave attenuation.

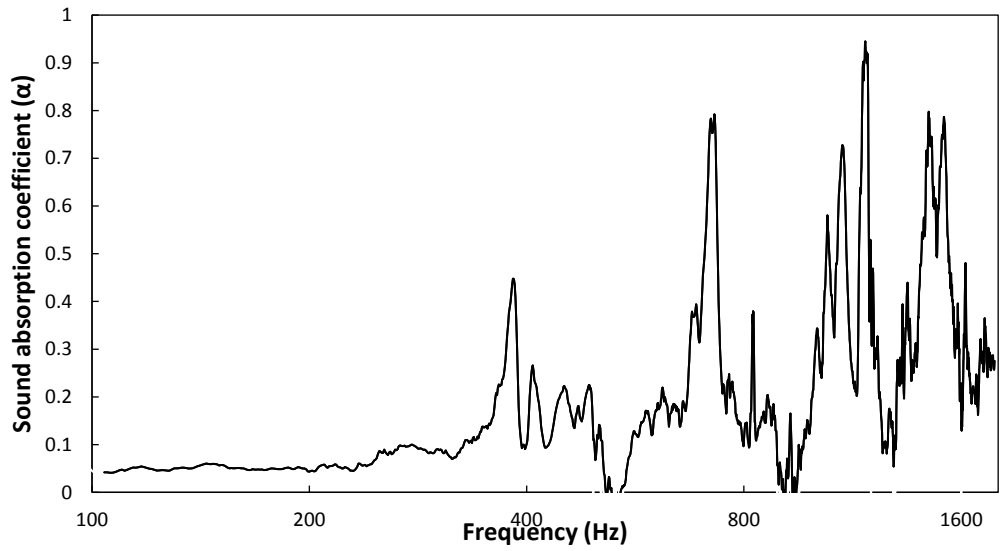


Figure 7.38: Sound absorption coefficient of two composite mats of PVA/CNTs with 5mm air gap and 3cm back cavity

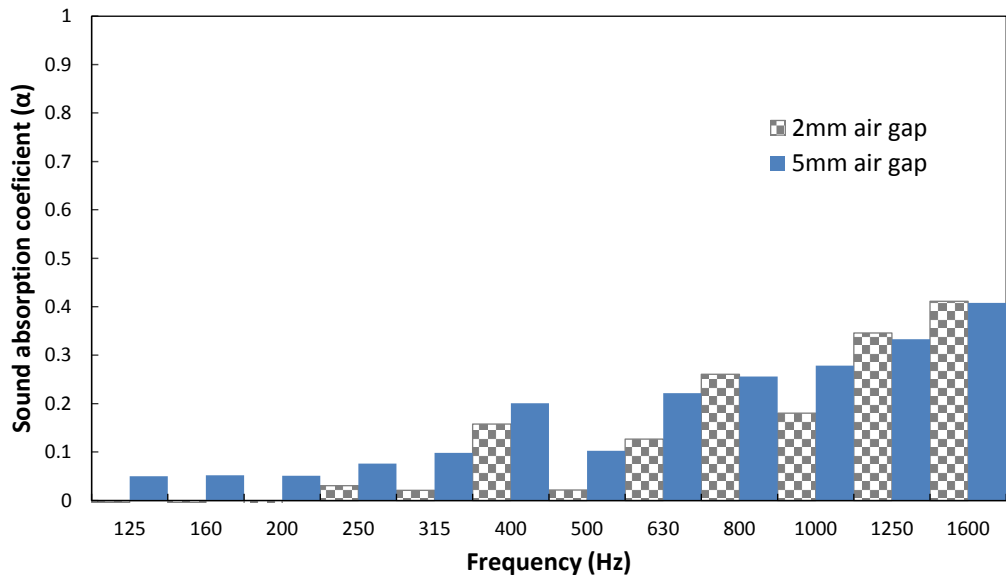


Figure 7.39: Sound absorption coefficient of two composite mats of PVA/ CNTs with 2mm and 5mm air gap and 3cm back cavity (1/3 octave plot)

Other composite mats PVA/GN were also tested. The gaps separation used between mats were 2mm and 7mm. These samples show a duplication in the values of the sound absorption coefficient of single mat at different ranges of frequencies 315, 400, 500, 630, 1000 and 1600Hz while the absorption at the other frequency bands is generally enhanced, as seen in Figure 7.40, Figure 7.41 and Figure 7.42.

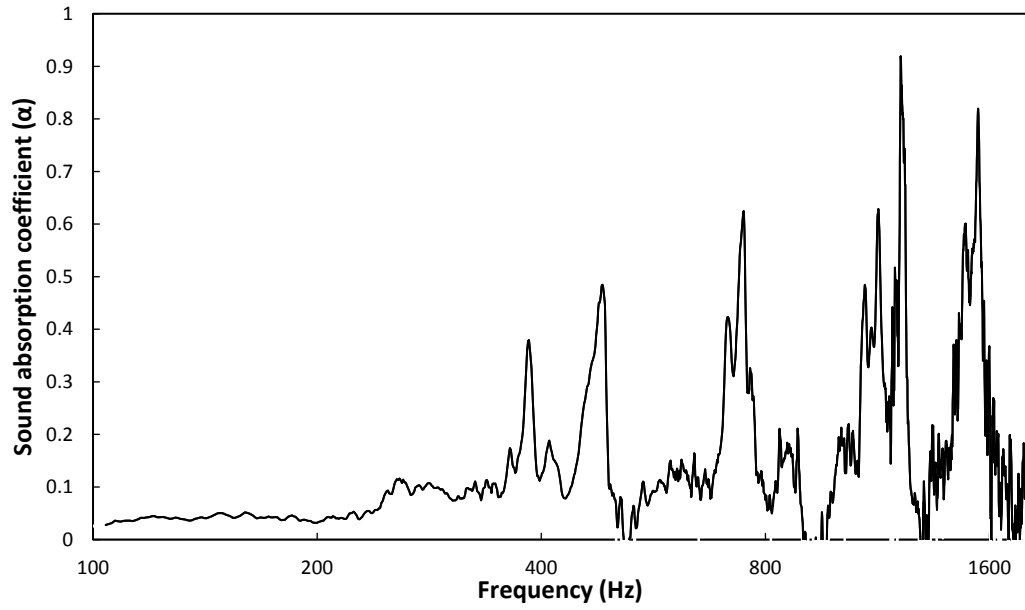


Figure 7.40: Sound absorption coefficient of two composite mats PVA/ GN with 2mm air gap and 3cm back cavity

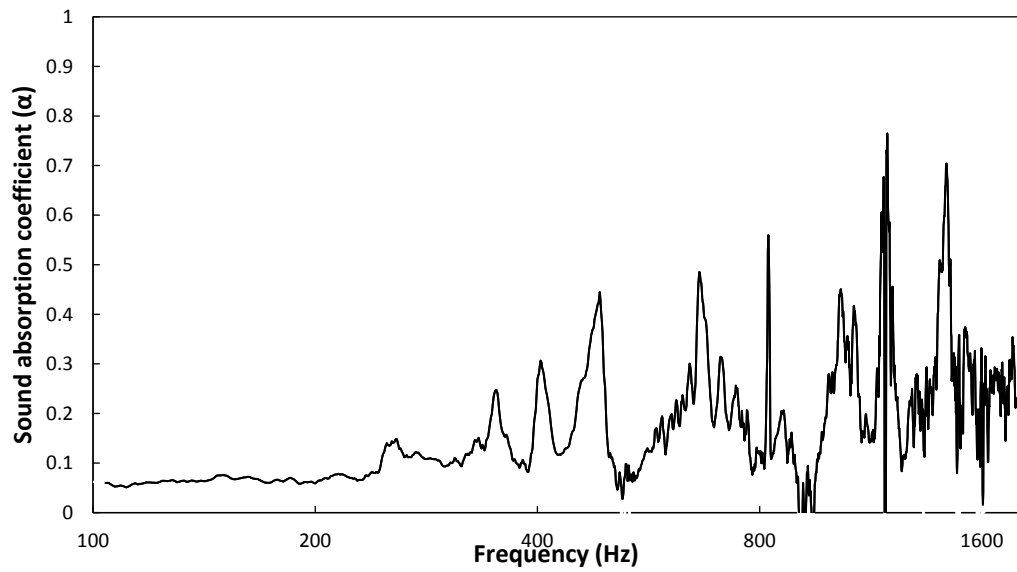


Figure 7.41: Sound absorption coefficient of two composite mats PVA/GN with 7mm air gap and 3cm back cavity

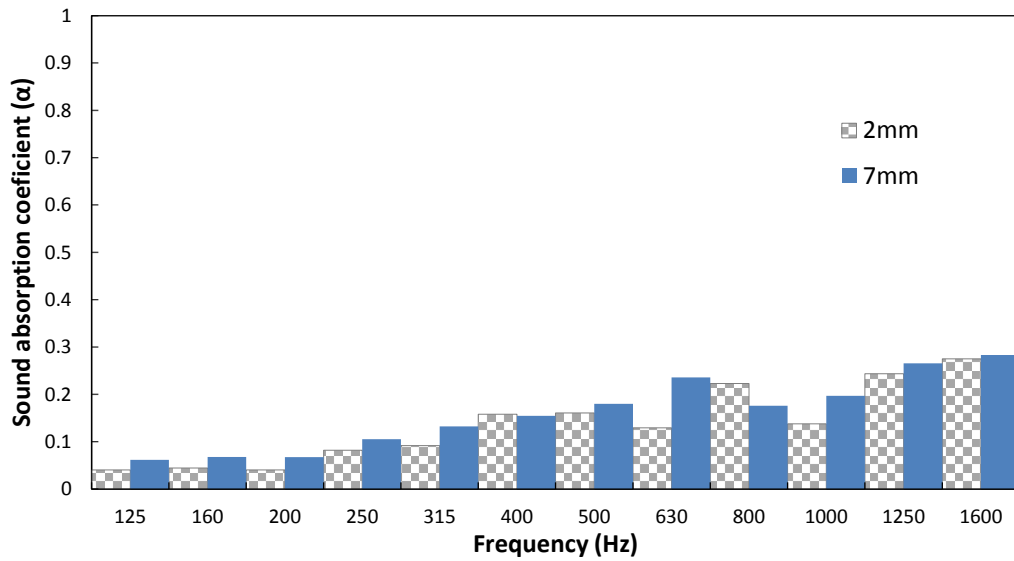


Figure 7.42: Sound absorption coefficient of two composite mats of PVA/GN with 2mm and 7mm air gap and 3cm back cavity (1/3 octave plot)

Furthermore, four composite mats of PVA/GN were used with separation air gaps and 3cm cavity. The arrangement of this bundle was PVA9GN5-2mm-PVA9GN10-1mm-PVA12GN5-2mm- PVA12GN10. The thickness of the samples and air gaps together was about 7mm. A noticed improvement in the sound absorption coefficient reaches 0.48 at 1250 and 1600 Hz as observed in Figure 7.43. The sound traveled through different mediums, and passed through different fiber diameters as it moved between mats and air. As the sound waves travel through the mats, the deformation causes mechanical losses via conversion of part of the sound energy into heat, resulting in acoustic attenuation, mostly due to the mat viscosity. Similar attenuation mechanisms apply for the air and any other medium through which sound travels.

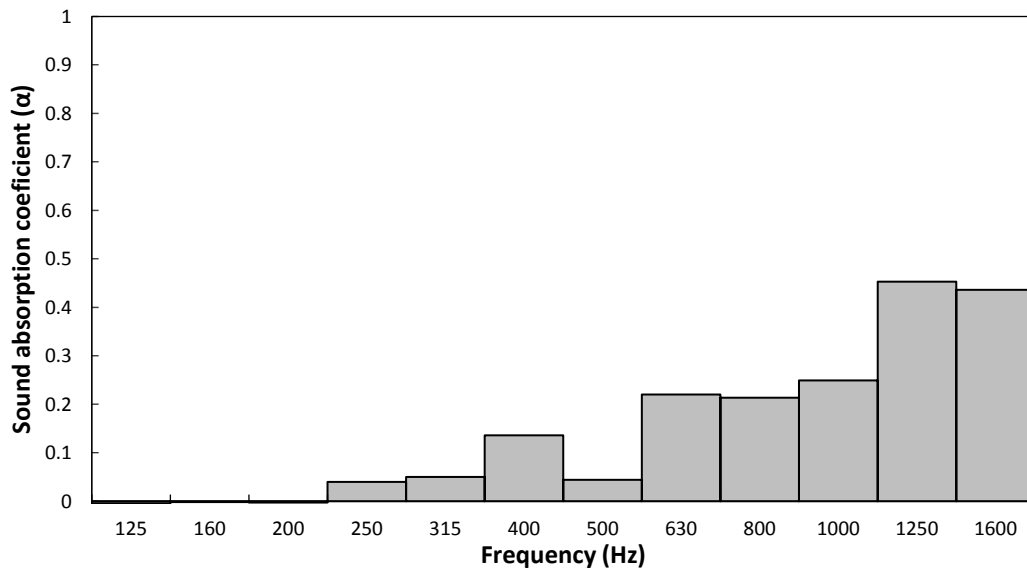
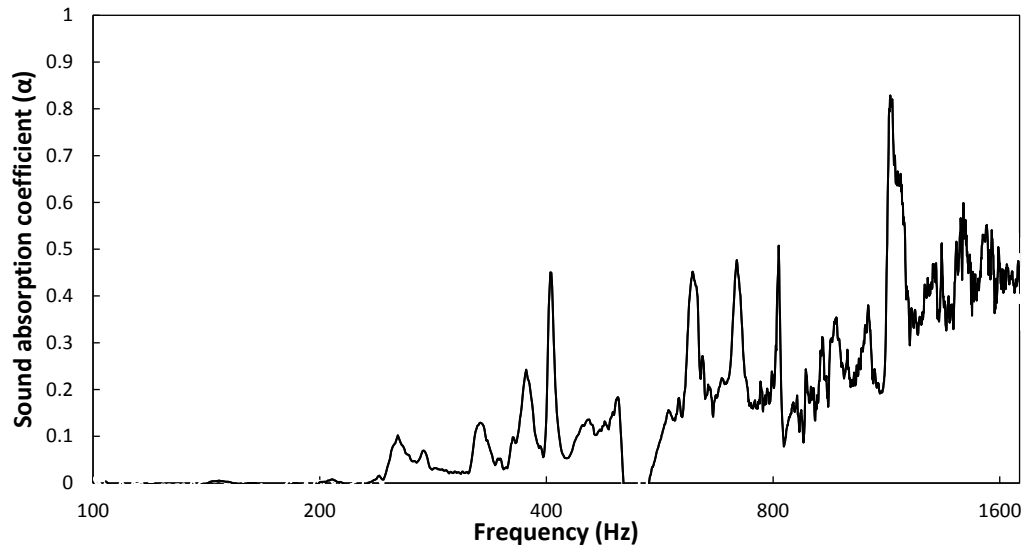


Figure 7.43: Sound absorption coefficient of four composite mats and air gaps (PVA9GN5-2mm PVA9 GN10- 1mm- PVA12GN5-2mm- PVA12GN10) at 3cm back cavity (FFT and 1/3 octave plot)

Another arrangement was used (PVA12GN5-2mm- PVA12GN10-1mm- PVA9GN5-2mm- PVA9GN10). This arrangement had the ability to absorb more sound waves than the previous arrangement as shown in Figure 7.44. The reason behind the changing in the sound absorption is related to the change in the fiber diameters of the mats that face the incident sound wave. The fiber diameters gradually decreased from the facing surface to sound waves the back surface.

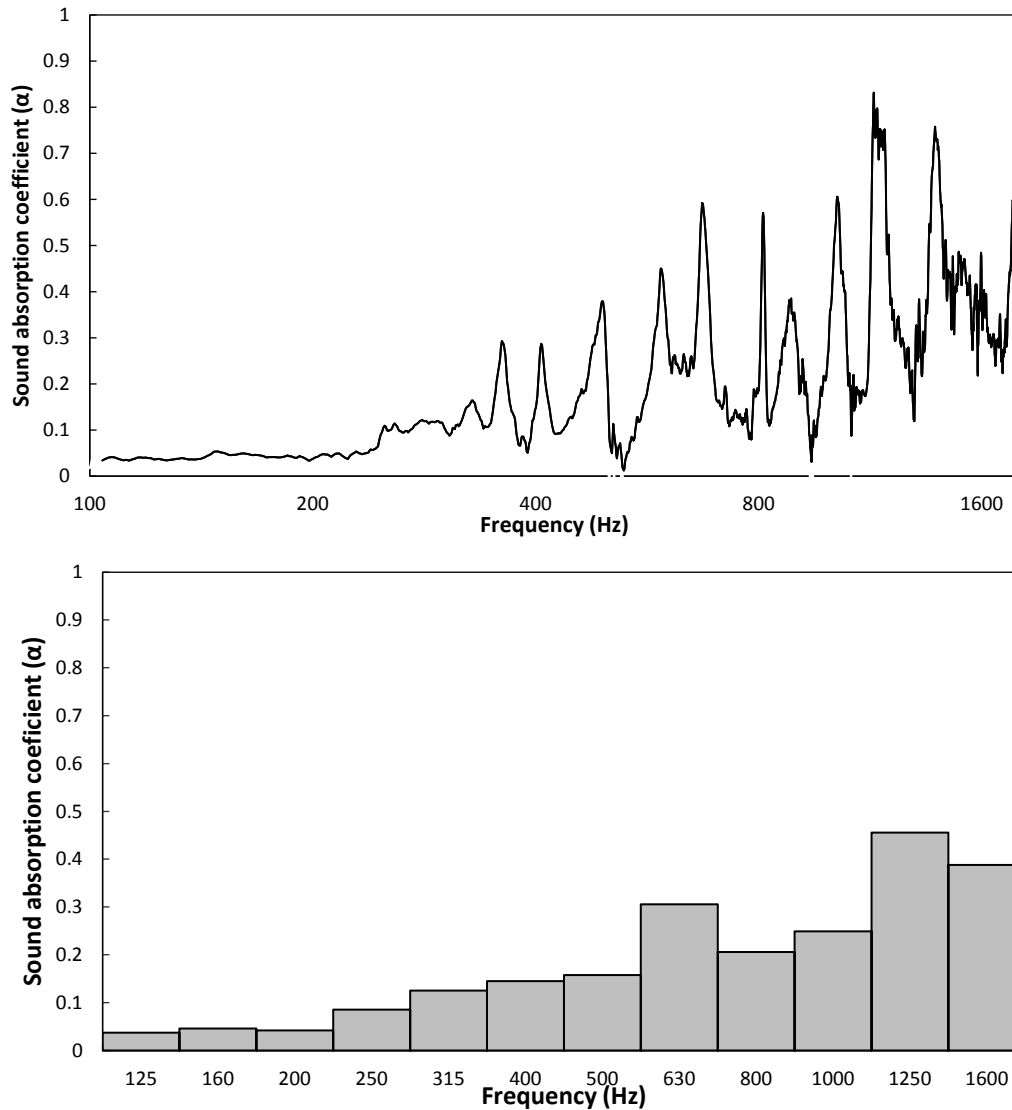


Figure 7.44: Sound absorption coefficient of 4 composite mats and air gaps (PVA12GN5-2mm- PVA12GN10 -1mm- PVA9GN5-2mm- PVA9GN10) and 3cm back cavity (FFT and 1/3 octave plot)

7.3.3 Sound absorption of multi-layer mats PVA-PS-PVA

Mats with multi-layers were produced using two types of polymers. The layers were produced in sequence as follows; a layer of PVA then a layer of PS followed by a layer of PVA. Two different concentrations of PVA (9 and 12wt %) and PS (10 and 20wt %) were used. The sound absorption of a multilayer mat of PVA12PS10PVA12 was measured at zero and 3cm back cavity as shown in Figure 7.45 and Figure 7.46. Figure 7.47 illustrates that there is a significant improvement in the sound absorption due to the existence of the 3cm back cavity. The sound absorption duplicated at these ranges of frequencies 630, 800, 1000, 1250, and 1600Hz.

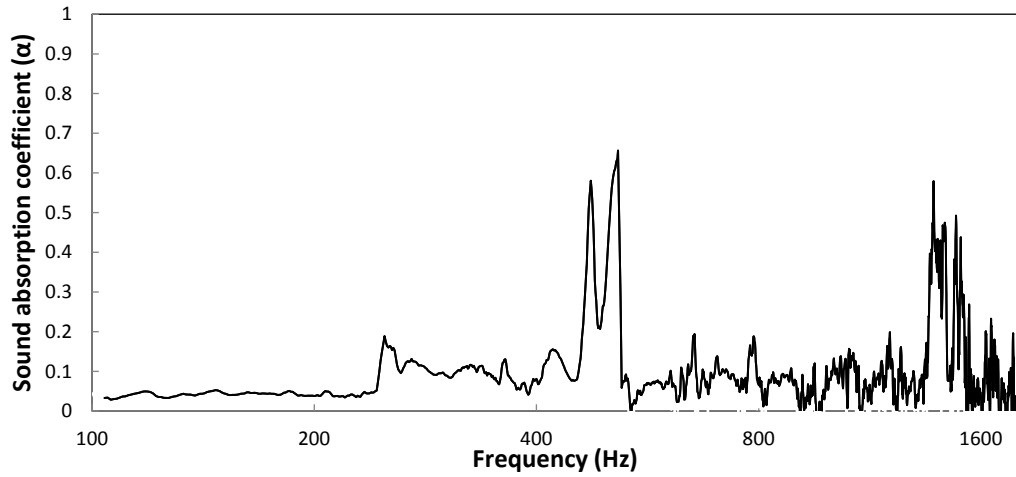


Figure 7.45: Sound absorption coefficient of a multi-layer PVA12 PS10PVA12 without back cavity

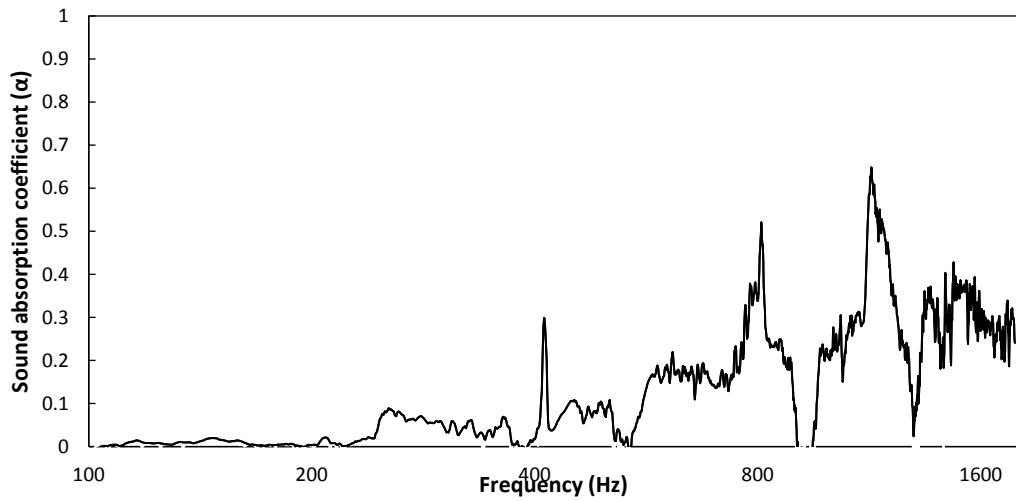


Figure 7.46: Sound absorption coefficient of one mat consists layers of PVA 12wt% PS10wt% PVA12wt% respectively at 3cm back cavity

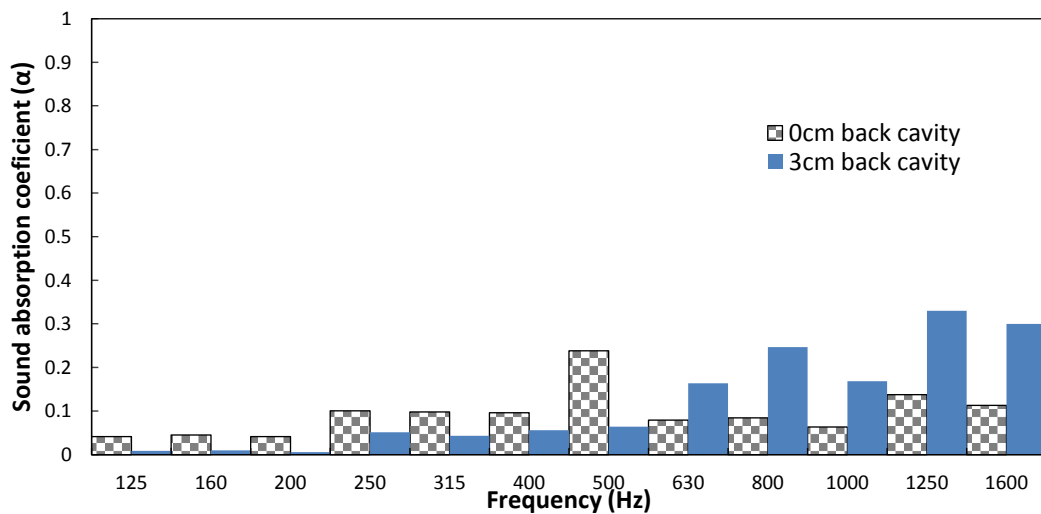


Figure 7.47: Sound absorption coefficient of one mat consists layers of PVA 12wt% PS10wt% PVA12wt% respectively at 0cm and 3cm back cavity (1/3 octave plot)

Others two mats of PAV and PS were prepared with different concentrations and their sound absorption was measured at 3cm back cavity. The first mat was PVA9PS10PVA9 and the second mat was PVA9PS20PVA9. The second mat displayed high improvement in sound absorption from (0.2- 0.82) at a frequency range of (500- 1600Hz) as shown in Figure 7.49 due to the gradient in fiber diameter distribution between PVA and PS. In addition, the increase in PS concentration leads to increase the fiber diameters, which offers a larger fiber diameters difference across the mat as well as a beads free structure, which enhanced the sound absorption.

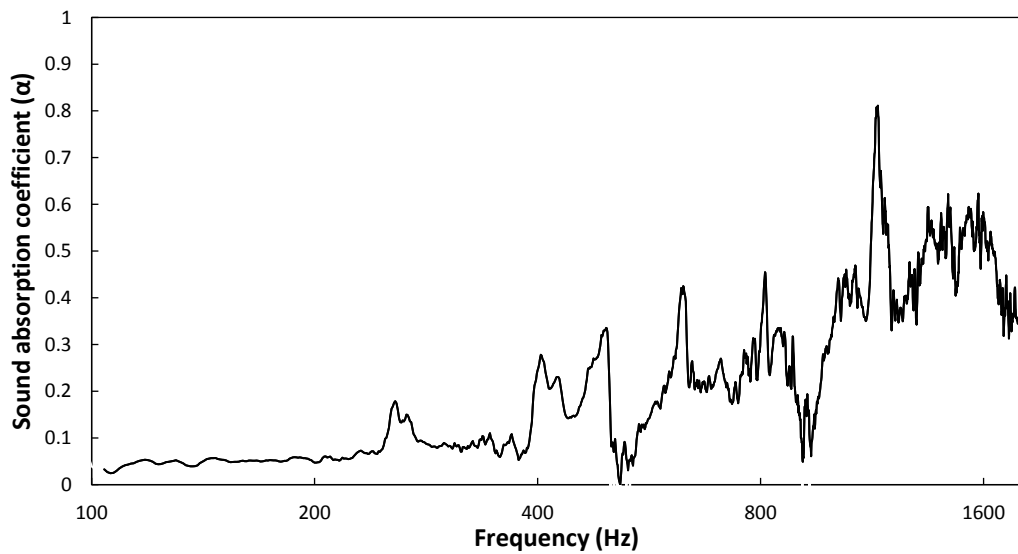


Figure 7.48: Sound absorption coefficient of one mat consists layers of PVA 9wt% PS 10wt% PVA 9wt% respectively at 3cm back cavity

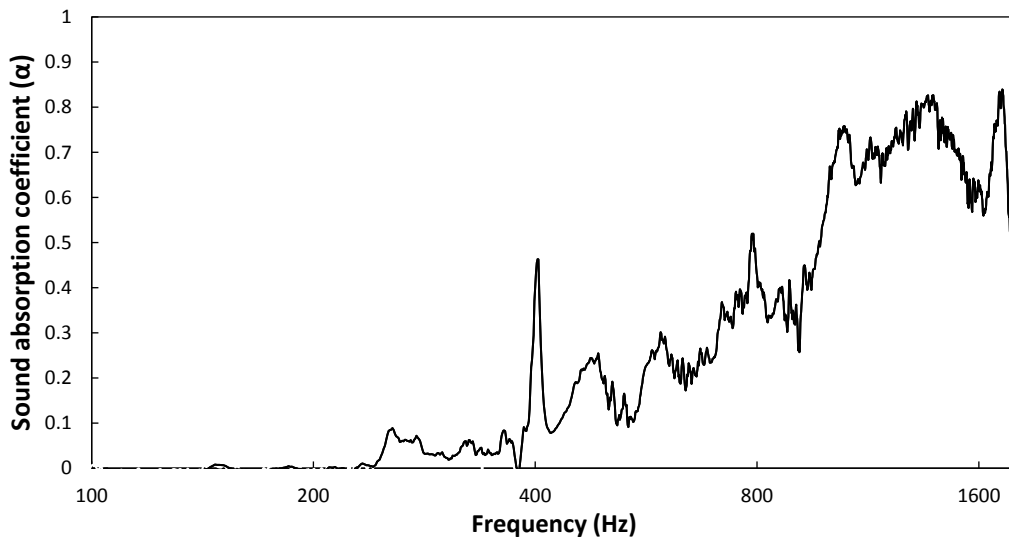


Figure 7.49: Sound absorption coefficient of one mat consists layers of PVA 9wt% PS20wt%PVA9wt% respectively at 3cm back cavity

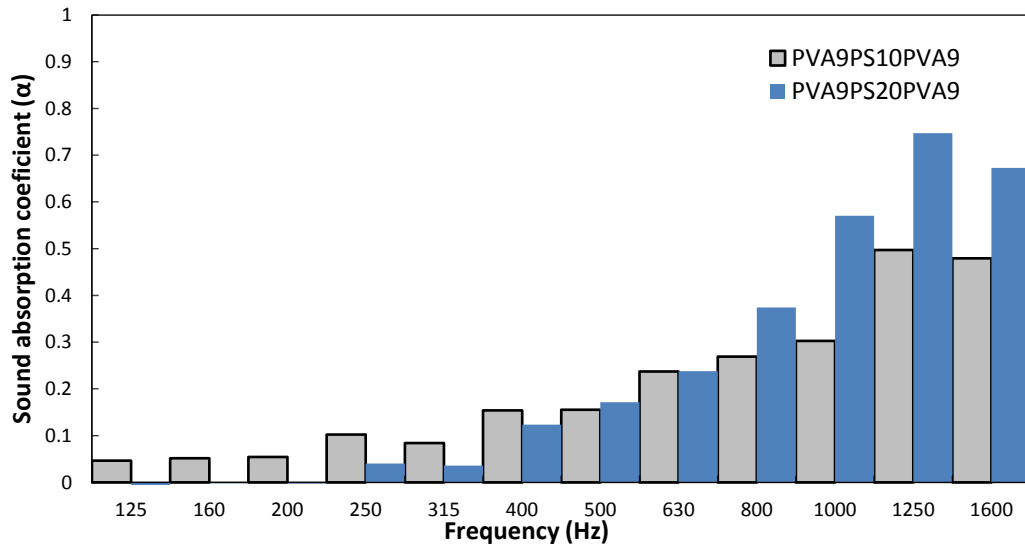


Figure 7.50: Sound absorption coefficient of mats PVA9PS10PVA9 and PVA9PS20PVA9 respectively at 3cm back cavity (1/3 octave plot)

Sound absorptions of the combination of two multi-layer mats with 3mm air gap was measured at different values of the back cavity (i.e. 5mm and 3cm). The first mat was PVA9PS20PVA9 and the second is PVA12PS20PVA12. It was noticed that the sound absorption increased as the back cavity increased as illustrated in Figure 7.53. The sound absorption increased and shifts towards the low frequency with increasing back cavity from 5mm to 3cm as figured in Figure 7.51 and Figure 7.52.

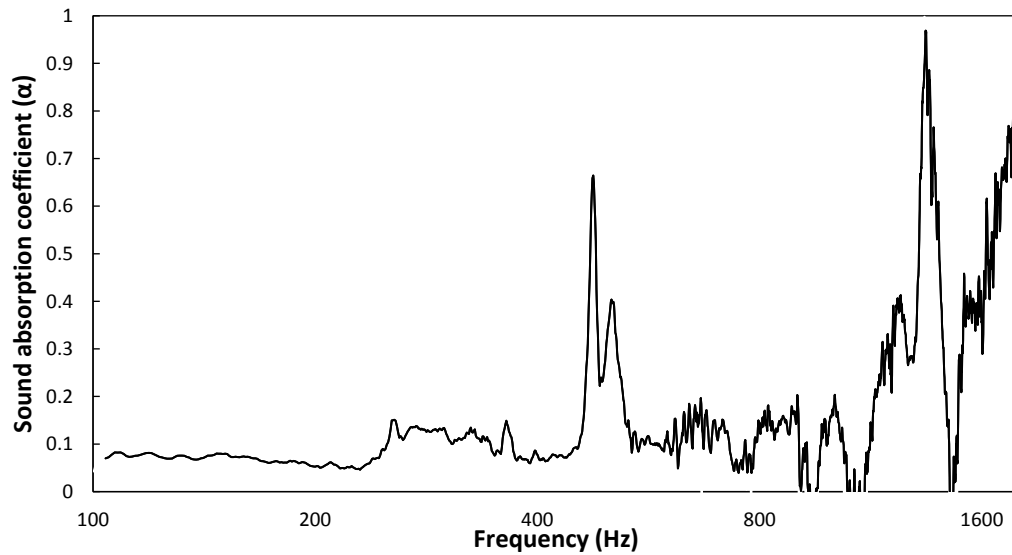


Figure 7.51: Sound absorption coefficient of two multilayer PVA9PS20PVA9 with 3mm gap PVA12PS20PVA12 at 5mm back cavity

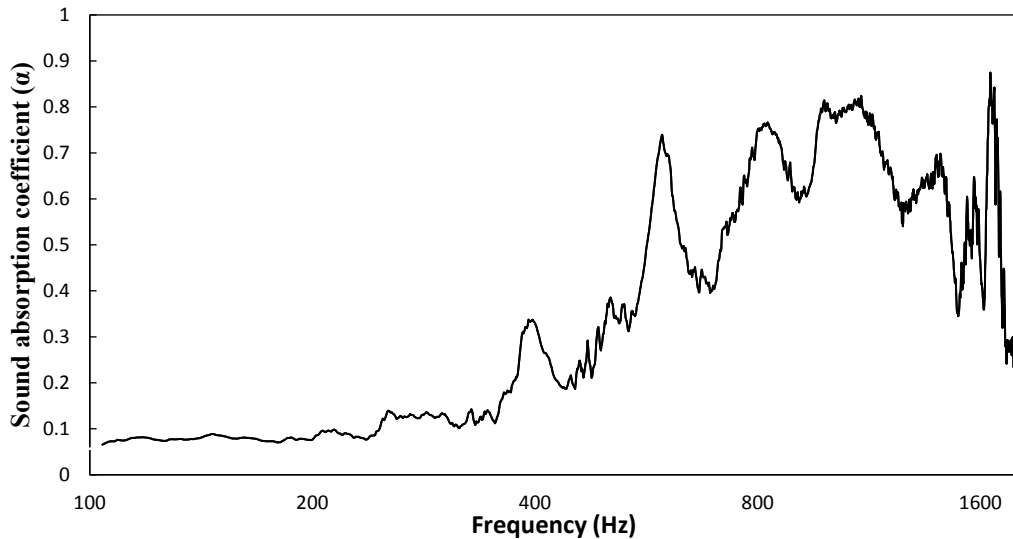


Figure 7.52: Sound absorption coefficient of two multi-layers PVA9PS20PVA9 with 3mm gap PVA12PS20PVA12 at 3cm back cavity

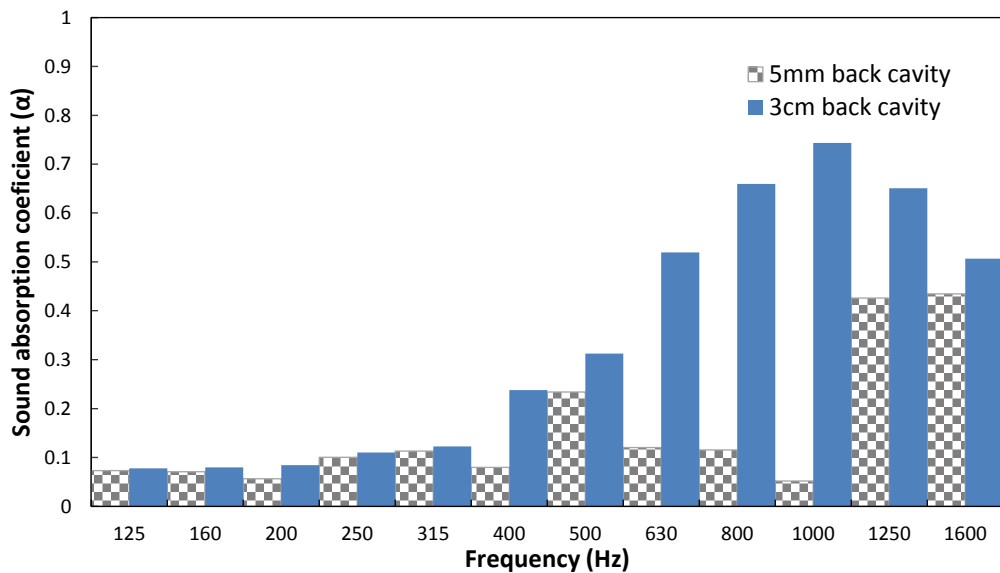


Figure 7.53: Sound absorption coefficient of two multilayer PVA9PS20PVA9 with 3mm gap PVA12PS20PVA12 at 5mm and 3cm back cavity(1/3 octave plot)

Moreover, four layers were used to construct the multi-layer mat. The mats were arranged with separation air gaps as follows; PVA9PS20PVA9- 3mm- PVA12PS10PVA12- 5mm- PVC12PS20PVC12- 2mm- PVC12PS10PVC12 and the sound absorption coefficient are measured at different back cavities (i.e. 2mm, 1cm, 2cm, and 2.5cm). It was observed that as the back cavity became deeper, the sound absorption shifted to the low-frequency region except for frequency at 1250 and 1600Hz as shown in Figure 7.58.

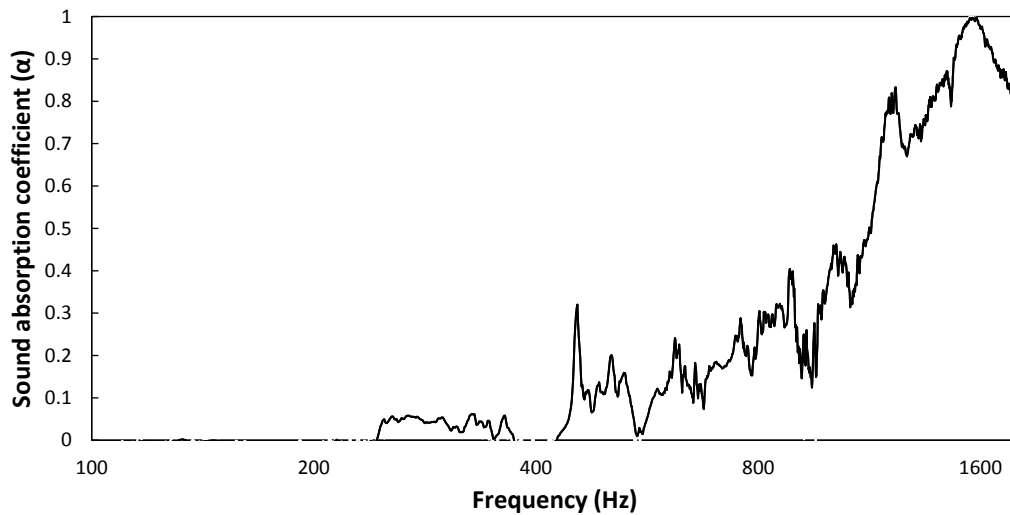


Figure 7.54: Sound absorption coefficient of PVA9PS20PVA9- 3mm- PVA12PS10PVA12- 5mm- PVC12PS20PVC12- 2mm- PVC12PS10PVC12 with 2mm cavity

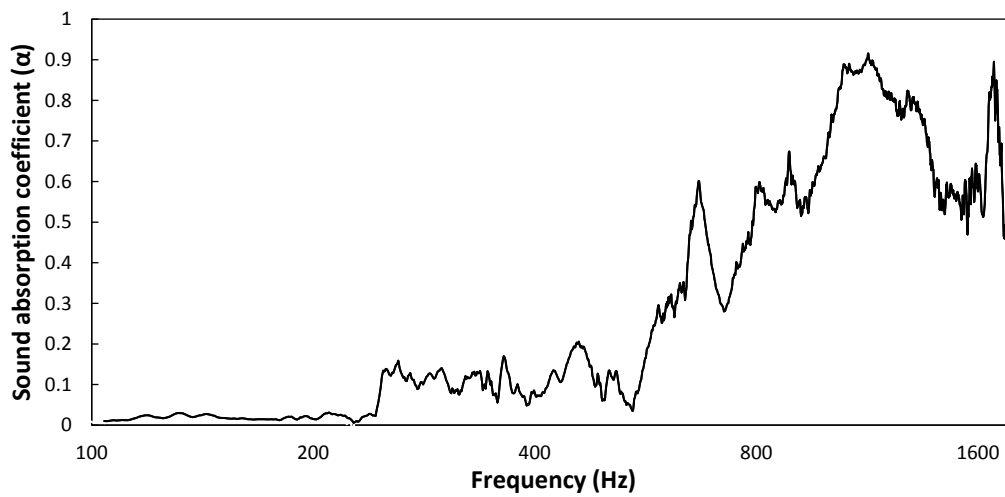


Figure 7.55: Sound absorption coefficient multi-layer mats of PVA9PS20PVA9- 3mm- PVA12 PS10pvA12- 5mm- PVC12PS20PVC12- 2mm- PVC12PS10PVC12 with 1cm back cavity

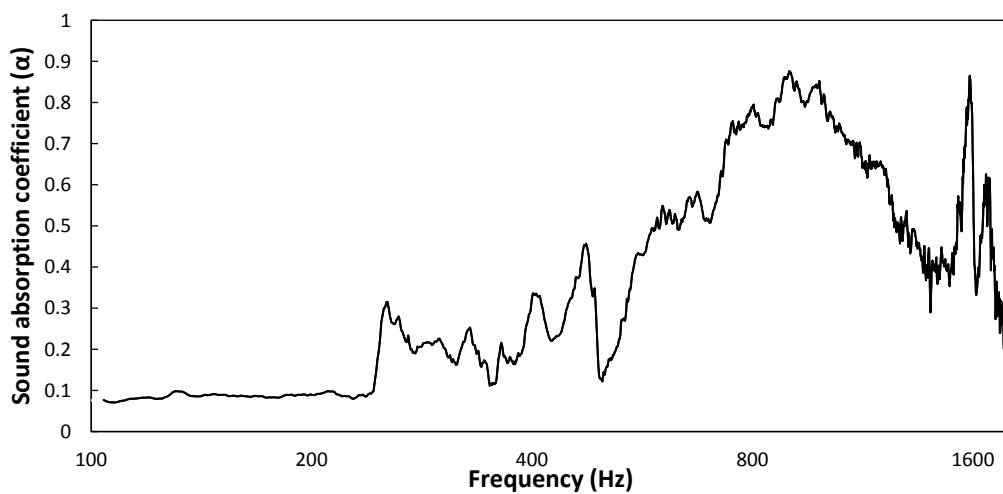


Figure 7.56: Sound absorption coefficient multi-layer mats of PVA9PS20PVA9- 3mm- PVA12 PS10pvA12- 5mm- PVC12PS20PVC12- 2mm- PVC12PS10PVC12 with 2cm back cavity

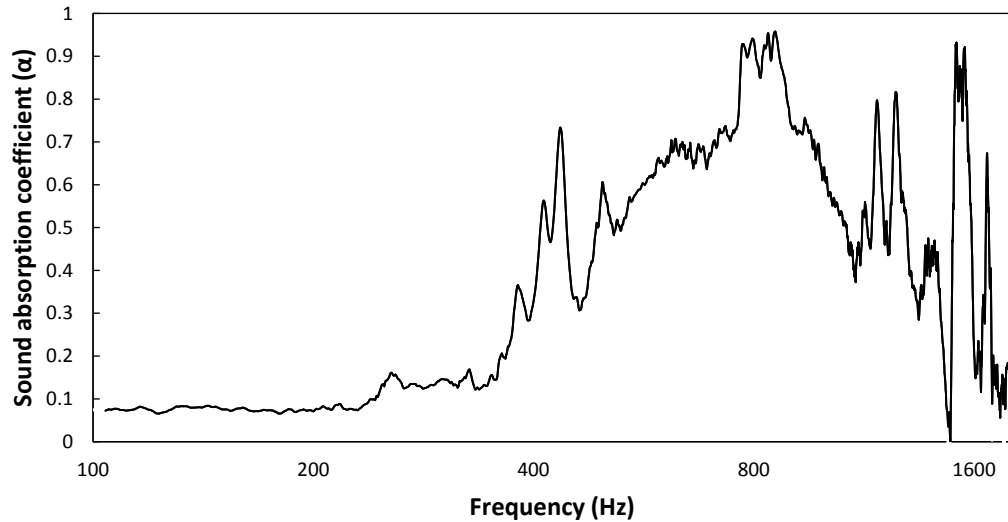


Figure 7.57: Sound absorption coefficient of PVA9PS20PVA9- 3mm- PVA12PS10PVA12- 5mm PVC12PS20PVC12- 2mm- PVC12PS10PVC12 with 2.5cm cavity

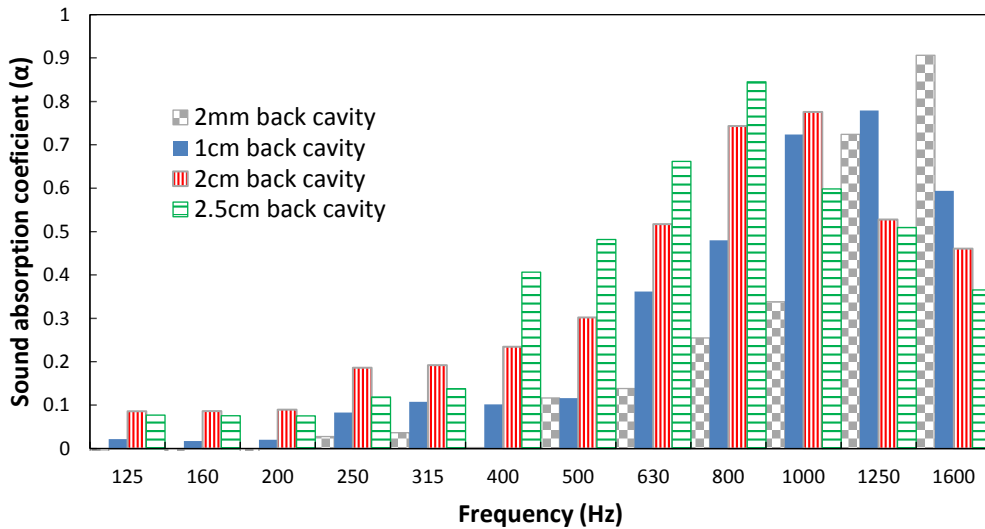


Figure 7.58: Sound absorption coefficient of PVA9PS20PVA9- 3mm- PVA12PS10PVA12- 5mm-PVC12PS20PVC12- 2mm- PVC12PS10PVC12 at 2mm, 1cm, 2cm, 2.5cm cavity (1/3 octave plot)

7.3.4 Sound absorption of PVA mats with graded structure

The sound absorption of the graded structure foams was investigated in our lab (Aeroacoustics and Noise Control Laboratory at UOIT) and the results showed that the graded structure improves the ability of the foam to absorb the sound waves. Regarding this result, mats with graded fiber diameters were produced and the results were investigated as shown in Figure 7.59. The first, mat was produced from PVA 9wt% by applying different flow rates (i.e. 0.1, 0.2, 0.3ml/h) and fixed the other parameters to obtain different fiber diameters. This mat had three layers of fibers with different diameters as follows: 129nm, 141nm and, 158nm, respectively. Another mat was

prepared from three different concentrations of PVA (i.e. 7, 9, 12 wt%) and electrospun at fixed flow rate 0.3ml/h. The fiber diameters of the mat layers were 109nm, 158nm and, 267nm, respectively. It was noticed that the sound absorption for the second mat was better than the first because the difference in the diameters of graded fibers is larger. Also, the graded fiber mats show a better sound absorption than the mats with no graded fibers.

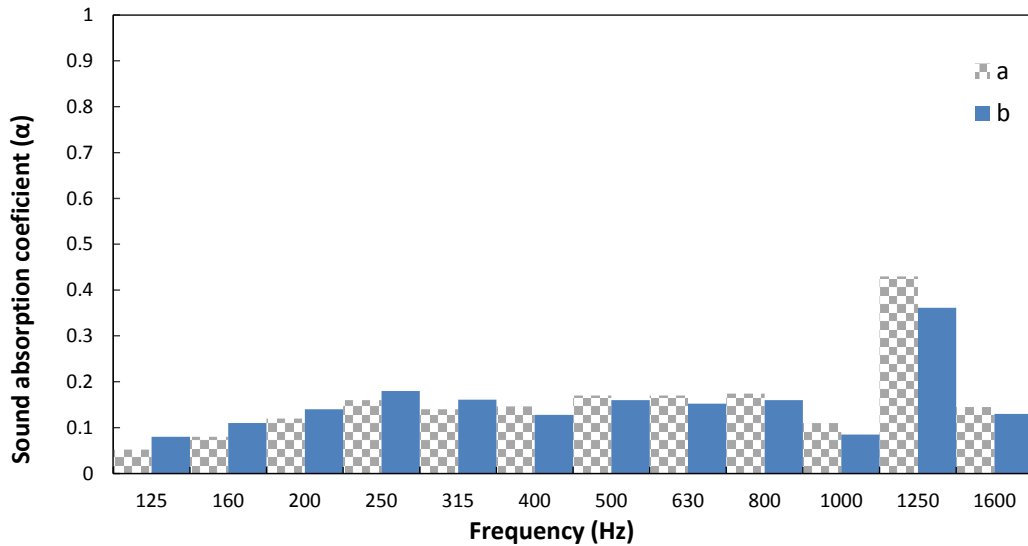


Figure 7.59: Sound absorption coefficient of PVA mats with graded structure a) PVA9% with different flow rates b) mat from PVA 7, 9, 12wt% with fixed flow rate.

7.3.5 Sound absorption of PVA mats with different thickness

The three mats of PVA 9wt% with different thickness 33.9μm, 80.6μm, and 123.1μm were produced by electrospun PVA solution for 3.5h, 7h, and 10.5h, respectively. Figure 7.60 illustrates that as the mats' thickness increased the sound absorption increased and Table 7.1 shows the percent of improving in the sound absorption with increasing the mats' thickness.

Table 7.1: Percent of sound absorption improved with increasing the mats' thickness

Thickness increased (μm)	Frequency (Hz)											
	125	160	200	250	315	400	500	630	800	1000	1250	1600
From 33.9 to 80.6μm	223%	249%	132%	174%	117%	105%	79%	61%	59%	79%	78%	18%
From 80.6 to 123.1μm	---	---	16%	---	14%	12%	17%	18%	19%	28%	---	33%

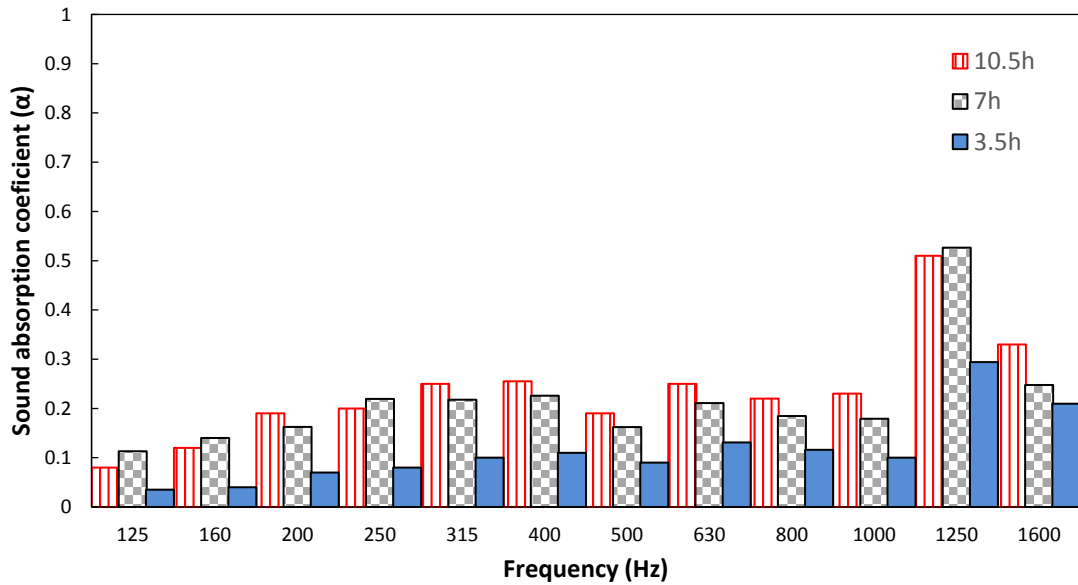


Figure 7.60: Sound absorption coefficient of PVA mats electrospun for different time 10.5h, 7h, and 3.5h

7.4 Nanofiber membrane with conventional sound absorbing material

Rockwool (DD2) is a conventional sound absorbing material with 6cm thickness. It has a good sound absorption characteristic in mid and high-frequency ranges. The addition of nanofibers membrane to the surface of DD2 was studied and the sound absorption coefficient for the samples were measured after using nanofiber membranes. The addition of nanofiber membranes improved the sound absorption at the low-frequency range. Adding PVA mat in the front of DD2 sample enhanced the sound absorption in the low-frequency range at (300- 425Hz) as shown in Figure 7.62. In addition, adding two layers of PVA mats in the front and back of DD2; the sound absorption increased in the low-frequency range where the absorption curve shifted to the lower frequency and the absorption value increased as shown in Figure 7.63. The results obtained from the three sound absorption measurements were compared in Figure 7.64. The percent of sound absorption improving for DD2 at low frequencies by adding PVA mats are shown in Table 7.1.

Table 7.2: Percent of sound absorption improving of DD2 using PVA mats

Frequency (Hz)	Percent of improvement of sound absorption	
	PVA mat at front of DD2	PVA mats at front and back of DD2
200	29.5%	46.2%
250	21.4%	122.0%
315	49.1%	164.6%
400	28.9%	70.6%

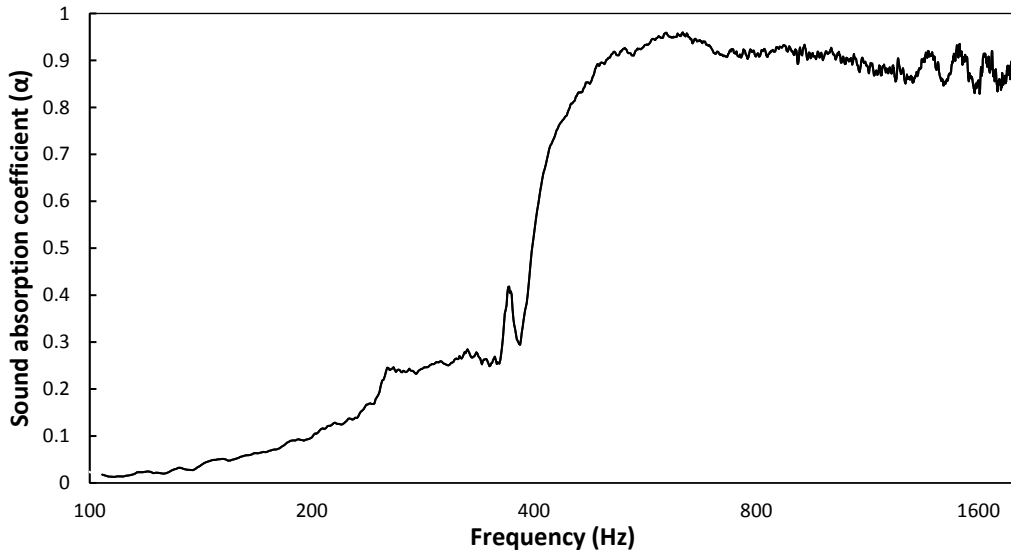


Figure 7.61: Sound absorption coefficient of DD2

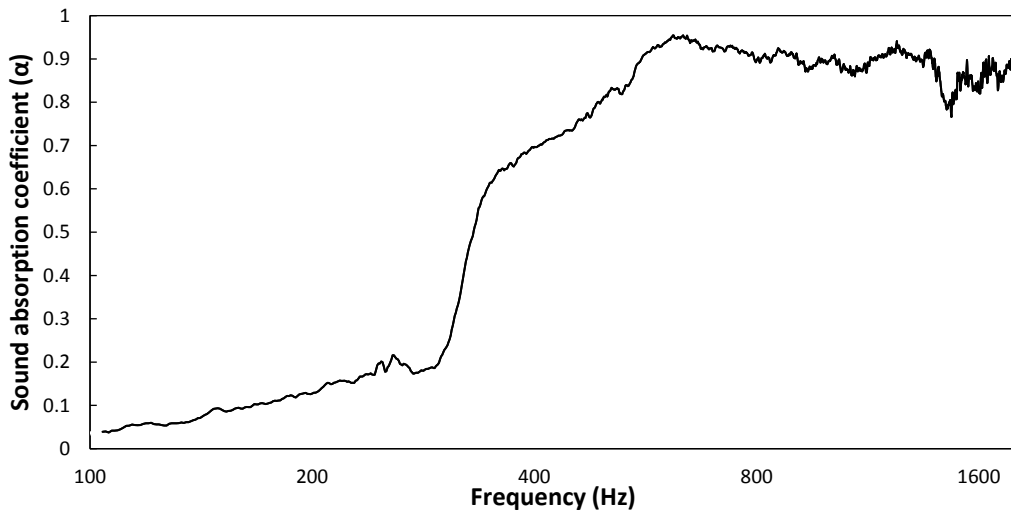


Figure 7.62: Sound absorption coefficient of DD2 with PVA nanofiber membrane at front

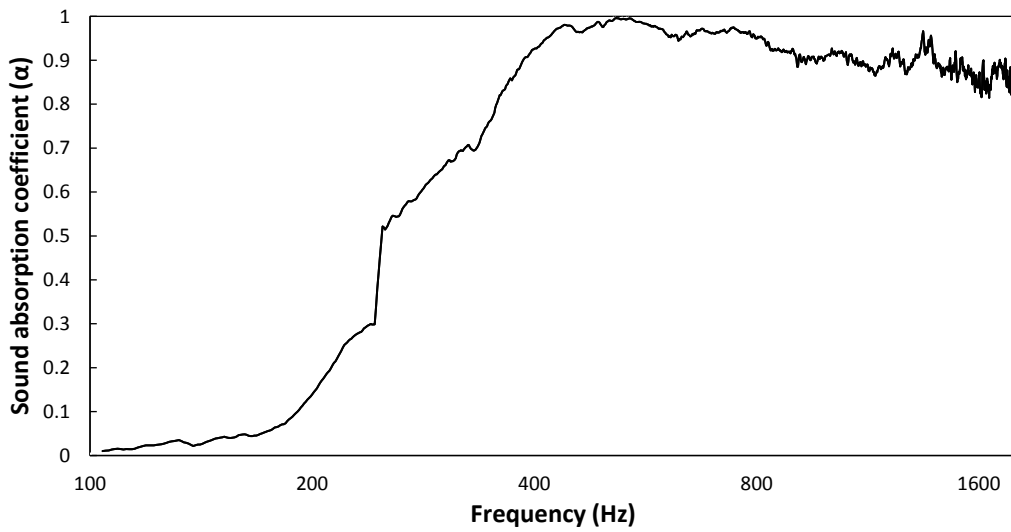


Figure 7.63: Sound absorption coefficient of DD2 with two PVA nanofiber membranes at both sides

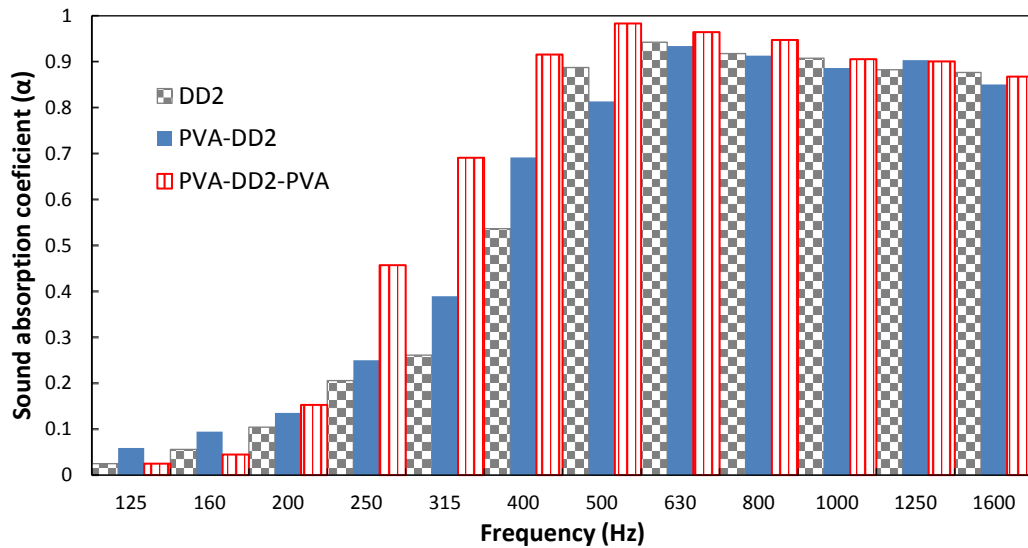


Figure 7.64: Sound absorption coefficient of (DD2), (PVA-DD2), and (PVA-DD2- PVA)

Nanofiber membranes that contained several layers of different polymers are used with DD2. Adding a multi-layer of nanofiber membrane (PVA12-PS20-PVA12) to DD2 increased the sound absorption efficiency at low frequency as shown in Figure 7.65. This multi-layer mat consisted of three layers of nanofiber mat as follows; PVA layer on the top, bottom, and PS in the middle. The sound absorption for the multilayer mat shows noticed improvements due to the graded structure in fiber diameters distribution. Its measurement result is close to the sample of (PVA-DD2-PVA).

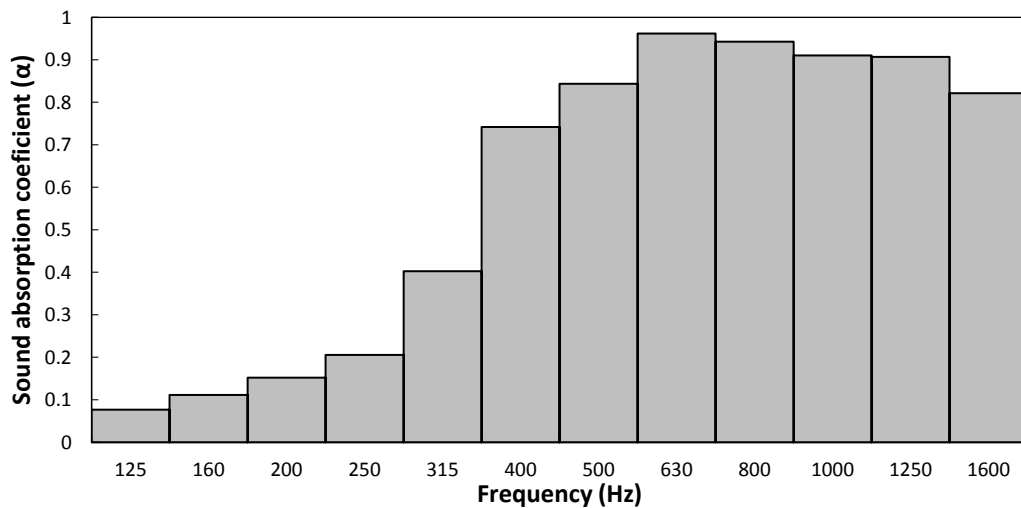
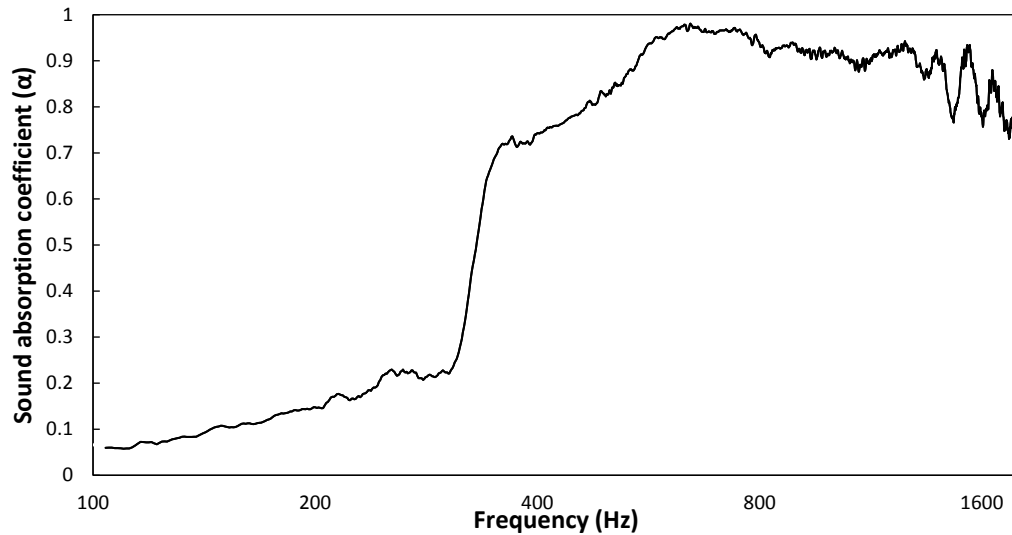


Figure 7.65: Sound absorption coefficient of DD2 with PVA12-PS20-PVA12 nanofiber membrane at front (FFT and 1/3 octave plot)

7.5 Summary

The nanofiber mats were used as a sound absorbing material. The measurements of sound absorption coefficient show that nanofibers mats are a promising candidate to be sound absorbing materials at low and mid frequency range. Using nanofiber mats instead of conventional sound absorbing material will save weight and volume used for the conventional one. The sound absorption mainly depends on the type of polymer used in producing this mat. PVA shows an effective behavior as a sound absorbent. Different fillers have different effects on the sound absorption of nanofiber mats; it sometimes improves the sound absorption at different frequencies. Decreasing the diameters of fibers improves the ability to absorb the sound as shown for PVA mats. It is improved between 110% to 53% at different frequencies and when the diameters decrease from

267nm to 158nm. The existence of beads decreases the efficiency of nanofiber mats to absorb sound as illustrated for PS 10wt%. Back cavities were found to improve the sound absorption, for instance, the sound absorption of PVC12PS10PVC12 mat has been improved by 48% at 794Hz when the cavity was increased from 3 to 5cm. Gaps between the fibers mat improve the sound absorption of the samples especially at low-frequency regions, for example, increasing air gap between two mats PVA/CNTs improves the sound absorption by 28% at 379Hz. Multi-layers samples show a significant sound absorption results at low-mid frequency regions. The mats with graded fibers' diameter shows better sound absorption than mat have the same fibers' diameters. Increasing the thickness of the mats enhances the sound absorption. Adding nanofibers mats to the conventional sound absorbing materials improve its ability to absorb sound at the low-frequency region by 20% for 198Hz, 56% for 315Hz and 30% for 397Hz.

Chapter 8: Conclusions, contributions and future work

Electrospinning is a novel technology, which applies an electric field to form fibrous materials from a polymer solution. Unlike traditional spinning techniques, fibers with diameters in the range of 100nm can be produced for applications where nanoscale fibers are necessary because of the unique advantages that they offer. Nanofiber materials have very high surface area compared to their volume to interact with sound waves and therefore have better sound dampening ability in a given volume. This is particularly useful for dampening sound in the mid and low-frequency ranges. In this work, a number of polymers have been electrospun successfully, including polyvinyl alcohol (PVA), polystyrene (PS), and polyvinyl chloride (PVC). These have also been reinforced by fillers to enhance mechanical and acoustic properties.

8.1 Conclusions

- A statistical model had been developed for effects of processing parameters during the fabrication of PVA nanofibers in the field of interest. This model evaluated five of the main parameters that affect the electrospinning production process, namely, polymer concentration, flow rate, high voltage, fiber collection distance, and the rotation speed of the drum.
- The effects of noise variables on the control factors were studied by subjecting them to Signal to Noise Ratio (S/N) test in the domain of interest. It was found that high voltage was influenced the most by the noise variables.
- Polyvinyl alcohol (PVA), polystyrene (PS), and polyvinyl chloride (PVC) mats had been successfully produced, and their sound absorption coefficients were quantified in the frequency range from 100-1900Hz using a 3cm back cavity. Single mats as well as multiple combinations produced from these materials had also been investigated.

- Filler materials such as carbon nanotubes, wollastonite, graphene and fiberglass had been used and were found to improve the sound absorption of nanofibers along with the improvement of mechanical properties.
- The fibers with bead formations were also studied, and it was determined that they do not have significant deteriorative effects on sound absorption results.
- It was found that as the fiber diameters decreased, its ability to absorb the sound increased.
- The multi-layered samples show effective sound absorption due to their graded structure as each layer has different fibers diameters that made sound waves move in different medium and dissipated their energy.
- The back cavity had a significant effect in improving the ability of nanofiber mats to absorb sound.
- The existence of air gaps between combinations of several mats increased the sound absorption, especially in the low-frequency range. As the gap increased, the sound absorption shifted towards the lower frequency.
- The mats produced from the blends of two polymers had a better ability to absorb sound than mats produced from a single polymer.
- The sound absorption improved by using mats that have graded fiber diameters structure.
- Increasing the mats' thickness enhances the sound absorption.
- Nanofibers mats enhanced the performance of conventional sound absorbing materials to absorb the sound by 32% at the low-frequency range.

8.2 Contributions

- Developed a statistical model for evaluating the effects of five processing parameters on the production of PVA nanofibers in the field of interest. This model can be

adjusted to evaluate the effects of the noise variables by carrying out signal to noise ratio (S/N) tests.

- A number of pure and filled polymeric systems were identified as capable of dampening sound while occupying significantly smaller volume.
- The multi-layered nanofiber mats were developed in which each layer had fibers of different diameters. This causes sound waves to transition in a different medium over very short distances enhancing the dampening efficiency.
- The use of air gap between combinations of several mats was shown to increase the sound absorption in the low-frequency range. As the gap increased, the sound absorption shifted towards the lower frequency.
- The mats produced from the blend of two polymers were shown to be more effective at absorbing sound compared to mats produced from a single polymer.

8.3 Recommendation and future work

- Evaluate mats fabricated from other types of materials, which may have high sound absorption abilities.
- Study the effect of adding other filler types such as Nano-clay, titanium dioxide (TiO₂) and wood fibers on acoustic performance, morphology, and mechanical properties.
- Develop a mathematical model for estimating the acoustic properties of nanofiber mats in terms of their fiber diameters and the material properties.
- Study the effect of increasing mat thicknesses on the acoustic performance.
- Study the effect of using hollow fibers on the sound absorption.

References:

- [1] He, Ji-Huan, Yong Liu, Lu-Feng Mo, Yu-Qin Wan, and Lan Xu. "Electrospun nanofibres and their applications." *Smithers Rapra Technology*, Shawbury (2008).
- [2] Z.-M. Huang, Y.-Z. Zhang, M. Kotaki, and S. Ramakrishna, "A review on polymer nanofibers by electrospinning and their applications in nanocomposites," *Compos. Sci. Technol.*, vol. 63, no. 15, pp. 2223–2253, 2003.
- [3] J. Wang, H. E. Naguib, and A. Bazylak, "Electrospun Porous Conductive Polymer Membranes," vol. 8342, pp. 1–13, 2012.
- [4] J. Doshi and D. H. Reneker, "Electrospinning process and applications of electrospun fibers," *J. Electrostat.*, vol. 35, no. 2–3, pp. 151–160, Aug. 1995.
- [5] W. Lu, J. Sun, and X. Jiang, "Recent advances in electrospinning technology and biomedical applications of electrospun fibers," *J. Mater. Chem. B*, vol. 2, no. 17, pp. 2369–2380, 2014.
- [6] D. H. Reneker and I. Chun, "Nanometre diameter fibres of polymer, produced by electrospinning," *Nanotechnology*, vol. 7, no. 3, pp. 216–223, Sep. 1996.
- [7] A. Greiner and J. H. Wendorff, "Electrospinning: a fascinating method for the preparation of ultrathin fibers.," *Angew. Chem. Int. Ed. Engl.*, vol. 46, no. 30, pp. 5670–703, Jan. 2007.
- [8] H. Xiang, S. Tan, X. Yu, Y. Long, X. Zhang, N. Zhao, and J. Xu, "Sound absorption behavior of electrospun polyacrylonitrile nanofiber membranes," *Chinese J. Polym. Sci.*, vol. 29, no. 6, pp. 650–657, Aug. 2011.
- [9] Q. Wang, J. Dai, W. Li, Z. Wei, and J. Jiang, "The effects of CNT alignment on electrical conductivity and mechanical properties of SWNT/epoxy nanocomposites," *Compos. Sci. Technol.*, vol. 68, no. 7, pp. 1644–1648, 2008.
- [10] L. Bokobza, "Multiwall carbon nanotube-filled natural rubber: Electrical and mechanical properties," vol. 6, no. 3, pp. 213–223, 2012.
- [11] A. S. Luyt, M. D. Dramićanin, Ž. Antić, and V. Djoković, "Morphology, mechanical and thermal properties of composites of polypropylene and nanostructured wollastonite filler," *Polym. Test.*, vol. 28, no. 3, pp. 348–356, 2009.
- [12] Y. J. Qian, D. Y. Kong, Y. Liu, S. M. Liu, Z. B. Li, D. S. Shao, and S. M. Sun, "Improvement of sound absorption characteristics under low frequency for micro-perforated panel absorbers using super-aligned carbon nanotube arrays," *Appl. Acoust.*, vol. 82, pp. 23–27, Aug. 2014.

- [13] R. Asmatulu, W. Khan, and M. B. Yildirim, "Acoustical properties of electrospun nanofibers for aircraft interior noise reduction," in ASME 2009 International Mechanical Engineering Congress and Exposition, 2009, pp. 223–227.
- [14] R. Nayak, R. Padhye, I. L. Kyratzis, Y. Truong, and L. Arnold, "Recent advances in nanofibre fabrication techniques," *Text. Res. J.*, p. 40517511424524, 2011.
- [15] X. Xing, Y. Wang, and B. Li, "Nanofiber drawing and nanodevice assembly in poly (trimethylene terephthalate)," *Opt. Express*, vol. 16, no. 14, pp. 10815–10822, 2008.
- [16] J. R. Capadona, O. Van Den Berg, L. A. Capadona, M. Schroeter, S. J. Rowan, D. J. Tyler, and C. Weder, "A versatile approach for the processing of polymer nanocomposites with self-assembled nanofibre templates," *Nat. Nanotechnol.*, vol. 2, no. 12, pp. 765–769, 2007.
- [17] Ramakrishna, Seeram, K. Fujihara, W. E. Teo, T-Ch Lim, and Z. Ma. "An introduction to electrospinning and nanofibers. 2005." Singapura: World Scientific Publishing Company.
- [18] R. Dersch, T. Liu, A. K. Schaper, A. Greiner, and J. H. Wendorff, "Electrospun nanofibers: Internal structure and intrinsic orientation," *J. Polym. Sci. Part A Polym. Chem.*, vol. 41, no. 4, pp. 545–553, 2003.
- [19] J. D. Hartgerink, E. Beniash, and S. I. Stupp, "Self-assembly and mineralization of peptide-amphiphile nanofibers," *Science (80-.)*, vol. 294, no. 5547, pp. 1684–1688, 2001.
- [20] J. Fang, H. Niu, T. Lin, and X. Wang, "Applications of electrospun nanofibers," *Chinese Sci. Bull.*, vol. 53, no. 15, pp. 2265–2286, 2008.
- [21] B. Ding and J. Yu, *Electrospun Nanofibers for Energy and Environmental Applications*. Springer, 2014.
- [22] S. Ramakrishna, K. Fujihara, W.-E. Teo, T.-C. Lim, and Z. Ma, *An introduction to electrospinning and nanofibers*, vol. 90. World Scientific, 2005.
- [23] R. Asmatulu, M. B. Yildirim, W. Khan, A. Adeniji, and H. Wamocha, "Nanofiber Fabrication and Characterization for the Engineering Education," pp. 1–9, 1845.
- [24] M. Ziabari, V. Mottaghitalab, and A. K. Haghi, "Application of direct tracking method for measuring electrospun nanofiber diameter," *Brazilian J. Chem. Eng.*, vol. 26, no. 1, pp. 53–62, 2009.
- [25] W. E. Teo and S. Ramakrishna, "A review on electrospinning design and nanofibre assemblies," *Nanotechnology*, vol. 17, no. 14, pp. R89–R106, Jul. 2006.

- [26] J. Deitzel, "Controlled deposition of electrospun poly(ethylene oxide) fibers," *Polymer (Guildf)*., vol. 42, no. 19, pp. 8163–8170, Sep. 2001.
- [27] T. Subbiah, G. S. Bhat, R. W. Tock, S. Parameswaran, and S. S. Ramkumar, "Electrospinning of nanofibers," *J. Appl. Polym. Sci.*, vol. 96, no. 2, pp. 557–569, Apr. 2005.
- [28] P. K. Baumgarten, "Electrostatic spinning of acrylic microfibers," *J. Colloid Interface Sci.*, vol. 36, no. 1, pp. 71–79, 1971.
- [29] I. Hayati, A. I. Bailey, and T. F. Tadros, "Investigations into the mechanisms of electrohydrodynamic spraying of liquids: I. Effect of electric field and the environment on pendant drops and factors affecting the formation of stable jets and atomization," *J. Colloid Interface Sci.*, vol. 117, no. 1, pp. 205–221, 1987.
- [30] Anton, Formhals. "Process and apparatus for preparing artificial threads." U.S. Patent No. 1,975,504. 2 Oct. 1934.
- [31] Anton, Formhals. "Artificial thread and method of producing same." U.S. Patent No. 2,187,306. 16 Jan. 1940.
- [32] V. G. Drozin, "The electrical dispersion of liquids as aerosols," *J. Colloid Sci.*, vol. 10, no. 2, pp. 158–164, Apr. 1955.
- [33] C. J. Buchko, L. C. Chen, Y. Shen, and D. C. Martin, "Processing and microstructural characterization of porous biocompatible protein polymer thin films," *Polymer (Guildf)*., vol. 40, no. 26, pp. 7397–7407, Dec. 1999.
- [34] G. Taylor, "Disintegration of water drops in an electric field," in *Proceedings of the Royal Society of London A: Mathematical, Physical and Engineering Sciences*, 1964, vol. 280, no. 1382, pp. 383–397.
- [35] A. Goktas, "Electrospinning of polystyrene/butyl rubber blends: a parametric study." Middle East Technical university, 2008.
- [36] H. L. Simons, "Process and apparatus for producing patterned non-woven fabrics." Google Patents, 18-Oct-1966.
- [37] L. Wannatong, A. Sirivat, and P. Supaphol, "Effects of solvents on electrospun polymeric fibers: preliminary study on polystyrene," *Polym. Int.*, vol. 53, no. 11, pp. 1851–1859, 2004.
- [38] S. H. Tan, R. Inai, M. Kotaki, and S. Ramakrishna, "Systematic parameter study for ultra-fine fiber fabrication via electrospinning process," *Polymer (Guildf)*., vol. 46, no. 16, pp. 6128–6134, 2005.
- [39] K. H. Lee, H. Y. Kim, H. J. Bang, Y. H. Jung, and S. G. Lee, "The change of bead

- morphology formed on electrospun polystyrene fibers,” *Polymer (Guildf)*., vol. 44, no. 14, pp. 4029–4034, 2003.
- [40] Z. Li and C. Wang, *One-dimensional Nanostructures: Electrospinning Technique and Unique Nanofibers*. Springer, 2013.
- [41] A. Koski, K. Yim, and S. Shivkumar, “Effect of molecular weight on fibrous PVA produced by electrospinning,” *Mater. Lett.*, vol. 58, no. 3–4, pp. 493–497, Jan. 2004.
- [42] J. Tao and S. Shivkumar, “Molecular weight dependent structural regimes during the electrospinning of PVA,” *Mater. Lett.*, vol. 61, no. 11–12, pp. 2325–2328, May 2007.
- [43] M. . Demir, I. Yilgor, E. Yilgor, and B. Erman, “Electrospinning of polyurethane fibers,” *Polymer (Guildf)*., vol. 43, no. 11, pp. 3303–3309, May 2002.
- [44] Y. Y. Zhao, Q. B. Yang, X. F. Lu, C. Wang, and Y. Wei, “Study on correlation of morphology of electrospun products of polyacrylamide with ultrahigh molecular weight,” *J. Polym. Sci. Part B Polym. Phys.*, vol. 43, no. 16, pp. 2190–2195, Aug. 2005.
- [45] M. G. McKee, J. M. Layman, M. P. Cashion, and T. E. Long, “Phospholipid nonwoven electrospun membranes.,” *Science*, vol. 311, no. 5759, pp. 353–5, Jan. 2006.
- [46] P. Heikkilä and A. Harlin, “Parameter study of electrospinning of polyamide-6,” *Eur. Polym. J.*, vol. 44, no. 10, pp. 3067–3079, 2008.
- [47] C. Mit-uppatham, M. Nithitanakul, and P. Supaphol, “Ultrafine Electrospun Polyamide-6 Fibers: Effect of Solution Conditions on Morphology and Average Fiber Diameter,” *Macromol. Chem. Phys.*, vol. 205, no. 17, pp. 2327–2338, 2004.
- [48] H. Fong, I. Chun, and D. H. Reneker, “Beaded nanofibers formed during electrospinning,” *Polymer (Guildf)*., vol. 40, no. 16, pp. 4585–4592, 1999.
- [49] S. Sukigara, M. Gandhi, J. Ayutsede, M. Micklus, and F. Ko, “Regeneration of *Bombyx mori* silk by electrospinning—part 1: processing parameters and geometric properties,” *Polymer (Guildf)*., vol. 44, no. 19, pp. 5721–5727, Sep. 2003.
- [50] Q. Yang, Z. Li, Y. Hong, Y. Zhao, S. Qiu, C. Wang, and Y. Wei, “Influence of solvents on the formation of ultrathin uniform poly(vinyl pyrrolidone) nanofibers with electrospinning,” *J. Polym. Sci. Part B Polym. Phys.*, vol. 42, no. 20, pp. 3721–3726, Oct. 2004.

- [51] Z. Li and C. Wang, "One-dimensional Nanostructures: Electrospinning Technique and Unique Nanofibers," Springer, 2013, pp. 15–29.
- [52] X. Geng, O.-H. Kwon, and J. Jang, "Electrospinning of chitosan dissolved in concentrated acetic acid solution," *Biomaterials*, vol. 26, no. 27, pp. 5427–5432, 2005.
- [53] E. Zussman, A. Yarin, and D. Weihs, "A micro-aerodynamic decelerator based on permeable surfaces of nanofiber mats," *Exp. Fluids*, vol. 33, no. 2, pp. 315–320, 2002.
- [54] A. Varesano, R. A. Carletto, and G. Mazzuchetti, "Experimental investigations on the multi-jet electrospinning process," *J. Mater. Process. Technol.*, vol. 209, no. 11, pp. 5178–5185, Jun. 2009.
- [55] Z.-M. Huang, Y.-Z. Zhang, M. Kotaki, and S. Ramakrishna, "A review on polymer nanofibers by electrospinning and their applications in nanocomposites," *Compos. Sci. Technol.*, vol. 63, no. 15, pp. 2223–2253, Nov. 2003.
- [56] Z. Li and C. Wang, "Effects of Working Parameters on Electrospinning," in *One-Dimensional nanostructures*, Springer, 2013, pp. 15–28.
- [57] J. Deitzel, J. Kleinmeyer, D. Harris, and N. . Beck Tan, "The effect of processing variables on the morphology of electrospun nanofibers and textiles," *Polymer (Guildf)*, vol. 42, no. 1, pp. 261–272, Jan. 2001.
- [58] V. Beachley and X. Wen, "Effect of electrospinning parameters on the nanofiber diameter and length," *Mater. Sci. Eng. C*, vol. 29, no. 3, pp. 663–668, 2009.
- [59] Rasel, Sheikh Md. "An advanced electrospinning method of fabricating nanofiber patterned architectures with controlled deposition and desired alignment." PhD diss., 2015.
- [60] X. Yuan, Y. Zhang, C. Dong, and J. Sheng, "Morphology of ultrafine polysulfone fibers prepared by electrospinning," *Polym. Int.*, vol. 53, no. 11, pp. 1704–1710, Nov. 2004.
- [61] H. Niu, X. Wang, and T. Lin, "Needleless Electrospinning : Developments and Performances," 2008.
- [62] J. Liu, G. Chen, H. Gao, L. Zhang, S. Ma, J. Liang, and H. Fong, "Structure and thermo-chemical properties of continuous bundles of aligned and stretched electrospun polyacrylonitrile precursor nanofibers collected in a flowing water bath," *Carbon N. Y.*, vol. 50, no. 3, pp. 1262–1270, 2012.

- [63] C. L. Casper, J. S. Stephens, N. G. Tassi, D. B. Chase, and J. F. Rabolt, "Controlling Surface Morphology of Electrospun Polystyrene Fibers: Effect of Humidity and Molecular Weight in the Electrospinning Process," *Macromolecules*, vol. 37, no. 2, pp. 573–578, Jan. 2004.
- [64] S. De Vrieze, T. Van Camp, a. Nelvig, B. Hagström, P. Westbroek, and K. De Clerck, "The effect of temperature and humidity on electrospinning," *J. Mater. Sci.*, vol. 44, no. 5, pp. 1357–1362, Oct. 2008.
- [65] J. M. Deitzel, N. C. BeckTan, J. D. Kleinmeyer, J. Rehrmann, and D. Tevault, "Generation of Polymer Nanofibers Through Electrospinning.," DTIC Document, 1999.
- [66] 'Nanofiber spinning equipment,' www.mecc.co.jp/en/html/nanon/collector.
- [67] Q. P. Pham, U. Sharma, and A. G. Mikos, "Electrospinning of polymeric nanofibers for tissue engineering applications: a review," *Tissue Eng.*, vol. 12, no. 5, pp. 1197–1211, 2006.
- [68] Y. Si, T. Ren, Y. Li, B. Ding, and J. Yu, "Fabrication of magnetic polybenzoxazine-based carbon nanofibers with Fe₃O₄ inclusions with a hierarchical porous structure for water treatment," *Carbon N. Y.*, vol. 50, no. 14, pp. 5176–5185, Nov. 2012.
- [69] L. Yang, A. Raza, Y. Si, X. Mao, Y. Shang, B. Ding, J. Yu, and S. S. Al-Deyab, "Synthesis of superhydrophobic silica nanofiber membranes with robust thermal stability and flexibility via in situ polymerization," *Nanoscale*, vol. 4, no. 20, pp. 6581–6587, 2012.
- [70] D. Yang, B. Lu, Y. Zhao, and X. Jiang, "Fabrication of aligned fibrous arrays by magnetic electrospinning," *Adv. Mater.*, vol. 19, no. 21, pp. 3702–3706, 2007.
- [71] D. Li, Y. Wang, and Y. Xia, "Electrospinning nanofibers as uniaxially aligned arrays and layer-by-layer stacked films," *Adv. Mater.*, vol. 16, no. 4, pp. 361–366, 2004.
- [72] J. J. Stankus, J. Guan, and W. R. Wagner, "Fabrication of biodegradable elastomeric scaffolds with sub-micron morphologies.," *J. Biomed. Mater. Res. A*, vol. 70, no. 4, pp. 603–14, 2004.
- [73] Jirsak, Oldrich, and Stanislav Petrik. "Needleless electrospinning-history, present and future." In *Proceedings of the 7th International Conference-TEXSCI*, pp. 6-8. 2010.

- [74] Dosunmu, O. O., George G. Chase, W. Kataphinan, and D. H. Reneker. "Electrospinning of polymer nanofibres from multiple jets on a porous tubular surface." *Nanotechnology* 17, no. 4 (2006): 1123.
- [75] Petrik, Stanislav. "Production Nozzle-Less Electrospinning Nanofiber Technology Stanislav Petrik and Miroslav Maly Elmarco sro V Horkach 76/18, CZ-46007 Liberec, Czech Republic."
- [76] O. Jirsak, F. Sanetnik, D. Lukas, V. Kotek, L. Martinova, and J. Chaloupek, "Method of nanofibres production from a polymer solution using electrostatic spinning and a device for carrying out the method," US7585437 B2, 08-Sep-2009.
- [77] O. Jirsak, P. Sysel, F. Sanetnik, J. Hruza, and J. Chaloupek, "Polyamic Acid Nanofibers Produced by Needleless Electrospinning," *J. Nanomater.*, vol. 2010, pp. 1–6, 2010.
- [78] Bijsterveld, Karin. *Mechanical sound: Technology, culture, and public problems of noise in the twentieth century*. MIT press, 2008.
- [79] H. G. Leventhall, "Low Frequency Noise and Annoyance," pp. 59–72, 2004.
- [80] G. Leventhall, "A Review of Published Research on Low Frequency Noise and its Effects," no. May, 2003.
- [81] G. Müller and M. Möser, *Handbook of engineering acoustics*. Springer Science & Business Media, 2012.
- [82] M. N. Mead, "Noise pollution: the sound behind heart effects," *Environ. Health Perspect.*, vol. 115, no. 11, p. A536, 2007.
- [83] G. W. Evans, P. Lercher, M. Meis, H. Ising, and W. W. Kofler, "Community noise exposure and stress in children," *J. Acoust. Soc. Am.*, vol. 109, no. 3, pp. 1023–1027, 2001.
- [84] L. Tzivian, A. Winkler, M. Dlugaj, T. Schikowski, M. Vossoughi, K. Fuks, G. Weinmayr, and B. Hoffmann, "Effect of long-term outdoor air pollution and noise on cognitive and psychological functions in adults," *Int. J. Hyg. Environ. Health*, vol. 218, no. 1, pp. 1–11, 2015.
- [85] S. Tabraiz, S. Ahmad, I. Shehzadi, and M. B. Asif, "Study of physio-psychological effects on traffic wardens due to traffic noise pollution; exposure-effect relation," *J. Environ. Heal. Sci. Eng.*, vol. 13, no. 1, p. 1, 2015.
- [86] S. L. Lusk, B. Gillespie, B. M. Hagerty, and R. A. Ziemba, "Acute effects of noise on blood pressure and heart rate," *Arch. Environ. Heal. An Int. J.*, vol. 59, no. 8, pp. 392–399, 2004.

- [87] X. Sagartzazu, L. Hervella, and J. M. Pagalday, "Review in Sound Absorbing Materials," vol. 981167000.
- [88] H. V Fuchs, *Applied Acoustics: Concepts, Absorbers, and Silencers for Acoustical Comfort and Noise Control: Alternative Solutions-Innovative Tools-Practical Examples*. Springer Science & Business Media, 2013.
- [89] H. Kuttruff, "Room Acoustics Spon Press," London, UK, 2000.
- [90] K. P. Waye, "Effects of Low Frequency Noise on Sleep," pp. 87–91, 2004.
- [91] M. Oud, "Low-frequency noise : a biophysical phenomenon," pp. 1–5, 2012.
- [92] Y.-Y. Kim, Y.-J. Kang, and J.-S. Lee, "Poroelastic acoustical foam having enhanced sound-absorbing performance." Google Patents, 06-Nov-2007.
- [93] T. L. Yang, D.-M. Chiang, and R. Chen, "Development of a novel porous laminated composite material for high sound absorption," *J. Vib. Control*, vol. 7, no. 5, pp. 675–698, 2001.
- [94] C. Nocke, C. Hilge, and J. Scherrer, "Micro-perforated sheets as day-light ceilings," in *Inter-noise 2014, Australia, 2014*, pp. 1–5.
- [95] Akasaka, Shuichi, Takahisa Kato, Shigeo Asai, and Hidetoshi Matsumoto. "Sound absorption characteristics of silica nanofiber sheet." *Sound absorption characteristics of silica nanofiber sheet (2014)*: 64-1.
- [96] K. K. M. Kucukali Ozturk, B. Nergis, C. Candan, "The Influence of Air Gap Between Nanofiber Layer and Rigid Wall on The Sound Absorption Behavior," in *Textile Science and the Economy*, pp. 37–40.
- [97] A. Trematerra and G. Iannace, "Acoustic Properties of Nanofibers," in *European Acoustics Association, 2014*, no. c, pp. 6–9.
- [98] K. Kalinová, "Nanofiber Resonant Membrane for Acoustic Applications," *J. Nanomater.*, vol. 2011, pp. 1–6, 2011.
- [99] M. K. Öztürk, B. Nergis, C. Candan, and K. Kalinova, "A study on the effect of fiber diameter on the acoustic behavior of the nanofiber membrane," in *Fiber Society Spring 2014 Conference: Fibers for Progress, 2014*.
- [100] J. Mohrova and K. Kalinova, "Different Structures of PVA Nanofiber Membrane for Sound Absorption Application," *J. Nanomater.*, vol. 2012, pp. 1–4, 2012.
- [101] Sundaray, Bibekananda, V. Subramanian, T. S. Natarajan, and K. Krishnamurthy. "Electrical conductivity of a single electrospun fiber of poly (methyl methacrylate) and multiwalled carbon nanotube nanocomposite." *Applied Physics Letters* 88, no. 14 (2006): 143114.

- [102] W. S. Khan, "Fabrication and characterization of polyvinylpyrrolidone and polyacrylonitrile electrospun nanocomposite fibers," 2010.
- [103] W. S. Khan, R. Asmatulu, and M. M. Eltabey, "Electrical and Thermal Characterization of Electrospun PVP Nanocomposite Fibers," vol. 2013, no. 1, 2013.
- [104] Y. Ji, C. Li, G. Wang, J. Koo, S. Ge, B. Li, J. Jiang, B. Herzberg, T. Klein, and S. Chen, "Confinement-induced super strong PS / MWNT composite nanofibers," vol. 56002.
- [105] W. Zhou, Y. Wu, F. Wei, G. Luo, and W. Qian, "Elastic deformation of multiwalled carbon nanotubes in electrospun MWCNTs – PEO and MWCNTs – PVA nanofibers," vol. 46, pp. 12689–12695, 2005.
- [106] L. Y. Yeo and J. R. Friend, "Electrospinning carbon nanotube polymer composite nanofibers," vol. 1, no. 2, pp. 177–209, 2006.
- [107] S. D. McCullen, D. R. Stevens, W. A. Roberts, S. S. Ojha, L. I. Clarke, R. E. Gorga, V. Uni, and N. Carolina, "Morphological , Electrical , and Mechanical Characterization of Electrospun Nanofiber Mats Containing Multiwalled Carbon Nanotubes," pp. 997–1003, 2007.
- [108] N. N. Yarns, B. F. Ko, Y. Gogotsi, A. Ali, N. Naguib, H. Ye, G. Yang, C. Li, and P. Willis, "Electrospinning of Continuous Carbon," vol. 1, no. 14, pp. 1161–1165, 2003.
- [109] M. J. Biercuk, M. C. Llaguno, M. Radosavljevic, J. K. Hyun, A. T. Johnson, J. E. Fischer, and Y. Heights, "Carbon nanotube composites for thermal management," vol. 80, pp. 1–12, 2002.
- [110] S. Wu, F. Li, H. Wang, L. Fu, B. Zhang, and G. Li, "Effects of poly (vinyl alcohol)(PVA) content on preparation of novel thiol-functionalized mesoporous PVA/SiO₂ composite nanofiber membranes and their application for adsorption of heavy metal ions from aqueous solution," *Polymer (Guildf)*, vol. 51, no. 26, pp. 6203–6211, 2010.
- [111] D. Yang, Y. Li, and J. Nie, "Preparation of gelatin/PVA nanofibers and their potential application in controlled release of drugs," *Carbohydr. Polym.*, vol. 69, no. 3, pp. 538–543, 2007.
- [112] "neographite_031_graphite_enhanced_polystyrene @ www.neotherm.ie." [Online]. Available: http://www.neotherm.ie/neographite_031_graphite_enhanced_polystyrene.html.

- [113] “expandable-polystyrene @ www.ceresana.com.” [Online]. Available: <http://www.ceresana.com/en/market-studies/plastics/expandable-polystyrene>.
- [114] “www.chemicalsafetyfacts.org.” [Online]. Available: <https://www.chemicalsafetyfacts.org/polystyrene-post/>.
- [115] Y. Fu, Q. Ni, Y. Yao, S. Xiao, W. Chen, and G. Liu, “Sound insulation performance of a glass fabric/PVC composite material.,” *Fuhe Cailiao Xuebao(Acta Mater. Compos. Sin., vol. 22, no. 5, pp. 94–99, 2005.*
- [116] C. Buratti and E. Moretti, “1 IMPACT NOISE REDUCTION: LABORATORY AND FIELD MEASUREMENTS OF DIFFERENT MATERIALS PERFORMANCES,” 2006.
- [117] B. Sundaray, D. Ph, V. J. Babu, V. Subramanian, and T. S. Natarajan, “Preparation and Characterization of Electrospun Fibers of Poly (methyl methacrylate) - Single Walled Carbon Nanotube Nanocomposites.”
- [118] P. W. Gibson, D. Ph, C. Lee, F. Ko, and D. Reneker, “Application of Nanofiber Technology to Nonwoven Thermal Insulation,” vol. 2, no. 2, 2007.
- [119] “Handbook of Noise Control Materials,” I. Section and V. Section, www.sounddown.com.
- [120] “features @ imagej.nih.gov.” [Online]. Available: <https://imagej.nih.gov/ij/features.html>.
- [121] B. ISO, “10534-2: 2001,” *Acoust. Determ. sound Absorpt. Coeff. impedance impedance tubes. Transf. method. Geneve, 2001.*
- [122] U. ISO, “10534-1: 2002,” *Acoust. Determ. sound Absorpt. Coeff. impedance impedance tubes, Part, vol. 1.*
- [123] E. N. ISO, “354: 2003,” *Acoust. Meas. sound Absorpt. a reverberation room, 2003.*
- [124] M. Hasan and M. Hodgson, “Effectiveness of reverberation room design: Room size and shape and effect on measurement accuracy,” in *PROCEEDINGS of the 22nd International Congress on Acoustics, 2016.*
- [125] I. T. Method and D. Filters, “Standard Test Method for Impedance and Absorption of Acoustical Materials Using a Tube , Two Microphones and a Digital Frequency Analysis,” pp. 1–12, 2014.
- [126] R. V. Lopes, “Design and Construction of a Low Cost Impedance Tube for Sound Absorption Coefficients Measurements,” no. Cobem, pp. 105–115, 2013.
- [127] A. G. MacDiarmid, W. E. Jones, I. D. Norris, J. Gao, A. T. Johnson, N. J. Pinto, J. Hone, B. Han, F. K. Ko, and H. Okuzaki, “Electrostatically-generated nanofibers

- of electronic polymers,” *Synth. Met.*, vol. 119, no. 1–3, pp. 27–30, 2001.
- [128] Rodoplu, Didem, and Mehmet Mutlu. "Effects of electrospinning setup and process parameters on nanofiber morphology intended for the modification of quartz crystal microbalance surfaces." *Journal of Engineered Fibers and Fabrics* 7, no. 2 (2012): 118-123.
- [129] C. J. Thompson, G. G. Chase, a. L. Yarin, and D. H. Reneker, “Effects of parameters on nanofiber diameter determined from electrospinning model,” *Polymer (Guildf.)*, vol. 48, no. 23, pp. 6913–6922, Nov. 2007.
- [130] Fong, Hao, and Darrell H. Reneker. "Elastomeric nanofibers of styrene-butadiene-styrene triblock copolymer." *Journal of Polymer Science Part B Polymer Physics* 37, no. 24 (1999): 3488-3493.
- [131] E. D. Boland, G. E. Wnek, D. G. Simpson, K. J. Pawlowski, and G. L. Bowlin, “Tailoring tissue engineering scaffolds using electrostatic processing techniques: a study of poly (glycolic acid) electrospinning,” *J. Macromol. Sci. Part A*, vol. 38, no. 12, pp. 1231–1243, 2001.
- [132] X. M. Mo, C. Y. Xu, M. Kotaki, and S. Ramakrishna, “Electrospun P (LLA-CL) nanofiber: a biomimetic extracellular matrix for smooth muscle cell and endothelial cell proliferation,” *Biomaterials*, vol. 25, no. 10, pp. 1883–1890, 2004.
- [133] D. S. Katti, K. W. Robinson, F. K. Ko, and C. T. Laurencin, “Bioresorbable nanofiber-based systems for wound healing and drug delivery: Optimization of fabrication parameters,” *J. Biomed. Mater. Res. Part B Appl. Biomater.*, vol. 70, no. 2, pp. 286–296, 2004.
- [134] S. Sukigara, M. Gandhi, J. Ayutsede, M. Micklus, and F. Ko, “Regeneration of Bombyx mori silk by electrospinning. Part 2. Process optimization and empirical modeling using response surface methodology,” *Polymer (Guildf.)*, vol. 45, no. 11, pp. 3701–3708, 2004.
- [135] O. Karatay and M. Dogan, “Modelling of electrospinning process at various electric fields,” *Micro Nano Lett.*, vol. 6, no. 10, p. 858, 2011.
- [136] M. M. Hohman, M. Shin, G. Rutledge, and M. P. Brenner, “Electrospinning and electrically forced jets. I. Stability theory,” *Phys. Fluids*, vol. 13, no. 8, p. 2201, 2001.
- [137] D. H. Reneker, A. L. Yarin, H. Fong, and S. Koombhongse, “Bending instability of electrically charged liquid jets of polymer solutions in electrospinning,” *J. Appl. Phys.*, vol. 87, no. 9, pp. 4531–4547, 2000.

- [138] T. A. Kowalewski and S. Barral, "Experiments and modelling of electrospinning process," vol. 53, no. 4, pp. 385–394, 2005.
- [139] T. A. Kowalewski, S. Barral, and T. Kowalczyk, "Modeling Electrospinning of Nanofibers," pp. 279–292.
- [140] O. S. Yördem, M. Papila, and Y. Z. Menceloğlu, "Effects of electrospinning parameters on polyacrylonitrile nanofiber diameter: An investigation by response surface methodology," *Mater. Des.*, vol. 29, no. 1, pp. 34–44, 2008.
- [141] Y. Dong, T. Bickford, H. J. Haroosh, K.-T. Lau, and H. Takagi, "Multi-response analysis in the material characterisation of electrospun poly (lactic acid)/halloysite nanotube composite fibres based on Taguchi design of experiments: fibre diameter, non-intercalation and nucleation effects," *Appl. Phys. A*, vol. 112, no. 3, pp. 747–757, 2013.
- [142] S. Y. Gu, J. Ren, and G. J. Vancso, "Process optimization and empirical modeling for electrospun polyacrylonitrile (PAN) nanofiber precursor of carbon nanofibers," *Eur. Polym. J.*, vol. 41, no. 11, pp. 2559–2568, 2005.
- [143] M. A. Lopez-Manchado and M. Arroyo, "Effect of the incorporation of pet fibers on the properties of thermoplastic elastomer based on PP/elastomer blends," *Polymer (Guildf.)*, vol. 42, no. 15, pp. 6557–6563, 2001.
- [144] R. Wächter and A. Cordery, "Response surface methodology modelling of diamond-like carbon film deposition," *Carbon N. Y.*, vol. 37, no. 10, pp. 1529–1537, 1999.
- [145] H. Trieu and S. Qutubuddin, "Poly (vinyl alcohol) hydrogels: 2. Effects of processing parameters on structure and properties," *Polymer (Guildf.)*, vol. 36, no. 13, pp. 2531–2539, 1995.
- [146] D. C. Montgomery, *Design and analysis of experiments*. John Wiley & Sons, 2008.
- [147] Sung, H. Park. "Robust design and analysis for quality engineering." (1996): 46-59.
- [148] P. Wang, J, and K. Tsai, "Semi-empirical model on work removal and tool wear in electrical discharge machining.," *J. Mater. Process. Technol.*, vol. 114, no. 1, pp. 1–17, 2001.
- [149] Phadke, M. S. "Quality engineering using design of experiments, quality control, robust design, and the Taguchi method." Wadsworth, Los Angeles, CA (1998).

- [150] S. F. Fennessey and R. J. Farris, "Fabrication of aligned and molecularly oriented electrospun polyacrylonitrile nanofibers and the mechanical behavior of their twisted yarns," *Polymer (Guildf)*, vol. 45, no. 12, pp. 4217–4225, 2004.
- [151] B. Ding, H. Kim, S. Lee, C. Shao, D. Lee, S. Park, G. Kwag, and K. Choi, "Preparation and characterization of a nanoscale poly (vinyl alcohol) fiber aggregate produced by an electrospinning method," *J. Polym. Sci. Part B Polym. Phys.*, vol. 40, no. 13, pp. 1261–1268, 2002.
- [152] Z. Qi, H. Yu, Y. Chen, and M. Zhu, "Highly porous fibers prepared by electrospinning a ternary system of nonsolvent/solvent/poly (l-lactic acid)," *Mater. Lett.*, vol. 63, no. 3, pp. 415–418, 2009.
- [153] L. Natarajan, J. New, A. Dasari, S. Yu, and M. A. Manan, "Surface morphology of electrospun PLA fibers: mechanisms of pore formation," *RSC Adv.*, vol. 4, no. 83, pp. 44082–44088, 2014.
- [154] C. Zhou, Q. Shi, W. Guo, L. Terrell, A. T. Qureshi, D. J. Hayes, and Q. Wu, "Electrospun bio-nanocomposite scaffolds for bone tissue engineering by cellulose nanocrystals reinforcing maleic anhydride grafted PLA," *ACS Appl. Mater. Interfaces*, vol. 5, no. 9, pp. 3847–3854, 2013.
- [155] A. R. Kakroodi, S. Cheng, M. Sain, and A. Asiri, "Mechanical, thermal, and morphological properties of nanocomposites based on polyvinyl alcohol and cellulose nanofiber from aloe vera rind," *J. Nanomater.*, vol. 2014, p. 139, 2014.
- [156] M. S. Peresin, Y. Habibi, J. O. Zoppe, J. J. Pawlak, and O. J. Rojas, "Nanofiber composites of polyvinyl alcohol and cellulose nanocrystals: manufacture and characterization," *Biomacromolecules*, vol. 11, no. 3, pp. 674–681, 2010.
- [157] H. Zhang, J. Huang, L. Yang, R. Chen, W. Zou, X. Lin, and J. Qu, "Preparation, characterization and properties of PLA/TiO₂ nanocomposites based on a novel vane extruder," *RSC Adv.*, vol. 5, no. 6, pp. 4639–4647, 2015.
- [158] J. Yao, C. W. M. Bastiaansen, and T. Peijs, "High strength and high modulus electrospun nanofibers," *Fibers*, vol. 2, no. 2, pp. 158–186, 2014.